ABSTRACT

Title of Document: HIGH TEMPERATURE STEAM GASIFICATION OF SOLID WASTES: CHARACTERISTICS AND KINETICS

Islam Ahmed Gomaa, Doctor of Philosophy, 2011

Directed by: Professor Ashwani K. Gupta
Department of Mechanical Engineering

Greater use of renewable energy sources is of pinnacle importance especially with the limited reserves of fossil fuels. It is expected that future energy use will have increased utilization of different energy sources, including biomass, municipal solid wastes, industrial wastes, agricultural wastes and other low grade fuels. Gasification is a good practical solution to solve the growing problem of landfills, with simultaneous energy extraction and nonleachable minimum residue. Gasification also provides good solution to the problem of plastics and rubber in to useful fuel.

The characteristics and kinetics of syngas evolution from the gasification of different samples is examined here. The characteristics of syngas based on its quality, distribution of chemical species, carbon conversion efficiency, thermal efficiency and hydrogen concentration has been examined. Modeling the kinetics of syngas evolution from the process is also examined. Models are compared with the experimental results.

Experimental results on the gasification and pyrolysis of several solid wastes, such as, biomass, plastics and mixture of char based and plastic fuels have been provided. Differences and similarities in the behavior of char based fuel and a plastic sample has been discussed. Global

reaction mechanisms of char based fuel as well polystyrene gasification are presented based on the characteristic of syngas evolution.

The mixture of polyethylene and woodchips gasification provided superior results in terms of syngas yield, hydrogen yield, total hydrocarbons yield, energy yield and apparent thermal efficiency from polyethylene-woodchips blends as compared to expected weighed average yields from gasification of the individual components. A possible interaction mechanism has been established to explain the synergetic effect of co-gasification of woodchips and polyethylene.

Kinetics of char gasification is presented with special consideration of sample temperature, catalytic effect of ash, geometric changes of pores inside char and diffusion limitations inside and outside the char particle.

HIGH TEMPERATURE STEAM GASIFICATION OF SOLID WASTES: CHARACTERISTICS AND KINETICS

By

Islam Ahmed Gomaa

Dissertation submitted to the Faculty of the Graduate School of the
University of Maryland, College Park, in partial fulfillment
of the requirements for the degree of
Doctor of Philosophy
2011

Advisory Committee:

Professor Ashwani K. Gupta, Chair
Professor Nam Sun Wang, Dean's Representative
Professor Michael Zachariah
Professor Gregory Jackson
Professor Bao Yang

Dedication

I would like to dedicate this thesis to my wife, Tahanie Thabet, and my parents, Professor Ibrahim Gomaa and Mrs. Soheir Saleh. They have been a great support for me throughout the years of my PhD study.

Acknowledgments

I would like to acknowledge my advisor, Professor A. K. Gupta for his help and support. Professor A. K. Gupta opened my eyes to the meaning of hard work. I am also thankful for his help in publishing a good number of journal papers.

Also, I would like to thank my wife and parents for their support. My wife turned down numerous job offers in order to stay next to me during the years of my study. My parents accepted the fact that I will be living away from them for years.

Finally, I would like to express my sincere gratitude to the Office of Naval Research (ONR), who supported this work.

Table of contents

List of Tables

List of Figures

Nomenclature

A pre-exponential factor ***(1/sec) or (1/min)***

C Gasifying agent concentration ***(mol/m^3)***

C_{carbon} is the initial carbon concentration in the char particle ***(mol/m^3)***

C_s Gasifying agent concentration at the char particle surface ***(mol/m^3)***

C_∞ Gasifying agent concentration far from the char particle ***(mol/m^3)***

Da Damkohler number (-)

$D_{effective}$ effective diffusivity inside the particle in the definition of Damkohler number ***(m^2/sec)***

$D_{ga\text{-}B}$ binary diffusion coefficients of the gasifying agent in gas *B* ***(m^2/sec)***

$D_{ga\text{-}C}$ binary diffusion coefficients of the gasifying agent in gas *C* ***(m^2/sec)***

D_o is the gasifying agent diffusivity in the gas phase ***(m^2/sec)***

D_p is effective diffusion coefficient of the gasifying agent inside the particle ***(m^2/sec)***

E_{act} Activation energy ***(kJ/mol)***

E_{yield} energy yield form PS gasification or pyrolysis ***(kJ)***

E_{0i} mean activation energy value in the distributed activation energy model ***(kJ/mol)***

f(X) is a function of conversion ***(X), (-)***

K reaction rate constant

K_i Reaction rate constant for pseudo reaction ***(i), (1/min)or (1/sec)***

$K_{observed}$ observed reaction rate constant in a chemically controlled experiment ***(1/sec)***

L characteristic length in the definition of Damkohler number ***(m)***

m char mass at time ***t (kg)***

N_e number of moles in each element ***n_e***

N_{H2} number of hydrogen moles evolved at time (***t***) from paper pyrolysis experiments

N_{H2}^{*} total number of hydrogen moles evolved from the sample during paper pyrolysis

N_{total} total number of moles in the particle

N_o initial number of moles in the char particle

n_{char} reaction exponent with respect to char (-)

n_e number of elements in the FEM solution

n_{ga} is the rate exponent with respect to gasifying agent

$n_{reaction}$ is the reaction rate exponent with respect to the gasifying agent in the definition of Damkohler number

n_{time} number of time intervals in the finite difference solution

q sample heating rate *($^oC/min$)*

R Universal gas constant *(J/kmol.K)*

R_{cd}^2 coefficient of determination (-)

r radius *(m)*

r_{char} char reactivity *(1/sec) or (1/min)*

r_e radius to the first node of element number **(*e*)**

r_{iso} isokinetic reactivity *(1/sec) or (1/min)*

r_p particle radius *(m)*

t time *(sec) or (min)*

T temperature *(K) or (^oC)*

T_{iso} isokinetic temperature *(K) or (^oC)*

T_o initial reactor temperature *(K)*

V_{CH4} amount of CH_4 evolved at time **(*t*)**

V^{*}_{CH4} maximum potential amount of CH_4

w_i weight of pseudo reaction **(*i*)** in paper pyrolysis kinetics, **(-)**

X Char conversion, **(-)**

X_e degree of conversion at the first node of element number ***(e)***

X_{total} Total conversion of the char particle **(-)**

y_B mole fraction of gas *B* **(-)**

y_C mole fraction of gas *C* **(-)**

y_{ga} gasifying agent mole fraction **(-)**

ρ density (kg/m^3)

Ψ is a dimensionless structural parameter in the random pore model **(-)**

α_j overall conversion of main syngas constituent **(*j*)** at time **(*t*)** from paper pyrolysis

α_i conversion of main syngas constituent from paper pyrolysis from pseudo reaction ***i***

$\eta_{app.}$ Apparent thermal efficiency **(-)**

λ tortuosity factor **(-)**

ε porosity of char at a given **(*r*)** and **(*t*)**, **(-)**

ε_o initial porosity of the char particle **(-)**

σ_i width parameter of the distribution in the distributed activation energy model ***(kJ/mol)***

Subscript

it index for time intervals

H_2O steam

CO_2 Carbon dioxide

Superscript

je index for number of nodes

Chapter I: Introduction

1.1. Motivations and Objectives

Many cities worldwide, in particular densely populated cities are confronted with the problem of acceptable means of disposing-off large quantities of municipal solid waste (MSW). Currently, landfills are the primary means of MSW disposal and account for about 80% of the residential waste generated in the USA. However, rising landfill tipping fees and their proven detrimental environmental impact have led engineers and scientists to search for cleaner and inexpensive alternatives for the disposal of municipal waste. Energy recovery from MSW, known as waste-to-energy (WTE), is one such alternative. One more motivation towards the WTE recovery is governmental regulations and plans such as, the Solid Waste Disposal Act of 1976 [1] (also known as Resource Conservation and Recovery Act-RCRA), which requires all states to implement 'Solid Waste Plans' that maximize waste reduction and recycling. Clean waste-to-Energy reduces the amount of materials sent to landfills, assists in preventing air/water contamination improves recycling rates and lessens the dependence on fossil fuels for power generation. Gasification of solid wastes is a good solution for not only the energy problem but also offers environmentally benign solution for waste destruction and management [2].

Specific problems rise from different types of solid waste. Dumping food waste in a landfill causes environmental problems. By volume, the dumped landfill waste causes the largest contribution to methane gas production [3]. It causes odor as it decomposes to cause public annoyance in addition to forming germs, and attracting flies and vermin. Another serious problem of food wastes is the generation of landfill leachate. Landfill leachate is liquid that leaks from the landfill and enters the environment. Once it enters the environment the leachate is at

risk for mixing groundwater near the site which then transports to some distances. Furthermore it has the potential to add biological oxygen demand (BOD) to the groundwater. BOD measures the rate of oxygen uptake by micro-organisms in a sample of water at a temperature of 20°C and over an elapsed period of five days in the dark.

Despite problems that arise from food wastes, they are biodegradable and can be decomposed easily. However, plastics and rubber are not biodegradable, but photo-degradable. Photo-degradation is a process in which the material brakes down by sunlight into smaller and smaller pieces, all of which are still polymer molecules, eventually becoming individual molecules of plastic, which are still difficult for the environment to accommodate.

Automobile tires alone are big problems not only in the USA but many countries worldwide. It is estimated that about 2 billion tires lie as trash in the USA and additional amounts worldwide. In addition over 200 million tires are added annually in the USA as wastes. It is estimated that about 80 to 90% of the plastics is disposed off improperly. The use of plastics in the cars has increase significantly over the years. For example in 1980 average amount of plastics in cars was 86 kg/vehicle, while in 1991 it was 163 kg/vehicle. The use of plastics is expected to increase in the future not only in cars in the transportation sector but also in other applications, such as appliances, toys and selected industrial and consumer applications.

Greater use of renewable energy sources is of pinnacle importance especially with the limited reserves of fossil fuels. It is expected that future energy use will have increased utilization of different energy sources, including biomass, municipal solid wastes, industrial wastes, agricultural wastes and other low grade fuels. The different types of wastes provide not only unique challenges for energy utilization, but also the energy yield and gas composition from gasification or pyrolysis is strongly impacted by the feed mixture composition. Development of

sustainable renewable energy technologies for their use in current and new power plants is of greater importance now than ever before due to several reasons. Some of these reasons include energy security and availability, independency from foreign oils and reduction of greenhouse gas emissions to provide cleaner environment for better health and plant and animal life. These reasons dictate the development of alternative and sustainable energy technologies. Gasification provides part of the solution towards dependable renewable energy source. Gasification is a robust solution to solve the growing problem of landfills, since energy can be fully extracted and the waste is destructed with minimum residue and with the properly developed process the remaining residue is non-leachable.

On the other hand, gasification provides an excellent solution to the problem of plastics and rubber in landfills by getting rid of the plastic and rubber wastes and recovering energy in the same time [4-7].

The goal of the new strategies in handling wastes must be garbage in and energy out in an environmentally acceptable manner [8].

The potential of gasification is attributed to several key advantages of the gasification process. For example, the IGCC power plants provide a very high thermal efficiency. Beside the high thermal efficiency of IGCC power plants, the gasification process can utilize a wide range of carbonaceous materials as feedstock (such as coal, biomass and wastes) and the gases produced can be used as fuel in power plants. The residue remaining from gasification, especially ash, can be used as construction material. Syngas from gasification can possess low, medium or high hydrogen content, with the remaining as carbon monoxide. Proper mixture of the two gases provides a potential of producing liquid fuels. Alternatively separating out hydrogen from the syngas can be used as good clean fuel in hydrogen engines or fuel cells.

Residues remaining from gasification are mainly ashes. Ash is not destructed by gasification or combustion. The ash remaining after the gasification process is a valuable product. For example, it can be used in the production of cement and other construction materials. The emission of hazardous pollutants is also eliminated or minimized. For example; NO_X formation is eliminated if steam and/or oxygen are used as gasifying agents. NO_X formation is also minimized even if air is used as the gasifying agent due to the lower reactor temperature as compared to that encountered in direct combustion of waste materials. Note that gasification temperatures are lower than the temperatures at which thermal NO_X is formed (1800^oC). Such high temperatures are common in combustion systems that have stoichiometric mixtures at selected regions of combustion chamber but not in the gasification studies conducted here. However, air gasification systems, runs on very rich equivalence ratios and the gasification temperatures are much lower. A considerable advantage of gasification over combustion is the reduction of volumetric gases products by a factor 5 to 20 which in turn reduces the size of gas conditioning/cleaning equipment [9].

1.2. What is Gasification?

Gasification is heating-up of solid or liquid carbonaceous material with some gasifying agent to produce gaseous fuel. The heating value of the gases produced is generally low to medium. This definition excludes combustion, because the product flue gas has no residual heating value from complete combustion of the fuel. It does include partial oxidation of fuel or fuel-rich combustion, and hydrogenation. In partial oxidation process the oxidant (also called the gasifying agent) could be steam, carbon dioxide, air or oxygen, or some mixture of two or more gasifying agents. The gasifying agent is chosen according to the desired chemical composition of the syngas and efficiency.

Pyrolysis and gasification are important to reform solid and liquid hydrocarbons to clean gaseous fuel which can be further processed to obtain clean and pure gaseous fuel or liquid fuel. Pyrolysis is a thermal degradation process of organic compounds in the absence of oxygen or air to produce various gaseous component yield as well as yield of tar and char residues. The heating rate of the sample, pyrolysis temperature, and particle size and distribution has an important effect on the products evolved and their distribution during pyrolysis [10].

Char gasification reactions have relatively high activation energy as compared to pyrolysis reactions. This difference in activation energies reveals higher sensitivity of gasification on the reactor temperature than that of pyrolysis. Higher values of activation energy in case of gasification result in longer gasification time. Consequently, char gasification is considered to be the rate limiting step in the overall gasification process [10].

Steam is usually used as a gasifying agent to achieve high hydrogen yield. Steam has been used as gasifying agent in this study to investigate the behavior of syngas during steam gasification and effect of steam flow rate on main syngas properties. The final composition of the syngas is a function of the gasification temperature, steam to carbon ratio and pressure. Consequently, adjustment of these parameters should be taken into consideration to optimize thermal efficiency. During the process of gasification of solid carbon, whether in the form of coal, coke, or char, the principle chemical reactions are those involving carbon, carbon monoxide, carbon dioxide, hydrogen, water (or steam), and methane [10]. These include

Combustion reactions:

$C+½O_2=CO,\ \Delta H=-111\ MJ/kmol$

$CO+½O_2=CO_2,\ \Delta H=-283\ MJ/kmol$

$H_2+½O_2=H_2O$, $\Delta H = -242$ MJ/kmol

The Boudouard reaction: $C+CO2 \Leftrightarrow 2CO\ \Delta H = +172$ MJ/kmol (1)

The water gas reaction: $C+H_2O \Leftrightarrow CO+H_2$, $\Delta H = +131$ MJ/kmol (2)

The methanation reaction: $C+2H_2 \Leftrightarrow CH_4\ \Delta H = -75$ MJ/kmol (3)

Reactions from (1), (2) and (3) are the most important reactions in the char-gasification step and both are endothermic reactions. These reactions are reduced to the following two homogeneous gas reactions.

Water-gas shift reaction: $CO + H_2O \Leftrightarrow CO_2 + H_2,\ \Delta H = -41 MJ/kmol$ (4)

The steam methane reforming reaction: $CH_4 + H_2O \Leftrightarrow CO_2 + 3H_2, \Delta H = +206 MJ/kmol$ (5)

A simplified reaction sequence for the gasification of carbonaceous matters is shown in Figure I-1. Figure I-2 shows the progress of a sample under pyrolysis and gasification conditions

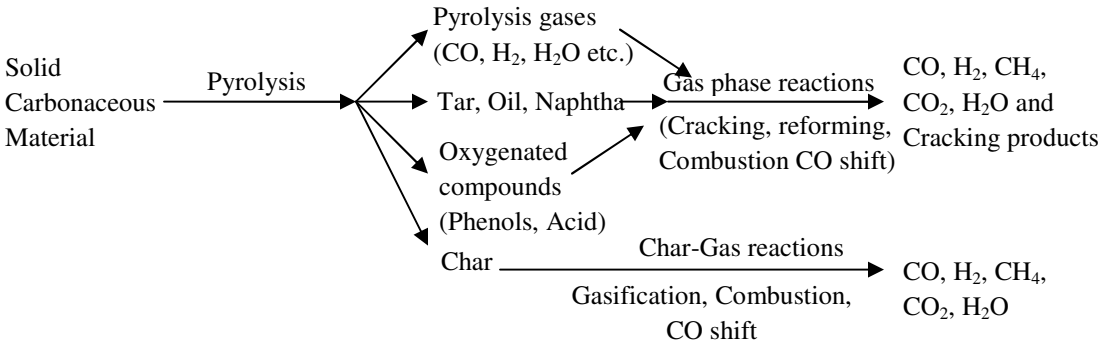

Figure I-1. Reaction sequence for gasification **[10]**

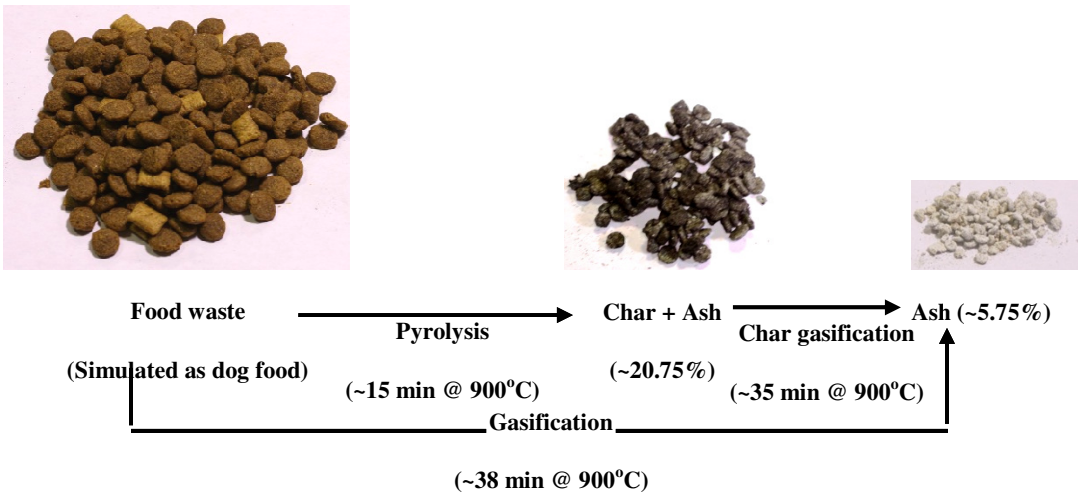

Figure I-2. Progress of food waste sample through pyrolysis and gasification

1.3. Characteristics of syngas evolution

1.3.1. Introduction

Samples other than coal have started to attract attention of researchers in the gasification field. Characteristics of syngas evolution from waste samples, such as, cardboard [11], paper [12], plastic [13] and food wastes [14] have been investigated. Results show that there is a great potential of using these materials as well as other waste materials as fuel for power generation in gasification power plants.

1.3.2. Gasification of char based fuel

Since cardboard forms a big percentage of MSW, gasification of cardboard has been investigated with specific focus on the evolutionary behavior of syngas chemical composition and its characteristics.

The investigation provides information on the evolutionary behavior of main gaseous produced in the syngas, such as hydrogen flow rate, hydrogen concentration, hydrogen to carbon monoxide ratio, syngas heating value and other properties concerning thermal efficiency and effectiveness

of the process. The effect of steam flow rate on the evolutionary behavior of syngas chemical composition and flow rates of main species has also been investigated. Information of the time dependent properties have been used to determine the overall yields and properties of the syngas, such as syngas yield, hydrogen yield, overall hydrogen to CO ratio, combustible part of the syngas (yield of pure fuel as percentage), heating values and other factors that describes the overall thermal effectiveness of the process. The effect of steam flow rate on the overall yield, syngas properties and apparent thermal efficiency has also been determined.

Paper represents approximately 1/3 of the waste composition in the municipal solid wastes. Therefore, paper has been investigated under gasification and pyrolysis conditions for reactor temperatures up to 1000^{o}C. Studies on paper will help assist in better design of advanced waste to energy conversion systems.

By definition, gasification of solid wastes includes a devolatilization process at beginning of the process. At high heating rates, the sample undergoes pyrolysis and gasification in parallel; however, at low heating rates the sample undergoes pyrolysis and gasification in series in the order of pyrolysis then char gasification (see figure I-1). Percentage of overlap between gasification and pyrolysis can be observed by plotting the evolution of syngas flow rate for both gasification and pyrolysis in the same figure. Our present results have shown an overlap between syngas flow from char gasification and gaseous yield from pyrolysis of 27% at low reactor temperature of 800^{o}C to ~ 95% overlap at high (1000^{o}C) temperature.

The main differences between the gasification and pyrolysis processes are examined here with special focus on the evolution of syngas flow rate, hydrogen flow rate and overall hydrogen yield, energy yield, apparent thermal efficiency, evolution of H_2 and CO mole fractions and the residue remaining from the process at temperatures of 600, 700, 800, 900 and 1000^{o}C. The main

difference between gasification and pyrolysis is absence of a gasifying agent in case of pyrolysis. Consequently, char inherently produced in the pyrolysis process remains in the product stream while steam-char reactions diminish the fixed carbon in sample with steam gasification.

Characteristics of food waste gasification and pyrolysis have been investigated as well. Main characteristics which have been investigated are syngas yield, hydrogen yield, energy yield and apparent thermal efficiency. The results show that food wastes offers a good potential for thermal treatment of the waste with the specific aim of power generation.

1.3.3. Gasification of plastics and rubber

Plastics have the advantage of higher heating value when compared to average heating value of cellulosic material. Plastics have the average LHV of 40 MJ/kg. However, the LHV for cellulosic wastes such as cardboard is 16 MJ/kg. Not only the plastics have the advantage of higher heating value than that of other components in municipal wastes but also, it has the potential of producing higher hydrogen yield when undergoing pyrolysis or gasification.

Plastics behave differently than other solid fuels such as coal, paper, cardboard or biomass when undergoing a gasification process. Plastics differ in the sense that there is no char or fixed carbon content in it. On the other hand, sample such as paper or biomass have on the average 18% fixed carbon and some ash depending on the sample heating rate. Based on this fact, when a biomass or cellulose based material undergo a pyrolysis process of slow or medium heating rate, only the volatile part of the sample evolves and the char remains in the reactor. However, under the same pyrolysis conditions, plastics will yield almost 99% of its mass as volatile products, leaving around 1% of ash and carbonaceous material. Since there is no char content in plastics, gasifying agents does not have the chance to react with the solid phase sample at low temperatures and the

benefit of syngas production is not gained unless the reactor temperature is high enough to accelerate the gasifying agent-sample reaction to a comparable rate to pyrolysis reaction rates.

Most of the research conducted in this area focus on the monomers yield from the polymers, such as the effect of operating conditions on olefins yield as compared to the paraffins either in the liquid phase or gaseous phase. Less attention has been devoted to the gaseous yield specially the hydrogen yield. The focus of this research is to determine the characteristics gaseous yield from the gasification or pyrolysis of polystyrene. Specific attention is given to effect of operating conditions on syngas yield, syngas quality, energy yield and specially hydrogen yield. Main investigated operating conditions examined are the reactor temperature and the presence of a gasifying agent, namely steam. Energy recovery from polystyrene form its solid phase to gaseous phase requires that the investigation should be conducted at higher temperature range than that in the research aiming for monomers and liquid hydrocarbons recovery.

Rubber wastes also have the advantage of high heating value and high hydrogen content. Rubber heating value is approximately 37.2 MJ/kg, which is close to the average heating value of plastic (~ 40 MJ/kg) and significantly higher than that of the biomass, which is about 18 MJ/kg.

The gasification of rubber has been investigated here with specific focus on the evolution of syngas flow rate, hydrogen flow rate in the syngas, amounts of syngas yield, hydrogen yield and energy yield from a given amount of material. Results of syngas characteristics obtained from the gasification process have been compared to that obtained from the pyrolysis. The characteristics of syngas from rubber gasification have been compared to that from woody biomass samples, namely hard wood and wood chips.

1.3.4. Gasification of a mixture of a char based fuel and a plastic fuel

Gasification systems may run on single or multiple sources of feedstock. However, in many cases the gasification systems often encounter the problem of unsteady source of biomass feed throughout the year so that the biomass composition is rarely fixed. During off-season of a given biomass, another feedstock has to be mixed with the feedstock in order to maintain a steady supply of feedstock to the gasifier for seeking the desired output power from the gasification power plant. On the other hand, a gasification system might be designed to run on solid wastes, which consists of a mixture of different carbonaceous materials. However the composition of the waste can change both temporally and spatially.

The fate of multi-components as feed stock to the gasifier might be much different than the expected fate of single components. Misleading information might arise from the assumption that the syngas characteristics resulting from gasifying a mixture of materials are directly proportional to the weighted average properties of syngas evolved from individual components of materials in the gasification process. This assumption ignores the possibility of material-material interaction between the mixed multi-component feed stock samples. An interaction might occur between the volatile matters evolved from each sample or between the volatile matter of a certain sample and the fixed carbon of another sample or both. Most probably an interaction on the volatiles evolved between the samples will occur among similar materials, such as two or more biomass samples. However, the interaction between volatiles from a certain material and fixed carbon from another material most probably occurs between different types of materials, such as, plastics and biomass or biomass and coals. The volatiles from plastics generally start to evolve at a higher temperature range (300~500K) as compared to those from biomass or coals (200~400K). Having an overlapping temperature range of gasification from the

two different materials suggest the existence of a combination of interactions between the volatiles released and fixed carbon.

For example, volatile matter evolving from coal pyrolysis is known to contain species of low molecular weight in the form of free radicals. On the other hand, hydrocarbon species originated from cleavage of plastics bond contributes in stabilizing the radicals generated from the coal, resulting in higher weight loss of coal and lower yield of char. However, in terms of volatile-char interactions, the hydrogen deficient active sites of char extract hydrogen from the plastic resulting in the formation of liquid molecule sites [15].

Some research in the area of mixture co-pyrolysis and/or co-gasification has been conducted at the low temperature range. Consequently, the research was focused on synergistic effect on liquid hydrocarbons yield [15, 16]. Other researchers have focused on the behavior of mixed sample from a pure thermogravimetric point of view that involves weight loss as a function of temperature of the sample.

Not much attention has been given to the synergistic effect of mixed samples on the characteristics of syngas yield at high temperature gasification. Consequently, this section forms a basis for investigating the behavior of two compounds in the sample feedstock on the evolved syngas behavior. Mixtures of different amounts of plastics in the biomass sample to form a mixture of woodchips and polyethylene is investigated under high temperature steam gasification conditions at atmospheric pressure. Characteristics of syngas have been evaluated based on the evolution of syngas flow rate/yield, evolution of hydrogen flow rate/yield, output power and energy yield, evolution of hydrocarbons flow rate/yield, and apparent thermal efficiency. The results obtained clearly showed that properties of syngas generated from a mixed sample are not

a weighted average of syngas properties obtained from separate gasification of each sample, which suggests synergistic effect due to co-gasification of woodchips and polyethylene.

1.4. Kinetics of char gasification

1.4.1. Introduction

Char gasification is slower than pyrolysis and is the rate limiting step in the overall gasification process.

Kinetics of biomass char and food wastes char gasification has not received the same attention as kinetic of coal char gasification. Kinetic parameters for coal char gasification are abundant in the literature, while kinetic parameters for biomass char and food wastes gasification are scarce. It is important to develop a rate expression for biomass and food wastes chars gasification which can be used in modeling the overall gasification process.

The progress of char particle gasification is a function of the particle size, porosity [17], gasifying agent chemical composition [18], gasifying agent partial pressure[19, 20], reactor temperature [21-22], geometry of the particle, pore structure [23], number of active sites, number of reactive sites [24], ash content[25-27], inhibitors partial pressure [28, 29], total pressure [30, 31] and thermal history of char which emanates from the heating rate during the pyrolysis process [32].

1.4.2. Gasification kinetics of Woodchips char

The objective of this part of the investigations is to compare the behavior of woodchips char during gasification using steam or CO_2 as the gasifying agents. The comparison will be conducted in term of geometric evolution of sample pores during the process, gasification duration, average reaction rate and effect of partial pressure of the gasifying agent. Reactor

temperature and total pressure were held constant at 900^{o}C and 2 bars, respectively. Steam and CO_2 flow rates was adjusted to have equal oxygen content for accurate comparison

Random pore model is well known to be used in modeling coal char gasification; however, very few numbers of investigations used the RPM in modeling kinetics of chars from biomass samples. Kinetic parameters of the random pore model have been determined for woodchips char gasification using steam and CO_2 as the gasifying agents.

1.4.3. Catalytic effect of ash on char gasification

One of the most important parameters which have been investigated is the catalytic effect of ash content on char gasification. Catalytic effect of ash on char gasification has been investigated for several biomass samples. Kinetics of food waste char gasification did not draw the attention of researchers in this field. Since food waste has considerable ash content, its catalytic effect must be investigated. Results show that ash has a positive effect on char reactivity. Kinetic parameters have been calculated for different degrees of conversion. Values of kinetic parameters were found to be affected by the degree of conversion. Quantitative analysis of kinetic parameters dependency on sample conversion has been examined here. Quantifying the catalytic effect of ash on char kinetics will help assist improving gasifiers design.

1.4.4. Kinetics of char gasification under diffusion resistance conditions

In this section, the effect of particle size, porosity and reactor temperature/reaction rate constant on the progress of particle conversion is investigated by numerically solving the transport equation inside a reacting char particle. These are the main parameters affecting the conversion of char particle.

Figure I-3 shows different cases of a reacting char particle. The first case, figure I-3a, shows the general case where, the chemical reaction rate and diffusion rate play an equal role in the process. Figure I-3b shows the extreme case of a diffusion controlled char gasification process, in which the reaction rate is very fast and the particle has low porosity. In this case the reaction occurs in outer shell of the particle and the gasifying agent concentration is almost zero at the particle surface. Figure I-3c show extreme case of a chemically controlled process, in which the reaction rate is very low and the particle is porous enough to allow for high effective diffusivity inside the particle. The gasifying agent concentration, in this case, is a horizontal line parallel to the *X-axis*.

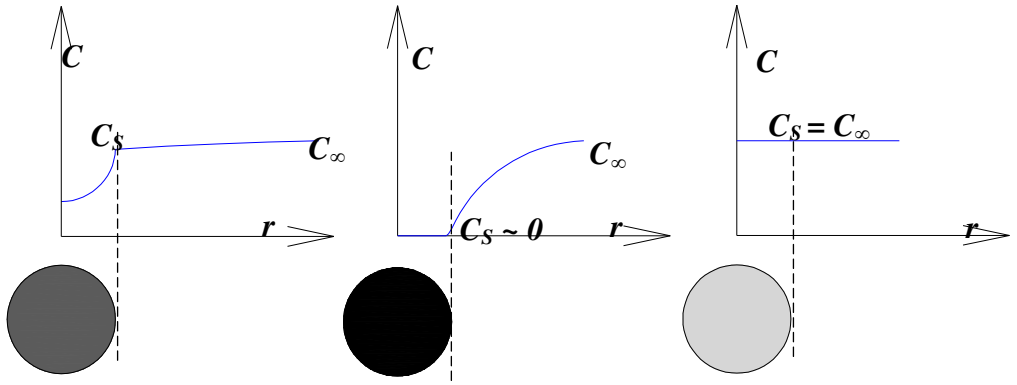

Figure I-3. Schematic of gasifying agent concentration profiles inside different char particles; (a) general case of medium porosity particle, (b) very low porosity particle and (c) highly porous particle

The model used in this section is the exposed core model [33]. In this model the gasifying agent has to diffuse from the surrounding to the surface of the particle and into the particle. In order to calculate the degree of conversion as a function of time and space, *X(r, t)*, the distribution of gasifying agent concentration inside the particle has been calculated. The concentration profiles

were determined by numerically solving the transport equation inside the particle using the finite element method. The Rayleigh-Ritz method has been used to determine the weight function and the approximation function [34]. The degree of conversion, *X(r, t)*, has been calculated by numerically solving the char reaction rate equation using the finite difference method.

The assumption of constant effective diffusion coefficient is usually used to solve the transport equation inside the particle analytically. The finite volume method is usually used for obtaining numerical solution of the Sturm–Liouville equation$\left[-\frac{d}{dx}\left[p(x)\frac{dy}{dx}\right]+q(x)y=\lambda w(x)y\right]$ to assist with the problem of unknown coefficients. Solving the problem using the finite element method is presented here as a different approach. In the solution presented here, the assumption of constant diffusion coefficient was eliminated as well as the assumption of constant gasifying agent concentration outside the particle. Presented also is the experimental method for determining the kinetic parameters and experimental validation of the model.

Numerical simulations have been conducted for three cases of two extreme cases and one general case, Da = 57.56. The two extreme cases correspond to large Damkohler number and small Damkohler number. The high Damkohler number corresponds to a high reaction rate, large particle size and low porosity particle. The small Damkohler number corresponds to a low reaction rate, small particle size and highly porous particle. The third case corresponds to an intermediate value of Damkohler number.

Chapter II: Literature review

2.1. Characteristics of syngas evolution during pyrolysis and gasification

2.1.1. Gasification of char based fuel

2.1.1.1. Reaction mechanisms of cellulose and lignin pyrolysis

Cellulose is a main constituent of biomass and has been investigated by several investigators in terms of reaction mechanisms and behavior under pyrolysis and gasification conditions. Shin et al. [35] investigated the kinetics of cellulose derived products, such as, levoglucosan, under pyrolysis conditions. They modeled the pyrolysis of levoglucosan using a three compound model; primary, secondary and tertiary compound. The primary compound, levoglucosan, decreases with the increase in temperature, the secondary compounds peaks at a certain temperature and the tertiary compounds increases with the increase in temperature. The secondary compounds where found to be carbonyl compounds and hydroxyl derivatives, such as, methanol, acetaldehyde, acrolein, glyoxal and furans compounds. Tertiary compounds were found to be carbon monoxide and other gaseous hydrocarbons.

Balat [36] categorized the steps at which cellulose reacts during pyrolysis in terms of the following temperature ranges:

Table II-1. Steps of cellulose pyrolysis as suggested by Balat [36].

Temperature	reaction	products
< 575 K	elimination of water, and depolymerization	Formation of carbonyl and carboxyl, evolution of CO and CO_2, and mainly a charred residue
575<T<725K	Breaking of glycosidic	Mixture of levoglucosan, anhydrides, and

	linkages of polysaccharide	oligosaccharides in the form of a tar fraction
> 725 K	scission of sugar units	Formation of carbonyl compounds such as acetaldehyde, glyoxal, and acrolein
> 775 K	mixture of all above processes	A mixture of all above products
Condensation	condense and cleave to char	Char

A review of the mechanistic pathways of cellulose pyrolysis is shown in figure II-1 [37-43]. Broido-shafizadeh [37] and modified Broido-Shafizadeh models [38] are based on an activation step followed by parallel competing reactions between char formation and evolution of gas and volatiles. In the modified mechanism [38] levoglucosan is added as an intermediate before char formation. The Vatirhegyi model [39] eliminated the active cellulose step based on the absence of any variations in mass during TGA experiments and worse fit if the activation step is not eliminated. The Vatirhegyi mechanism is based on parallel competing reactions of oligomers formation and a series of solids and gases formation. Luo et al [40] considered the formation of char from dehydration of active cellulose. Active cellulose then undergoes parallel depolymerization reactions and fragmentation reactions. Tar is formed by repolymerization of levoglucosan. Banyasz et al [42] presented a mechanism in which CO and CO_2 are formed from competing parallel routes. CO is favored at high heating rates and high temperatures. Lin et al. [43] presented a mechanism in which fragmented compounds, such as, aldehydes and ketones are formed from dehydrated sugars in contrast to their formation by direct fragmentation form active cellulose.

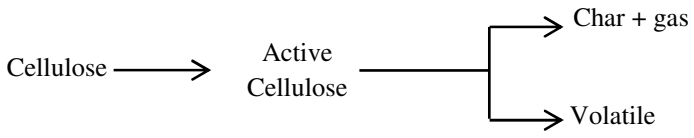

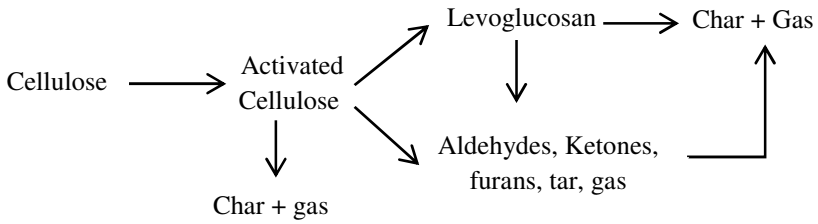
Cellulose
Activated Cellulose
Levoglucosan
Char + Gas
Aldehydes, Ketones, furans, tar, gas
Char + gas

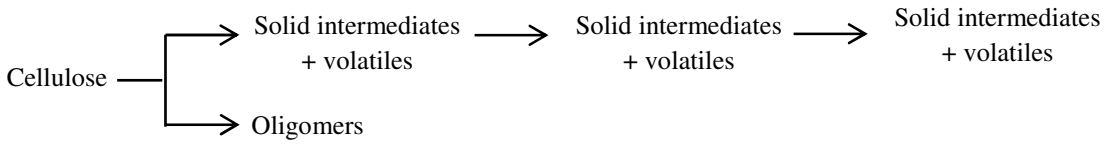
Cellulose
Solid intermediates + volatiles
Solid intermediates + volatiles
Solid intermediates + volatiles
Oligomers

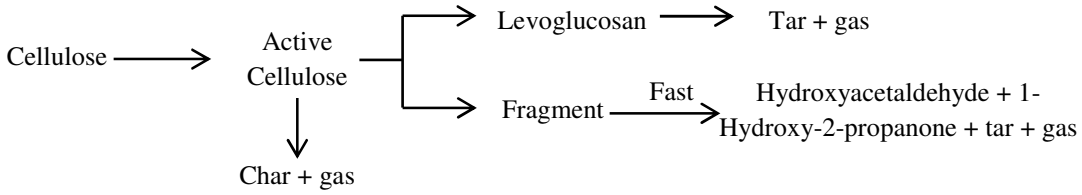
Cellulose
Active Cellulose
Levoglucosan
Tar + gas
Fragment
Fast
Hydroxyacetaldehyde + 1-Hydroxy-2-propanone + tar + gas
Char + gas

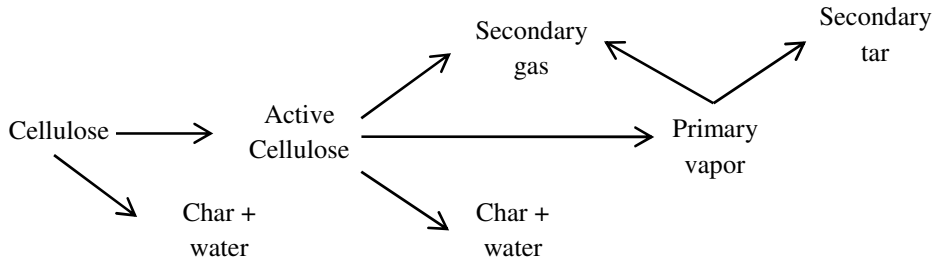
Secondary gas
Secondary tar
Cellulose
Active Cellulose
Primary vapor
Char + water
Char + water

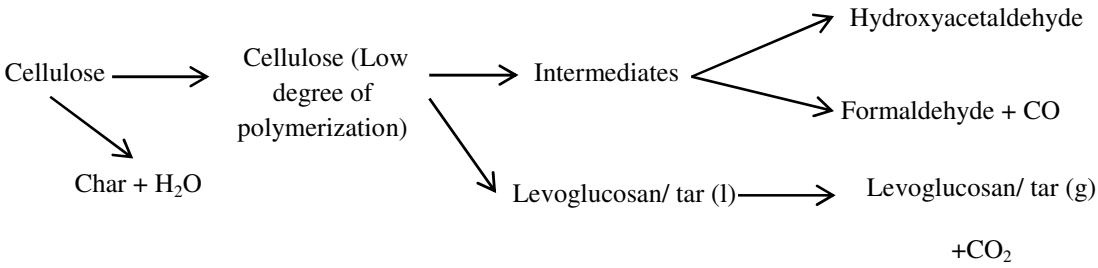
Cellulose
Cellulose (Low degree of polymerization)
Intermediates
Hydroxyacetaldehyde
Formaldehyde + CO
Char + H_2O
Levoglucosan/ tar (l)
Levoglucosan/ tar (g)
+CO_2

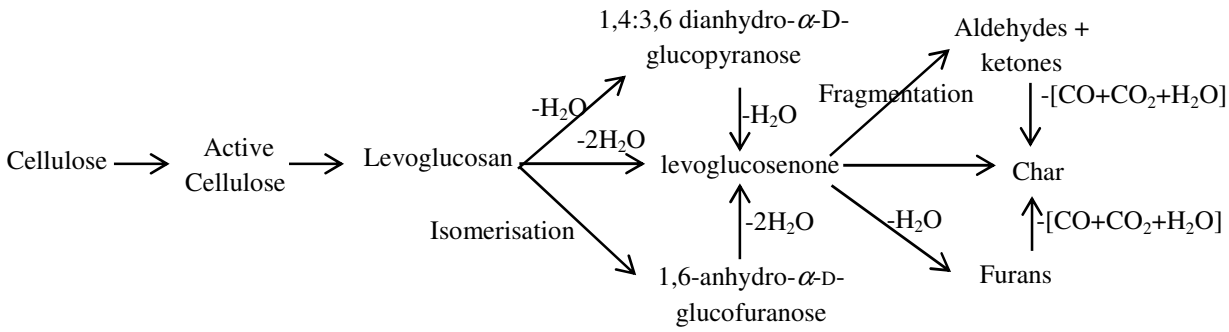

Figure II-1. Cellulose reaction mechanisms [37-43]

Petrocelli and Klein [44] investigated initial steps of lignin pyrolysis using model compounds; 1, 2-diphenylethane (DPE) [C_6H_5-CH_2-CH_2-C_6H_5], stilbene [C_6H_5-CH=CH-C_6H_5], diphenylmethane (DPM) [C_6H_5-CH_2-C_6H_5], and triphenylethylene (TPE) [C_6H_5-CH=C-$(C_6H_5)_2$]. Reactor temperature ranged from 400 to 600^{o}C.

DPE initially decomposed to hydrogen rich benzene and toluene accompanied with the hydrogen deficient ethylbenzene [C_6H_5-CH_2-CH_3], styrene [C_6H_5-CH=CH_2] and stilbene. Stilbene and styrene undergoes further decomposition and oligomerization to form hydrogen deficient species and hydrogen radicals. Hydrogen radical in turn, combines with benzyl and phenyl radicals to form more toluene and benzene.

DPM decompose to form phenyl radical, benzyl radical in parallel with hydrogen deficient species, fluorene [C_6H_4-CH_2-C_6H_4] and hydrogen radicals. Hydrogen radical in turn, combines with benzyl and phenyl radicals to form toluene and benzene. On the other hand, initial steps of TPE pyrolysis involve three routs; the first is unimolecular decomposition to form toluene and DPM. The second is decomposition of TPE to form benzene and stilbene or DPE. Figure 4 shows reactions sequence during PDE, DPM, stilbene and TPE pyrolysis.

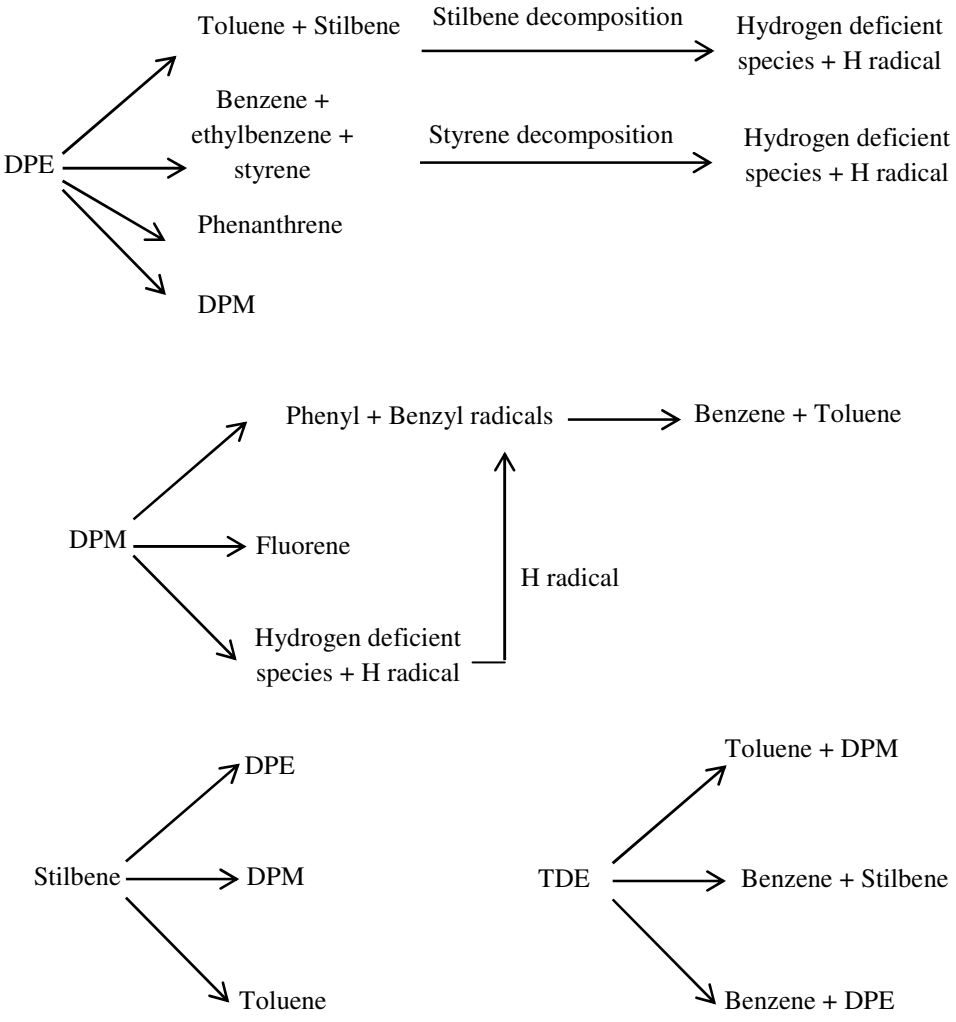

Figure II-2. Reactions sequence during PDE, DPM, stilbene and TPE pyrolysis.

2.1.1.2. Effect of operational conditions

2.1.1.2.1. Effect of steam flow rate

Gil et al. [45] investigated the effect of steam to oxygen ratio in the gasifying agent on the syngas properties and concluded that LHV decreases with decrease in H_2O/O_2 ratio, because of in-situ combustion of some gas components with the addition of O_2 fed to the reactor. However, when gasifying agent-to-biomass ratio (for a given H_2O/O_2 ratio) is increased, the LHV

decreases by the same reason (since more O_2 is introduced) [45, 46]. Consequently the thermal efficiency decreases with increase in gasifying agent-to-biomass ratios [45].

The general trend of increase in the steam to sample ratio is to increase the yield of total syngas, H_2, and CO_2, while the yield of CO and CH_4 decreases [47-52]. The increase in H_2 and CO_2 yield and the decrease in CO yield are attributed to the acceleration of the forward reaction rate of the water gas shift reaction ($CO + H_2O \Leftrightarrow CO_2 + H_2$) [47, 49-52]. On the other hand the increase in steam to sample ratio increases the methane reforming reaction to cause a reduction in the yield of methane [48]. Therefore, increase in steam to sample ratio results in a direct increase in the ratio of H_2/CO [48, 50].

Chaudhari et al [53] studied effect of steam flow rate on total amount of gas produced, and its composition from bagasse char and commercial char gasification. Formation of product gas was, approximately, doubled when steam flow rate increase from 1.25 to 10 g/h/g of char. They attributed this increase in gaseous products to the increase in the amount of steam, being one of the reactants, in the reaction leads to higher conversion as well as higher gas production. H_2/CO ratio in the synthesis gas obtained for bagasse char was decreased while it was increased for commercial char with increasing the steam flow rate from 1.25 to 10 g/h/g of char. heating value of the product gas did not change much and ranged between 270 and 290 Btu/scf for bagasse char and from 250 to 280 Btu/scf for commercial char.

2.1.1.2.2. Air versus steam gasification

Steam gasification favors steam reforming reactions, while the air gasification promotes combustion reactions. The yield of H_2 and hydrocarbons with steam gasification are higher than those with air injection, whereas CO and CO_2 are lower, since the extent of combustion of char and volatiles is reduced by replacing air with steam. It is also expected that CH_4 and other

hydrocarbons concentrations would be lower, since the equilibrium of water gas-shift reaction favors H_2 production. Steam reforming of tars (Tar + $H_2O \Leftrightarrow xH_2 + zCO$) and of hydrocarbons ($C_nH_m + nH_2O \Leftrightarrow (n+m/2)\ H_2 + nCO$) favors H_2 production, accompanied with a decrease in hydrocarbons content in the exit gas [54, 55].

Ocampoa et al. [56] investigated experimentally the gasification of Colombian coal in a fluidized bed. Experimental results showed a maximum in the higher heating value (HHV) curves versus air to coal ratio. The highest gas heating value of 3.3 MJ/m^3 was obtained using a steam/coal ratio of 0.71 and an air/coal ratio of 2.6.

2.1.1.2.3. Reactor temperature

Gil et al. [45] investigated the effect of different operational condition on the syngas chemical composition and properties. As part of their investigation, they examined the effect of reactor temperature on thermal efficiency of the process which increased with increase in reactor temperature. This is attributed to the endothermicity of the gasification process.

The yields of H_2 and CO increase with increase in reaction temperature since the gasification reactions are endothermic. The data showed that the increase in gas yield with reaction temperature is partly achieved at the expense of tar and liquids [51, 52].

The LHV increases a little with increase in reactor temperature due to increase in the yields of C_2H_2, H_2, and CO. The C_2H_m species are formed by the (steam) cracking of aromatic components of the tar [46].

Demirbas [57] investigated gaseous products from biomass by pyrolysis and gasification. In their study they introduced the effect of reactor temperature on gaseous, liquid and char yield for the

pyrolysis process. Increasing the reactor temperature decreased the liquid and char yield. However, increasing reactor temperature increased the gaseous yield.

2.1.1.2.4. Catalytic gasification

The low heating value (LHV, kJ/m^3) of the gas decreases somewhat when dolomite is used in the gasifier bed. This decrease can be due to the decrease in the amounts of light hydrocarbons in the flue gas. However, it is again verified how some dolomite in the bed has a positive effect; it increases the thermal efficiency from 86 percent to about 96 percent [50, 54].

Corella et al. [58] investigated the effect of placing the dolomite in a secondary reactor downstream from the primary gasifier on properties of the syngas evolved. The study provided no important differences between the two locations of the dolomite (i.e., inside the primary gasifier or downstream of the primary gasifier). This finding reveals that increase in the amount of H_2 in the flue gas is compensated with the decrease in amount of CO and also by the non-important variation in the amounts of CH_4 and other hydrocarbons (C_2H_n) in the flue gas. Therefore, there is no difference between locating the dolomite in the same gasifier bed or at a downstream position in the reactor from the point of view of LHV of the gas.

2.1.1.3. Effect of heating rate

Milosavljevic et al [59] investigated thermal effects in cellulose pyrolysis. They investigated the effect of heating rate on char formation and pyrolysis heat absorption. A linear relationship between mass loss and heat absorption, observed at high heating rate, 60 K/min. They concluded that the processes responsible for net heat absorption are apparently quite constant throughout the process of rapid heating. In contrast to high heating rate the results obtained at lower heating rates show a deviation from a steady heat absorption curve, at some point. This deviation occurs at progressively lower extents of mass loss as the heating rate is lowered. They suggested that the

heats of pyrolysis depend upon the exothermic nature of char formation. They concluded that a large portion of the exothermic char formation is delayed to progressively later times during the pyrolysis process at higher heating rates.

2.1.1.4. Gasification using Supercritical water

Supercritical water mixes with most of the organic compounds so that rapid and homogeneous reactions of organic compounds are possible in supercritical water. Matsumura [60] investigated the energy efficiency, product gas composition and economic feasibility from supercritical water gasification. They showed that cellulose decomposes much more rapidly in supercritical water than in sub-critical water. They concluded that this high reactivity can be used to decompose organic materials into gases without any pretreatment of drying the feedstock. Therefore, supercritical water gasification is considered a promising technology for the gasification of wet biomass since it does not require drying of feedstock beforehand. Separation of the gas and water occurs after complete gasification, cooling down and depressurization of the process.

2.1.2. Gasification of plastics and rubber

Encinar et al. [61] investigated the thermal decomposition of natural polystyrene. The first order reaction model has been used to describe the reaction rate. These investigators determined Kinetic parameters using multiple linear regression approach. The activation energy and pre-exponential factor varied with the heating rate. The activation energy ranged from 286.5 to 168.1 kJ/mol for the heating rates ranging from 5 to 25 K/min. On the other hand Westerhout et al. [62] used the first model to interpret the experimental data. In their investigation the use of the first order power law model was restricted to the 70-90% of the conversion range. They attributed the reason for this restriction to the fact that the actual reaction order varies with the conversion. And this description is valid mostly in this conversion range from 70 to 90%.

Lin et al. [63] investigated the pyrolysis kinetics of a refuse-derived fuel (RDF) which consists of high plastic content: 20 wt.% of polystyrene, 30 wt.% of Polyethylene, 10 wt.% of PVC, and 40 wt.% of paper. The nth order reaction model was used and individual activation energies were determined. The polystyrene activation energy was found to be 120.9 kJ/mol. The global pyrolysis reaction rate was calculated from the weighed sum of the component fractions of RDF. Two stages have been identified to describe the conversion rate of the plastics mixture. The obtained activation energy and reaction order for the first stage were 83.6 kJ/mol and 1.9, respectively. However, for the second stage the activation energy and reaction order were 138 kJ/mol and 1.7, respectively. In a similar study by Cozzani et al. [64], RDF pyrolysis has been investigated. They identified two weight loss steps as well. Temperature of the first step ranged from 300 to 400^{o}C and the second step ranged from 450 to 500^{o}C. The first step corresponded to the degradation of cellulosic materials while the second step corresponded to plastics. Similar conclusions were obtained when sawdust-polyethylene mixture was investigated. Sawdust degradation took place at reactor temperature between 230 to 430^{o}C; however, polyethylene degradation took place between 430 to 530^{o}C [65].

Bockhorn et al. [66] calculated the degree of conversion for a mixture of PVC, PS and PE (1:1:1 by weight) for stepwise low temperature pyrolysis (330, 380 and 440^{o}C). Calculations were conducted based on isothermal kinetic parameters from the literature. At 330°C about 10% of the polystyrene decomposes (reaction time 30 min). At 380°C depolymerization of the major part of polystyrene into its monomer takes place and about 10% of the PVC decomposed (reaction time 60 min). At higher temperatures (440°C) the decomposition of polyethylene and of the major part of the residue from of PVC occurs.

Ponzio et al. [67] investigated the effect of steam injection on hydrogen yield in the gasification of plastic containing waste. Compared to air gasification, the relative proportion of H_2 in syngas for steam gasification experiments was higher. This was attributed to steam reforming ($C+H_2O \Rightarrow H_2+CO$) and water gas shift ($CO+H_2O \Rightarrow H_2+CO_2$) reactions. In a similar study by He et al. [5] on catalytic steam gasification of municipal solid waste (MSW), an increase in syngas flow rate and decrease in gasification period was observed by increasing the reactor temperature. Gasification period at 700^{o}C was 90 minutes and 39 minutes for reactor temperature 950^{o}C.

Kaminsky et al. [68] investigated the pyrolysis of mixed plastics (Polyolefins 57%, Polystyrene 19%, PVC 13.7%, and other materials 10.3%) in a fluidizing medium, namely steam, in the temperature range of 600 to 800^{o}C. They found very interesting results concerning the distribution of gaseous yield in this temperature range. At 700^{o}C, the highest yield of C_2, C_3 and C_4 alkenes was observed. On the other hand the amount of carbon oxides and the highly hydrogenated gases such as methane and hydrogen increased with increase in reaction temperature. In a similar study by Simon et al. [69] on the pyrolysis of polyolefins with steam, the investigators noticed that high amounts of olefins are obtained at temperatures around 700^{o}C, with 20-31 % ethene, 14-18 % propene, and 3-6 % butenes. Clearly the role of temperature and material properties are critical for the amounts of hydrogen and other gas yield in the syngas. Therefore, the focus of our research is to provide further insights on the pyrolysis and gasification of polystyrene at different reactor temperatures and determine the kinetics parameters for their future use in modeling the process.

Tongamp et al. [6] developed a process to produce hydrogen from polyethylene $[–CH_2–]_n$ (PE) by milling with $Ca(OH)_2$ and $Ni(OH)_2$ followed by heating the milled product. Different mixtures were heated from 20 to 700^{o}C at a heating rate of 20^{o}C/min. H_2 release occurred

between 400 and 500°C, and H_2 concentration of 95% was obtained from the mixture of PE/$Ca(OH)_2$/$Ni(OH)_2$ (C:Ca:Ni = 6:14:1) sample. The role of milling, $Ca(OH)_2$ and $Ni(OH)_2$ was described as follows. Milling is necessary to avoid separate decomposition of PE and hydroxides and to stimulate interaction between them when heat is applied. With the well milled samples, heating at a low temperature simply leads to the formation of calcium carbonate, and release of hydrogen at the same time. When nickel hydroxide is well dispersed within PE and calcium hydroxide, this process allows for the onsite formation of fine nickel particles that function as catalyst to facilitate the formation of hydrogen. The overall process reaction was given as: $6[CH_2] + 12Ca(OH)_2 + Ni(OH)_2 = 6CaCO_3 + 18H_2 + 6CaO + H_2O + Ni$

Several researchers have investigated the kinetics of weight loss of rubber containing samples [70-72]. The results reveal that the kinetics of rubber gasification can be described using parallel first order independent reactions. The results obtained on activation energies depended on the heating rate and the range of investigated temperatures. The activation energy value ranged from 40 to 210 kJ/mol.

Castaldi et al. [73] proposed a reaction mechanism of Styrene–Butadiene Rubber (SBR) decomposition under pyrolysis conditions. The mechanism suggested was based on simultaneous thermogravimetric analyzer (TGA) and gas chromatograph/ mass spectrometer (GC/MS) measurements. These investigators have suggested the following decomposition steps for SBR; first, there is a breakage between the ligand and butadiene backbone, which results in some hydrogen liberation. The backbone continues to be hydrogenated to form butane and n-butane. The styrene ligand undergoes various transformations, hydrogenation and removal of methylene groups, leading to the substituted polycyclic aromatic hydrocarbons (PAHs), such as, ethyl-benzene and toluene.

Several researchers have investigated the porosity of char obtained from rubber pyrolysis. San Miguel et al. [74] found that char obtained from pyrolysis of scrap tires developed poor porosity and limited internal pores surface area. On the other hand, Helleur et al. [75] concluded that the poor porosity of the obtained char was enhanced by further carbonization using steam and CO_2 activation. Using steam at 900^oC for three hours produced an activated carbon with good surface area (302 m^2/g). Steam was observed to generate a narrower but more extensive micro-porosity than carbon dioxide [76, 77]. On the other hand, Vizuete et al. [78] concluded that chemical treatment of residual rubber using HNO_3 resulted in large pore structure in the material.

2.1.3. Co-gasification and Co-pyrolysis of mixed fuels

Aznar et al. [79] investigated the gasification of a mixture of plastic waste, pine wood sawdust and coal in an air fired fluidized bed gasifier. Among other parameters they studied the effect of feed stock composition on syngas yield, energy content, syngas LHV and syngas chemical composition. Mixture ratios of 80%-10%-10%, 60%-40%-0%, 60%-0%-40% and 60%-20%-20% of coal-biomass-plastic were investigated. A peak value of energy content and LHV was obtained at a mixture ratio of 60% coal - 40% plastic while syngas yield was minimal from the same mixture. The peak value of energy yield and syngas LHV is attributed to the high LHV of plastics. In a similar study, pinto et al. [52] investigated steam gasification of biomass mixed with plastic wastes in a fluidized bed gasifier. Presence of 20% polyethylene (PE) increased H_2 concentration from 28% to 50% and decreased the CO concentration from 38% to 28%. Presence of PE is effective only up to 20% PE. Any further increase in PE percentage did not increase the H_2 concentration or decrease the CO concentration. Constant concentration of H_2 and CO was retained.

Vélez et al. [80] investigated co-gasification of Colombian coal and biomass in a fluidized bed gasifier. Several samples of these blends were used in the experiments by mixing 6% or 15% of biomass, (sawdust, rice or coffee husk), with coal. The thermal efficiency was calculated for the six investigated mixtures. Increasing the mass percentage of rice and coffee husk from 6 to 15% increased the thermal efficiency; however, increasing the sawdust percentage did not change the thermal efficiency of the process. The energy efficiency of the process reached a peaked value of approximately 60%.

Sharypov et al. [81] investigated the co-pyrolysis of wood biomass and synthetic polymer mixtures. Characteristics of thermal degradation of separate biomass and plastic samples and their mixture were investigated using a thermogravimetric analyzer (TGA). The mutual influence of biomass and plastics during the thermal decomposition was not apparent from the results obtained. In other words, the degradation of single components in biomass and plastic mixtures were clearly revealed to be independent.

The influence of biomass/plastic mixture composition on the products yield from the co-pyrolysis was investigated at 400°C [81]. Yields of both light and heavy liquid fractions increased with the presence of plastic material. A maximum yield of light liquids was obtained for a mixture of 20% biomass and 80% plastic. One interesting result observed was that more than two times higher yield of light liquid hydrocarbons was obtained from the 20-80% biomass-plastic mixture as compared to the expected yield from individual materials, i.e., the sum of light liquid fractions produced from the pyrolysis of each separate component. They supposed that the olefinic products from plastics thermal conversion react with some products from the biomass depolymerization to result in the formation of light liquids.

Kumabe et al. [82] examined co-gasification of woody biomass and coal with air and steam using a downdraft type fixed bed gasifier at 1173 K. The biomass to coal ratio was varied from 0 to 1 based on the carbon content. The conversion to syngas increased with increase in biomass in the feedstock. However, the conversion to char and tar decreased with increase in biomass. The increase in biomass fraction resulted in a decrease in H_2 composition and increase in CO_2 composition. The cold gas efficiency increased from 65% to 85% when biomass fraction increased from 0 to 1. Similar results were obtained by Lapuerta et al. [83] on the thermal efficiency of an air blown circulating flow gasifier who reported exponential increase of cold gas efficiency from ~15% to 40% with the addition of biomass to coal. The reason for higher thermal efficiency from the use of biomass was attributed to different C-C bonds in the two materials. The coal structure (char) consists of mainly C=C bonds derived from its significant heavy polycyclic aromatic hydrocarbons (PAH's) content which requires high activation energy to break such bonds. However, the cellulose and lignin content of the biomass consists mainly of weaker bonds, such as, R–O–R (phenols, aldehydes, ketones, etc.), which can easily be broken.

Sharypov et al. [16] investigated the interaction between coal and polyolefinic plastic (PP) during co-pyrolysis using TGA, GC-MS and HPTLC diagnostics. From the TGA experiments it was established that the mass looses are non-additive for the blends examined so that it can be assumed that plastic–coal interaction occur during the thermal treatment. Predicted values for co-pyrolysis of the coal/PP mixtures were calculated based on additive contribution of the suitable value of coal or PP obtained from the experiments. The yield of liquid hydrocarbons was identified according to their boiling point. Hydrocarbons with boiling point below 180^{o}C represented fraction 1, hydrocarbons with boiling point in the range 180 to 350^{o}C represented fraction 2 and distillate residues represented fraction 3. It is to be noted that the amounts of

fraction 1 are non-additive. Experiments lead to an overproduction of liquids. Second, the observed increases correspond to a decrease of fraction 3. This phenomenon could be explained from the change in distribution of the hydrocarbons produced by the degradation of polymers. The interaction between coal and plastic was explained as follows; coal promotes radical formation leading to the production of lighter hydrocarbons from the polymer. On the other hand, polymer plays the role of hydrogen donor to enhance conversion of coal. Radicals that promote the coal-plastic interaction are alkyl aromatic compounds and contribute to mainly liquids of fraction 2. These alkyl aromatic compounds are not found in the products of coal or plastic when reacted alone. These compounds were considered as molecular probes for chemical interactions between the coal and polymers.

Caia et al. [15] investigated the synergistic effect between the low volatile coal (LVC) and plastic (polypropylene, PP, low density polyethylene, LDPE and high density polyethylene, HDPE). A difference in weight loss (ΔW) was defined as the difference between the weight loss for a blend and the theoretical weighted average loss of each sample examined separately. ΔW was less than ±1% before 400°C, since at this temperature plastic did not decompose and no interaction occurred between LVC and plastic. The weight loss (ΔW) reached 2.0–2.7% at reactor temperature higher than 530°C, which indicates synergistic effect during pyrolysis at high temperatures. The kinetic parameters (activation energy and pre-exponential factor) of coal and plastic pyrolysis were determined by assuming a first order reaction. Results showed that activation energy and pre-exponential factor of the coal/plastic blends are different from those of the individual materials. This directly suggests that the pyrolysis mechanism of coal/plastic blends is different than that for the individual components present in the mixture.

Sakurovs [84] investigated the effect of adding polypropylene (PP), polystyrene (PS), polyacrylonitrile (PAN), $(CH_2\text{-}CH\text{-}CN)_n$) or polyphenylene sulfide (PPS) to three different Australian coking coals on the coal fluidity (plasticity). Polystyrene strongly reduced the fluidity of coal. Polypropylene did not affect the fluidity in two of the coking coals. Polyphenylene sulfide (PPS) reduced the fluidity of the coals at temperatures near the solidification temperature of the coals. Polyacrylonitrile (PAN) increased the coal fluidity at temperatures near the softening temperature. Sakurovs [84] attributed this change in coal fluidity to chemical interactions between coal and plastics, which involve transfer of hydrogen, either to the coal that results in an increase in fluidity, or from the coal that results in a decrease in fluidity.

A lot of countries in the EU gained considerable experience with co-gasification and co-combustion of coal and biomass or coal and sewage sludge because of their participation in the APAS Clean Coal Technology program (1992-1994), (Activite de Promotion, D'Accompagnement et de Suivi). Synergic effects were reported by some researchers such as Sjostrom et al. [85] who report synergies in Fluidized bed co-gasification of wood and coal mixtures and de Jong et al. [86] who report synergies with co-gasification of coal, miscanthus and straw in an air-blown Fluidized bed gasifier. On the other hand, Rudiger et al. [87] reported an absence of any synergistic effects between the different fuels. They attributed this absence of synergistic effect to the difference in temperature ranges within which devolatilization of coal and biomass take place.

Kuznetsov et al. [88] studied the Co-pyrolysis and co-hydropyrolysis of biomass/polyolefine mixtures. Experiments were held in the temperature range of 300 to 500^{o}C. They found that hydropyrolysis of biomass/plastic mixture results in higher degree of conversion and increased yield of light liquids as compared to co-pyrolysis in an inert atmosphere. They attributed this

increase in conversion and liquid hydrocarbons yield to the hydrogen assisted rupture of C-O and C-C bonds. The hydrogen atoms can stabilize the radical products during the thermal degradation of polymer. A similar study was conducted by Kuznetsov [89] using a coal/polyethylene (PE) mixture. The following catalytic processes were applied: pyrolysis in an inert atmosphere, hydropyrolysis and water–steam cracking. The highest degree of coal conversion was achieved in the hydropyrolysis process at 430^{o}C and working pressure 6 MPa. The maximum yield of light distillate products was observed for the water–steam cracking at 430^{o}C and 1 MPa.

Most researchers conducted their experiments in a continuously fed reactor in order to understand the effect of operational conditions on syngas properties. The syngas was analyzed at the exit of the reactor, so that the syngas analyzed was a result of all the reactions that occur inside the reactor. In this study the experimental setup is designed to resolve this issue of global averaging by monitoring the evolution of syngas chemical composition in the time domain. This procedure allows one to also determine the global composition, if desired. This investigation provides better understanding of syngas evolution form solid fuels while flowing through the space domain in gasifiers. Monitoring the evolution of syngas in the time domain allowed for calculating the cumulative yield of key properties of the syngas such as cumulative yield of syngas, hydrogen, energy with time, and efficiency.

2.2. Kinetics of char gasification

2.2.1. Effect of reactor pressure

Roberts et al. [20] investigated the effect of pressure on apparent and intrinsic reaction kinetics. The apparent reaction rate at 10% conversion for the char-CO_2 reaction is a function of pressure. The results showed that pressure increases the apparent reaction rate of the char-CO_2. However, this increase is not constant over the pressure range 1-30 atm. As the pressure is increased to

above 10 atm., effect of pressure is less and apparent reaction order is almost zero at pressures of 20-30 atm. However, the intrinsic reaction rate was not found to be affected by the pressure that much. This supports that the shift in apparent reaction order at high pressures is not due to fundamental change in the reaction mechanism. They attributed this decrease in reaction order due to the following: at atmospheric pressure the surface of the sample is not saturated and the reaction rate is proportional to the number of surface complexes. As the pressure increases, more surface complexes are formed to result in an increase in reaction rate. At high enough pressures the surface will be saturated with complexes, such that increases in pressure will not lead to the formation of further surface complexes and the reaction rate will not increase. Consequently, the apparent reaction order is zero.

Cetin et al.[30] studied the CO_2 gasification kinetics of chars from biomass species within the temperature range of 800–950^{o}C and pressures between 1 and 20 bar using thermogravimetric analysis (TGA). Pressure has been found to have no effect on reactivity during char conversion while it has a dramatic effect on the chemical and physical structure during the pyrolysis process. They found that increase in total pressure decreases the average reactivity of gasification of pine chars. During these experiments, partial pressure of CO_2 was kept constant while the total pressure was varied. The total pressures used in these experiments were identical to those used during pyrolysis to generate the char samples. They concluded that the difference shown in reactivities could be due to the role of pyrolysis pressure on the intrinsic reactivity and/or the effect of total gasification pressure on the apparent reactivity. To distinguish the effect of pyrolysis pressure on the intrinsic reactivity, radiata pine chars generated at different pressures were gasified at 850^{o}C and 1 bar for comparison with the biomass char. They suggested that the difference in intrinsic reactivity can only be assigned to the effect of pyrolysis pressure rather

than the total surface area effect. They used the x-ray diffraction (XRD) technique to quantify the effect of pyrolysis pressure by characterizing the atomic structure of the char samples. Results showed that the reactivity difference can be linked to the graphitic structure found in chars generated at pressures greater than atmospheric pressure. Consequently, they concluded that the difference in gasification reactivities under different gasification pressures is mainly due to graphitization in biomass char structure at higher pressures.

Everson et al [28] investigated the effect of CO presence in the reactor on the reaction kinetics of pulverized coal-chars. to evaluate the parameters for the intrinsic reaction rate they conducted two sets of experiments, (1) with carbon dioxide and an inert (nitrogen), and (2) with carbon dioxide and carbon monoxide. A comparison between char reactivities for the two experiments, CO was found to have an inhibiting effect of carbon monoxide.

Reaction rate for steam gasification was found to be double than that from CO_2 gasification [18]. A reaction order of 0.5 to 0.8 was found for H_2O and CO_2 gasifying agents, respectively. The investigators have indicated that the reaction order is not affected by pressure of up to 10 bars. However, it decreased for reactor pressures above 10 bars [20]. In general, the increase in reactor temperature resulted in an exponential increase in reaction rate, especially in the chemically controlled regime.

Hydrogen and carbon monoxide were found to have an inhibition effect in both steam and CO_2 gasification. Wall et al [29] confirmed that the inhibition effect of CO and H_2 is more significant at high reactor pressures, higher than 10 bars. They also indicated that the inhibition of H_2 and CO is explained in terms of the Langmiur-Hinshilwood reaction mechanism; CO and H_2 are adsorbed to active cites, resulting in less free active sites for the gasifying agent to react with the char.

Cetin et al [30] investigated the effect of total pressure on char gasification. Cetin et al [30] have shown that total pressure has no effect on intrinsic reactivity of char. They also, investigated the effect of pyrolysis pressure on the reactivity of char. Cetin et al [30] measured the qualitative presence of graphite structures in chars obtained at high pyrolysis pressures. Graphite structures increased with the increase in pressure. Graphite structures during pyrolysis decreased the apparent reactivity of char during gasification.

2.2.2. Effect of geometric changes on kinetics of char gasification

Kajitani et al. [19] investigated the kinetics of coal char gasification in a pressurized drop tube furnace at a high temperatures range, from 1100 to 1500^{o}C. The peak reaction rate was at a conversion value of approximately 0.4. Reaction order with respect to CO_2 was found to be 0.73 and 0.86 for steam. The random pore model (II-E1) was used to fit the experimental data.

$$\frac{dX}{dt} = A.C^{n_{ga}} e^{-\frac{E_{act}}{RT}} (1-X)(1-\psi \ln(1-X)^{1/2} \quad \text{(II-E1)}$$

Structural parameter was found to be 3 in case of steam and CO_2 and 14 in case of using oxygen as the gasifying agent. In a similar study by Ochoa et al. [90] the structural parameter, ψ, value was 4.7 for sub-bituminous coal and 7 for high volatile bituminous coal.

Zou et al. [22] conducted modeling investigation for studying the reaction kinetics of petroleum coke gasification with CO_2. They deduced that higher temperatures lead to shorter time of gasification and higher gasification rate. The random pore model was used in their study and they found that the gasification rate increased with the increase in conversion then followed by a rapid decrease after reaching a maximal rate around a conversion value, *X*, *of* 0.3. They attributed the lower gasification rate initially to the poor porosity initially, which is also, the main reason of the occurrence of a peak gasification rate.

The random pore model has also been used to model the gasification of low rank coal char, such as, Thai-lignite. Sangtong and Narasingh [91] compared results from the random pore model with results obtained from fitting the homogeneous model for two types of chars. The random pore model provided better fitting than the homogeneous model. Structural parameters obtain from the random pore model fitting was 0.61 for char sample A and 2.2 for char sample B.

Bhat et al [92] investigated the kinetics of rice husk gasification using steam as gasifying agents. The investigated temperature range was from 750^{o}C to 900^{o}C. They used both the volume reaction model represented by the conversion–time relation; $-ln(1-X) = (KC)t$, and the shrinking non-reacting core model represented by; $t = (\rho r_p/KC)[1-(1-X)^{1/3}]$. Their results show that the gasification reaction of rice husk char is chemically controlled up to a temperature of 850^{o}C. The activation energy obtained by volume reaction model and shrinking core model were close in agreement. The activation energy calculated was in the order of 180 to 200 kJ/mol. This value is higher than the value obtained for paper char gasification in this study using the same reacting volume model. This discrepancy may be attributed to the high ash content of paper which may have a catalytic effect on the process.

Bhatia and Perlmutter [23] developed a model which accounts for the change in pore structure resulting in a change in internal surface area with time/conversion. This change in internal surface area results in a proportional change in the char conversion rate. The random pore model developed by Bhatia and Perlmutter [23], is usually used to describe the presence of a peak value of reaction rate/conversion rate.

Yamashita et al [17] modeled the char particle is a three-dimensional cube. The cube is composed of a large number of small, randomly arranged lattices classified as char, ash, or

macropores. The porosity of the particle was expressed as a large void in the center of the particle. They indicated that when the porosity is high, the reaction occurs on both an internal void surface and an external surface.

2.2.3. Catalytic effect on char gasification

Tancredi et al. [25] investigated the catalytic effect of ash on char gasification for eucalyptus wood chars. The ash content in char was of the order of 1.45% on mass basis. The reactivity of the char increases monotonically with conversion. At low and intermediate conversion, it can be attributed to the increase in surface area as gasification proceeds. At high conversion levels a steeper increase in reactivity has been observed, which cannot be explained by the development of surface area. This region of the reactivity-conversion curves can be better explained as the result of an increase in catalytic effect of the metallic constituents (mainly Na and K) present as inorganic matter in the chars. Here CO_2 was used as the gasifying agent. Activation energies determined were found to vary within a narrow range of 230 to 257 kJ/mol. Arrhenius plots showed parallel lines for different degrees of conversion. Parallel line of Arrhenius plot indicates similar activation energies. The increase in reactivity was mainly due to an increase in pre-exponential factor. In a similar study by Montesinos et al. [26], steam gasification and CO_2 gasification of grape fruit skin char were investigated. They also observed an increase in reactivity at high values of conversion. However, a different trend of activation energies values was observed; in the case of CO_2 gasification, as the conversion increased, a decrease in activation energy was observed. On the other hand an increase in activation energy was observed in case of steam gasification. This increase in activation energy was also, observed by Mars et al. [93]. The decrease in activation energy values in the case of CO_2 gasification was accompanied by a decrease in pre-exponential factor as well. This behavior is called the compensation effect

[94]. Montesinos et al. obtained a value of isokinetic temperature of 1150 K. The isokinetic temperature is the temperature at which all reactivities are equal for different conversions. An isokinetic temperature of 1449 K was obtained by Dhupe et al [95] for CO_2 gasification using catalyzed sodium lignosulfonate. Feistel et al [96] found this temperature to be 1425 K, obtained using potassium-catalyzed steam gasification.

Gokarn and Muhlen [97] investigated the gasification of char using two types of catalysts and a mixture of both the catalysts. The investigated catalysts were calcium lignosulfonate and sodium lignosulfonate. The carbon matrix was saturated by calcium lignosulfonate at 10% by weight. However, this saturation did not affect the catalytic effect of sodium lignosulfonate in the mixed catalytic system.

Li and Cheng [98] investigated the catalytic gasification of coal char using Na_2CO_3 and K_2CO_3 as catalysts. Effect of catalyst loading was investigated. Increase in catalysts loading was found to be effective until 25% by weight of K_2CO_3 loading and 20% by weight of Na_2CO_3 loading. Further increase in catalysts loading resulted in a decrease in char reactivity. The results of reactivity versus conversion plots showed an increase in char reactivity initially. Further increase in conversion showed a decrease in char reactivity. They attributed this decrease to the char pores blocking the catalyst at high degrees of conversion. A compensation effect was observed and an isokinetic temperature of 1289^{o}C for Na_2CO_3 and 1466^{o}C for K_2CO_3 were obtained.

Iwaki et al [99] investigated the catalytic effect of molten carbonates mixtures on waste paper conversion. Li, Na and K carbonates and their mixtures were used in their experiments. They found that the melting point is an essential factor to be considered. Usually a mixture of carbonates has a lower melting point than a single carbonate compound. The results show that

carbon conversion varies significantly with one, two and three carbonate components. They attributed this variation in carbon conversion to a lower melting point associated with the mixture catalyst as compared to a single catalyst from the improved contact efficiency between the gasifying agent and wastepaper using a mixture.

Tomishige et al. [100] investigated the cellulose gasification using $Rh/CeO_2/SiO_2$ catalysts. They investigated the dependence of carbon conversion (C-conversion) and cold gas efficiency in the gasification of cellulose on CeO_2 content in $Rh/CeO2/SiO_2$ catalysts. There was a maximum in the C-conversion and the cold gas efficiency at 35 mass % CeO_2 content. The presence of a peak was justified as follows. The BET surface area decreased with increase in CeO_2 content in the catalyst. On the other hand, using Rh/SiO_2 with no addition of CeO_2 showed low performance of the gasification of cellulose and showed an elevated value of tar and solid carbon yield. However, addition of 10% CeO_2 decreased the yield of tar and solid carbon drastically, and this indicates that CeO_2 promoted the gasification reaction significantly. On the other hand, the addition of CeO_2 decreased the catalyst surface area, and this can make the particle size of Rh metal large and reduce the activity. So, the addition of CeO_2 has both positive and negative aspects to the gasifier performance. In a similar study by Asadullah et al [101] Rhodium metal loaded on CeO_2 (Rh/CeO_2) was found to be an excellent catalyst for cellulose gasification at low temperatures that resulted in 100% C-conversion to syngas.

Watanabe et al [102] investigated Catalytic hydrogen generation from biomass simulated as glucose and cellulose with ZrO_2 in supercritical water. They found that gasification efficiency with zirconia was twice as much as that without catalyst at all the experimental conditions. For comparison, they conducted the experiments using alkali hydroxide (NaOH) for glucose and cellulose. For all the experiments, the gasification efficiency with NaOH was the highest and the

yield of CO was negligibly small. Negligible CO yield was attributed to the acceleration in the water gas shift reaction.

Most researchers have used the TGA to investigate the kinetics of char gasification. The implicit assumption here is that the carbon–steam reactions that occur are the main sources for weight loss. It is to be noted that char contains approximately 15 % hydrogen and oxygen (on a mass basis). In the work presented here, this assumption is eliminated; the reactivity of carbon in the char particle is calculated based on monitoring the carbon content in the syngas stream. Consequently, the kinetic parameters obtained are not subjected to the error of mass loss due to hydrogen and oxygen evolution from the char particle.

2.3. Kinetics of syngas evolution during pyrolysis

Heterogeneous substances such as coal and biomass have a complex structure. Detailed reaction mechanisms than include necessary elementary reactions for cellulose, lignin or coal pyrolysis are still under development. Consequently, coal and biomass pyrolysis are usually modeled using simple semi-empirical models as an approximation using experimental data. [103]

Pseudo parallel first-order model: the heterogeneous sample is thought to be composed of pseudo-components, where a pseudo-component is a group of reactive species that exhibit similar reactivity. A first-order kinetic equation is assumed for each pseudo-component. The resulting mass loss rate curve is the weighted sum of the individual $d\alpha_i/dt$ reaction rates:

$$\frac{d\alpha_j}{dt} = \sum C_i \frac{d\alpha_i}{dt} \quad \text{(II-E2)}$$

$$and \ \frac{d\alpha_i}{dt} = K_i(1-\alpha_i) \quad \text{(II-E3)}$$

where, α_j is the overall conversion at time t, α_i is the conversion from pseudo reaction i, C_i is the weight of reaction i and K_i is the reaction rate constant for reaction i.[104]

Pseudo parallel nth-order model: due to the complex structure of the biomass or coal samples, the reactivity of a certain functional group may depend on its physical position and concentration of other groups. The application of n^{th} order kinetics is a simple way to fit experimental results to the model;

$$\frac{d\alpha_i}{dt} = K_i(1-\alpha_i)^n \quad \text{(II-E4)}$$

Distributed activation energy model (DAEM): The pyrolysis process sometimes is expressed using infinite number of reactions that differ only in the activation energy value. This way, the activation energy can be expressed as a continuous distribution function, $D_j(E_{act})$. [106]

$$D_i(E_{act}) = (2\pi)^{1/2}\sigma_i^{-1}exp[-(E_{act}-E_{oi})^2/2\sigma_i^2] \quad \text{(II-E5)}$$

where E_{0i} and σ_t are the mean value and the width parameter (variation) of the distribution.

Chapter III: Experimental setup and experimental conditions

3.1. Description of experimental setup

Figures III-1and III-2 show a photograph and a schematic diagram of the laboratory scale experimental facility used for pyrolysis and gasification experiments. Pure steam is generated by stoichiometric combustion of hydrogen and oxygen. Steam generated is then introduced into the gasifying agent conditioner section, an electronically controller tube furnace (LINDBERG/BLUE M MINI-MITET^{M}). The furnace is used to ensure that the gasifying agent temperature is at the same temperature as that of the main reactor in which the gasification occurs. The sample material undergoes gasification in the main reactor. The main reactor is a 2 inch tube section of the furnace, (LINDBERG/BLUE M 1200°C SPLIT-HINGE TUBE FURNACE). The tube furnace unit consists of an electric heater and a temperature control unit. The controller provides uniform temperature in the test section of the reactor. The uniformly heated length of the reactor is 12 inches. The sample is placed in a stainless steel mesh then introduced to the main reactor via a fast connection located at the rear end of the main reactor. The mesh is 1.8 inches in diameter and 7 inches in length see figure III-3. Steam at a defined temperature is then introduced to the main reaction chamber.

The syngas flowing out from the main reaction chamber is sub-divided into two branches; one passes to the sampling line while the other is passed through the exhaust system. The bypass line has a non-return valve and a flow meter to assure a unidirectional flow out from the reactor. The syngas sample is then introduced to a condenser followed by a low pressure filter and a moister

absorber (anhydrous calcium sulfate). Syngas flow is then introduced to a three way valve that allows one to fill the sampling bottle or introduce the syngas directly to the micro GC for detailed analysis of the syngas produced. The sampling line, condenser and sampling bottles were purged with argon prior to each experiment. The Argon purging step ensures that the sampling line, condenser and sampling bottles are free of air or syngas samples from a previous test run. Sampling bottles are used only when short sampling intervals are needed (0.5 to 1 min). Direct sampling and analysis are carried out by the GC when longer sampling time intervals are allowed. A constant flow rate of inert gas (nitrogen) is introduced with the oxygen flow in the steam generation section. The nitrogen is detected by the GC and is used to determine the flow rate of different syngas species by comparing the detected species mole fraction with the known nitrogen mole fraction.

In order to assure that the oxygen to hydrogen ratio is stoichiometric, steam is condensed and nitrogen flow is analyzed in the Agilent 3000 micro GC. If trace amounts of hydrogen and/or oxygen are detected, the hydrogen and/or the oxygen flow rate are finely adjusted. These steps are repeated until the oxygen and hydrogen content in the nitrogen flow is negligible. Oxygen would result in a bigger error in the syngas flow rate and composition, consequently, the H_2 and O_2 flow rates where finely adjusted to have trace amount of excess hydrogen (~0.08%) and no detectable oxygen concentration.

The semi-batch reactor is very useful in the process analysis and understanding the characteristics of each stage of the process for better design and development of advanced gasification systems. The semi-batch reactor has the following advantages:

- The system allows one to monitor the variation in syngas flow rate and chemical composition with time. At the beginning, the high flow rate due to pyrolysis is observed and quantified. The extended low value of syngas flow rate due to char gasification is observed as well.

- The temperature can be easily controlled and set to a constant value.

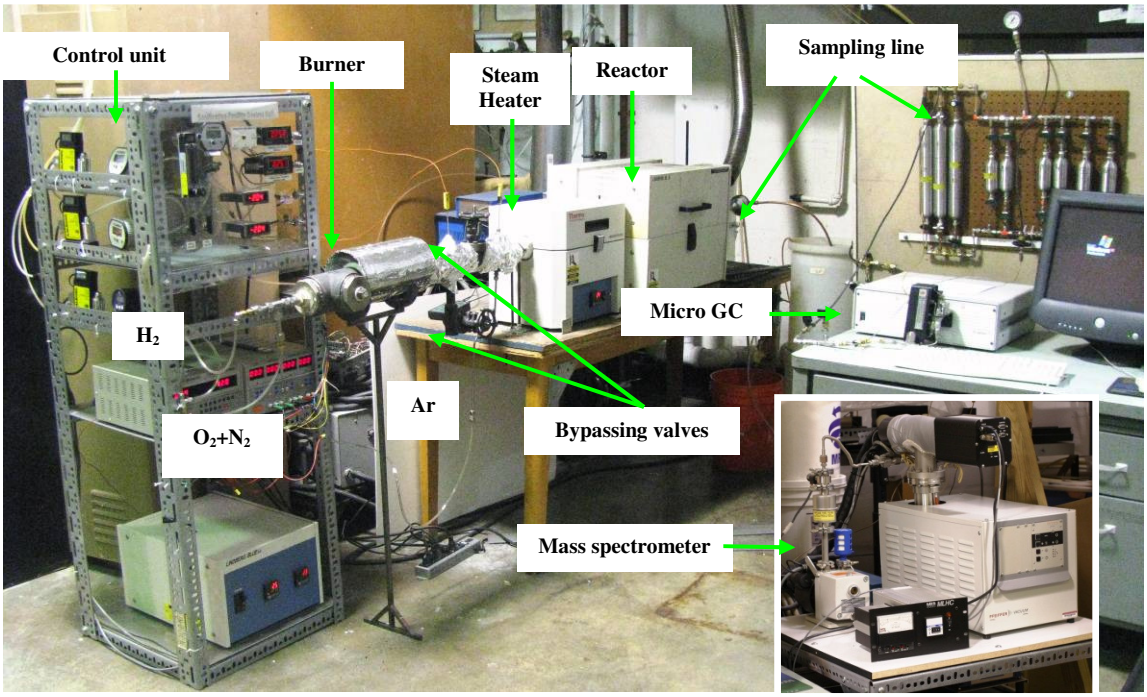

Figure III-1. A photograph of the experimental facility

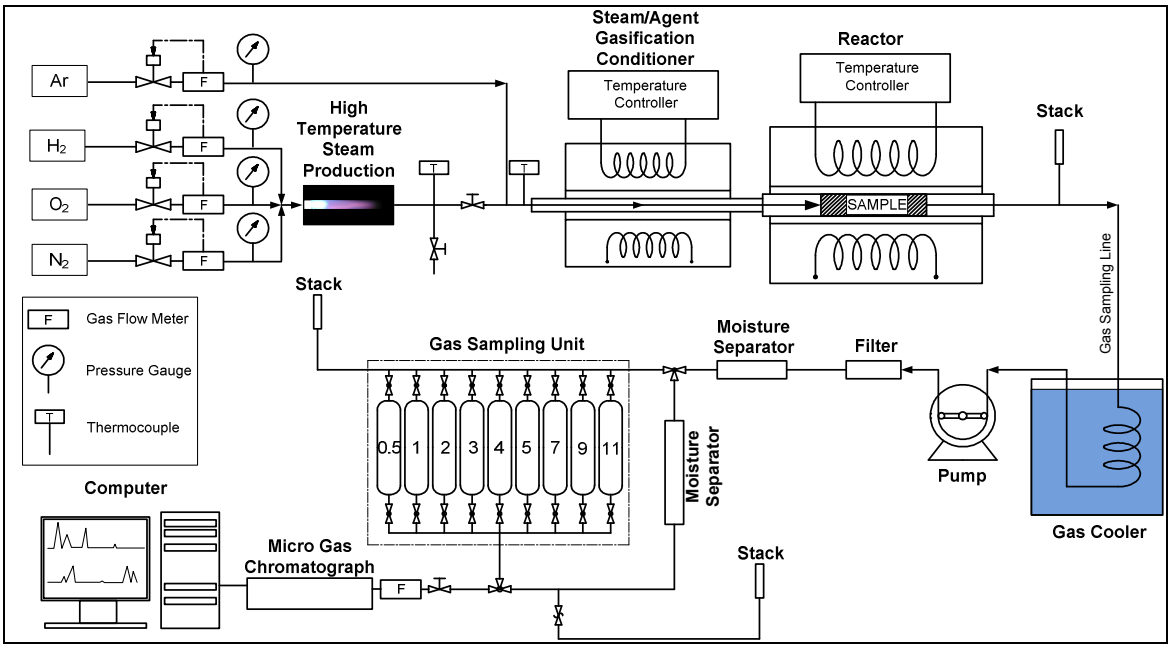

Figure III-2. Schematic diagram of the experimental setup

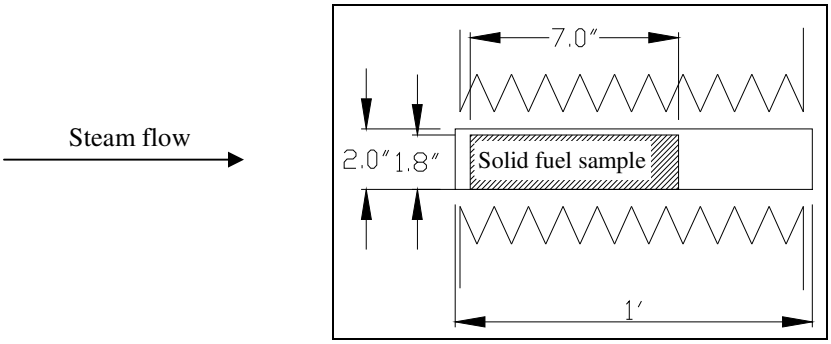

Figure III-3. Detailed drawing of the reactor

3.2. Char preparation

For char preparation, both the main and gasifying agent conditioning reactors were heated up to 900°C. A continuous flow of helium was introduced to both reactors during and after heating. Then a sample was introduced to the main reactor through a fast connection located at the reactor exit. The helium gas was kept flowing through the reactor to provide an inert medium for charring and to sweep the volatile mater out of the reactor. The sample was kept at a charring temperature of 900°C for an hour. In order to insure that the pyrolysis process has been

completed, a sample of the exit gases was analyzed using the mass spectrometer [MKS PPT Quadrupole Residual Gas Analyzer]. The charring process is considered complete when the analyzed exhaust contained only helium in the stream flow.

3.3. Procedures of reactivity determination

In order to examine the catalytic effect of ash the char gasification a mass spectrometer was used. Data from the mass spectrometer was used to calculate the reactivity of carbon in the sample char. Carbon in the sample will evolve in the form of carbon monoxide through the water gas reaction ($C + H_2O \Leftrightarrow CO + H_2$) and in the form of carbon dioxide through the water gas shift reaction ($CO + H_2O \Leftrightarrow CO_2 + H_2$). Consequently, monitoring the evolution of CO and CO_2 flow rate helps to calculate the carbon consumption rate from the sample. Helium was used as an inert gas in the reactivity experiments to avoid the confusion between CO and N_2 in the mass spectrometer. The mass spectrometer was used to measure the flow rate of CO and CO_2 obtained by relating the partial pressure of CO and CO_2 with the partial pressure of Helium. For this purpose the flow rate of Helium was kept constant at a known flow rate. From the carbon flow rate–time, relationship one can calculate the total yield of carbon and instantaneous sample mass inside the reactor at time (t).

3.4. Experimental conditions and samples properties

Table III-1. Tested samples and experimental conditions

Sample (Mass)	**Reactor temperature(s)**	**Gasifying agent (Flow rate(s))**	**Trace gas/ Inert medium for pyrolysis**

			(Flow rate)
Cardboard (35 g)	900°C	Steam (3.312, 4.122, 5.00, 6.33, 7.655 and 8.9 g/min)	-
Paper (35 g)	600, 700, 800, 900 and 1000°C	Steam (8 g/min)	Nitrogen (2.6 LPM)
Rice husk (35 g)	800, 900 and 1000°C	Steam (8 g/min)	Nitrogen (2.33 g/min)
Sugarcane bagasse (15 g)	800, 900 and 1000°C	Steam (8 g/min)	Nitrogen (2.33 g/min)
Food waste (35 g)	800 and 900°C	Steam (8 g/min)	Nitrogen (2.6 LPM)
Polystyrene (C_8H_8) (35 g)	700, 800 and 900°C	Steam (8 g/min)	Nitrogen (3 g/min)
rubber tires (35 g)	800 and 900°C	Steam (8 g/min)	Nitrogen (2.33 g/min)
Polyethylene-	900°C	Steam	Nitrogen

woodchips mixture from 0% to 100% in 20% intervals (35 g)	(7.72 g/min)	(2.33 g/min)

Table III-2. Operational conditions for char gasification kinetics experiments

Sample (mass)	**Charring temperature and duration***	**Pressure**	**Gasifying agent (flow rate)**	**Reactor temperature**	**Trace gas (flow rate or partial pressure)**
Food waste (35 g)	900°C (1 hr)	1 atm	Steam (8 g/min)	750, 800, 850 and 900°C	Helium 1.1 g/min
Woodchips (35 g)	900°C (1 hr)	2 bars	Steam (4.42 g/min) CO_2 (5.4 g/min)	900°C	Argon 0.5, 0.8, 1.1 and 1.4 bars
Activated charcoal (1 g)	-	1 atm	Steam (7.72 g/min)	775, 800, 825 and 850°C	Nitrogen (2.33 /min)

* A flow of inert gas was used for charring the sample

Table III-3. Sample properties; ultimate and proximate analysis

Sample	Volatile matter (%)	Fixed carbon (%)	Ash (%)	C	H	O	N	S	Heating value (MJ/kg)
paper	79	21	8.5	40.7	5.6	45.2	-	-	-
Cardboard [106]	19.9	80.1	5	44	5.9	44.6	0.3	0.2	-
Rice husk [107]	15.80	63.60	20.60	38.30	4.36	35.45	0.83	0.06	HHV: 14.89
sugarcane bagasse [107]	14.95	73.78	11.27	44.80	5.35	39.55	0.38	0.01	HHV: 17.33
yellow pines woodchips [108]	-	-	-	C 52.60	H 7.0	O 40.1	N 0	S 0	LHV: 22.3
Rubber tires [109]	-	-	8.74	72.25	6.74	9.67	0.36	1.23	-
Polyethylene [110]	100	-	-	86	14	-	-	-	LHV: 42.978
Activated charcoal properties									
Particle size 100~150 μm				Porosity 0.0705(-)					Density 1300~ 1700 kg/m^3

Chapter IV: Results and discussion

4.1. Characteristics of syngas evolution from wastes gasification and pyrolysis

4.1.1. Paper gasification and pyrolysis

In this section, main characteristics of gaseous yield from steam gasification have been investigated experimentally. Results of steam gasification have been compared to that of pyrolysis. The temperature range investigated were 600 to 1000^{o}C in steps of 100^{o}C. Results have been obtained under pyrolysis conditions at same temperatures. Investigated characteristics were evolution of syngas flow rate with time, hydrogen flow rate, chemical composition of syngas, energy yield and apparent thermal efficiency. Residuals from both processes were quantified and compared as well. Material destruction, hydrogen yield and energy yield were better in case of gasification as compared to that of pyrolysis. This advantage of the gasification process is attributed mainly to char gasification process. Char gasification was found to be more sensitive to the reactor temperature than pyrolysis. A partial overlap between gasification and pyrolysis has been observed. This partial overlap increases with increase in temperature.

4.1.1.1. Syngas flow rate

Figures IV-1, IV-2 and IV-3 show the syngas flow rate for both pyrolysis and gasification at different temperatures. Flow rates from pyrolysis and gasification show similar trend at the first few minutes. The values are almost the same in both cases. Pyrolysis shows a rapid increase in flow rate at the beginning of the process followed by a rapid decrease in flow rate until the flow rate reaches an asymptotic value of zero. In contrast, results from gasification process show positive values of flow rate for longer period of time, indicating the presence of char-steam

reaction. The area confined between the pyrolysis curve and the gasification curve reveals presence of char gasification. One can see this area is almost zero in the case of 600°C. This indicates less contribution from char gasification process at this temperature. This is further confirmed by the results on residuals remaining given in section 4.1.1.4. Increase in temperature decreased char gasification time as shown in figures IV-1, IV-2 and IV-3. One can notice the partial overlap in time between gasification and pyrolysis at 700°C. This partial overlap increases with the increase in temperature. For example, at reactor temperature of 800°C, pyrolysis ends at about 15 minute while gasification ends at ~ 45 minute. Overlap between gasification and pyrolysis is extended from the 4th minute until the 15th minute. This overlap at the 800°C represents around 27% of the char gasification process. An examination of the data at 900°C (figure IV-2b), shows that the overlap exists between the 3rd and the 10th minute, while char gasification ends at about 17th minute. These values reveal a 50% overlap between gasification and pyrolysis. The overlap at 1000°C temperature is almost 95% of the char gasification time.

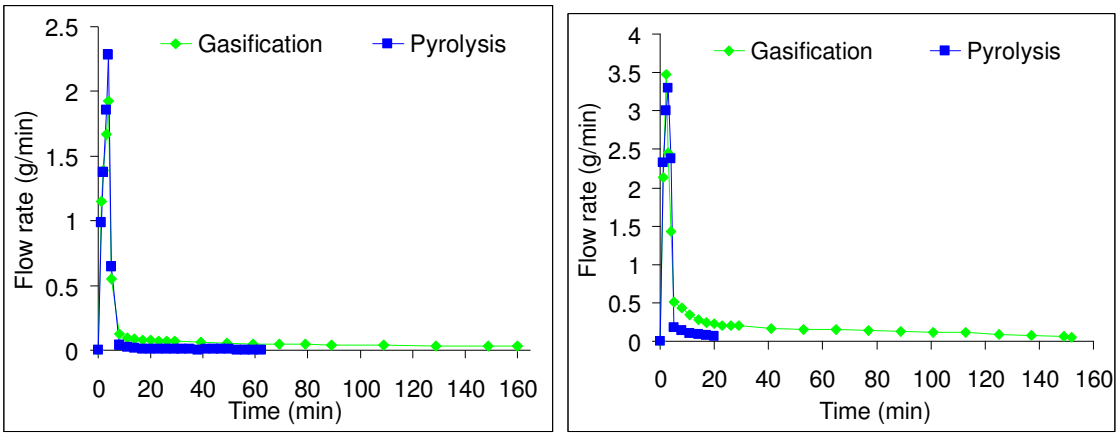

(a) (b)

Figure IV-1. Syngas flow rate from pyrolysis and gasification at (a) 600°C and (b) 700°C

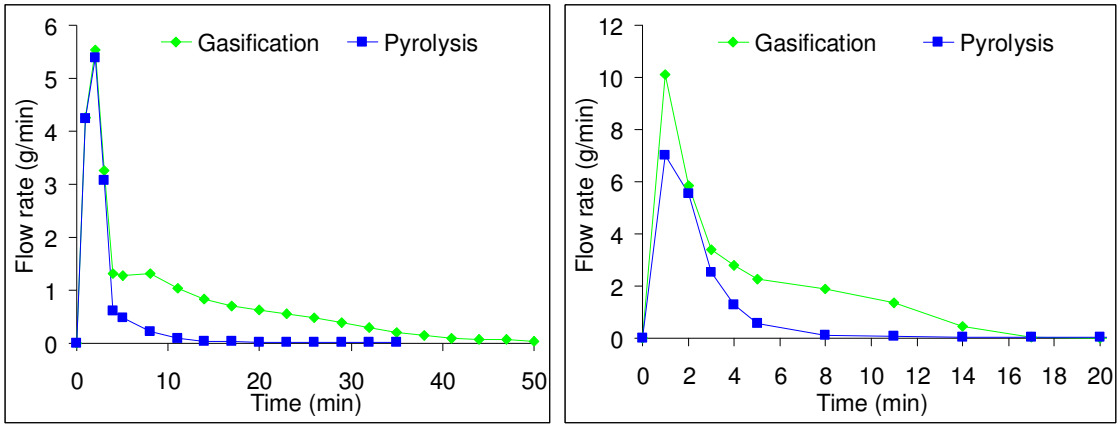

(a) (b)

Figure IV-2. Syngas flow rate from pyrolysis and gasification at (a) 800°C and (b) 900°C

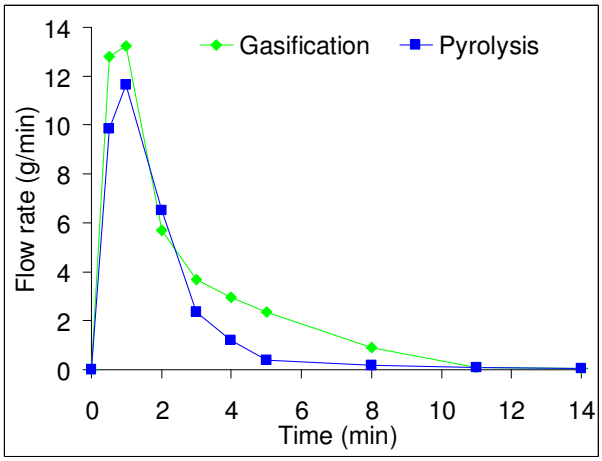

Figure IV-3. Syngas flow rate from pyrolysis and gasification at 1000°C

4.1.1.2. Hydrogen flow rate and yield

Figures IV-4 and IV-5 show the effect of reactor temperature on hydrogen flow rate for both gasification and pyrolysis processes. The common effect of increase in reactor temperature in both processes is that increase in reactor temperature increases hydrogen flow rate and decreases the time of hydrogen release. This is attributed to the endothermicity of hydrogen release for both processes and increase in reaction rates with the increase in reactor temperature. However, gasification shows higher hydrogen flow rates than pyrolysis at same process

temperature. Additional hydrogen production is attributed to gasification of char with steam and also from the partial contribution of water gas shift reaction. One more important result is that hydrogen evolution in case of gasification is relaxed over a longer period of time than hydrogen evolution from pyrolysis. This is due to the slower reaction kinetics of char gasification, which leads to the extension of the gasification process for a longer time duration. For example, at 800^{o}C the results for both pyrolysis and gasification shows that hydrogen release in the case of pyrolysis is almost zero at the 12th minute, while one can see considerable flow rate of hydrogen at 20th minute in case of gasification. For the 600^{o}C case, gasification and pyrolysis yielded same amount of hydrogen as shown in figure IV-6. This is attributed to almost negligible gasification reactions at this temperature.

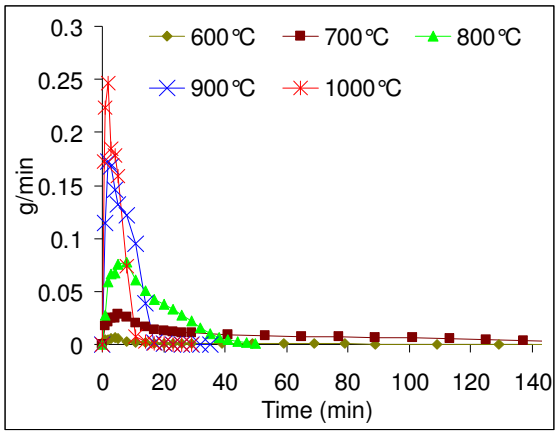

Figure IV-4. Hydrogen flow rate from gasification

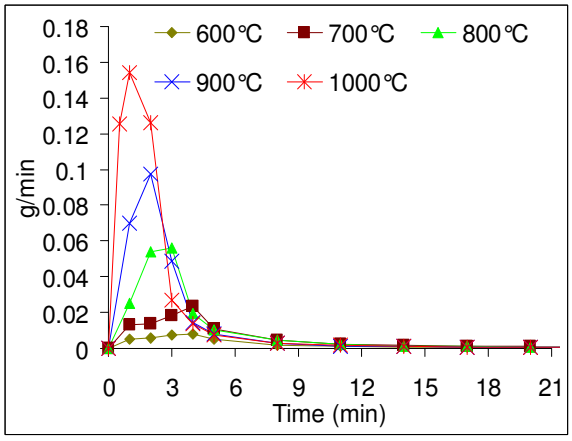

Figure IV-5. Hydrogen flow rate from pyrolysis

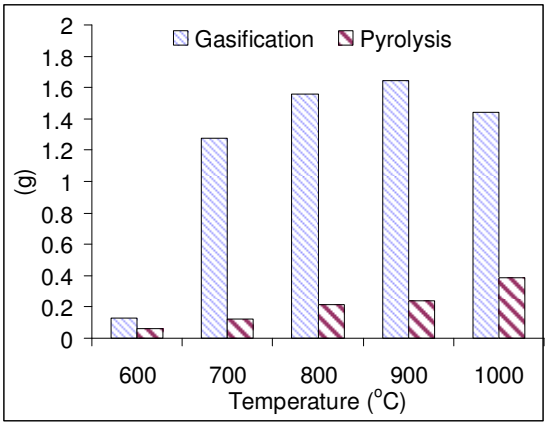

Figure IV-6. Hydrogen yield from pyrolysis and gasification

4.1.1.3. Evolution of H_2 and CO mole fraction

Figures IV-7(a), IV-7(b), IV-8(a) and IV-8(b) show the effect of temperature on evolution of H_2 and CO mole fraction during gasification and pyrolysis. Except for the 600°C data, all other temperatures examined here show the same trend. At the beginning, both gasification and pyrolysis show a good overlap in the mole fraction values. For example at reactor temperature of 700°C (figure IV-7b) one can see an overlap in mole fraction of H_2 and CO for the first five minutes. This overlap is reduced with the increase in reactor temperature. Overlap in the 900°C run is only for one minute. This overlap is attributed to the time taken by the sample to reach reactor nominal temperature. Overlap in mole fraction indicates pyrolysis of the sample at the beginning of the gasification process. Long periods of overlap at low temperatures are attributed to slow kinetics of char gasification at these low temperatures and indicate the sensitivity of char gasification to reactor temperature. For reactor temperatures higher than 600°C, H_2 mole fractions for gasification are higher than that of pyrolysis and CO mole fractions for gasification are lower than that of pyrolysis. The increase in H_2 mole fraction in case of gasification is attributed to char gasification by steam and the water gas shift reaction. However, lower values of mole fraction of CO are attributed to water gas shift reaction and

presence of trace amount of oxygen emanated from the steam generation system. It is important to note the relative increase in steam mole fraction in the reactor with time and the relative decrease in carbon mole fraction with time. This results in the consumption of CO mole fraction by the water gas shift reaction (figure IV-9) and the gain of H_2 at the same time. The 600°C run does not follow the same trend as in for the other temperatures due to the absence of steam-char gasification reactions at this low temperature.

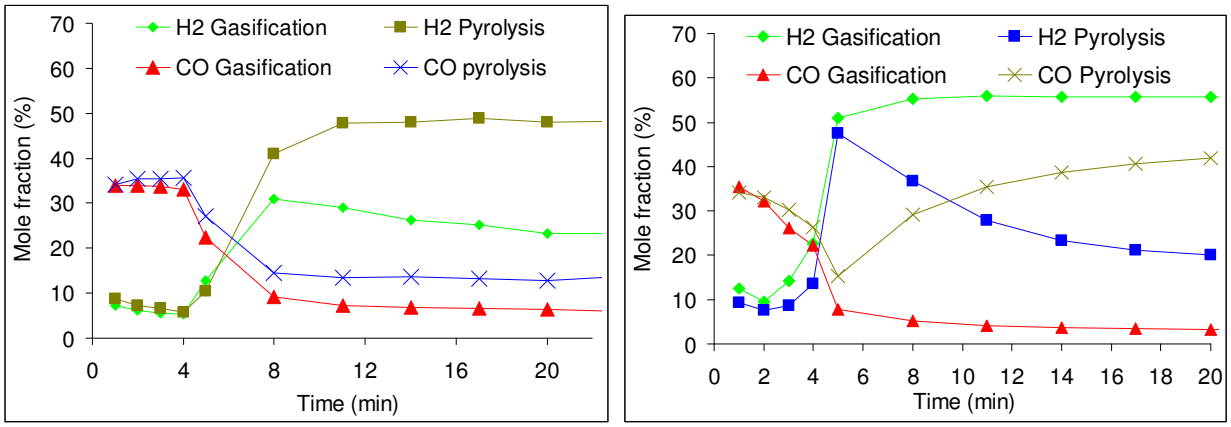

(a) (b)

Figure IV-7. H_2 and CO mole fraction for pyrolysis and gasification at (a) 600 and (b) 700°C

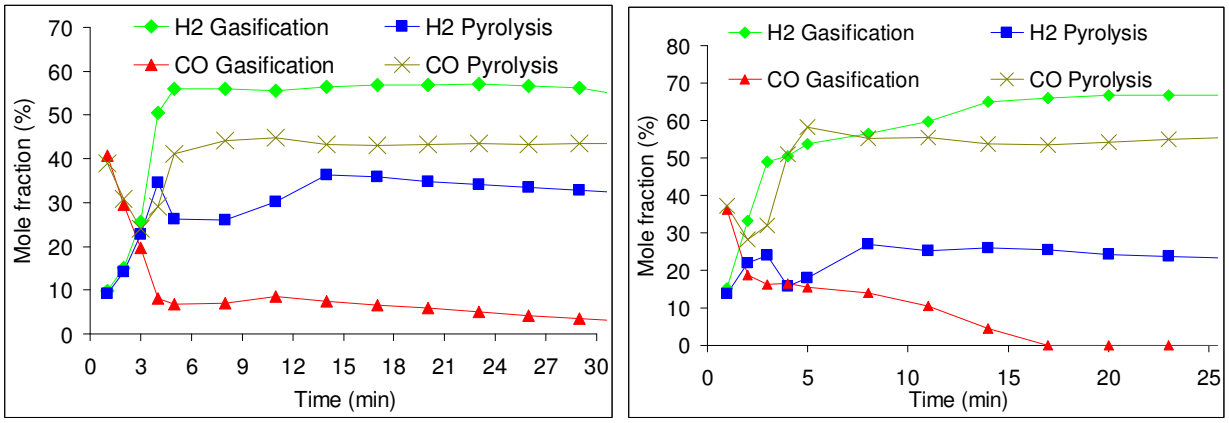

(a) (b)

Figure IV-8. Evolution of H_2 and CO mole fraction during pyrolysis and gasification at (a) 800 and (b) 900°C

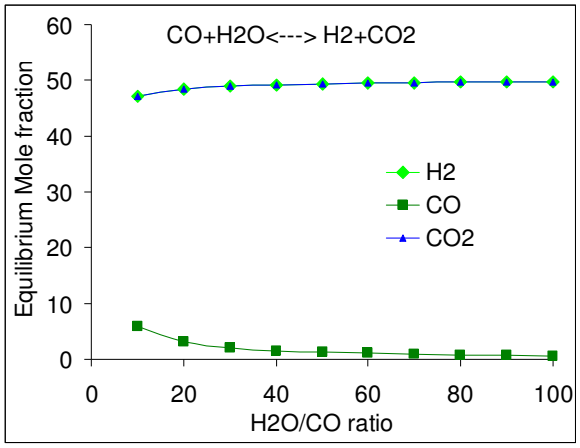

Figure IV-9. Equilibrium mole fraction for H_2O/CO reaction

4.1.1.4. Residue Material after Pyrolysis and Gasification

Figure IV-10 shows residual material leftover after the pyrolysis and gasification process. As shown in (figure IV-10), pyrolysis shows higher percentage of residual material as compared to that obtained from the gasification process. Residual materials from the pyrolysis process are mainly the char remaining from the devolatilization process. On the average the char percentages is about 20% of the initial sample mass from pyrolysis. This value represents the amount of fixed carbon in the sample as shown by the dark color material collected. In contrast, the residual materials in the case of gasification are white ash (no dark color material). Ash represents about 8~9% in the paper. The residuals percentage being of the order of 8% in case of gasification, confirms the gasification of all the char (fixed carbon) left over from the pyrolysis process. The gasification of all the carbon content in the sample is also confirmed by the presence of only white color ashes leftover from the gasification process versus the black color char leftover from the pyrolysis process (see figure IV-11). It is important to note the absence of steam-char reactions at low temperatures (less than 700^{o}C). Residuals from the gasification process at 600^{o}C showed considerably higher values than that at successively increased temperatures. Mass of Residuals at 600^{o}C (for gasification) was 23% of the initial sample which is comparable to the

residuals mass from a pyrolysis process. This indicates that only pyrolysis took place at this 600^{o}C temperature.

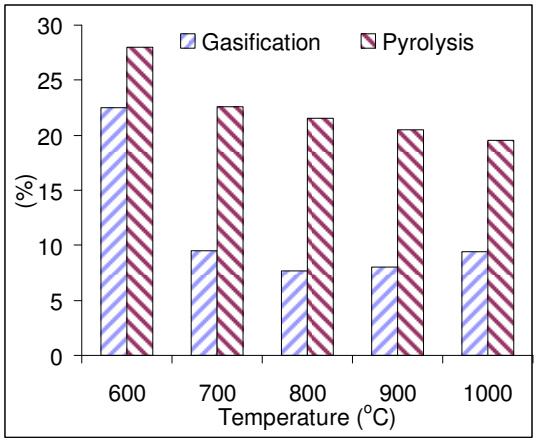

Figure IV-10. Percentage of Char residues from pyrolysis and ash residues from gasification

Figure IV-11. Char leftover from pyrolysis (left) and ash leftover from gasification (right)

4.1.1.5. Energy yield

Figure IV-12 shows the effect of reactor temperature on energy yield and apparent thermal efficiency from the paper sample. Increase in reactor temperature increases the energy yield from the sample for both pyrolysis and gasification cases. In case of the pyrolysis process, increase in temperature allow for better breakdown of long chains of hydrocarbons and consequently allow the release of more gaseous yield from the process. More specifically increase in the pyrolysis temperature increases the CO yield at the expense of CO_2 yield. This increase in CO yield at the expense of CO_2 yield raises the quality of syngas beside the initial increase in overall syngas yield. As for gasification same trend is observed; increase in the

reactor temperature increases energy yield from the sample. This is attributed to two reasons. First, the gasification process starts with rapid devolatilization of volatile component in the sample (pyrolysis) which is enhanced with the increase in reactor temperature. Second, it promotes in better steam-tar reforming process at elevated temperatures. In general, gasification shows higher energy yields than pyrolysis. However, the energy yields from gasification and pyrolysis at 600^{o}C are comparable. Gasification did not show higher energy yield than pyrolysis at this low temperature. The same would be expected if the experiments were carried out at even lower temperatures. This indicates the absence of char gasification reactions at this temperature. This is confirmed by the residual material results shown in figureIV-10. The material remaining from the gasification process at 600^{o}C is considerably higher than that obtained at successively increased temperatures.

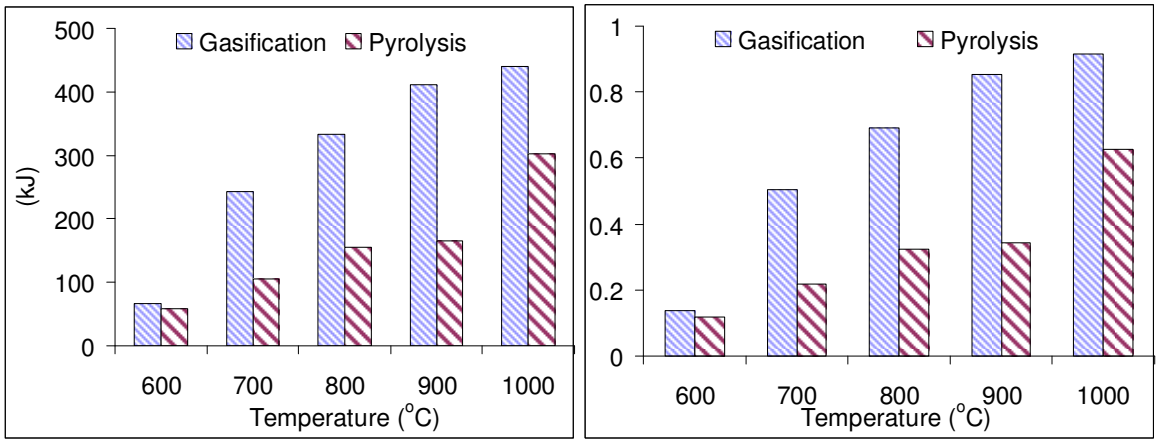

(a) (b)

Figure IV-12. (a) Energy yield from pyrolysis and gasification and (b) apparent thermal efficiency of pyrolysis and gasification

4.1.2. Rice husk gasification

Evolution of syngas from rice husk pyrolysis and gasification has been investigated at reactor temperatures of 800, 900 and 1000°C. Steam has been used as the gasifying agent. Evolution of main syngas constituents has been investigated. Results confirm that gasification occurs in two stages with the first stage as pyrolysis and the second stage being gasification of char. Pyrolysis experiments have been conducted at the same reactor temperatures as gasification to provide direct comparison. Hydrogen and CO yields from pyrolysis increased with the increase in reactor temperature. However, for gasification, hydrogen decreased slightly with increase in temperature while the CO yield remained almost constant. The behavior of hydrogen yield as well as CO yield form gasification and pyrolysis can be explained in terms of hydrogen and carbon content in char, liquid hydrocarbons (HCs) and syngas.

4.1.2.1. Evolution of CO and H_2 mole fractions

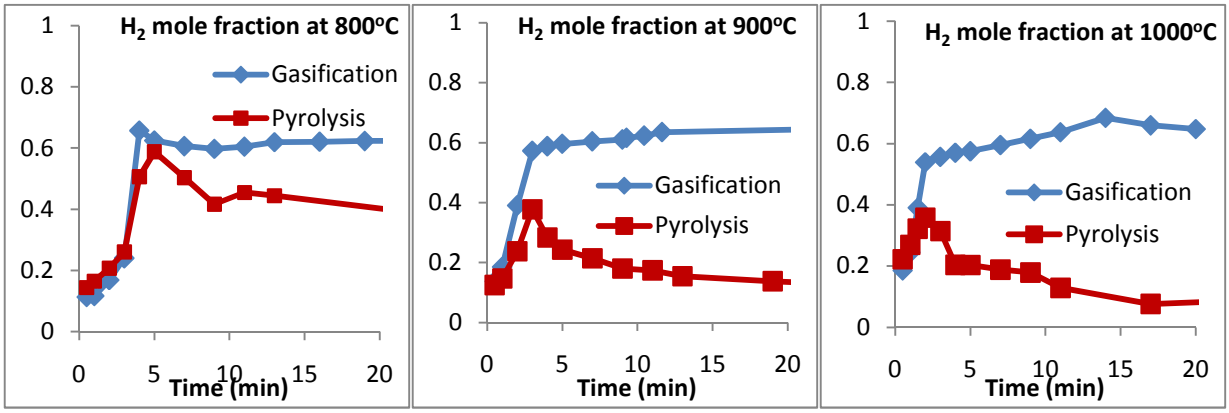

(a) **(b)** **(c)**

Figure IV-13. Evolution of H_2 mole fraction for reactor temperatures (a) 800, (b) 900 and (c) 1000°C

Figures IV-13a, IV-13b and IV-13c show the evolution of H_2 mole fraction from rice husk at 800, 900 and 1000°C reactor temperatures. Initially the mole fraction of H_2 from gasification coincides to that from pyrolysis. This overlap is longer in case of reactor temperature

of 800°C. After the initial stage in which H_2 mole fraction from gasification coincides with that from pyrolysis, H_2 mole fraction from gasification continues to increase until it reaches an asymptotic value. The increase in H_2 mole fraction in case of gasification is mainly attributed to the water gas reaction and the water gas shift reaction.

Figures IV-14(a), IV-14(b) and IV-14(c) show the evolution of CO mole fraction from gasification and pyrolysis at three different temperatures. In contrary to the behavior of H_2 mole fraction in gasification experiments, CO mole fraction from gasification continues to decrease to reach an asymptotic value. CO mole fraction is affected by two competing reactions in the stage of char gasification; the CO mole fraction tends to increase by the water gas reaction and tend to decrease by the water gas shift reaction ($CO + H_2O \Leftrightarrow H_2 + CO_2$). However, since the steam to CO ratio in the later stages of char gasification is high, the water gas shift reaction tends to shift towards more H_2, CO_2 and less CO. Results of equilibrium concentration of the water gas shift reaction at 900°C confirms the forgoing discussions, see figure IV-9.

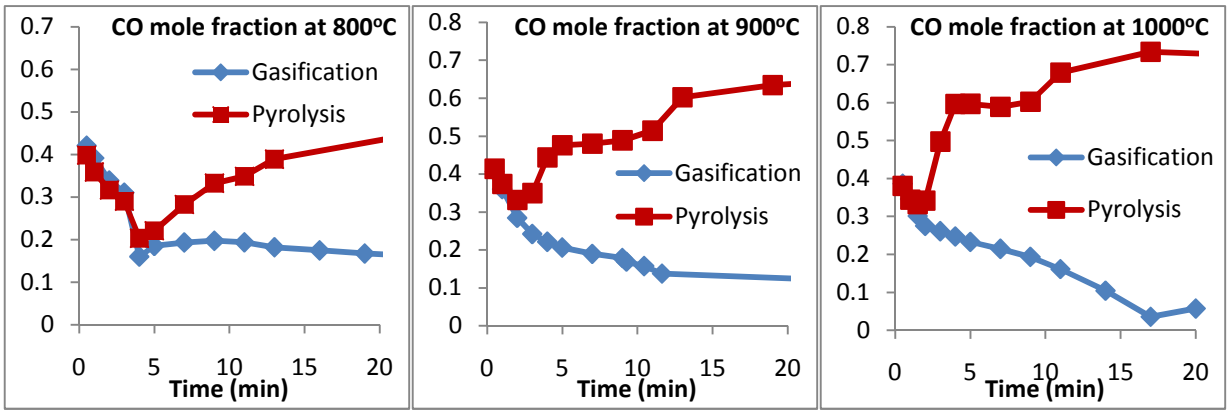

(a) **(b)** **(c)**

Figure IV-14. Evolution of CO mole fraction for reactor temperatures (a) 800, (b) 900 and (c) 1000°C

4.1.2.2. Total yield of main syngas constituents

Figure IV-15 shows the total yield of main syngas constituents from pyrolysis and gasification of rice husk at the selected 3 reactor temperatures. Hydrogen yield from pyrolysis tends to increase with the increase in reactor temperature as shown in figure IV-15(a). CO yield increase with the increase in reactor temperature in case of pyrolysis. On the other hand hydrogen slightly decreases with the increase in temperature in the case of gasification and CO yield is almost constant. The behavior of hydrogen yield as well as CO yield form gasification and pyrolysis can be explained in terms of hydrogen and carbon content in char, liquid hydrocarbons (HCs) and syngas. Under non-isothermal pyrolysis conditions, char yield is maximized at the conditions of low temperature and low heating rates. The liquid hydrocarbons yield is maximized at the conditions of intermediate reactor temperatures and high heating rates. The syngas yield is maximized for the conditions of high heating rate and high reactor temperatures.

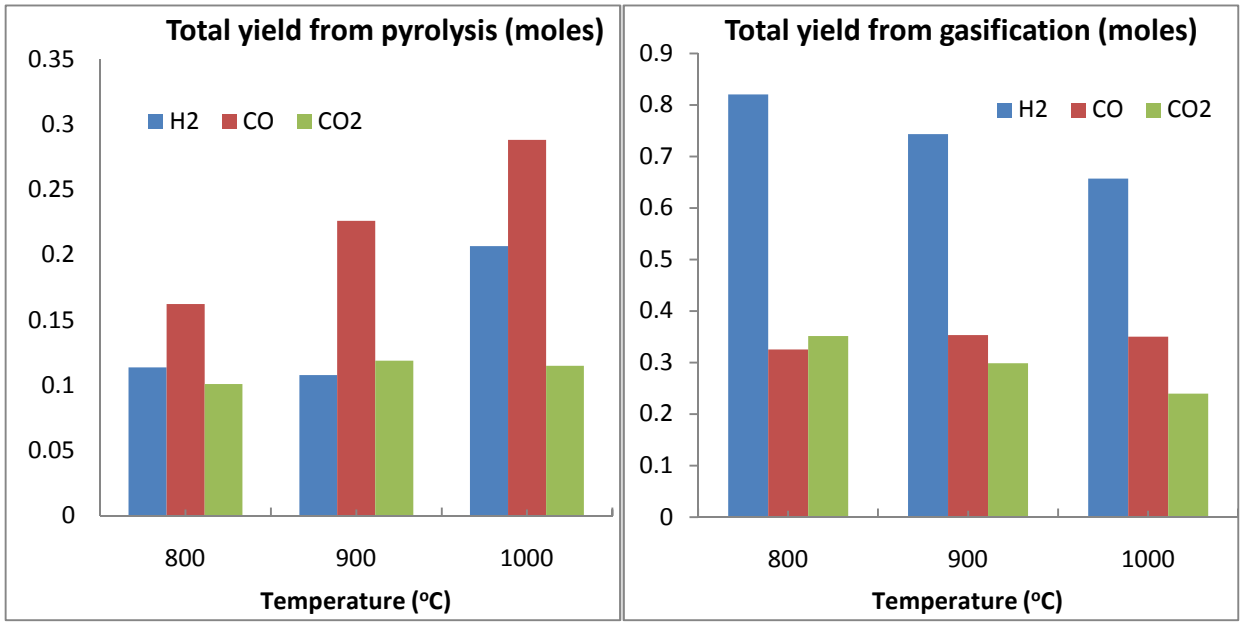

(a) **(b)**

Figure IV-15. Total yield of H_2, CO and CO_2 from (a) pyrolysis and (b) gasification

Based on the above mentioned behavior of char, liquid hydrocarbons and syngas yields according to reactor conditions, the increase of H_2 and CO with increase in temperature is in order. However, it might look contradictory to have a decrease in hydrogen yield from gasification and a constant CO yield. Hydrogen yield form gasification is attributed to the pyrolysis part as well the char gasification part. The increase in reactor temperature tends to increase the hydrogen yield in the form of syngas, but it also tends to increase the hydrogen content in the liquid hydrocarbons and tends to decrease the char formed. A schematic representation of the competing routes during biomass gasification is shown in figure IV-16.

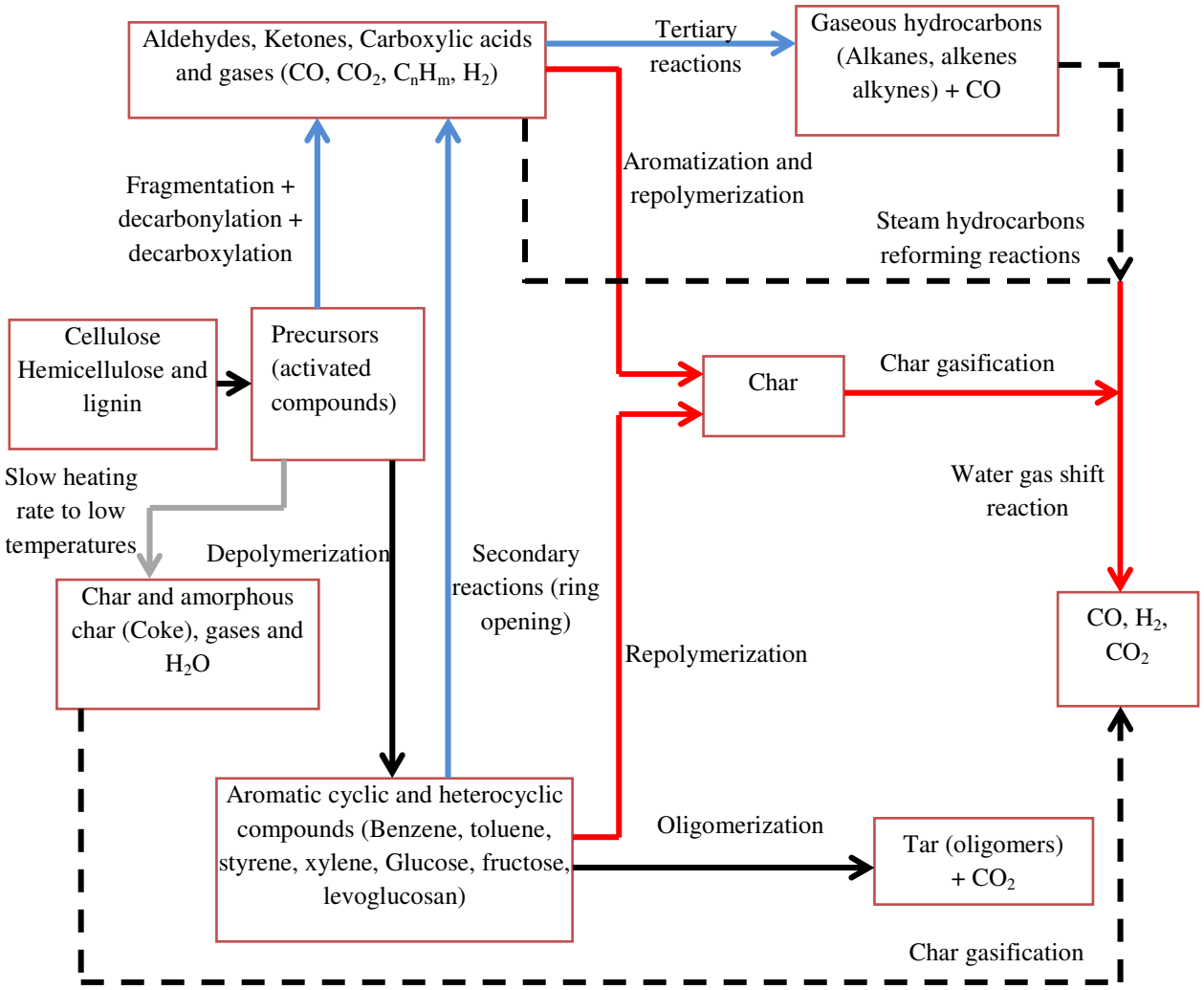

Figure IV-16. Reaction mechanism of biomass gasification. Blue line represents pyrolysis route which are accelerated with increase in reactor temperature. Red line represents char formation route and consequent CO production route through char gasification. This route is favored at lower temperatures

Having less char formed resulted in less yield of hydrogen in the syngas from the char gasification ($C+H_2O \rightarrow CO + H_2$). The decrease in hydrogen yield is mainly attributed to competing effects of syngas increase due to increase in temperature and less char formed and in turn less hydrogen formation via the water gas reaction. Same discussion applies for the CO behavior; CO yield increases directly with the increase in reactor temperature and heating rate by pyrolysis. However, in contrast the carbon yield in form of char decreases as the reactor temperature increases. However, the competing effect results in almost a flat yield of CO. Decreasing yield of CO_2 from gasification can be explained in terms of the water gas shift reaction equilibrium. The WGS tends to yield more products at the lower temperatures. Consequently, CO_2 yield decreases at higher temperatures.

4.1.3. Gasification and pyrolysis of sugarcane

Sugarcane bagasse gasification starts with pyrolysis, followed by the gasification of char. The characteristics of syngas evolved during gasification strongly depend on the heating rate and the sample temperature. The pyrolysis process consists of a complex series of hydrocarbons breakdown, fragmentation, isomerization and repolymerization. At high heating rates and high reactor temperatures steam gasification and steam reforming reactions occur in parallel with some of the pyrolysis reactions. The evolution of syngas characteristics will be discussed in lights of a global reaction mechanism which includes the pyrolysis step in conjunction with possible steam reforming/gasification reactions.

4.1.3.1. Global reaction mechanism of sugarcane gasification

Figure IV-17 show the evolution of syngas flow rate with time at reactor temperatures of 800, 900 and 1000°C. The flow rate starts with a high value at approximately 30 seconds followed by a steep decrease in flow rate. In the case of 800°C experiment, the steep decrease in flow rate is followed by a mild slope of syngas flow rate that is attributed to char gasification. However, at 900°C, the char gasification period is partially merged with the syngas evolution from pyrolysis, which resulted in a local peak at the second minute. In the 1000°C test case, one can see a total merging between the pyrolysis step and the char gasification step. The evolution of hydrogen showed similar behavior, see figure IV-18. The behavior of syngas evolution during gasification can be explained using the reaction mechanism presented in figure IV-19, and the evolution of sample temperature, presented in figure IV-20.

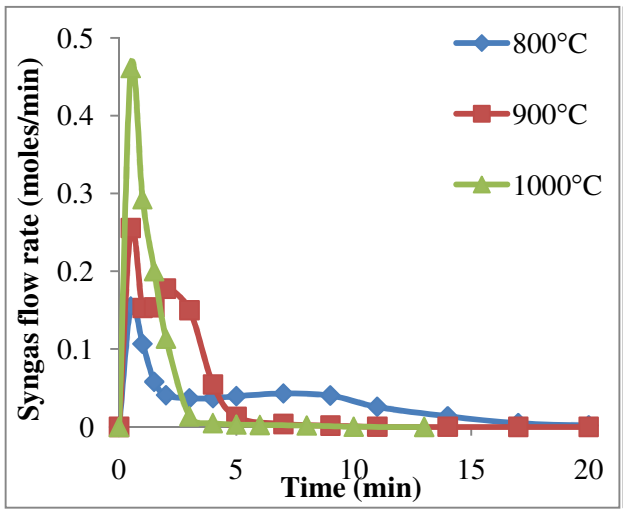

Figure IV-17. Evolution of syngas flow rate for reactor temperatures 800, 900 and 1000°C

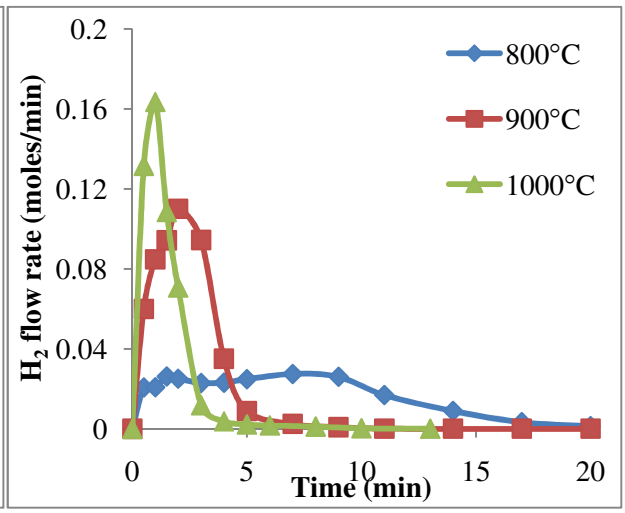

Figure IV-18. Evolution of H_2 flow rate for reactor temperatures 800, 900 and 1000°C

In the mechanism presented below the main constituting blocks of biomass are; cellulose, hemicellulose and lignin. The first step is activation of these compounds. After activation, the precursors undergo parallel reactions during initial stages of pyrolysis. The precursors might

undergo fragmentation reactions by carbon bonds scission, decarbonylation and decarboxylation, resulting in fragmented hydrocarbons; ketones, aldehydes and acetic acids. On the other hand the activated compounds might undergo depolymerization to form cyclic and heterocyclic compounds. The fragmentation route is favored at high heating rates and high reactor temperatures. However, the depolymerization route is favored at high/medium heating rates and intermediate reactor temperatures.

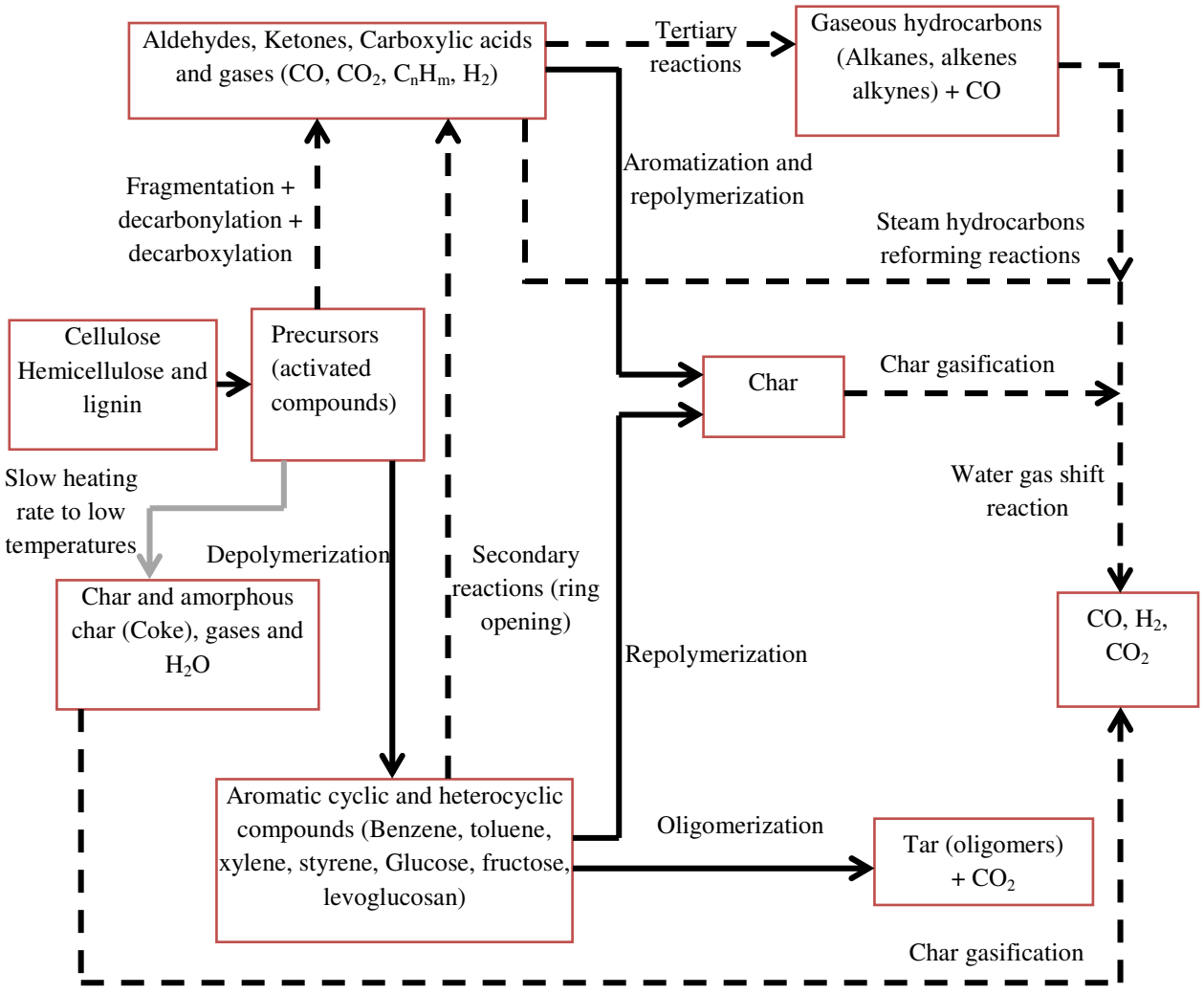

Figure IV-19. Reaction mechanism of biomass gasification. The dotted line represents routes which are favored at high heating rates and high reactor temperatures.

Cyclic compounds might undergo fragmentation through secondary reactions to yield gaseous hydrocarbons and fragmented hydrocarbons, which in turn, might undergo tertiary reactions to yield gaseous hydrocarbons and carbon monoxide [35].

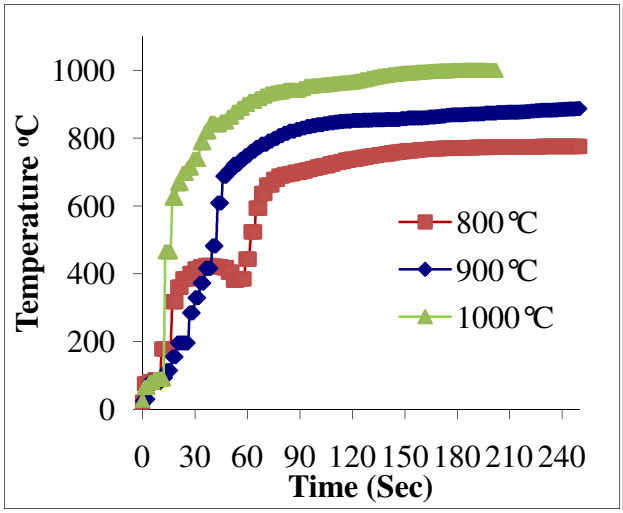

Figure IV-20. Evolution of sample temperature with time for reactor temperatures 800, 900 and 1000°C

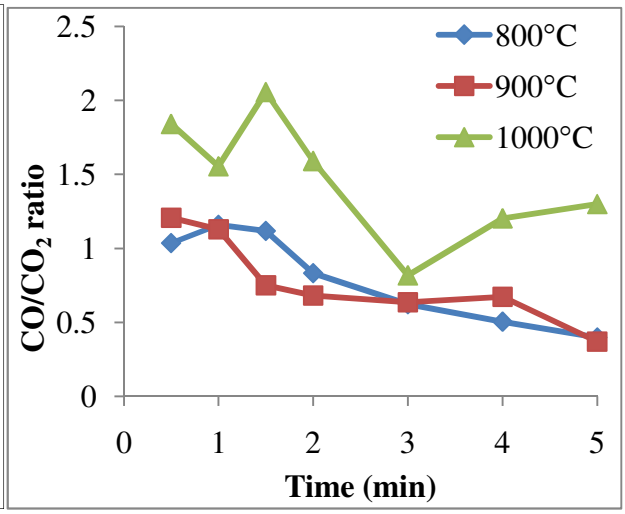

Figure IV-21. Evolution of CO/CO_2 ratio (molar basis)

Char is formed by three routes; the first is charring and coke formation at low heating rates and low temperatures. The second route is aromatization and repolymerization from fragmented hydrocarbons. The third route is repolymerization of cyclic and heterocyclic compounds. Tar and carbon dioxide are formed by oligomerization of precursors such as levoglucosan to form oligomers. It has been reported in the literature that CO and CO_2 are formed from competing parallel routes [42]. CO production route is favored at high heating rates at high reactor temperatures. However CO_2 route is favored at intermediate heating rates and intermediate temperatures. Based on the above mentioned observations, CO and CO_2 evolutions in this mechanism are generated from competing routes. This conclusion is confirmed from the

results of CO/CO_2 ratio shown in figure IV-21. CO/CO_2 ratio at reactor temperature of 1000^oC is higher than that at reactor temperatures of 800 and 900^oC.

The behavior of syngas flow rate can be explained in lights of the presented reaction mechanism. The increase in reactor temperature results in an increase in the heating rate, see figure IV-20. Consequently routes of fragmentation, secondary fragmentation, tertiary reactions, steam-hydrocarbons reforming reactions and char gasification reactions are accelerated. As a result of the acceleration in these routes syngas flow rate is increased. It is important to note that the precursors for char formation are the depolymerized cyclic and heterocyclic and fragmented hydrocarbons, which are consumed by tertiary reactions and steam reforming reactions as well. Consequently, the increase in reactor temperature results in less char formation and shorter time duration for char gasification.

Figure IV-18 shows the evolution of hydrogen flow rate for the investigated temperatures. The peak value of hydrogen flow rate shifts towards a high reactor temperature and longer residence time as compared to the peak syngas flow rate. For example, hydrogen flow rate peaks at the second minute for reactor temperatures of 800 and 900^oC and peaks during the first minute for reactor temperature of 1000^oC. However, the syngas flow rate peaks at about 30 second for the temperatures reported here. Hydrogen is mainly produced by fragmentation, secondary reactions, tertiary reactions, reforming reactions and char gasification reaction. All these routes are favored at high heating rates and high reactor temperatures.

4.1.3.2. Energy yield and apparent thermal efficiency

Figure IV-22 and IV-23 show the energy yield and the apparent thermal efficiency at the three reactor temperatures. The increase in reactor temperature resulted in an increase in energy

yield and apparent thermal efficiency. Although the increase in reactor temperature did not provide a consistent effect on syngas and hydrogen yield, see figure IV-24, the enhancement in syngas quality at the 1000°C case resulted in an increase in the energy yield. The enhancement in syngas quality is mainly attributed to the increase in CO and C_nH_m yields at 1000°C.

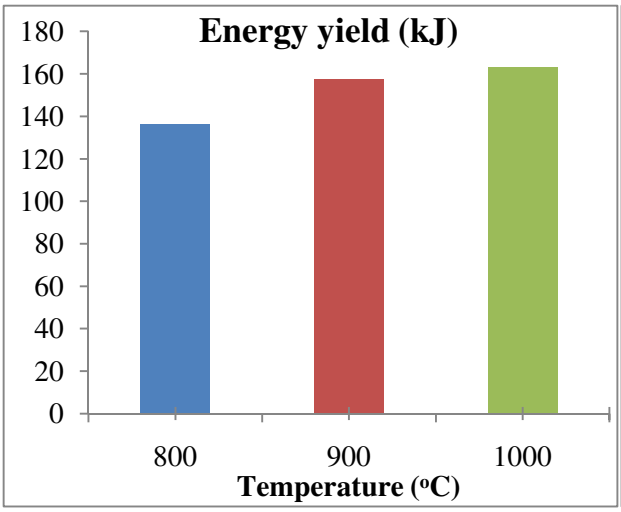

Figure IV-22. Energy yield at reactor temperatures of 800, 900 and 1000°C

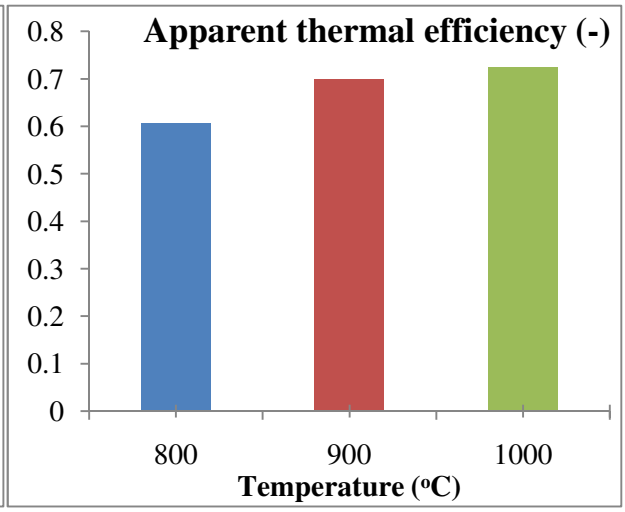

Figure IV-23. Energy yield at reactor temperatures of 800, 900 and 1000°C

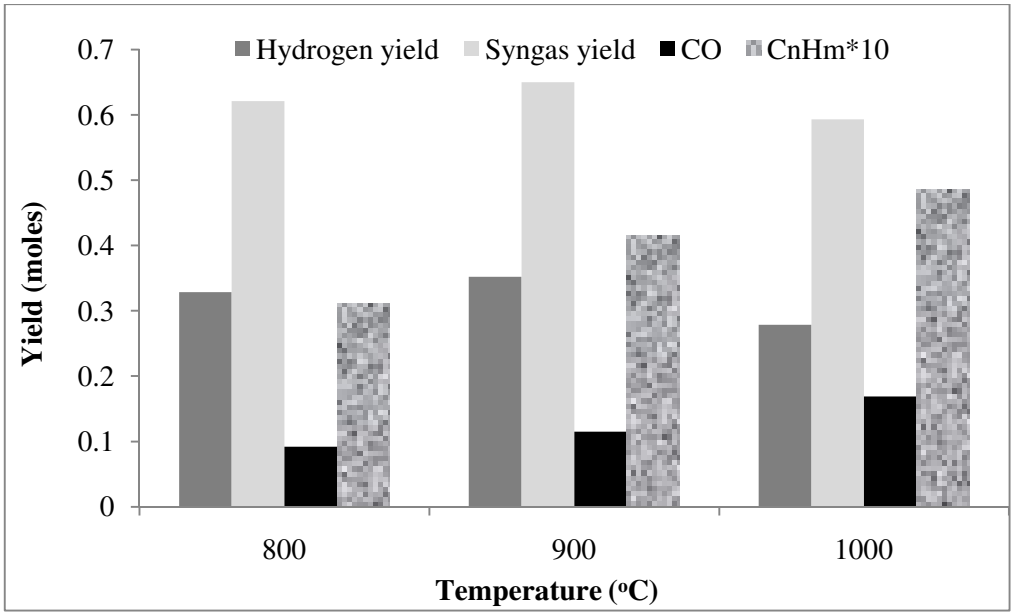

Figure IV-24. Syngas, hydrogen, CO and C_nH_m yield at reactor temperatures of 800, 900 and 1000°C

4.1.3.3. Cumulative yield of syngas, hydrogen and energy from sugarcane gasification

Figure IV-25, IV-26 and IV-27 show the evolutionary behavior of cumulative yield of syngas, hydrogen and energy. The vertical lines represent the time at which syngas, hydrogen and energy yields reached 99% of the total yield. The purpose of these figures, figures IV-25 to IV-27, is to set a criterion to define time duration of gasification. The sample might take up to 20 minutes for its complete conversion or absolute zero flow rate of syngas. On the other hand, it took only 8 minutes to reach 99% of sample conversion or 99% of total syngas yield. From figure IV-26, one can see that the increase in reactor temperature resulted in a significant decrease in time duration for energy conversion, based on the proposed criterion. This definition of time duration is more significant in determining the required residence time for a char particle to reach a certain degree of conversion. Note that there was no control on the residence time of gaseous and volatile yields during the experiment as they follow with the steam flow from the reactor. Therefore, the presented residence time in figures IV25-27 corresponds to the char content in the sample.

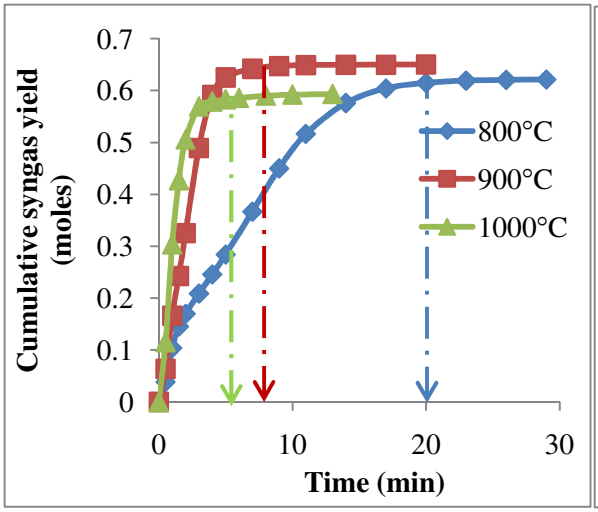

Figure IV-25. Cumulative syngas yield at reactor temperatures of 800, 900 and 1000°C

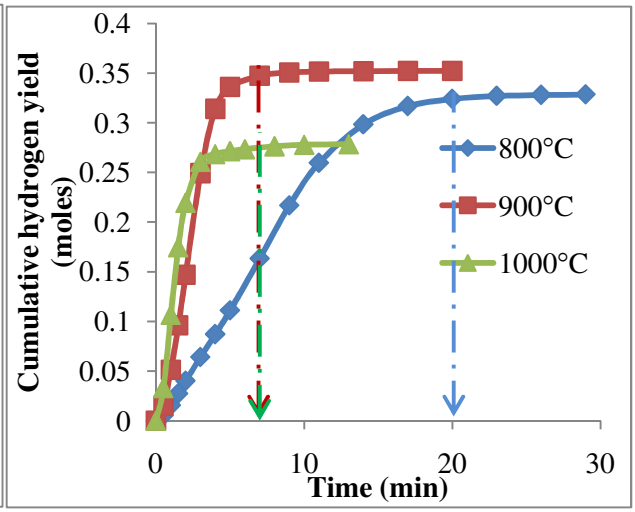

Figure IV-26. Cumulative hydrogen yield at reactor temperatures of 800, 900 and 1000°C

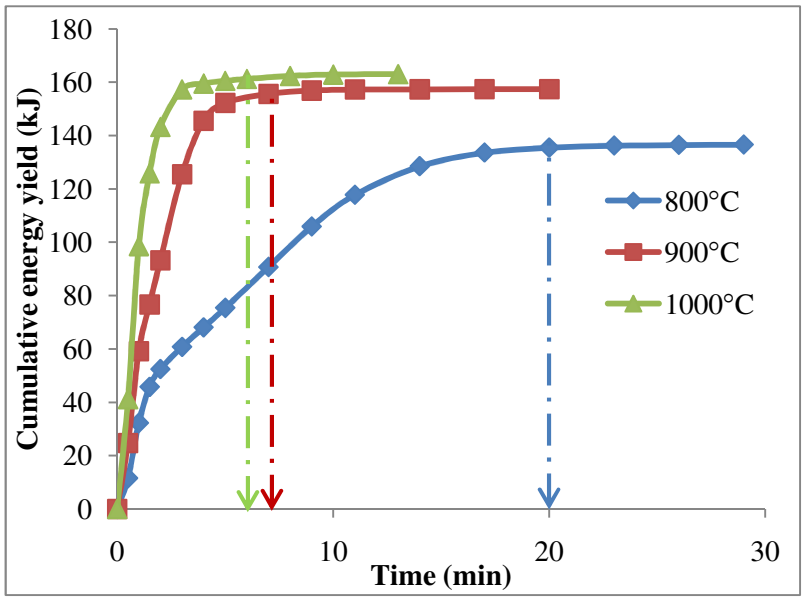

Figure IV-27. Cumulative energy yield at reactor temperatures of 800, 900 and 1000°C

4.1.4. Polystyrene gasification and pyrolysis

Polystyrene (PS) pyrolysis and gasification have been examined in a semi-batch reactor at temperatures of 700, 800 and 900°C. Characteristic differences between pyrolysis and gasification of polystyrene (PS) has been evaluated with specific performance focus on the evolution of syngas flow rate, evolution of hydrogen flow rate, evolution of output power, syngas yield, hydrogen yield, energy yield, apparent thermal efficiency and syngas quality. Behavior of (PS) under either pyrolysis or gasification processes is compared to that of char based sample, such as, paper and cardboard. In contrast to char based materials, PS gasification yielded less syngas, hydrogen and energy than pyrolysis at 700°C. However, the gasification of PS yielded more syngas, hydrogen and energy than pyrolysis at 900°C temperature. Gasification of PS is affected by reactor temperature more than PS pyrolysis. Syngas, hydrogen and energy yield increased exponentially with temperature in case of gasification. However, syngas and

energy yield increased linearly with temperature having rather a mild slope in the case of pyrolysis. Pyrolysis resulted in higher syngas quality at all temperatures.

4.1.4.1. Evolution of syngas flow rate

Figures IV-28a, IV-28b and IV-28c show the evolution of syngas from polystyrene (PS) pyrolysis and gasification at three different temperatures of 700, 800 and 900^{o}C. The results show a peak at certain time of the process. This is attributed to transient heating of the sample after introduction of the sample into the main reactor. One can clearly see the shift in peak position towards shorter times at higher reactor temperatures. This behavior is more obvious in the pyrolysis runs. This can be explained by assuming that the evolution of volatiles in the case of pyrolysis follows an nth order single step reaction, i.e., $dX/dt = K*(1-X)^n$ where X represents the conversion at time t and K is the reaction rate constant. Increase in the reactor temperature is equivalent to increasing the heating rate of the sample, especially in the first few minutes of the process. Increase in the heating rate means that the sample will reach the same temperature in shorter time. Consequently, the rate constant k will reach a higher values in a shorter time and the term representing the volatile amount remaining in the sample, $(1-X)^n$, will have a higher value. Consequently the reaction rate, dX/dt, will reach its peak in a shorter period of time.

The increase in reactor temperature has a positive effect on syngas flow rate in both pyrolysis and gasification. However, the effect of reactor temperature is more significant in gasification than pyrolysis. At 700^{o}C, the syngas flow rate for pyrolysis is higher than that of gasification. Increase in the reactor temperature to 800^{o}C resulted in increase in the syngas flow rate for both pyrolysis and gasification. In addition, the syngas yield from gasification was more than that from the pyrolysis. The increase in syngas flow rate at 900^{o}C was even more significant. One can say that the syngas flow rate increased quasi-linearly with temperature for the pyrolysis process

and increased exponentially for the gasification process over the investigated temperature range of 700 to 900°C. These results can be directly seen from the data shown in figure IV-31 where the overall syngas yield flow rate is presented. Of course these relations are not expected to hold for all other temperature values and temperature ranges. Therefore, further investigations should be carried out in order to determine the behavior of syngas evolution at higher (or lower) reactor temperatures.

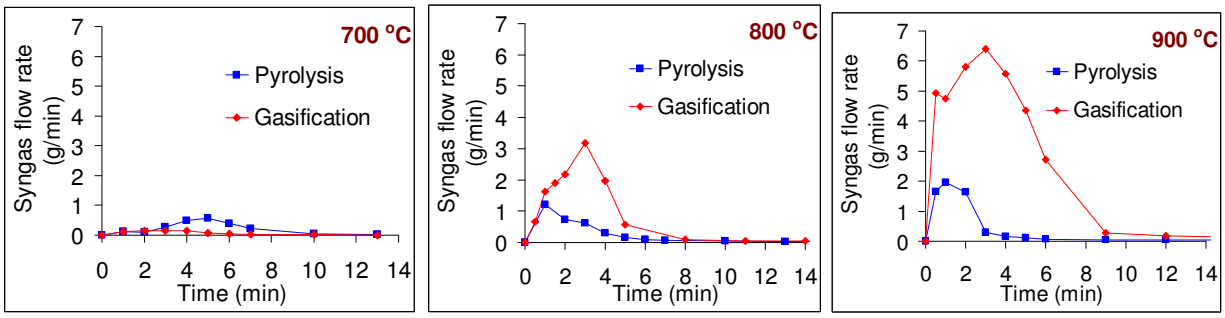

(a) **(b)** **(c)**

Figure IV-28. Evolution of syngas flow rate from pyrolysis and gasification for reactor temperatures (a) 700 °C, (b) 800 °C and (c) 900 °C

4.1.4.2. Evolution of hydrogen flow rate

Figures IV-29a, IV-29b and IV-29c show the evolution of syngas from the pyrolysis and gasification of PS at the three investigated temperatures, namely 700, 800 and 900°C. Similar to the syngas flow rate results shown above, all curves show a peak at a certain time in the process. A shift in peak position towards shorter time with increase in the reactor temperature is observed. This behavior is seen for both the pyrolysis and gasification experiments. This shift is attributed to the increase in sample heating rate, which increases the reaction rate constant to provide a shorter time. On the other hand, it was expected that the presence of steam will increase the hydrogen flow rate and yield at all temperatures. However, at reactor temperature of 700°C, hydrogen flow rate from the gasification experiment was less than that from the pyrolysis

experiment. This suggests a competing reaction of PS with steam that forms condensable hydrocarbons. This competing reaction is more favorable at reactor temperature of 700°C.

The increase in reactor temperature increased the hydrogen flow rate for both pyrolysis and gasification. If the goal from the pyrolysis and gasification of PS is the production of hydrogen gas, then it is not useful to use the gasification process unless the reactor temperature is higher than 800°C, see figures IV-29 and IV-32. One can see from the hydrogen flow rate results, figure IV-29, as well as the overall hydrogen yield results, figure IV-32, that hydrogen yield from gasification at reactor temperature of 700 and 800°C is lower than that from pyrolysis.

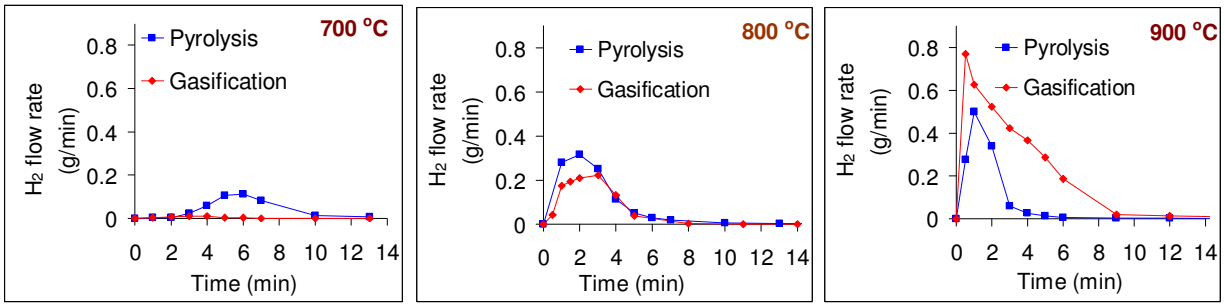

(a) **(b)** **(c)**

Figure IV-29. Evolution of hydrogen flow rate from pyrolysis and gasification for reactor temperatures (a) 700°C, (b) 800°C and (c) 900°C

4.1.4.3. Evolution of output power

Figure IV-30a, IV-30b and IV-30c show the evolution of output power (kJ/min) associated with the chemical energy in the syngas. The figures represent the output power from pyrolysis and gasification at reactor temperatures 700, 800 and 900°C. Gasification yielded less power than pyrolysis at 700°C, almost the same power at 800°C and more power at 900°C. If chemical energy form PS in its original solid form is to be recovered in reformed gaseous form, it is recommended to use gasification process only at reactor temperatures higher than 800°C.

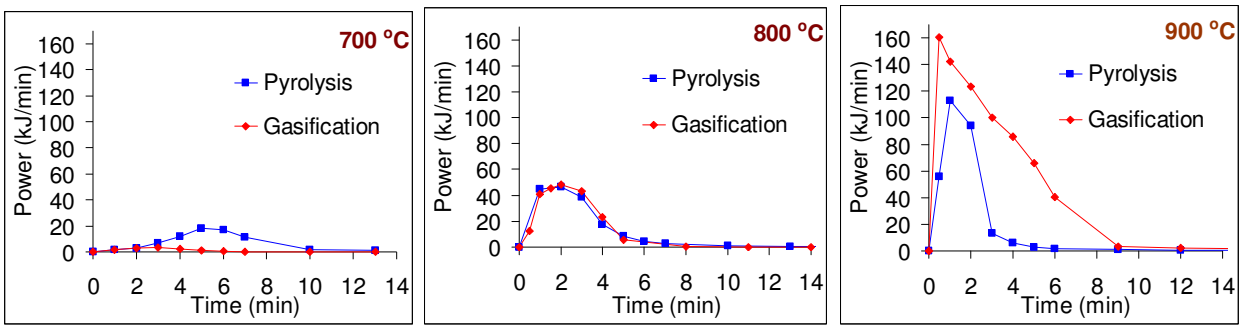

(a) (b) (c)

Figure IV-30. Evolution of output power from pyrolysis and gasification at reactor temperatures of: (a) 700°C, (b) 800°C and (c) 900°C

4.1.4.4. Syngas yield

Polystyrene yields almost 99 % volatile matter under pyrolysis or gasification conditions. Around 2 % of black carbon has been observed for pyrolysis experiment carried out at 700°C. Besides this all the experiments yielded negligible amount of black carbon, accounting to less than 1%. The volatile yield is either in the gas phase or condensable phase. The condensable phase contains liquid hydrocarbons and wax. The change in gaseous yield with reactor temperature can help describe pyrolysis and gasification of PS using simple models. One can consider the pyrolysis of PS as if it undergoes two parallel competing reactions with two different reaction rates of k_1 and k_2, *where* k_1 corresponds to the reaction yielding gaseous form and k_2 corresponds to the reaction yielding condensable hydrocarbons. This model can be represented as follows:

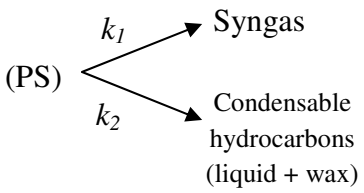

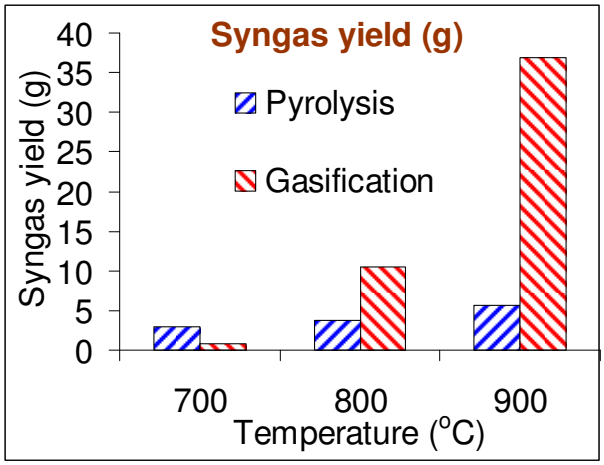

Figure IV-31. Overall syngas yield from pyrolysis and gasification

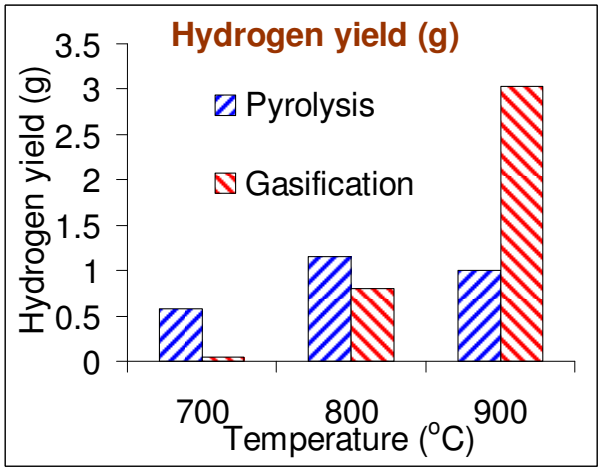

Figure IV-32. Overall hydrogen yield from pyrolysis and gasification

Examinations of the syngas yield from pyrolysis reveal an increase in both syngas flow rate and yield with increase in temperature, see figure IV-31. This behavior indicates that PS pyrolysis process favors the syngas production route (k_1) at increased temperatures.

Results of syngas flow rate and overall syngas yield show that at 700°C, gaseous yield form gasification is lower than that of pyrolysis; however, at 900°C the yield from gasification is higher than that of pyrolysis, see figure IV-31. This behavior is different from the behavior of cellulosic based material. In a previous study by the authors, Ahmed and Gupta [13, 27] showed that steam gasification always yielded more syngas than pyrolysis at all temperatures. One further major difference between PS and cellulosic based material is the hydrogen yield. Steam gasification always increased the hydrogen yield for cellulosic material as compared to pyrolysis, and one would expect similar behavior for PS also. On the contrary a decrease in hydrogen flow rate and yield was observed with steam gasification at 700°C as compared to pyrolysis.

Hydrogen flow rate and overall hydrogen yield are shown in figure IV-29 and figure IV-32, respectively. Putting this information together reveals that the presence of a PS-steam reaction that yields condensable hydrocarbons (liquid + wax). This reaction is competing with

the gasification reactions. Consequently, in the simplest model, the gasification process has to be represented by four competing parallel reactions as given below:

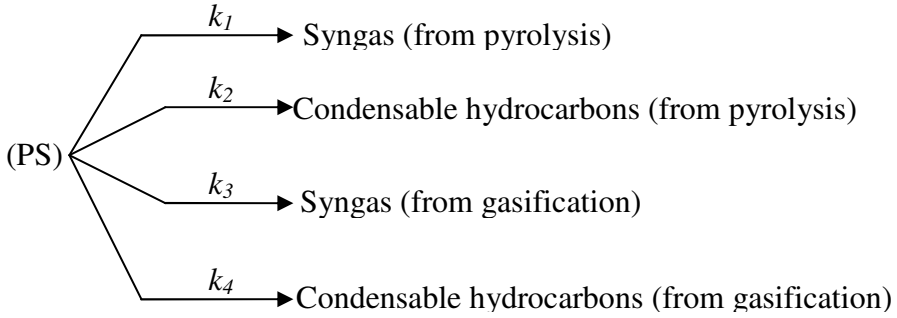

From the results of syngas yield and hydrogen yield shown in figures IV-31 and IV-32, one can conclude the domination of reaction (k_4) at reactor temperature of 700^{o}C. However, at reactor temperature of 900^{o}C, the third reaction (k_3), dominates. In order to support this conclusion, a comparison between condensable yield from pyrolysis and gasification has been conducted. The sample size and experimental conditions was as follows:

- Sample: 18 grams of polystyrene (PS)
- Reactor temperature: 700^{o}C for both pyrolysis and gasification
- Steam flow rate for gasification: 8 g/min
- Nitrogen flow rate for pyrolysis: 3 g/min

The sample mass was reduced because the condenser was designed to condense only a fraction of the flow for gas analysis. In this experiment the entire product stream was directed to the condenser with no bypass of the sample. Condensable hydrocarbons are collected in the condenser and a small flask was placed after the condenser. Gaseous products were directed to the exhaust system. In the case of gasification experiments the condensable hydrocarbons got mixed with the condensed water. Separation of condensable hydrocarbons from the condensed water was performed using the difference in density in a long column. Condensate from

pyrolysis was approximately 4.4 grams or 24.4 % of the initial sample mass. However for gasification the condensate was approximately 11 grams, representing 61.1 % of the initial sample mass. Getting more hydrocarbons condensate from gasification than pyrolysis emphasize the presence of reaction four (k_4), which represents the condensable hydrocarbons formation as a result of steam-PS reactions. An accurate mass balance could not be performed due to the error emanating from condensate which was not retrieved from the condenser as well as the escaped volatiles which were not condensed. Considering that the factors causing the error are equally affecting the pyrolysis and gasification experiments, the fact that gasification yields more condensable hydrocarbons than pyrolysis is still true. Figure IV-33 shows a photograph of a sample from the condensed hydrocarbons and they are labeled to show the global fractionation.

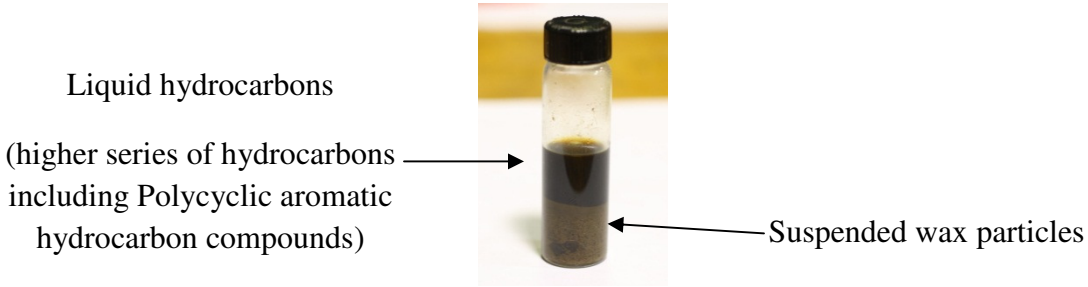

Figure IV-33. Condensable hydrocarbons from PS gasification

4.1.4.5. Hydrogen yield

Figure IV-32 shows the effect of reactor temperature on overall hydrogen yield. Hydrogen yield from gasification shows a consistent increase with an increase in reactor temperature. Gasification yielded more hydrogen than pyrolysis only at the examined reactor temperature of 900^{o}C.

4.1.4.6. Energy yield and apparent thermal efficiency

Figure IV-34a and IV-34b show the energy yield and apparent thermal efficiency for gasification and pyrolysis at reactor temperatures of 700, 800 and 900^{o}C. The apparent thermal

efficiency was based on a LHV of 41 kJ/kg.[111] The increase in reactor temperature increases the energy yield and apparent thermal efficiency for both the processes of pyrolysis and gasification. For reactor temperature less than 800^{o}C, gasification yielded less energy and lower apparent thermal efficiency than pyrolysis. At reactor temperature of 900^{o}C, gasification yielded almost three times the amount of energy than that from pyrolysis. Energy yield and apparent thermal efficiency increases quasi-linearly with temperature in case of the pyrolysis process. The increase in energy yield and apparent thermal efficiency with increase in temperature for gasification can be described best using an exponential function in temperature similar to that of the Arrhenius equation. This indicates that the effect of temperature on energy yield is similar to that on the reaction rate. A simple curve fitting can put these behaviors to provide an equation of the form:

- $E_{yield}(T) = 0.7422T - 621.85$ $\{for\ 700^{o}C < T < 900^{o}C\}$ *Pyrolysis*
- $E_{yield}(T) = 2.20685*10^{11}*exp[-22831/T]$ $\{for\ 700^{o}C < T < 900^{o}C\}$ *Gasification*
- $\eta_{app.} = 0.0005T - 0.4333$ $\{for\ 700^{o}C < T < 900^{o}C\}$ *Pyrolysis*
- $\eta_{app.} = 146128948*exp[-22820/T]$ $\{for\ 700^{o}C < T < 900^{o}C\}$ *Gasification*

where, E_{yield} is the energy yield in kJ, T is the reactor temperature in K and $\eta_{app.}$ is the apparent thermal efficiency (dimensionless).

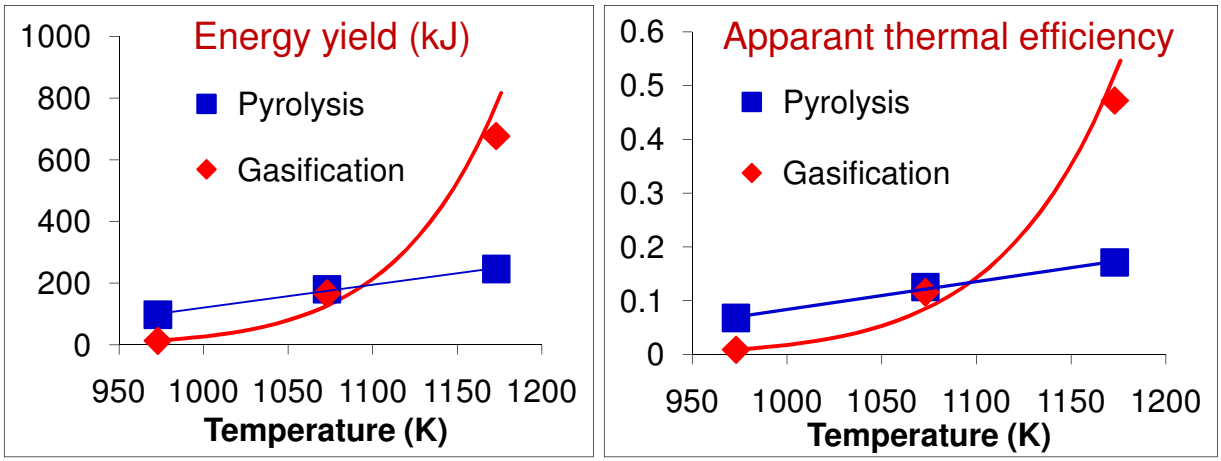

(a) **(b)**

Figure IV-34. (a) Energy yield and (b) apparent thermal efficiency for pyrolysis and gasification

4.1.4.7. Syngas quality

The objective of part of this study was to determine the effect of reactor temperature on overall syngas quality and to compare the quality of syngas resulting from the pyrolysis process with the gasification process. The criteria upon which the syngas quality will be determined are based on overall hydrogen mole fraction, figure IV-35, and overall pure fuel percentage (molar basis), figure IV-36. The pure fuel mole fraction is determined by subtracting CO_2 yield form the total syngas yield. Pyrolysis shows better syngas quality at all temperatures based on both the above criteria. It is important to note that the criteria here are only the mole fraction and not the total yield of pure fuel or hydrogen. Gasification yields much more energy than pyrolysis as shown in section (**4.1.4.6.**) above.

From the results on the effect of temperature on syngas quality one can see that increase in temperature causes a quasi-linear increase in pure fuel percentage in the case of gasification. On the other hand, temperature has no effect on pure fuel percentage in the case of pyrolysis. The fuel percentage for the pyrolysis experiments is almost 99%. This value of fuel percentage is higher than that reported by the authors for cardboard pyrolysis, which was 77% and 80% at

reactor temperatures of 800 and 900°C, respectively.[112] The percentage of pure fuel from gasification at 900°C was 92.6%. This value is higher than that was reported for cardboard gasification, which was approximately 78% for similar experimental conditions.[11]

Neither pyrolysis nor gasification shows a consistent trend of hydrogen mole fraction yield as a function of reactor temperature. However, pyrolysis resulted in higher hydrogen mole fraction than gasification at all temperatures.

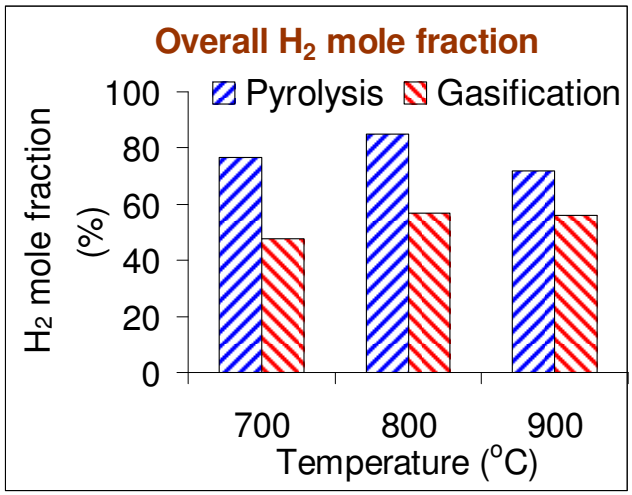

Figure IV-35. Overall hydrogen mole fraction for pyrolysis and gasification

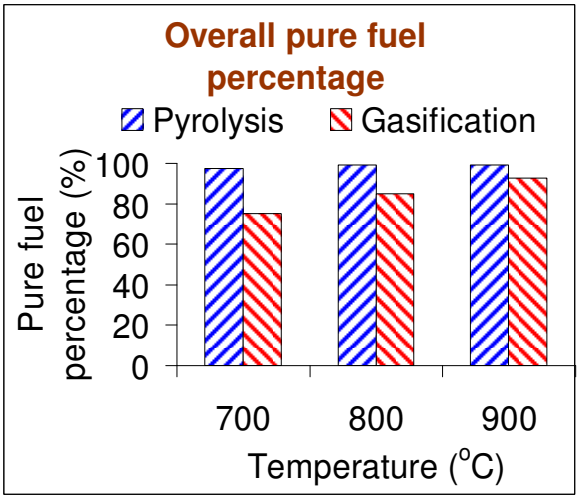

Figure IV-36. Overall pure fuel percentage in syngas for pyrolysis and gasification

4.1.5. Rubber gasification and pyrolysis

The characteristics of syngas evolution during pyrolysis and gasification of waste rubber have been investigated. A semi-batch reactor was used for the thermal decomposition of the material under various conditions of pyrolysis and high temperature steam gasification. The results are reported at two different reactor temperatures of 800 and 900°C and at constant steam gasifying agent flow rate of 7.0 g/min and a fixed sample mass. The characteristics of syngas were evaluated in terms of syngas flow rate, hydrogen flow rate, syngas yield, hydrogen yield and energy yield. Gasification resulted in 500% increase in hydrogen yield as compared to

pyrolysis at 800°C. However, at 900°C the increase in hydrogen was more than 700% as compared to pyrolysis. For pyrolysis conditions, increase in reactor temperature from 800 to 900°C resulted in 64% increase in hydrogen yield while for gasification conditions a 124% increase in hydrogen yield was obtained. Results of syngas yield, hydrogen yield and energy yield from the rubber sample are evaluated with that obtained from woody biomass samples, namely hard wood and wood chips. Rubber gasification yielded more energy at the 900°C as compared to biomass feedstock samples. However, less syngas and less hydrogen were obtained from rubber than the biomass samples at both temperatures.

4.1.5.1. Evolution of syngas and hydrogen flow rates

Figure IV-37 shows the evolution of syngas flow rate with time. The flow rate starts with a high value of syngas followed by a steep decrease in the flow rate. This is then followed by an extended period of monotonically decreasing syngas flow rate. The initial high value of syngas flow rate and the subsequent steep decrease in the flow rate are mainly attributed to the evolution of volatile matter from the rubber sample. This is also confirmed by the similarity in flow rate trend observed initially on the evolution of syngas flow rate from gasification and pyrolysis, compare Figures IV-38 and IV-39. The extended period of monotonically decreasing syngas flow rate is attributed to the presence of reinforcing fibers in the tires.

Figure IV-38 shows the evolution of syngas flow rate from the pyrolysis of rubber tire. Note the different scales in the two figures IV-37 and IV-38. The syngas flow rate starts at a high value followed by a steep decrease in flow rate. The peak value of syngas flow rate at 900^{o}C was higher than that at 800^{o}C. This is attributed to the higher heating rate of volatile matter in the sample in case of the higher reactor temperature. The increase in reactor temperature shifts the

peak value of flow rate toward shorter residence time in the reactor and is attributed to the higher heating rate in case of the high reactor temperature.

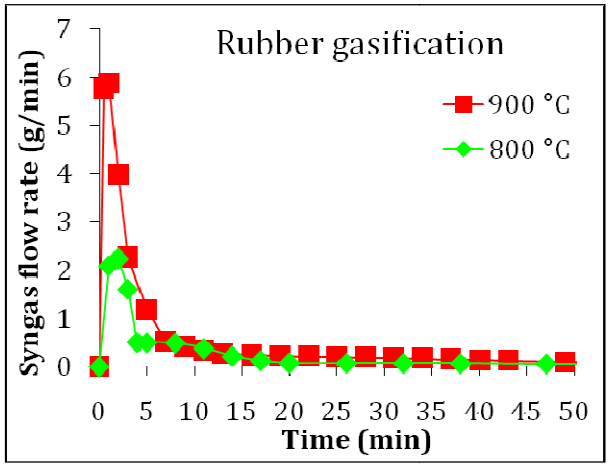

Figure IV-37. Evolution of syngas flow rate during rubber gasification

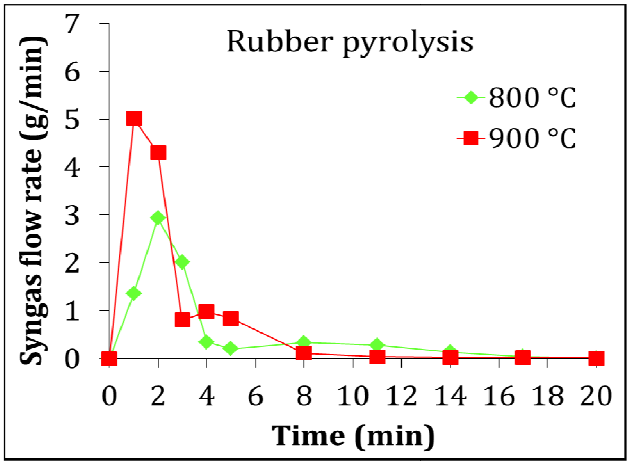

Figure IV-38. Evolution of syngas flow rate during rubber pyrolysis

Figure IV-39 shows the evolution of hydrogen flow rate from the pyrolysis of rubber at the same two temperatures of 800 and 900°C as that examined under gasification condition. The results show the same trend as the syngas flow rate. The hydrogen flow starts with a peak value followed by a steep decrease in the flow rate. The increase in reactor temperature from 800 to 900°C increased the peak value of hydrogen from approximately 0.023g/min to 0.053g/min. and this significant increase of over 50 percent is attributed to enhanced thermal breakdown of long chains of hydrocarbons in the sample with increase in temperature.

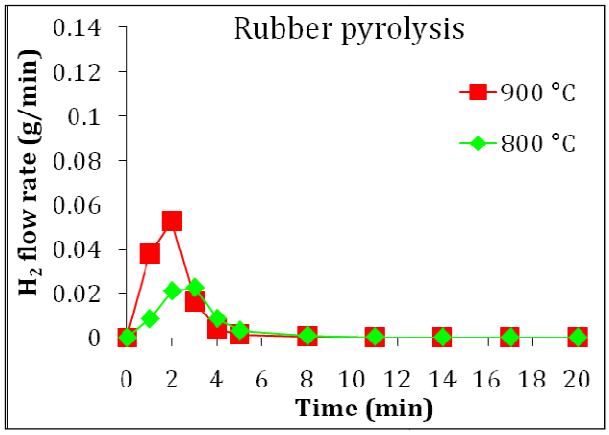

Figure IV-39. Evolution of hydrogen flow rate during rubber pyrolysis

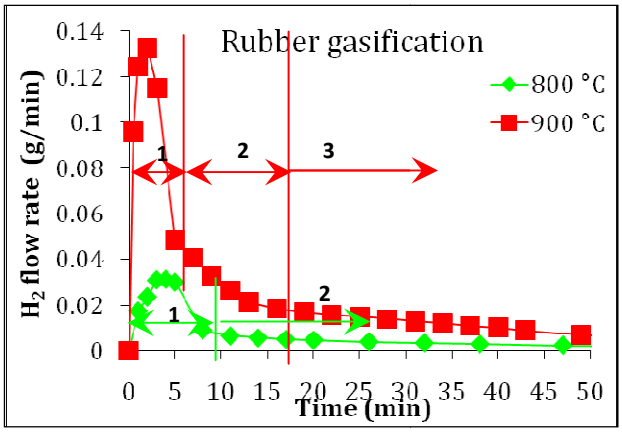

Figure IV-40. Evolution of hydrogen flow rate during rubber gasification

Figure IV-40 shows the evolution of hydrogen flow from the gasification of rubber at 800 and 900°C. It is important to note the tremendous increase in the peak value of hydrogen associated with the increase in reactor temperature from 800 to 900°C in case of gasification. The peak value of hydrogen flow increased from approximately 0.031g/min to approximately 0.132 g/min. This clearly indicates that steam hydrocarbons reforming reactions increase with the increase in reactor temperature. The hydrogen flow rate curve for the 800°C can be divided into two regions wherein the first region is dominated by hydrogen evolution due to pyrolysis and is characterized by a steep increase in flow rate followed by steep decrease in flow rate. The second region is dominated by hydrogen evolution due to char gasification and is characterized by monotonically decreasing flow rate of hydrogen.

In contrast, the hydrogen evolution for the 900°C run case can be divided into three regions. The first region is dominated by hydrogen evolution due to rubber pyrolysis, the third region is hydrogen evolution due to char gasification and the middle region is the hydrogen flow rate due to simultaneous evolution of hydrogen from rubber pyrolysis, steam reforming reactions

and steam char reactions A possible reason for the slow reaction rate, and extended duration for char gasification, could be from the third region shown in Figure IV-40 wherein the diffusion limited char oxidation region might be hindered by increased value of ash with time in the char-steam reaction. One can see that the slope of hydrogen flow rate represents an average value of hydrogen evolution from region one and region three.

4.1.5.2. Syngas, hydrogen and energy yield

The effect of reactor temperature on overall yield of syngas, hydrogen and energy from gasification and pyrolysis conditions are now discussed.

Figure IV-41 show the overall yield of syngas from gasification and pyrolysis at the two reactor temperatures of 800 and 900^{o}C. Gasification always yielded higher syngas as compared to pyrolysis. The increase in reactor temperature increased the syngas yield from both gasification and pyrolysis.

Figure IV-42 shows a direct comparison of the overall yield of hydrogen from gasification and pyrolysis at reactor temperatures of 800 and 900^{o}C. Gasification resulted in significant increase in hydrogen yield at both the temperatures examined here. Gasification resulted in 500% increase in hydrogen yield as compared to pyrolysis at 800^{o}C. However at 900^{o}C, the gasification resulted in more than 700% increase as compared to pyrolysis. Increase in reactor temperature from 800 to 900^{o}C under pyrolysis conditions resulted in 64% increase in hydrogen yield. However, under gasification conditions the corresponding increase in hydrogen yield was 124%. This suggests that the gasification results in not only increased amounts of hydrogen in the syngas but also at higher gasification temperatures the percent increase of hydrogen is higher. The results suggest that high temperature conditions are favorable for increased amounts of syngas yield, energy yield and hydrogen yield in the case of steam assisted

gasification. At low temperature conditions the amounts of energy yield is similar from pyrolysis and gasification. This is because the gasification reactions dominate only at higher temperatures. For biomass wastes the gasification reactions dominate at temperatures greater than 700°C while for the rubber sample the gasification reactions become important at temperatures close to 900°C.

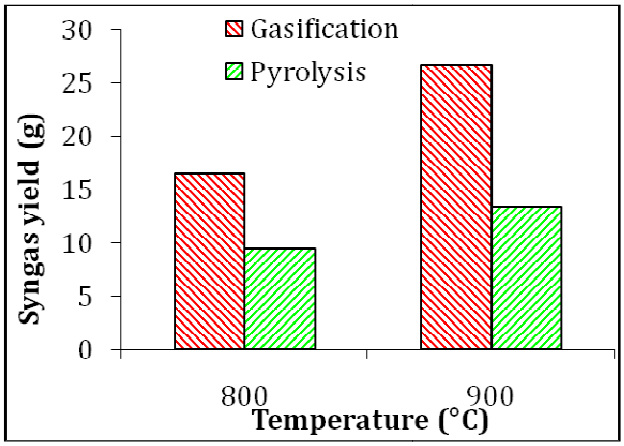

Figure IV-41. Syngas yield from rubber gasification and pyrolysis

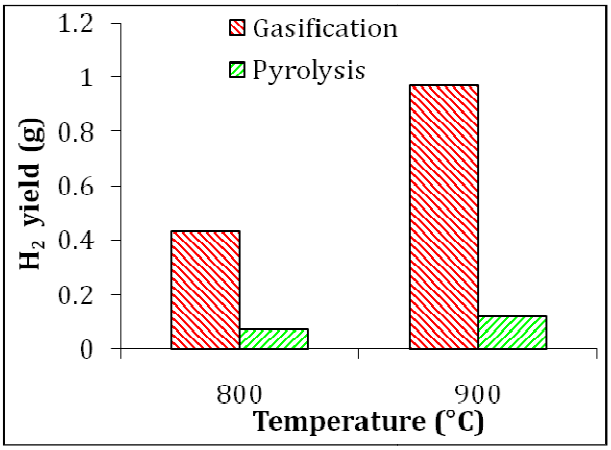

Figure IV-42. Hydrogen yield from rubber gasification and pyrolysis

Figure IV-43 shows the overall yield of energy from the rubber sample obtained from gasification and pyrolysis at reactor temperatures of 800 and 900°C. Gasification yielded almost the same energy as pyrolysis at a reactor temperature of 800°C. This behavior is significantly different from that observed for a cellulosic sample, such as paper, cardboard and woodchips, at this temperature. Gasification always yielded more energy than pyrolysis at 800°C. Consequently, if energy yield is the main focus from a process it is important to maintain a higher reactor temperature (900°C) for the gasification of rubber. At this temperature the gasification time is also shorter.

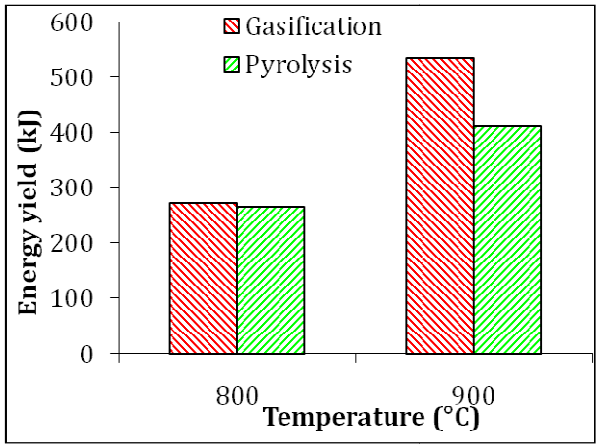

Figure IV-43. Energy yield from rubber gasification and pyrolysis

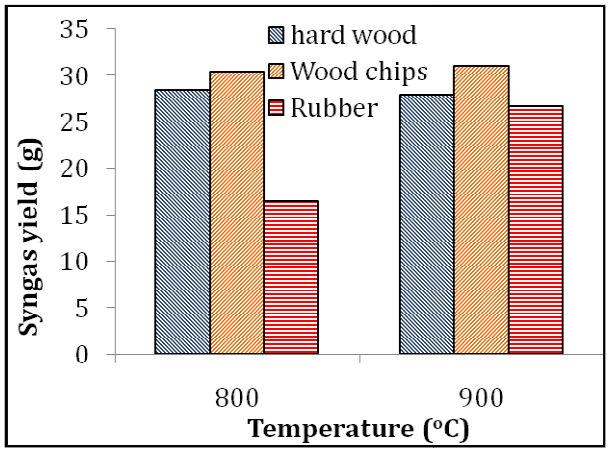

Figure IV-44. Syngas yield from hard wood, wood chips and rubber gasification

4.1.5.3. Comparison with biomass samples

A comparison between rubber gasification and woody biomass samples is now presented with focus on syngas yield, hydrogen yield and energy yield.

Figure IV-44 shows the syngas yield form the gasification of hard wood, wood chips and rubber at two reactor temperatures of 800 and 900°C. The results show that reactor temperature did not affect the overall syngas yield from any of the woody samples. On the other hand, increase in reactor temperature increased the syngas gas yield from the rubber sample. This indicates the importance of reactor temperature in enhancing steam hydrocarbons reforming reactions for the rubber sample.

Figure IV-45 shows the hydrogen yield from the gasification of hard wood, wood chips and rubber at two different temperatures of 800 and 900°C. Increase in reactor temperature slightly increased the hydrogen yield in case of the woody biomass samples. However, for rubber gasification, increase in reactor temperature doubled the hydrogen yield. It is to be noted that

rubber yielded less hydrogen than the biomass samples for all the cases examined here. This is because of low hydrogen to carbon ratio in the rubber as compared to woody biomass.

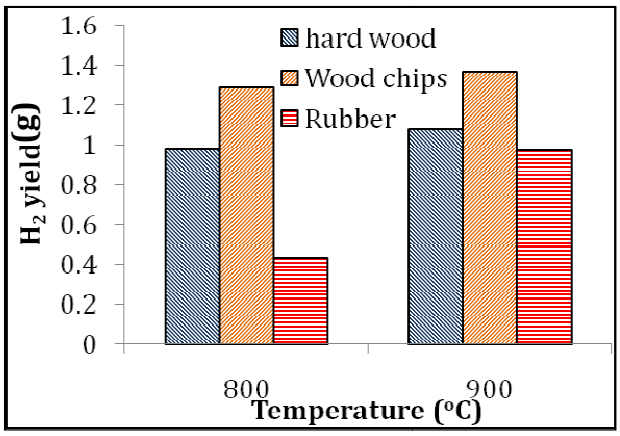

Figure IV-45. Hydrogen yield from hard wood, wood chips and rubber gasification

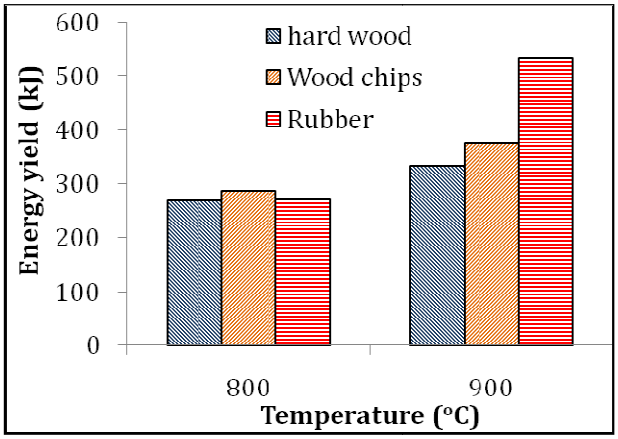

Figure IV-46. Energy yield from hard wood, wood chips and rubber gasification

Figure IV-46 shows the energy yield from the two biomass samples and its comparison with the rubber sample. The energy yield from all samples was almost the same at gasification temperature of 800°C. However, at the 900°C rubber yielded much more energy than the two biomass samples. The increase in energy in case of the biomass samples is attributed to enhancement of syngas quality, namely the increase of CO mole fraction. This is because the total syngas yield in case of the hard wood and wood chips is not affected by the reactor temperature. However, the enhancement in energy yield in case of rubber gasification is attributed to both the quantitative and qualitative effects, see figure IV-44. Getting more energy from the rubber gasification than that from the biomass sample indicates the great potential of using rubber waste as fuel in gasification systems. It also indicated that some amounts of rubber are favorable for the co-gasification of wastes. Our previous results on the gasification of plastics and biomass wastes suggests increased yield of syngas and energy from a mixture of biomass

and plastics than the individual gasification of either of the materials. This requires further examination with the use of biomass-rubber mixtures.

Figure IV-47 show the mass of hydrocarbon yield from the gasification of rubber and its direct comparison with hard wood and wood chips at two different reactor temperatures of 800 and 900^{o}C. Rubber yielded more hydrocarbons at both the temperatures. Increase in reactor temperature increased the hydrocarbon yield from rubber gasification. However, the increase in hydrocarbons yield with the increase in temperature did not have the same effect on hard wood and wood chips. These results indicate that the percentage of energy gained from the rubber sample that is in the form of hydrocarbons is higher than that from the biomass samples.

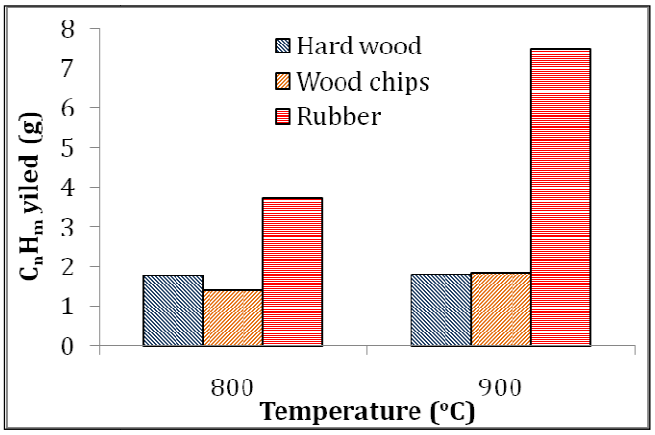

Figure IV-47. Hydrocarbons yield from gasification of hard wood, wood chips and rubber

4.1.6. Cardboard gasification and pyrolysis

Evolutionary behavior of syngas characteristics evolved during the gasification of cardboard has been examined using a semi-batch reactor with steam as a gasifying agent. Evolutionary behavior of syngas chemical composition, mole fractions of hydrogen, CO and CH_4, as well as H_2/CO ratio, LHV (kJ/m^3), hydrogen flow rate, and percentage of combustible fuel in the syngas evolved has been examined at different steam flow rates with a fixed mass of

cardboard waste. The effect of steam to carbon ratio as affect by the steam flow rate on overall syngas properties has therefore been examined. A new parameter, coefficient of energy gain (CEG), has been introduced to provide information on the energy gained from the process. This new parameter elaborates the importance of optimizing the sample residence time in the reactor.

4.1.6.1. Evolutionary behavior of syngas characteristics and the effect of steam flow rate

The evolutionary behavior of syngas chemical composition (mole fraction of H_2, CO, and CH_4) as well as H_2/CO ratio, LHV (kJ/m^3) and pure fuel percentage has been examined at steam flow rates of 3.31 4.12, 5.0, 6.33, 7.65 and 8.9 g/min. The major chemical species determined here where: H_2, CH_4, CO, CO_2 and C_nH_m (consisting of mainly C_2H_2, C_2H_4, C_2H_6, C_3H_8 and C_3H_6). Pure fuel flow rate is defined here as syngas flow rate minus CO_2 flow rate. Pure fuel percentage is defined as the pure fuel flow rate divided by the syngas flow rate. Figure IV-48 shows characteristic evolutionary behavior of selected major gases in the syngas during gasification (Figure IV-48a and b) and during pyrolysis at same temperature (Figure IV-48c). The inclusion of pyrolysis results at same temperature is to aid explaining the syngas behavior in the first three minutes of gasification and for comparison as well.

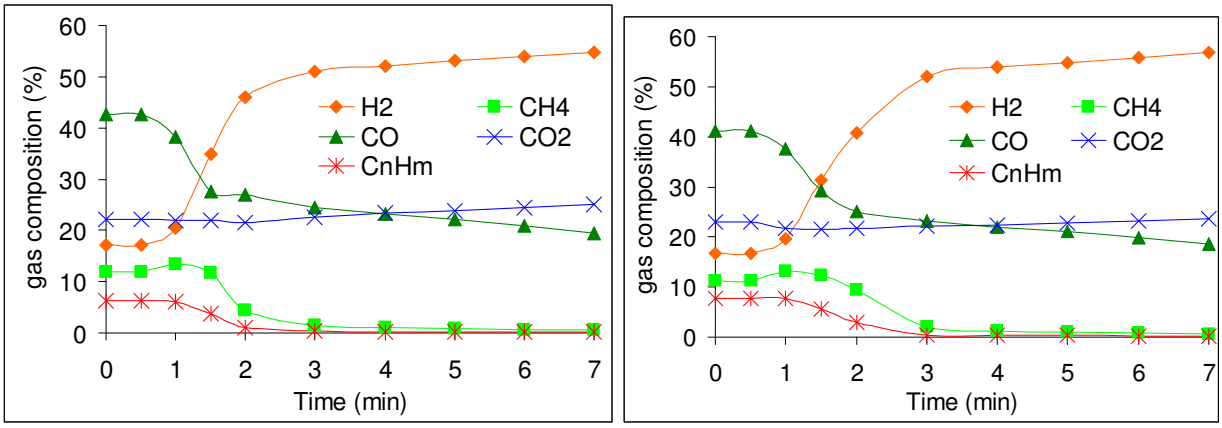

(a) (b)

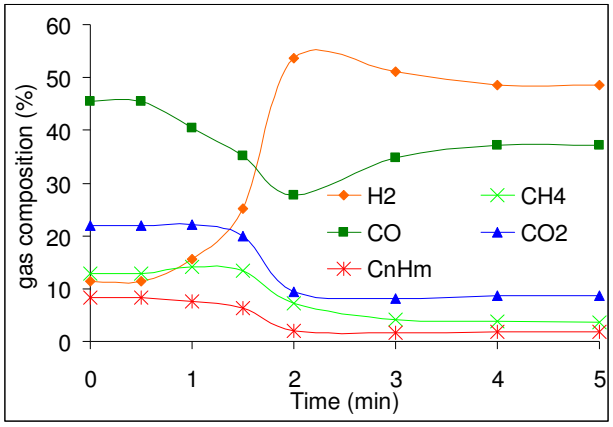

(c)

Figure IV-48. Evolutionary behavior of syngas chemical composition (a) gasification at steam flow rates of 4.12 g/min (b) gasification at steam flow rates of 5.0 g/min and (c) Pyrolysis at same temperature (900^{o}C)

The results show that the evolutionary behavior of syngas at all the steam flow rates examined provides the same trend qualitatively. Hydrogen in the syngas starts at a relatively small mole fraction followed by a steep increase between the first and the second minute into gasification. Higher gasification times beyond 2 minutes results in a slow and linear increase in hydrogen molar ratio. On the other hand carbon monoxide mole fraction starts at a high concentration then experience a steep decrease between the first and the second minute. This is attributed to the rapid pyrolysis process occurring at the beginning (the sample temperature is raised from room temperature to reactor temperature in a very short time). The increase in hydrogen formation is due to the endothermicity of hydrogen formation (from the water gas reaction: $C + H_2O \Leftrightarrow CO + H_2O + 131$ KJ/Kmol). The rapid increase in hydrogen mole fraction and rapid decrease in CO mole fraction can be better explained by considering pyrolysis results of syngas chemical composition with time (see figure IV-48c). In the pyrolysis results one can see that hydrogen starts with a relatively small mole fraction and CO starts with a high mole

fraction. However, between the first and second minute there is a steep increase in hydrogen mole fraction accompanied by a steep decrease in CO mole fraction. This behavior is similar to that of gasification in the first two minutes. This similarity indicates the domination of pyrolysis at the beginning of gasification. On the other hand, there is a difference in mole fractions behavior after the second minute between gasification and pyrolysis. In case of gasification hydrogen mole fraction keep on increasing and CO mole fraction keep on decreasing. In case of pyrolysis, hydrogen mole fraction is showing a peak and CO mole fraction is showing a minimum at the same time. This difference in behavior between gasification and pyrolysis after the third minute is attributed to presence of char gasification in case of steam gasification.

The results show a linear decrease in CO mole fraction and an increase in the CO_2 mole fraction after the third minute. This is attributed to the effect of the water gas shift reaction ($CO + H_2O \Leftrightarrow CO_2 + H_2$) which favors the formation of H_2 and CO_2 at the expense of CO. The water gas shift reaction has this tendency because of the gradual increase of steam to sample ratio with time in the batch reactor. This increase in steam to sample ratio increases the steam concentration in the reactor which accelerates the forward reaction rate for the water gas shift reaction.

Mole fractions of hydrocarbons like CH_4 and C_nH_m are showing a considerable mole fraction at the beginning followed by a rapid decrease between the first and third minute. This behavior is consistent in both gasification and pyrolysis runs. Consequently, Hydrocarbons yield in the gasification process is mainly attributed to sample pyrolysis in the initial stage of gasification.

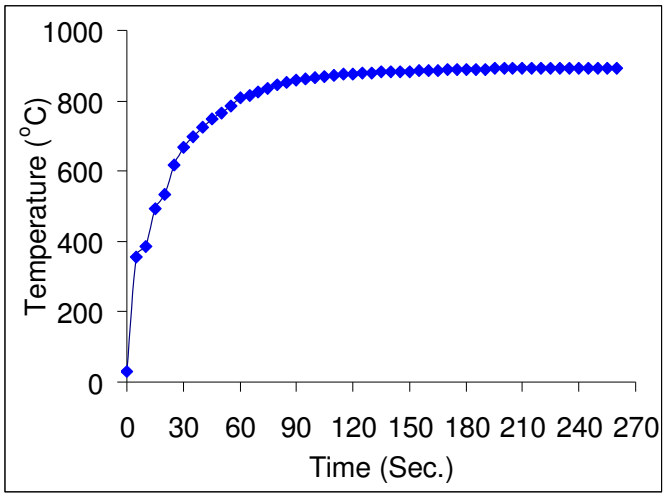

Figure IV-49. Change of sample temperature with time

Figure IV-50 shows the evolution of H_2 flow rate. The hydrogen flow rate increases with increase in steam flow rate. This is because of the increase in forward reaction rate in the water gas reaction ($C + H_2O \Leftrightarrow CO + H_2$ +131 KJ/Kmol), water gas shift reaction ($CO + H_2O \Leftrightarrow CO_2 + H_2$) and steam-hydrocarbons reforming reactions ($C_nH_x + mH_2O \Leftrightarrow nCO + (m + x/2)\ H_2$) and steam-tar reforming reactions. The above curve (Figure IV-50) exhibits a peak in hydrogen flow rate between the first and the second minute. This peak is implicitly a result of two evolutionary behaviors of syngas; the first is the increase in hydrogen molar concentration with time. The second is the decrease in bulk flow rate of syngas with time. The increase in hydrogen molar fraction tends to increase the hydrogen flow rate, while the decrease of bulk flow rate of syngas tends to decrease the hydrogen flow rate. Combination of these two behavior results in a peak flow rate of hydrogen at approximately the second minute. In addition the evolution of H_2 due to pyrolysis also occurs at elevated temperature in the range of 550–800^{O}C and the sample is expected to reach this temperature in about 90 seconds, see figure IV-49**.**

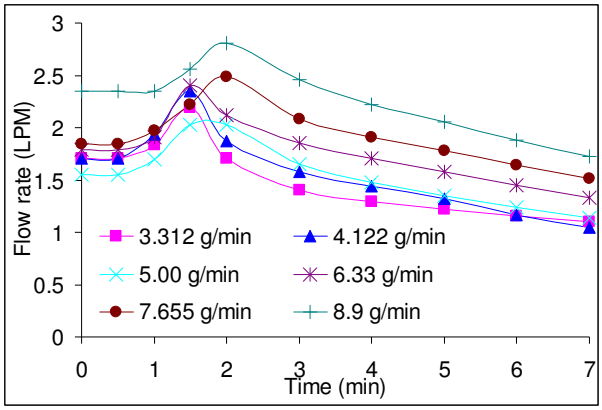

Figure IV-50. Evolutionary behavior of H_2 flow rate at different steam flow rates

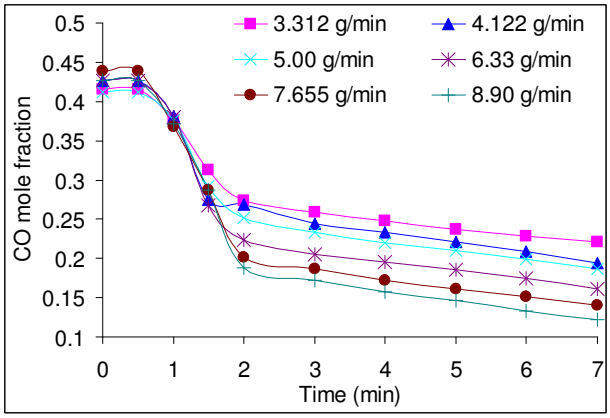

Figure IV-51. Evolutionary behavior of CO mole fraction at different steam flow rates

Figures IV-51, IV-52 and IV-53 show the evolution of CO mole fraction, CH_4 mole fraction and H_2/CO ratio at different steam flow rates, respectively. CO mole fraction for different steam flow rates is showing same qualitative behavior. As mentioned before the general trend of CO mole fraction is a high mole fraction of CO initially then a steep decrease between the first and second minute, then a monotonically decrease after the third minute. This is attributed to faster evolution of CO than hydrogen during pyrolysis. This is confirmed by the trend shown in figure IV-48c. Increase in steam flow rate resulted in a decrease in CO mole fraction for the same gasification timing. This is attributed to the water gas shift reaction.

Evolution of CH_4 mole fraction should be interpreted in terms of pyrolysis occurring initially, since formation of methane due to methanation reactions ($C + 2H_2 \Leftrightarrow CH_4$) is known to be so slow, especially if compared to fast devolatilization of cellulose during the pyrolysis process. Methane mole fraction shows a peak at the first minute (Figure IV-52). This peak indicates presence of two competitive factors. The first factor is presence of high volatile content in the sample initially, which decreases with time. The second factor is the continuous increase in sample temperature with time in the first 90 second. The first factor tends to favor a high

methane mole fraction initially with a steep decrease in mole fraction with time, while the second factor tends to increase volatile matter yield, including methane, with time. Increasing the steam flow rate didn't have a significant effect on CH_4 mole fraction. This confirms that methane evolution is mainly attributed to sample pyrolysis. The above interpretation can be summarized in the following equation.

$$\frac{dV_{CH_4}}{dt} = K(V^*_{CH_4} - V_{CH4})^n$$
$$K = A_o \exp[-E/RT]$$

Where V_{CH4}, V^*_{CH4} *and* K are the amount of CH_4 evolved, the maximum potential amount of CH_4 and the rate constant respectively. The $(V^*_{CH4} - V^*_{CH4})$ term decreases with time, while the rate constant, K, increases with time.

The evolutionary behavior of H_2/CO reveals the same qualitative behavior. However, the increase in steam flow rate increases the H_2/CO ratio (Figure IV-53). This effect is more pronounced at longer time (minutes) into gasification and not seen in the first 90 seconds. This is because at the beginning of gasification, pyrolysis takes place so that the loner hydrocarbon chains breaks down into small components of gaseous structures. Since all steam flow rates share the same pyrolysis process at the beginning of gasification, the H_2/CO ratio has the same value at all steam flow rates examined during the first 90 seconds. The monotonically increase in H_2 mole fraction and decrease of CO mole fraction after the third minute results from the water gas shift reaction ($CO + H_2O \Leftrightarrow CO_2 + H_2$).

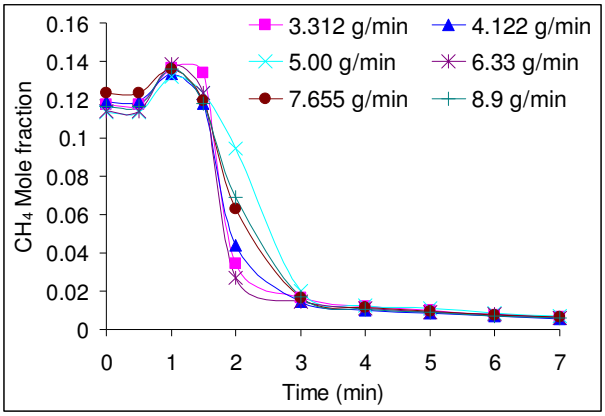

Figure IV-52. Evolutionary behavior of CH_4 mole fraction at different steam flow rates

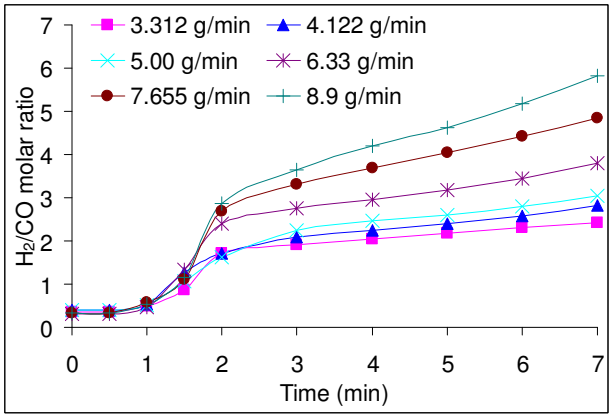

Figure IV-53. Evolutionary behavior of H_2/CO ratio at different steam flow rates

Figure IV-54 shows the evolutionary behavior of fuel (i.e., syngas – CO_2 in the syngas) at different steam flow rates. High steam flow rates results in increased fuel percentage at longer residence time (or higher steam/sample ratios). Figure IV-55 shows that LHV (kJ/m^3) starts at a high value and then decays with longer residence in the reactor. This is attributed to high concentration of carbon monoxide at the beginning of gasification which transforms CO and tars to fuel-rich syngas. At later times into gasification the concentration of carbon monoxide decreases and concentration of hydrogen increases which has less heating value (in kJ/m^3) as compared to the heating value of carbon monoxide. On the other hand increasing the steam flow rate increases the LHV (kJ/m^3) only slightly. However, fuel percentage remains almost constant with time. Increase in the steam flow rate increases the pure fuel percentage slightly due to the increase in hydrogen mole fraction in syngas.

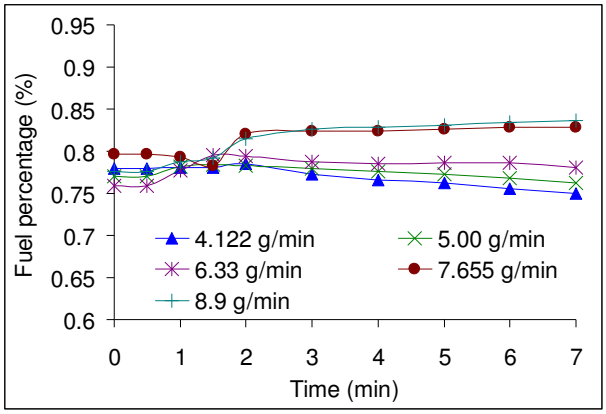

Figure IV-54. Evolutionary behavior of Fuel % in syngas at different steam flow rates

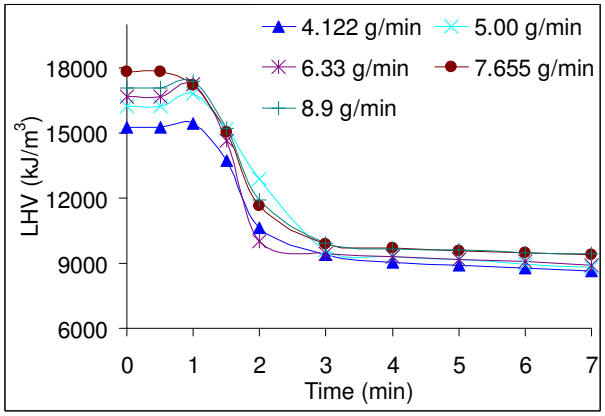

Figure IV-55. Evolutionary behavior of syngas LHV (kJ/m^3) at different steam flow

4.1.6.2. Effect of steam flow rate on overall syngas characteristics

The above results have clearly shown that the syngas properties change with time into gasification. The overall behavior of syngas, defined as the time integral of syngas properties, is now presented. For example, the overall syngas yield (in liters) is the time integral of syngas flow rate (LPM) and overall syngas heating value is the time integral of output power (kJ/min) divided by time integral of syngas flow rate (kg/min or LPM).

Figures IV-56 to IV-62 show the effect of steam flow rate on syngas composition, pure fuel yield (liters) and overall fuel percentage in syngas (%), apparent thermal efficiency and energy yield (kJ), overall LHV (kJ/m^3) and (kJ/kg), hydrogen yield (liters) and overall hydrogen to carbon monoxide molar ratio (Kmol/Kmol), carbon conversion and syngas yield (kJ), and coefficient of energy gain.

The major components in the syngas were evaluated as a function of the steam flow rate and are presented in figure IV-56. The results show an increase in hydrogen mole fraction in the syngas with increase in the steam flow rate. On the other hand both carbon monoxide and carbon dioxide mole fraction decreases with increase in the steam flow rate. Almost constant behavior

of the methane mole fraction shows that steam flow rate has insignificant effect on methane mole fraction. On the other hand increase in steam flow rate increases the pure fuel yield from 22 liters to 32 liters and slightly increases the pure fuel percentage from 77% to 80% which is a direct result of steam reforming process from long chains of hydrocarbons ($C_nH_x + mH_2O \Leftrightarrow nCO + (m + x/2)\ H_2$), see figure IV-57. The pure fuel yield increases due to the accelerated reaction rate with increase in the steam concentration in the reactor which in turn increases the syngas yield.

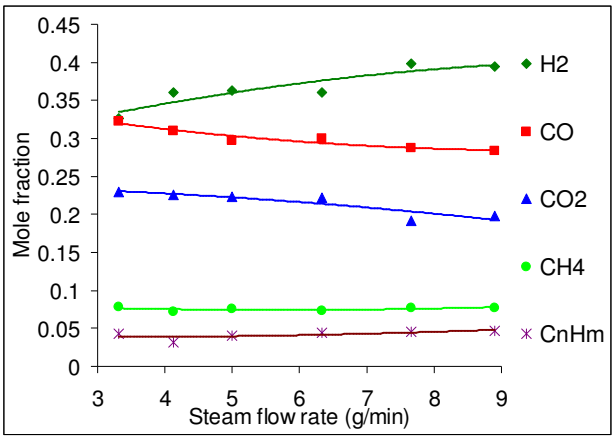

Figure IV-56. Effect of steam flow rate on syngas composition

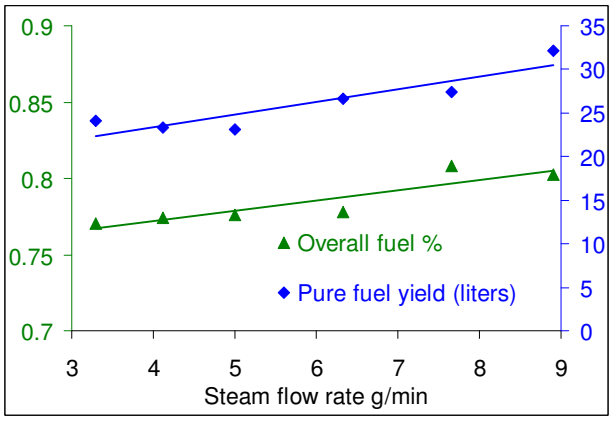

Figure IV-57. Effect of steam flow rate on pure fuel yield and pure fuel %

Apparent thermal efficiency is defined as energy yield from syngas divided by energy yield from the solid fuel sample. The results are shown in figure IV-58. The apparent thermal efficiency increases with increase in the steam flow rate. This is a direct result of the pure fuel yield increase with the increase in steam flow rate, which in turn increases the total out power accompanied from the syngas. Note that the thermal efficiency is described as an apparent thermal efficiency because of two reasons; first is that part of the hydrogen generated in the syngas is a result of the steam biomass reaction, and the second reason is that the heat required for the endothermic gasification reaction is provided by an outer source of heat supply (in this case an electric heating furnace).The increase in steam flow rates increases the LHV of the

syngas produced based on both volume and mass basis, see fig IV-59. At high steam flow rates examined here the LHV of the syngas obtained was about 14,000kJ/m^3. This is a quite high LHV of the syngas as compared to that reported in the literature from gasification of cellulose and paper waste.

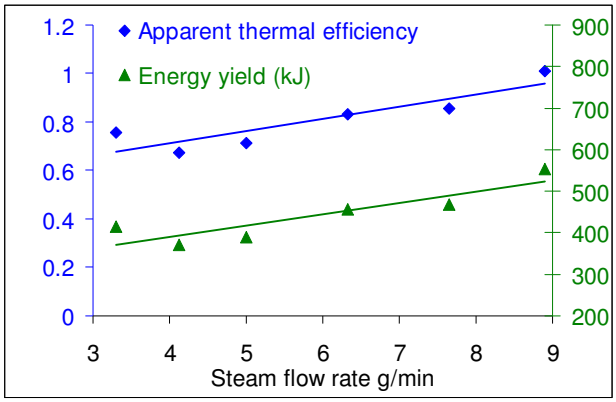

Figure IV-58. Effect of steam flow rate on apparent thermal efficiency and energy yield

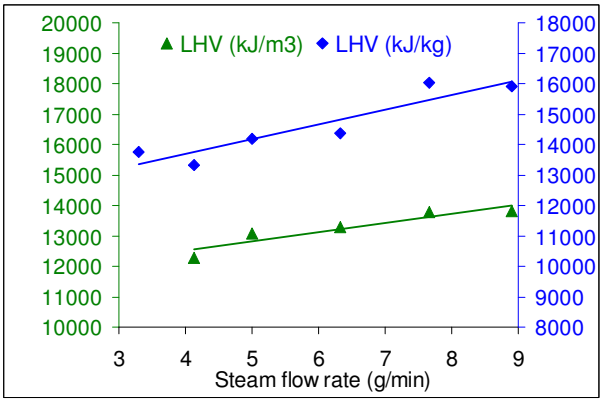

Figure IV-59. Effect of steam flow rate on overall LHV, (kJ/m^3) and (kJ/kg)

The increase in overall H_2/CO ratio and H_2 molar ratio with increase in the steam flow rate (figure IV-60) is due to two reasons; first the acceleration of forward reaction rate of the CO Shift reaction ($CO + H_2O \Leftrightarrow CO_2 + H_2$ -41 kJ/Kmol). Second is due to the acceleration of forward reaction rate of steam methane reforming reaction ($CH_4 + H_2O \Leftrightarrow CO_2 + 3H_2$ + 206 MJ/kmol). On the other hand increasing the steam flow rate increases the LHV on both mass and volume basis (kJ/kg) and kJ/m^3). This is due to the slight increase of pure fuel percentage in syngas with increase in the steam flow rate.

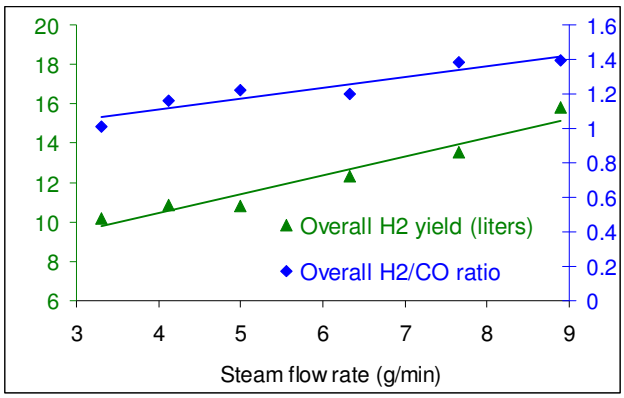

Figure IV-60. Effect of steam flow rate on H_2 yield and overall H_2/CO ratio

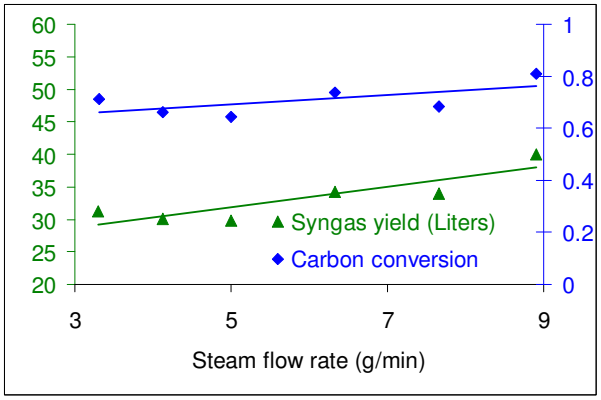

Figure IV-61. Effect of steam flow rate on carbon conversion (%) and syngas yield (liters)

The carbon conversion is defined as the ratio of carbon in syngas to the carbon initially contained in the sample. Increase in steam flow rate has a slight effect on increase in the carbon conversion. This is due to the acceleration of gasification forward reaction rates with the increased concentration of steam in the reactor. Both the carbon conversion and syngas yield increase with increase in steam flow rate (see figure IV-61).

4.1.6.3. Coefficient of energy gain (CEG)

The coefficient of energy gain (CEG) is defined as the ratio of energy gained by syngas to the total energy utilized in the gasification process. The total energy utilized is the time integral of the average power consumed by the electric heating furnace and the estimated energy needed for heating up the steam to the desired temperature. Despite the fact that more energy is needed for heating up the steam for higher steam flow rates, increasing the steam flow rate increased the CEG. Figure IV-62 shows the effect of steam flow rate on CEG at different residence time (1.5, 2, 3, 5 and 7 minutes) in the reactor. The results show that smaller residence time results in higher (average) CEG which is to be expected due to high flow rate of syngas at

the beginning of the process. While it is worthwhile to have a high CEG but at the expense of loss of total energy yield and total hydrogen yield since there will be not enough time to extract all the available energy in the sample, i.e., this will lower the apparent thermal efficiency and the carbon conversion.

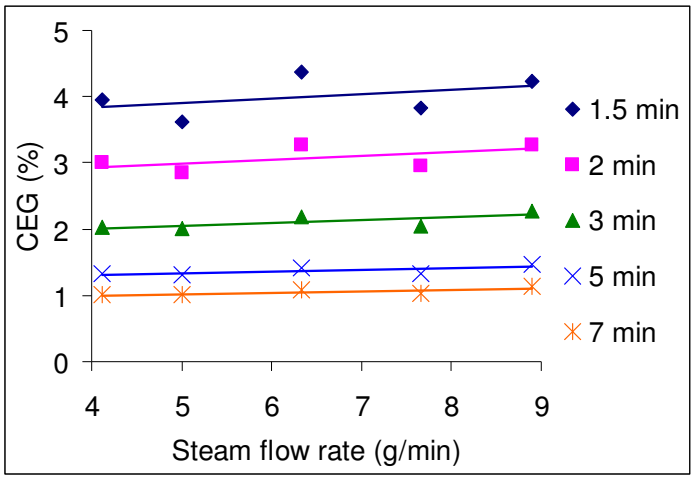

Figure IV-62. Effect of steam flow rate on coefficient of energy gain (CEG) at different sample residence time in the reactor

4.1.7. Cardboard pyrolysis

Evolutionary behavior on the yield of various gaseous components during pyrolysis of cardboard has been investigated using a semi-batch reactor. Specifically, the behavior of syngas flow rate and chemical composition of syngas have been examined at various pyrolysis temperatures with variation of cardboard residence time in the reactor. The syngas properties determined include evolutionary behavior of concentrations of hydrogen, CO, CO_2 and hydrocarbons in the syngas as well as temporal behavior of syngas flow rate. The temporal behavior of syngas heating value, output power, H_2/CO ratio, pure fuel percentage in syngas and apparent thermal efficiency have also been examined. The results showed that the reactor

temperature has distinct effect on the evolutionary behavior of syngas properties during pyrolysis, specially the peak position of hydrogen yield and H_2/CO molar ratio.

4.1.7.1. Evolutionary behavior of syngas characteristics

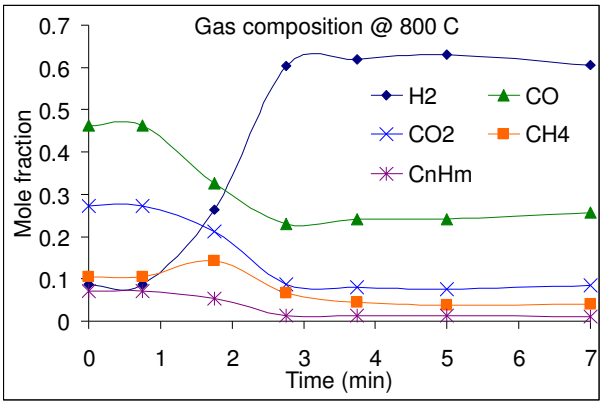

Figure IV-63. Evolution of syngas chemical composition at reactor temperature of 800^0C

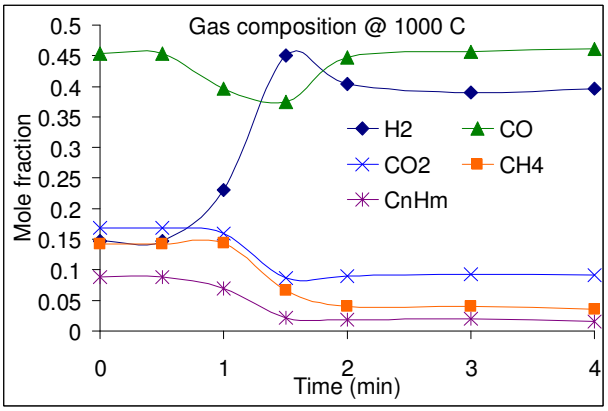

Figure IV-64. Evolution of syngas chemical composition at reactor temperature of 1000^0C

Figures IV-63 and IV-64 show a change in syngas chemical composition with residence time of the sample in the reactor. These results show that the trend is similar for all gaseous species except H_2 which showed a sharp increase in mole fraction at the beginning of the process. CO_2, CH_4 and C_nH_m show a gradual decrease with time. However, CO show an initial decrease in mole fraction followed by steady state levels at reactor temperature of 800^0C, while at 1000^0C reactor temperature a local minimum in mole fraction followed by steady state value is obtained at longer residence times in the reactor. Comparing figures IV-63 and IV-64 reveals an average increase in CO mole fraction and an average decrease in CO_2 mole fraction. This increase in CO mole fraction with the corresponding decrease in CO_2 mole fraction can be explained from the kinetics study of Banyasz et al.[42] which suggests a mechanism that support the presence of competing routes for CO and CO_2 formation. Their study showed that the CO formation route accelerates with the increase in heating rate (reactor temperature). However CO_2

formation mechanism is not affected equivalently with the increase in reactor temperature. Details of this mechanism are introduced in section 4.1.7.2.

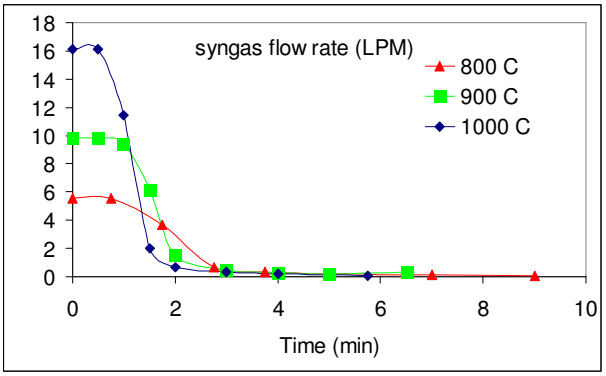

Figure IV-65. Evolution of syngas flow rate at different reactor temperatures

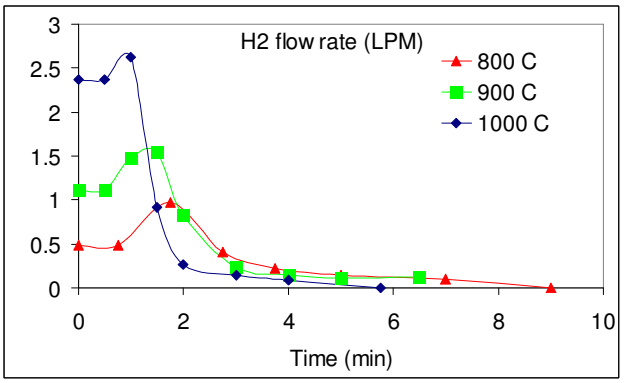

Figure IV-66. Evolution of H_2 flow rate at different reactor temperatures

Evolutionary behavior of syngas flow rate shows a high flow rate at the beginning of pyrolysis then a steep decrease in syngas flow rate between the first and the third minute see figures IV-65 and IV-66. The steep decrease depends strongly on the nominal reactor temperature. In general higher reactor temperature results in steeper decrease in hydrogen and syngas flow rate. For example; flow rate decreased from 16 LPM to 2 LPM in 1 minute at reactor temperature of 1000^{o}C, while it decreased from 6 LPM to 2 LPM in 1.75 minutes at reactor temperature of 800^{o}C. In contrast increase in the nominal reactor temperature increases the syngas flow rate. This effect is more evident during the initial first minute of pyrolysis. This is due to the endothermicity of cellulose cracking process and the increase in heating rate with the increase in reactor temperature.

Hydrogen flow rate showed a different evolutionary behavior than the syngas flow rate. Evolutionary behavior of hydrogen flow rate is characterized by a peak value in flow rate. The location of flow rate peak is affected by the reactor temperature. The location of peak value of

flow rate shifts towards shorter residence time at increased reactor temperature. Presence of a local peak in hydrogen flow rate is attributed to two competing effects. The first effect is the increase in hydrogen flow rate due increase in sample temperature and sample heating rate. The second effect is the decrease in hydrogen flow rate with time due to the decrease in hydrogen content in the solid sample. Eventually, hydrogen content in the sample reaches an asymptotic value of zero, consequently the hydrogen flow rate exhibits a decreasing trend until it reaches zero.

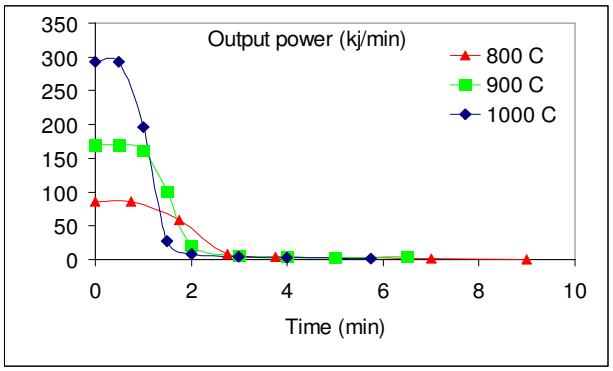

Figure IV-67. Evolution of output power at different reactor temperatures

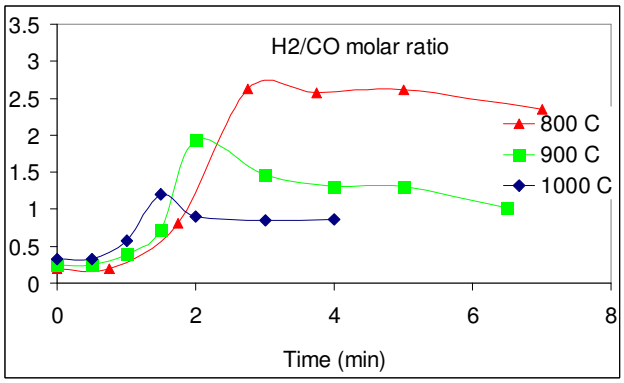

Figure IV-68. Evolution of H_2/CO ratio at different reactor temperatures

The output power is defined here as the syngas flow rate multiplied by the syngas heating value Output power released as chemical energy contained in the syngas was examined at various pyrolysis temperatures and the results are shown in figure IV-67. The output power obtained show a similar behavior to that of syngas flow rate (high output power initially then a steep decrease between the first and the second minute), as expected. Increase in reactor temperature increased the converted energy from the solid fuel to the gaseous fuel and hence increased output power.

The molar ratio of hydrogen to carbon monoxide shown in figure IV-68 reveal a qualitatively similar behavior of local peak occurrence at some residence time for the three reactor temperatures examined here. The peak value shifts towards lower reaction time with increase in the reactor temperature. At the beginning of pyrolysis process (first 1.75 minutes) increase in reactor temperature increased the ratio of hydrogen to carbon monoxide slightly, while this trend opposed after 2.5 minutes into pyrolysis. The overall effect of reactor temperature on H_2/CO ratio will be discussed further later on in the paper.

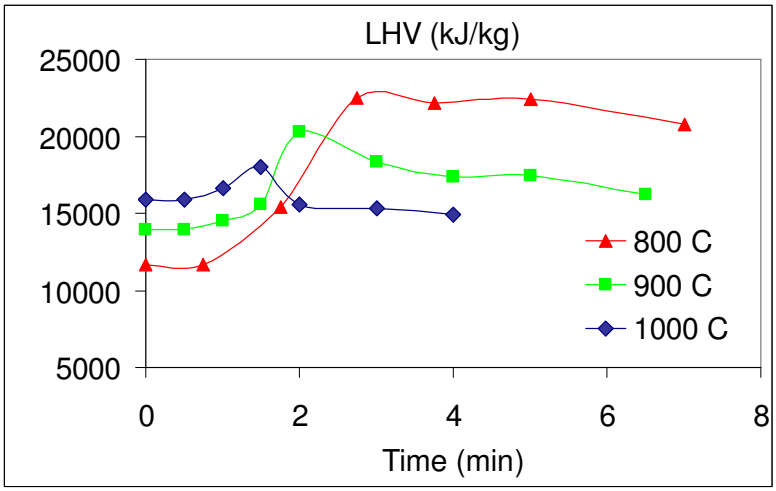

Figure IV-69. Evolution of LHV (kJ/kg) for different reactor temperatures

Increase in reactor temperature results in an increase in heating value (HV) of the syngas on mass basis (kJ/kg) for residence time less than 2 minutes, see figure IV-69. However, the data shows opposite trend after the second minute. By comparing this data to the plot of H_2/CO ratio data explains this behavior since the H_2/CO plot shows the same behavior (heating value of hydrogen based on units of kJ/kg is higher than that of carbon monoxide).

4.1.7.2. Characteristics of overall syngas yield

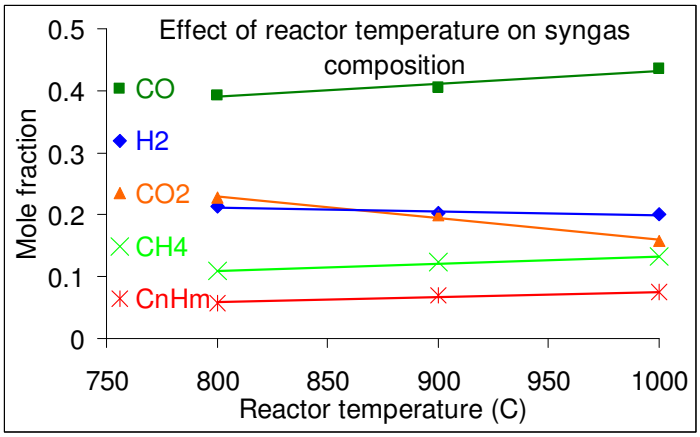

Figure IV-70. Effect of reactor temperature on syngas composition

The reactor temperature has a significant effect on the syngas mole fraction; increase in the reactor temperature increased the CO mole fraction and decreased the CO_2 mole fraction. Hydrogen showed a slight decrease in mole fraction. On the other hand, methane and higher hydrocarbons mole fraction increased slightly with increase in the reactor temperature, see figure IV-70.

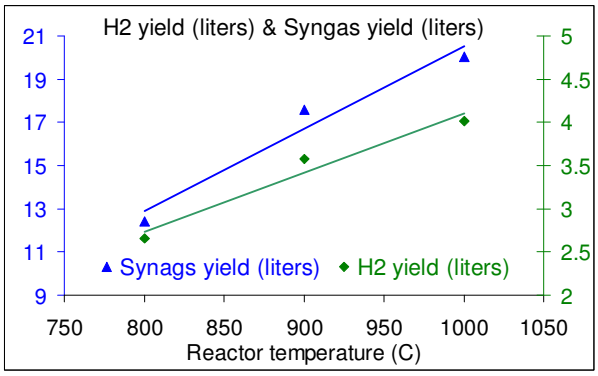

Figure IV-71. Effect of reactor temperature on syngas and H_2 yields

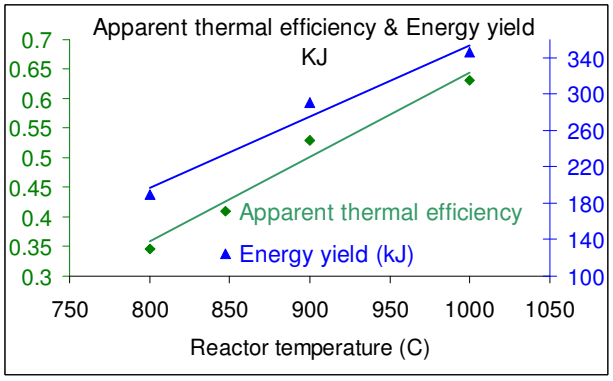

Figure IV-72. Effect of reactor temperature Energy yield (kJ) and apparent thermal efficiency

The overall syngas yield is defined as the time integral of syngas flow rate. Increase in the reactor temperature increased the syngas yield, see figure IV-71. This is due to the effective

breakdown of long chains of hydrocarbons in cardboard and tar into smaller fragments of gaseous hydrocarbons with increase in the reactor temperature. Similarly, increase in the reactor temperature increased the hydrogen yield from the sample. Increase in the reactor temperature assists in cracking of tar during the secondary tar cracking reaction which results in higher hydrogen yield, see figure IV-71.

Apparent thermal efficiency is defined as total energy yield from syngas divided by the energy provided by the solid fuel combustion. Figure IV-72 shows that the apparent thermal increases with increase in the reactor temperature and is from the direct result of increased energy yield with increase in the reactor temperature.

Overall hydrogen to carbon monoxide molar ratio decreased from 0.54 to 0.46 with increase in the reactor temperature, see figure IV-73. This is due to the increase in CO concentration at the expense of decreased CO_2 as mentioned before. Increase in the reactor temperature decreased the tar yields, see figure IV-73. This is because higher temperatures promote the cracking of tar via secondary reactions to smaller fragments of gaseous products.

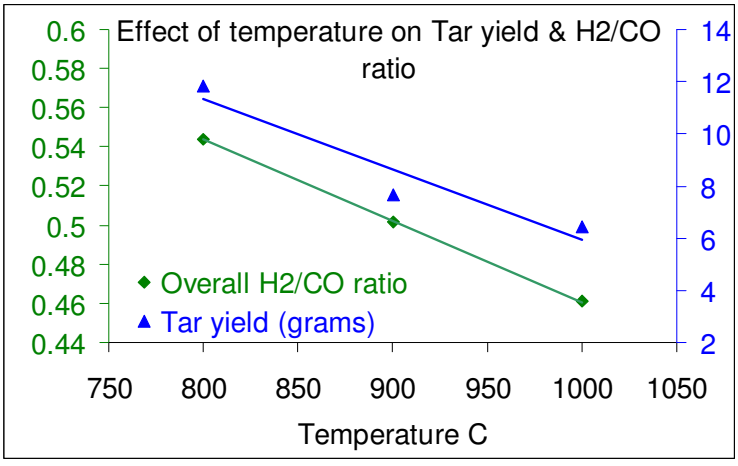

Figure IV-73. Effect of reactor temperature on overall H_2/CO ratio and tar yield (grams)

Banyasz et al.[42] investigated gas evolution and mechanism of cellulose pyrolysis in a two heating zone pyrolysis system. The two heating zone experiments indicated that a large portion of CO is formed from the decomposition of primary volatile products (aldehydes) during secondary reactions. However CO_2 is formed at early stages of cellulose pyrolysis during the primary reactions. In the two heating zone experiment, CO formation was found to be highly dependent on the temperature set at the second zone, while CO_2 was not affected by additional heating, thus indicating further decomposition of vapor products to produce CO [42, 113].

The behavior of CO_2 is adequately described by a single first order reaction. The effect of CO formation requires the incorporation of a competing reaction step into the mechanism. At high temperatures and fast heating rates $k_1 > k_2$ (see figure IV-74), so that at faster heating rate takes less time for conversion to CO while at low temperature the competing reaction preferentially converts the precursor to the competing products (CO_2 and levoglucosan). Therefore at high heating rates CO is preferable since k_1 is larger than k_2 at high temperatures and vice versa. Levoglucosan/tar is the probable predominant product of pathway (2) in the mechanism given below.

Pathway one is a major pyrolysis pathway for cellulose producing intermediates that undergo further reactions yielding formaldehyde, CO and other gases formed during secondary cracking reaction of intermediates generated in pathway one[42].

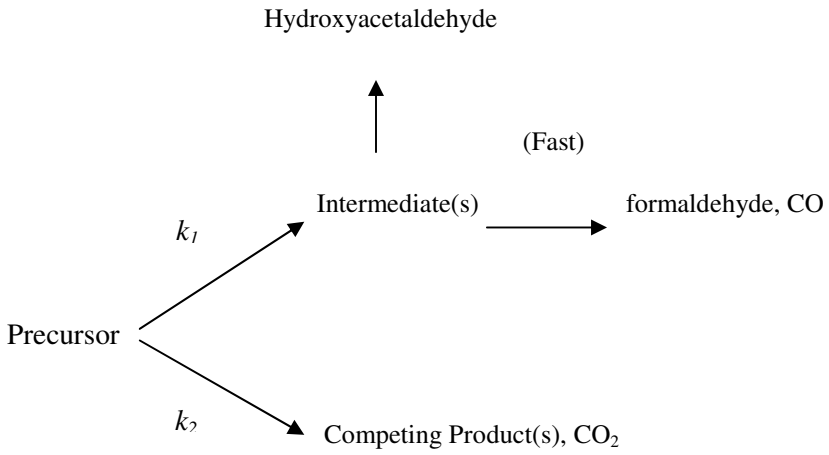

Figure IV-74. Cellulose pyrolysis mechanism [42]

Antal et al. [114] have provided a review on the current state of knowledge on the kinetics of cellulose pyrolysis in which they concluded that two major pathways are now recognized to be active during cellulose pyrolysis. The path leading to the formation of levoglucosan is a relatively stable product while the second yields in glycolaldehyde formation. Higher heating rates and temperatures favor the glycolaldehyde formation pathway[11]. This as well as the conclusion from Banyasz et al. [42] studies confirms that the intermediate forming the formaldehyde and CO is glycolaldehyde and the competing product in pathway (2) is levoglucosan (tar) and CO_2.

4.1.8. Mixture gasification

Gasification of polyethylene (PE) and woodchips (WC) mixtures have been investigated in a semi-batch reactor, using high temperature steam as the gasifying agent. The reactor temperature was maintained at 900^{o}C. The ratio of PE to WC was varied from 0% to 100% in 20% intervals. Characteristics of syngas were evaluated based on the yield of syngas, hydrogen,

energy, ethylene, total hydrocarbons and apparent thermal efficiency of the process. Results show that properties of syngas evolved during gasification of PE-WC blends cannot be determined from the weighted average syngas properties obtained from separate gasification of WC and PE. Superior results in terms of syngas yield, hydrogen yield, total hydrocarbons yield, energy yield and apparent thermal efficiency from PE-WC blends were obtained as compared to expected weighed average yields from gasification of individual components. Results confirm synergistic interaction between PE and WC during high temperature steam gasification of these mixtures. These results also provide the importance of mixing two or more compounds on the performance of stream gasification of wastes.

Presented in the first part of this section is the evolutionary behavior of syngas properties (syngas flow rate, hydrogen flow rate, output power, carbon flow rate, ethylene flow rate and total hydrocarbons flow rate) as affected by PE to WC ratio. The second part presents results on the overall yield of syngas properties (syngas yield, hydrogen yield, energy yield, apparent thermal efficiency, ethylene yield, total hydrocarbons yield and carbon yield).

4.1.8.1. Evolutionary behavior of syngas properties

Figures IV-75a and IV-75b show the evolution of syngas flow rate from 0 to 5 minutes and from 5 to 25 minutes, respectively, as affected by different percentages of PE in the feed stock. Syngas flow rate starts with a high value, from zero to three minutes, followed by a steep decrease in flow rate, from minute 2 to minute 5, followed by an extended period of low flow rate (notice the difference in X and Y axis scale between figure IV-75a and IV-75b. The reason for high syngas flow rate, initially is that the sample was initially at room temperature then injected to the reactor which is at an elevated temperature of 900^{o}C. Consequently the sample is subjected to high heating rate. Besides, the sample initially has its 100% volatile content as well.

Because of the high heating rate and high volatile content, initially, the syngas flow rate starts with a high value. After few minutes the sample becomes in equilibrium with the reactor temperature and a most of the volatile matter has evolved during the initial stage of the process, resulting in a steep decrease in syngas flow rate.

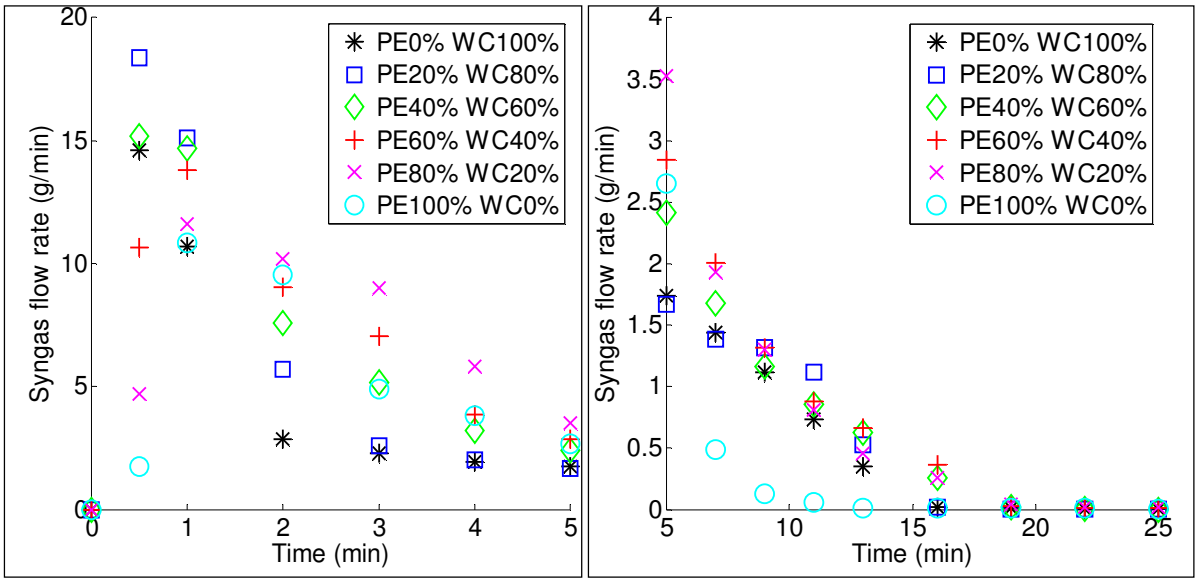

Figure IV-75. Evolution of syngas flow rate (a) from 0 to 5 minutes and (b) from 5 to 25 minutes

The increase in PE percentage tends to decrease the maximum value of syngas flow rate. Except for the 0% PE test conditions, a decrease in the peak value of syngas flow rate is observed. In contrast to the effect of PE% on syngas flow rate, the peak value of hydrogen flow rate increased with increase in the amounts of PE% present in the feed stock, see figure IV-76a. The evolution of hydrogen flow rate curve is also characterized by the initial high value of flow rate, followed by an extended period of lower flow rate, see figure IV-76b. In figure IV-76b, examination of the time period from minute 7 to minute 16, one can notice a lower hydrogen flow rate from the 100% PE run as compared to the other woodchips (WC) containing test

sample. This is attributed to the char - steam gasification reaction ($C + H_2O \Leftrightarrow CO + H_2$), which takes place in case of WC char gasification and absent in case of PE.

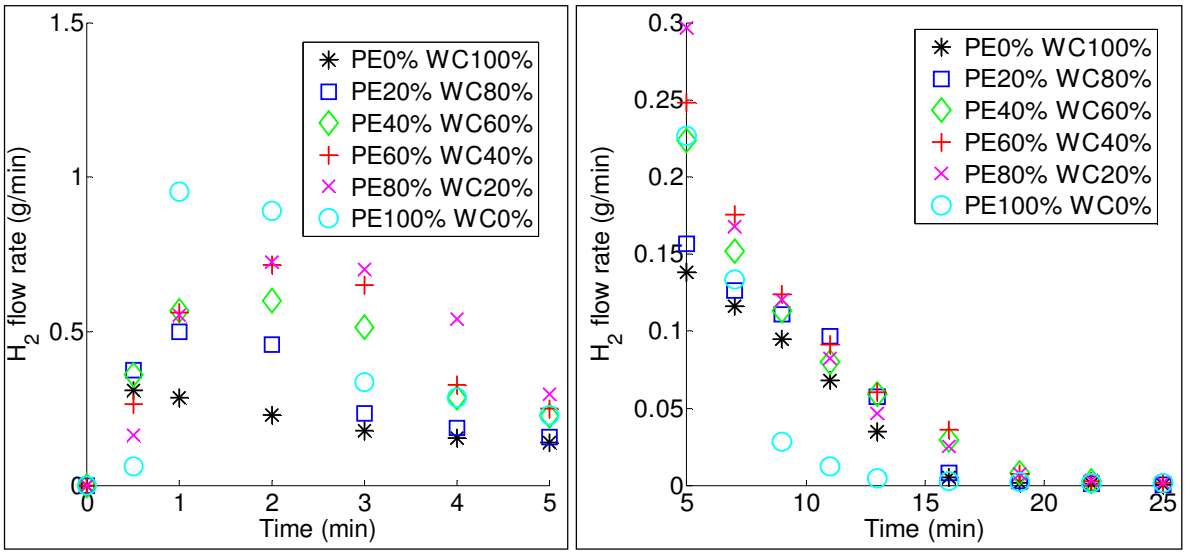

Figure IV-76. Evolution of hydrogen flow rate (a) from 0 to 5 minutes and (b) from 5 to 25 minutes

Figure IV-77a and IV-77b shows the evolution of ethylene flow rate and total hydrocarbons flow rate, including ethylene, respectively, for different percentages of PE in WC in the feed stock sample. As the monomer forming the PE plastic, ethylene is an indicator of PE thermal degradation. Evolution of hydrocarbons, including ethylene, did not extend for more than five minutes in the gasification process. Evolution of hydrocarbons is mainly attributed to thermal breakdown of long hydrocarbons chains in both PE and WC. Consequently, one can conclude that the syngas and hydrogen flow after the fifth minute is mainly attributed to gasification reactions and steam hydrocarbons reforming reactions.

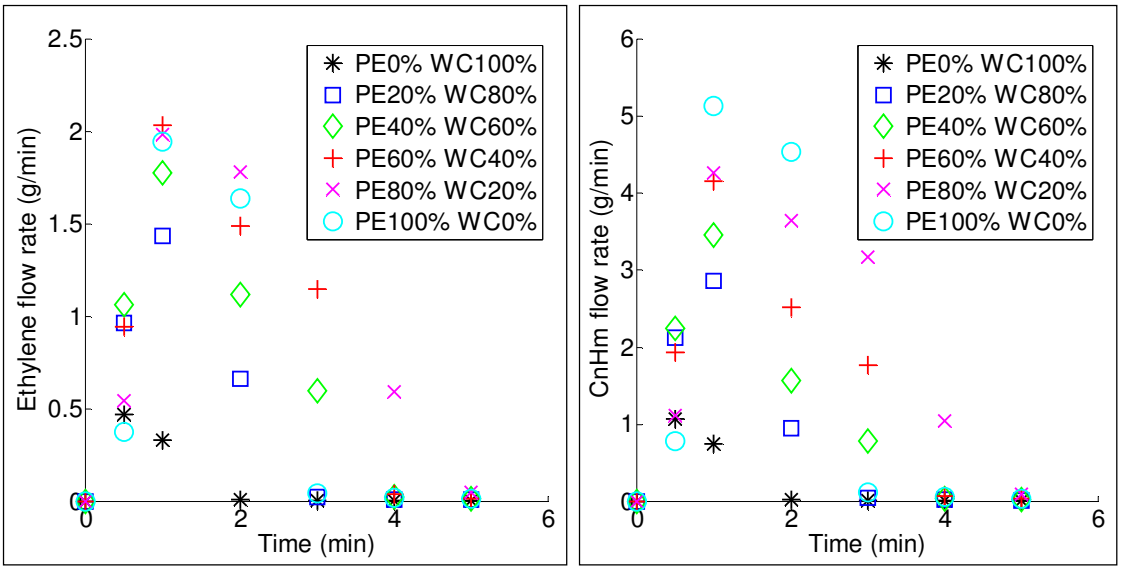

(a) **(b)**

Figure IV-77. Evolution of (a) ethylene flow rate and (b) total hydrocarbons flow rate

Figures IV-78a and IV-78b show the evolution of output power from 0 to 5 minutes and 5 to 25 minutes, respectively, for different percentages of PE in the feed stock sample. One can see from the output power evolution curve that most of the energy is being released in the first four to five minutes from the start of gasification. The increase in PE percentage tends to increase the peak value of output power. Figures IV-79a and IV-79b show the evolution of carbon flow rate from 0 to 5 minutes and 5 to 25 minutes. Carbon flow rate was calculated based on carbon content in the syngas. No apparent effect of PE percentage in the feed stock sample on the peak value of carbon flow rate could be observed.

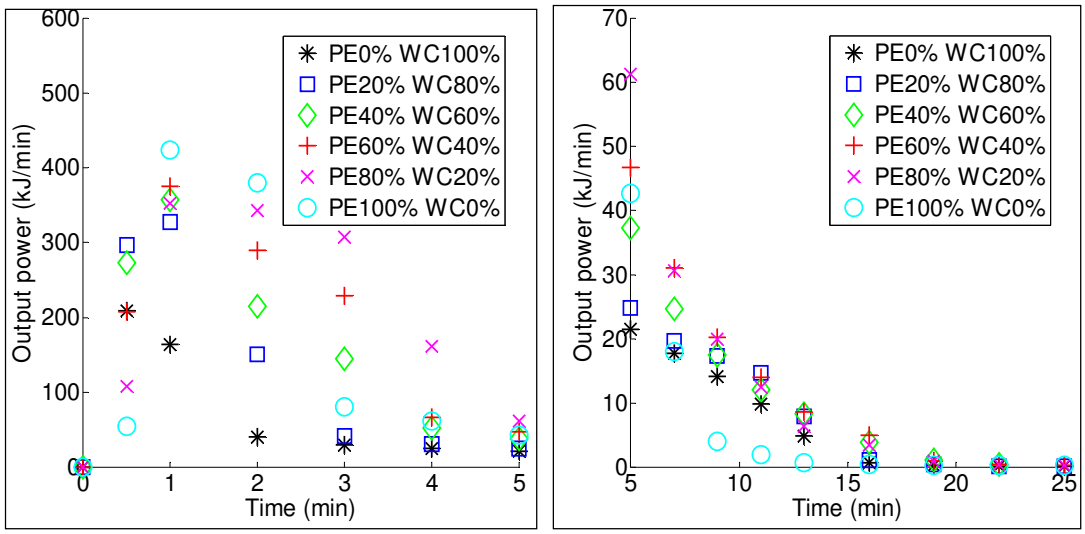

Figure IV-78. Evolution of (a) output power and (b) carbon flow rate

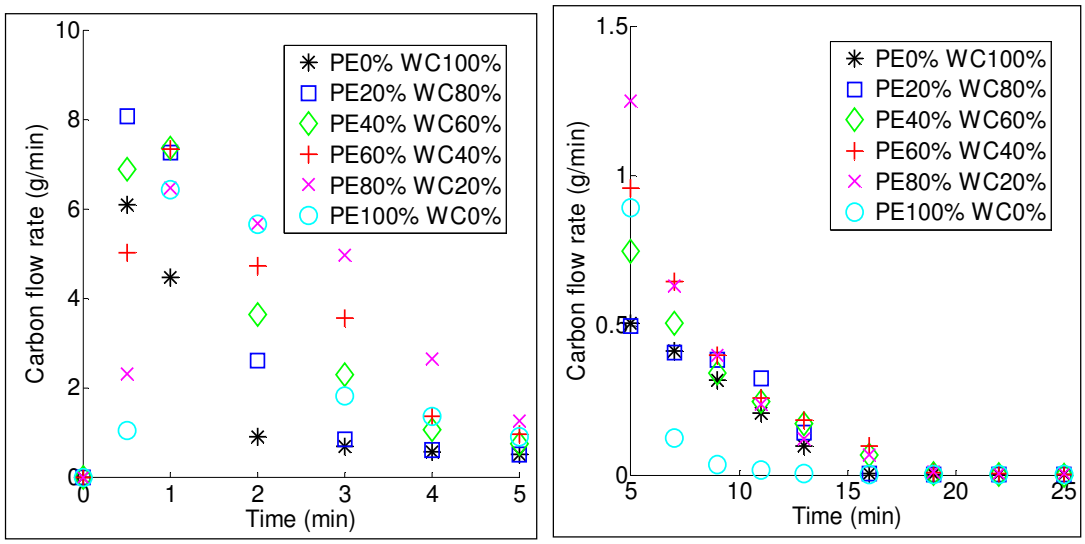

Figure IV-79. Evolution of carbon flow rate (a) from 0 to 5 minutes and (b) from 5 to 25 minutes

4.1.8.2. Overall yield of syngas properties

Figure IV-80 shows the syngas yield and hydrogen yield for different PE to WC ratios, varying from 0% PE to 100% PE in the feed sample. A peak value of syngas yield is shown at

PE percentage of approximately 80%. The syngas yield from separate gasification of PE or WC yielded less syngas than for any blend of their mixtures. Solid line in the figure represents the weighted average value of syngas yield based on separate syngas yield from the gasification of PE and WC. Same behavior is observed for the hydrogen yield. Results show a peak value of overall hydrogen yield at PE percentage value of 80%. The solid line in the figure also represents the weighted average yield. Hydrogen yield from the mixed samples was higher than that from the theoretical weighted average yield.

Figure IV-81 shows the yield of total hydrocarbons and ethylene yield at different PE to WC ratios, from 0% PE to 100% PE. The increase in PE percentage increased both hydrocarbon yield and ethylene yield, except for the 100%PE experiment. The maximum yields of ethylene and hydrocarbons were obtained at the 80%PE experiment. This indicates the synergistic effect of co-gasification of PE and WC. The increase did not follow the linear trend of weighted average yield form separate gasification of PE and WC. Blends of PE and WC always yielded higher values of hydrocarbons and ethylene.

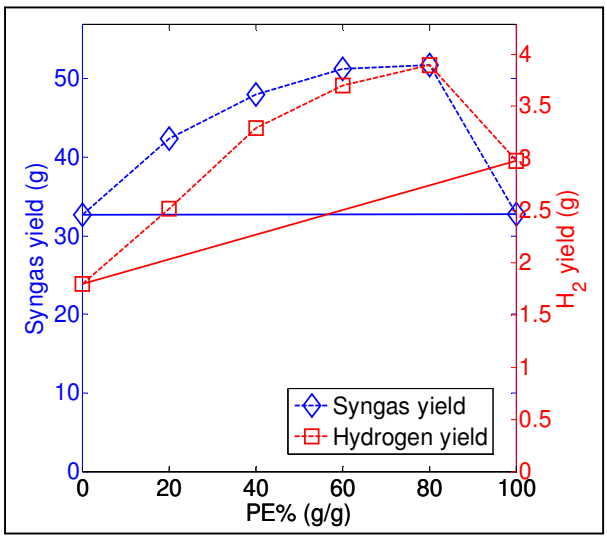

Figure IV-80. Syngas yield (left axis) and hydrogen yield (right axis)

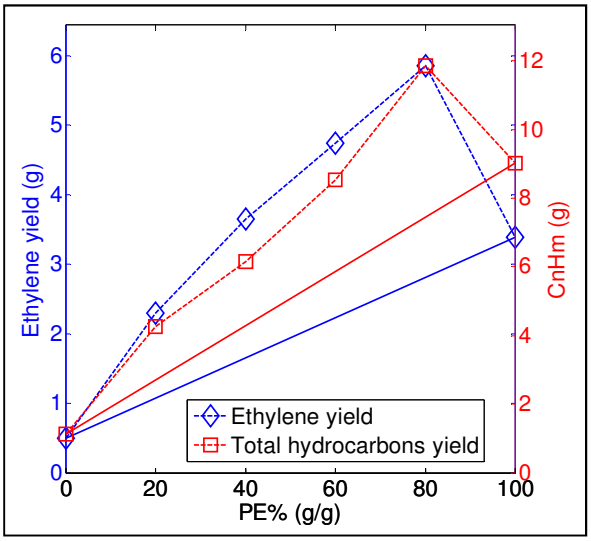

Figure IV-81. Total hydrocarbons yield (left axis) and ethylene yield (right axis)

Figure IV-82 shows the energy yield and apparent thermal efficiency for different PE to WC ratios in the feed stock. Following the trend of previous properties, energy yield and apparent thermal efficiency of PE-WC blends showed superior results as compared to weighted average values, represented by the solid line in the figure. Peak values of energy yield and apparent thermal efficiency were obtained at PE percentage of approximately 80%.

The PE is expected to yield more energy than the WC because of its higher heating value. However, adding small amount of WC, 20%, resulted in higher energy yield than that obtained from the 100% PE sample conditions. This means that the presence of a small percent of WC tremendously increases the energy gain from the PE considering the fact that PE (LHV: 42.98 MJ/kg) was replaced by high heating value of WC (LHV: 22.3 MJ/kg).

Figure IV-83 shows the carbon yield in gas phase for different PE to WC ratios. The carbon yield was calculated based on the carbon content in the syngas. Higher yield of carbon from PE-WC blends indicates the presence of steam-tar reforming reactions. The solid line in the figure represents the carbon content in the sample. The carbon content in the syngas is closer to the theoretical maximum for the mixed samples experiments than that for the single component samples.

Based on the results obtained on the overall yield of syngas properties, it can be confirmed that there is a synergistic interaction between PE and WC during gasification of the sample feed stock mixture. Superior results in terms of syngas yield, hydrogen yield, total hydrocarbons yield and energy yield from PE-WC blends were obtained as compared to the expected weighed average yield. A possible interaction mechanism is that PE acts as a hydrogen donor to radicals generated from WC pyrolysis, resulting in stabilizing those radicals and the production of higher yield of total hydrocarbons than that expected by the weighted average

yield. Enhancement in HCs was ~ 4 grams at 80% PE. However the enhancement in syngas yield was ~ 18 grams at the 80% PE run. This means that there is ~ 14 grams increase in CO, H_2 and CO_2 which is not explained by the hydrogen donor mechanism. In order to explain the enhancement in CO, H2 and CO2 yield, the arrangement of WC with respect to PE should be considered. A possible volatiles-char interaction mechanism is shown in figure IV-84. PE was always located upstream from WC for all experiments for consistency. WC char might have played a role in adsorbing volatile matter evolved from PE, and in turn, promoted steam-hydrocarbons reforming reaction, to result in excess H_2, CO and CO_2 than what expected by the weighted average yield alone, see figure IV-85. Promotion of the steam-hydrocarbons reforming reactions, is also evidenced from the closer carbon yield values to the theoretical maximum in case of mixed samples data points, see figure IV-83.

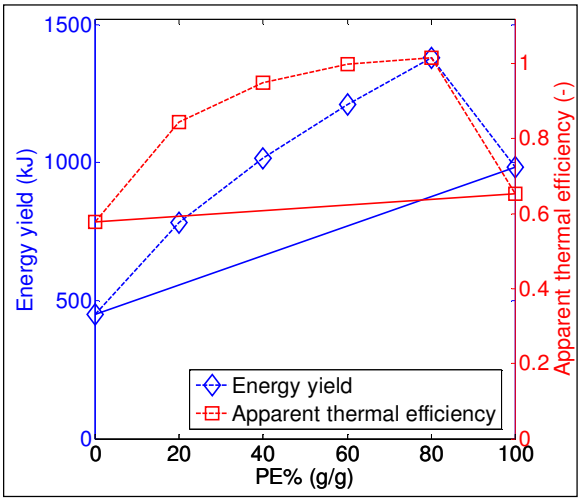

Figure IV-82. Energy yield (left axis) and apparent thermal efficiency (right axis)

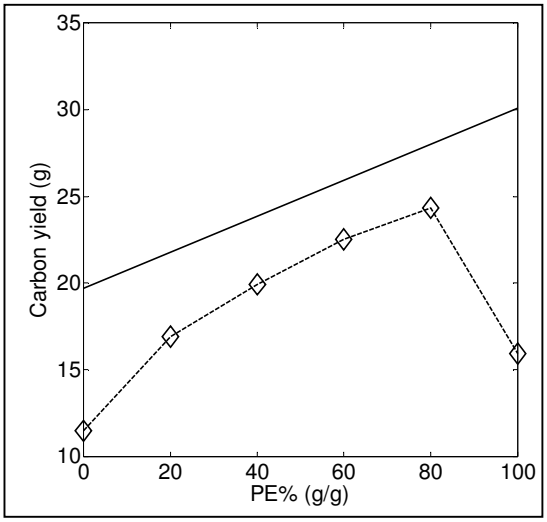

Figure IV-83. Overall carbon yield (based on carbon content in the syngas)

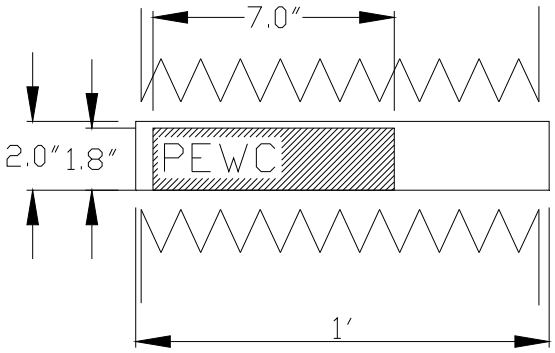

Figure IV-84. Arrangement of PE and WC sample in the reactor

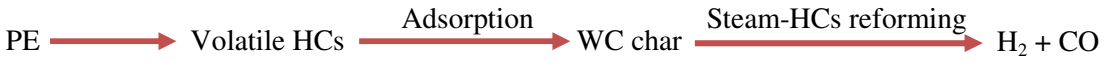

Figure IV-85. Possible volatiles-char interaction mechanism

4.1.8.3. Cumulative yield of syngas, hydrogen and energy

Presented in this section is the cumulative behavior of main syngas properties; syngas cumulative yield, hydrogen cumulative yield and energy cumulative yield. The cumulative behavior is very important in quantifying the yield-time relationship. The experiment might last for more than an hour before reaching an absolute zero value of syngas flow rate. On the other hand, 99% of the syngas might have evolved in a matter of minutes. The cumulative behavior might help in determining the required residence time and consequently gasifier size for a certain conversion degree of syngas, hydrogen or energy.

Figure IV-86 show the cumulative yield of syngas for the mixtures investigated. All plots coincide on each other during the initial stage, 0 to 2nd minute. Because of the high value of syngas flow rate initially, a steep slope of cumulative syngas yield is obtained. The steep slope gradually gets less steep until it reaches an asymptotic value approaching zero. This is attributed

to low flow rate values after the 10th minute. The horizontal solid lines represent the 99% syngas yield value for each mixture condition. The vertical lines represent the time at which 99% of the syngas has been evolved, see figure IV-89. Although a syngas flow was detected even after 40 minutes from the beginning of experiments, 99% of the syngas has evolved in less than 20 minutes.

Figure IV-87 shows the cumulative yield of hydrogen for all mixtures. 99% of hydrogen has evolved in the time duration range of 12 to 19 minutes. The solid horizontal and vertical lines are the 99% hydrogen yield mark and the time at which 99% of hydrogen has been evolved. For the woodchips containing experiments, the cumulative hydrogen yield is following the same trend; a steep slope initially followed by a gradual decrease in slop, followed by an asymptotic slope value to zero. The 100% PE run is showing a fast evolution of hydrogen in the first 10 minutes, consequently a shorter period of 99% hydrogen yield has resulted.

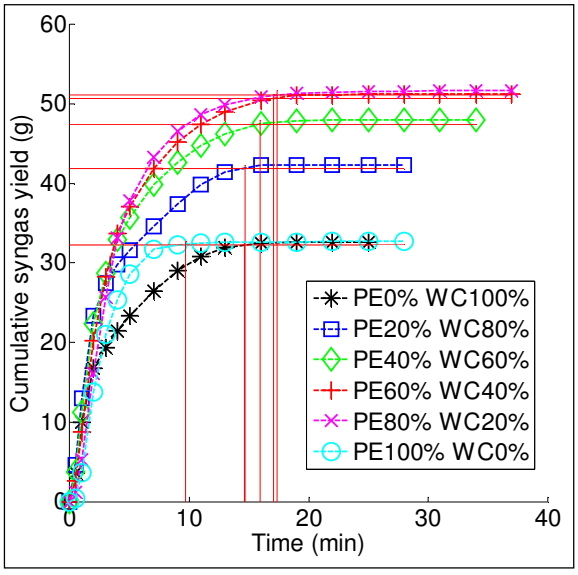

Figure IV-86. Cumulative syngas yield

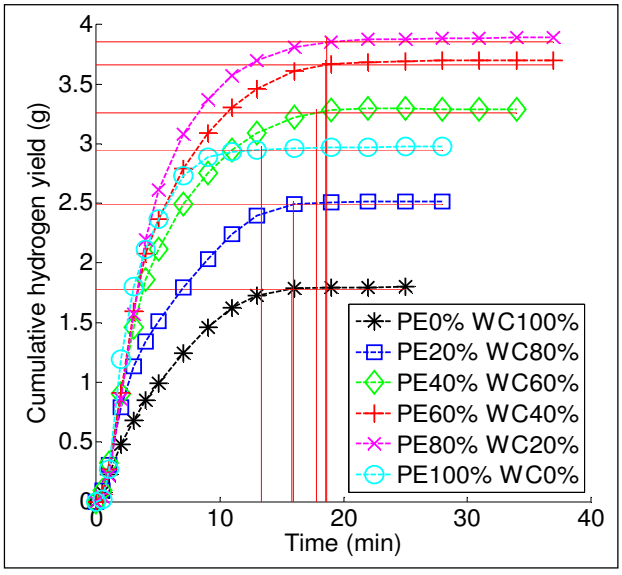

Figure IV-87. Cumulative hydrogen yield

Figure IV-88 shows the cumulative energy yield of all experiments. 99% of the energy has evolved around the 15th minute. 99% of the energy has evolved in less than 10 minutes in case of 100% PE run. One can see a tremendous enhancement in energy yield of the mixed samples as compared to that of the pure samples.

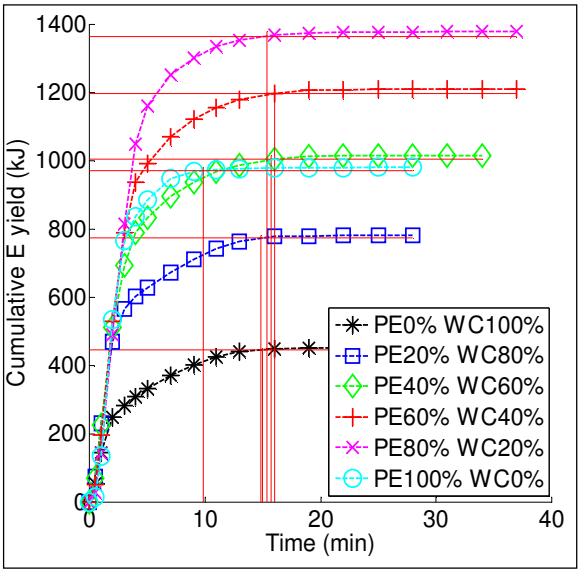

Figure IV-88. Cumulative energy yield

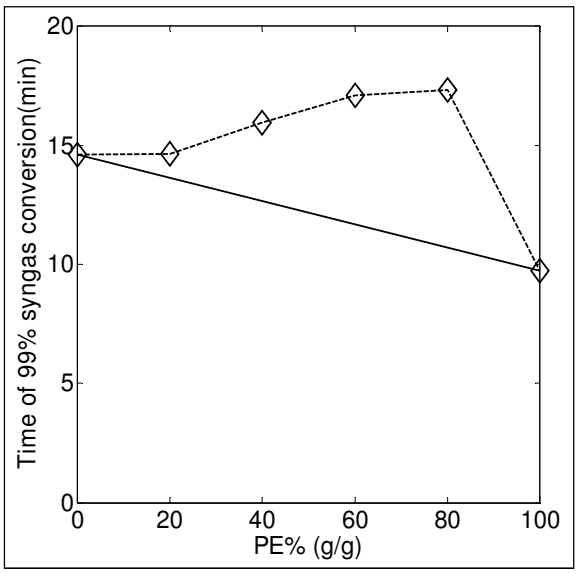

Figure IV-89. Time of 99% syngas conversion

4.2. Kinetics of syngas evolution from char gasification and pyrolysis

4.2.1. Gasification kinetics of paper char

The kinetics of char gasification is usually determined by monitoring the deterioration of mass of char with time using a Thermogravimetric analyzer (TGA). At low reactor temperatures (< 900°C) char gasification is assumed to be chemically controlled and rate constant is calculated based on a single step first order reaction, $r_{char} = -\frac{1}{m}\frac{dm}{dt}$, where, m, is the sample mass at time t and r_{char} is the reaction rate. After the end of the pyrolysis process the syngas yield is totally

attributed to the char gasification. It takes on the order of 8 to 12 minutes for the pyrolysis process to finish, which is enough time for the sample to reach the reactor temperature. This means that the char gasification process is accomplished under isothermal conditions. Based on the assumptions that the char gasification is chemically controlled and the reaction occurs isothermally, integration of the first order reaction rate yields the following expression $Kt = -\ln(1 - X)$, where K is the rate constant and X is the conversion.

In the present experiment there was no possibility to monitor the mass deterioration in the reactor with time. However, after making some assumptions, it is possible to roughly estimate the mass deterioration in the reactor based on the syngas flow rate and its carbon content. These assumptions are: the char leftover after the pyrolysis process is mostly carbon and the steam char reaction yields only gas phase products. Now, analogues to the first order reaction assumed above one can determine the kinetics of carbon conversion by the same way and under the same conditions. The rate constant is determined from figure IV-90 by calculating the slope of –ln(*1-X*) versus time. The activation energy and the pre-exponential factor are determined from fig IV-91, ln(*K*) versus *1/T*, where *T* is the isothermal temperature.

The activation energy obtained is this work was 149 kJ/mol, which is comparable to reported values in the literature for carbonaceous materials such as biomass chars [113] (apparent activation energy for the steam-char gasification ranges from 130 to 170 kJ/mol).

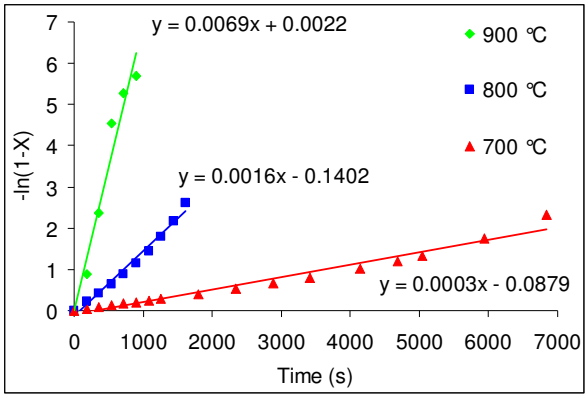

Figure IV-90. –ln(1-X) versus time

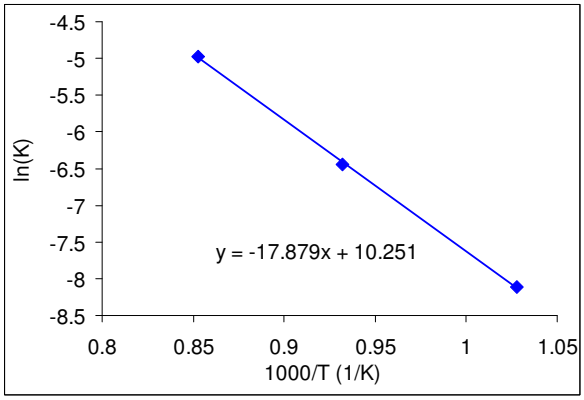

Figure IV-91. ln(K) or ln(r) versus 1/T

4.2.2.Gasification kinetics of food wastes char

Figure IV-92 shows the progress of the food waste sample during pyrolysis and char gasification and corresponding time duration for each process. The char gasification reaction is slowest in the overall gasification process. So, it is important to quantify how fast this process is.

The main constituent of char is carbon and main reaction in the char gasification process is the water gas reaction ($C+H_2O \Rightarrow CO + H_2$). The carbon-monoxide may undergo a water gas shift reaction $CO + H_2O \Leftrightarrow CO_2 + H_2$). Therefore, the carbon reactivity in the char can be inferred from the molar flow rate of carbon-monoxide and carbon dioxide. A mass spectrometer has been used to calculate the CO_2 and CO flow rate. From the CO and CO_2 flow rate, the total carbon yield and carbon conversion history can be determined. Figure IV-93 shows the change of carbon molar flow rate with time for temperatures 750, 800, 850 and 900^{o}C. One can see that higher the temperature shorter the char gasification period and higher the carbon flow rate. Figure IV-94 shows the carbon conversion versus time at temperatures of 750, 800, 850 and 900^{o}C. The plots are characterized by an initial constant slop. Results show that lower the temperature is longer the conversion time.

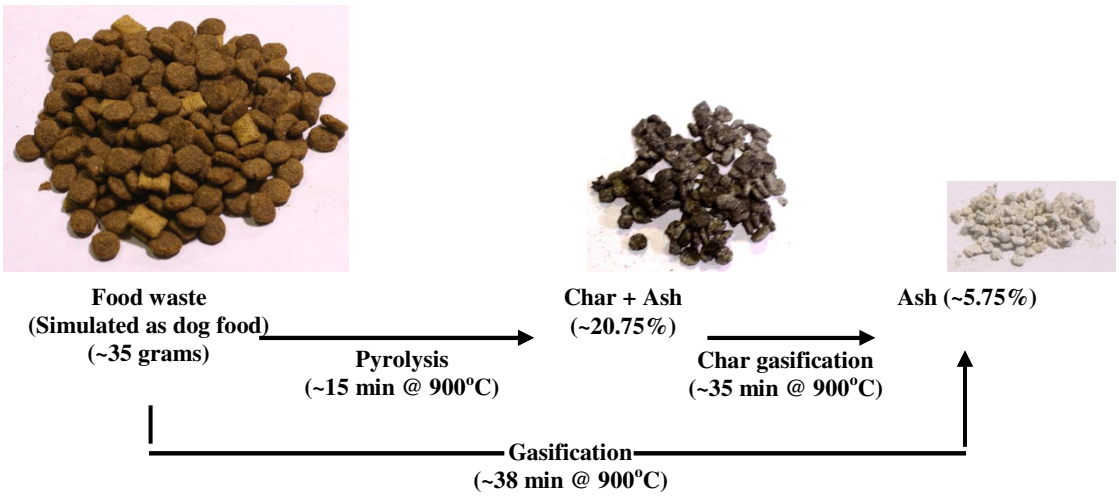

Figure IV-92. Progress of food waste sample through pyrolysis and gasification

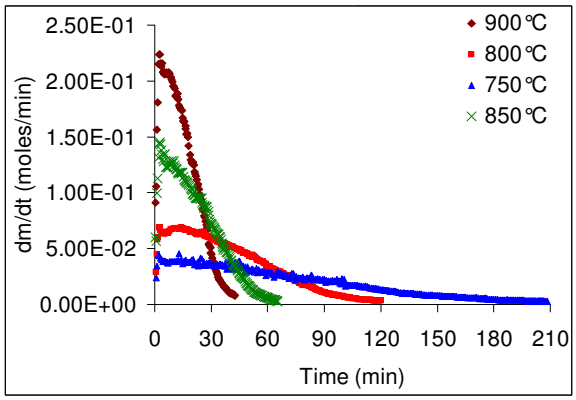

Figure IV-93. Carbon flow rate versus time for temperatures 750, 800, 850 and

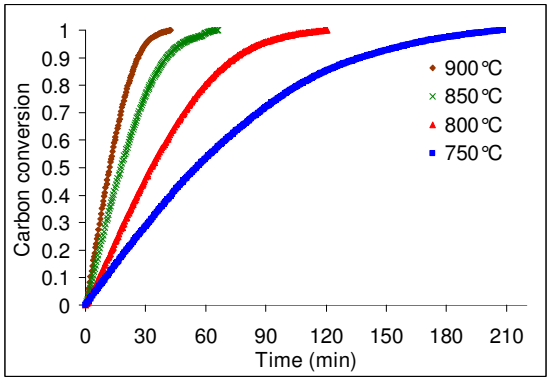

Figure IV-94. Conversion versus time for temperatures 750, 800, 850 and 900°C

Carbon reactivity was defined as $r_{char} = -\frac{1}{m}\frac{dm}{dt}$. Where, m is the mass at time (t). History of carbon mass inside the reactor was calculated from the carbon flow rate history. While, $\frac{dm}{dt}$ is the carbon mass flow rate measured by the mass spectrometer. Figure IV-95 shows the change of carbon reactivity with conversion. Carbon reactivity increases monotonically with conversion until conversion value of 0.7 followed by a steeper increase in reactivity. The steepness at lower temperature plots may not be observed because of the r values scale. The food waste char contains ~27.7% ash, most of which is salt. The inorganic components in char are the main

reason of reactivity increase, since they have a catalytic effect. From the reactivity information, kinetic parameters, activation energy *E* and pre-exponential factor *A*, were calculated. A first order reaction model has been used.

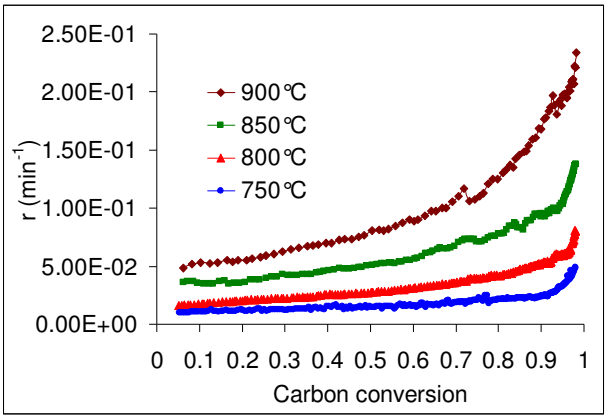

Figure IV-95. Char reactivity versus conversion for temperatures 750, 800, 850 and 900°C

Figure IV-96 shows the Arrhenius plot from which the activation energies and pre-exponential factors at different degrees of conversion (X) have been calculated. Results of the linear fittings of $ln(r_{char})$ versus $1/T$, pre-exponential factors and activation energies for conversion values from 0.1 to 0.9 are shown in table IV-1. From figure IV-96 one can see that the Arrhenius plots show almost parallel lines with increasing intercept with conversion. Parallel lines indicate constant values of activation energy. Values of activation energies in this range of conversion (0.1 to 0.9) were found to fluctuate around an average of 113 kJ/mol. However, values of pre-exponential factor increase with conversion. The trend of activation energies and pre-exponential factors indicates that the increase in reactivity in this range of conversion is attributed to increase in pre-exponential factor. In theory, the pre-exponential factor or frequency factor, *A*, depends on how often molecules collide with each other and whether the molecules are properly oriented or not. Although in solid reactions, the pre-exponential factor and activation

energy do not have the physical significance as in gas reactions [94] a logical reasoning can be introduced to explain the increase in pre-exponential factor. Ash may have increased the adsorption rate of steam to the char surface and consequently, raised the reaction rate.

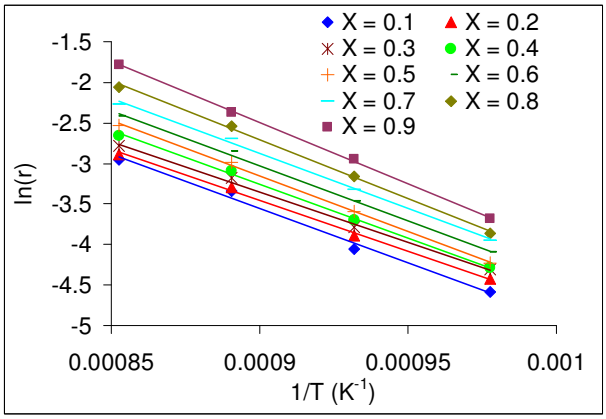

Figure IV-96. Arrhenius plot at different degrees of conversion; from 0.1 to 0.9

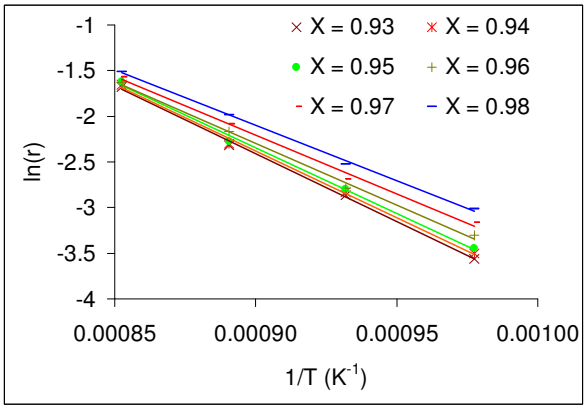

Figure IV-97. Arrhenius plot at different degrees of conversion; from 0.93 to 0.98

Table IV-1. Activation energies and pre-exponential factor at different degrees of conversion for X = 0.1 to 0.9

Carbon conversion	Arrhenius equation $\ln(r_{char}) = \ln(A) - \frac{E}{R}\frac{1}{T}$	Activation energy E, (kJ/mol)	Pre-exponential factor A, (min^{-1})
0.1	$ln(r_{char}) = 8.5228 - 13424\frac{1}{T}$	111.6	5028
0.2	$ln(r_{char}) = 7.7939 - 12501\frac{1}{T}$	103.9	2425
0.3	$ln(r_{char}) = 7.7964 - 12386\frac{1}{T}$	102.9	2431

0.4	$ln(r_{char}) = 8.6576 - 13241\frac{1}{T}$	110	5753
0.5	$ln(r_{char}) = 9.2199 - 13751\frac{1}{T}$	114.3	10096
0.6	$ln(r_{char}) = 9.1941 - 13579\frac{1}{T}$	112.8	9838
0.7	$ln(r_{char}) = 9.3624 - 13603\frac{1}{T}$	113	11642
0.8	$ln(r_{char}) = 10.337 - 14501\frac{1}{T}$	120.5	30853
0.9	$ln(r_{char}) = 11.124 - 15133\frac{1}{T}$	125.8	67778

Figure IV-97 show the Arrhenius plot for conversions from 0.93 to 0.98. A compensation effect was observed here, where there is a simultaneous decrease in activation energy and pre-exponential factor with increase in conversion, see table IV-2. The simultaneous decrease in activation energy and pre-exponential factor is called "the compensation effect" or "isokinetic effect" [94]. In a compensation effect behavior, Arrhenius plots should intersect at a single point at the isokinetic temperature and isokinetic reactivity. Since the plots do not intersect in the examined temperature range, an extrapolation for the linear fittings was used to find the isokinetic temperature and reactivity. The extrapolation is shown in figure IV-98. Since the lines do not intersect exactly at a single point, the weighted average of 15 intersections was used to find the isokinetic temperature and reactivity. According to Agrawal [94] in order to validate the presence of correct compensation effect, the linear plot of *ln(A)* versus *E* should have a slop of $1/RT_{iso}$, were T_{iso} is the isokinetic temperature and an intercept of $ln(r_{iso})$, where r_{iso}, is the isokinetic reactivity. *Ln(A)* versus *E* is shown in Figure IV-99. From the slop value in Figure IV-

99, the isokinetic temperature should be ~ 991°C and $ln(r_{iso})$ should be ~ -0.801. T_{iso} and $ln(r_{iso})$ values obtained from Figure IV-98 are 1001°C and -0.72 respectively, which is close to the values obtained from Figure IV-99. So, in summary, compensation effect is observed by the end of conversion but was not observed before conversion degree of 0.9.

Table IV-2. Activation energies and pre-exponential factors at different degrees of conversion from 0.93 to 0.98

Carbon conversion	Arrhenius equation $ln(r_{char}) = ln(A) - \frac{E}{R}\frac{1}{T}$	Activation energy E, (kJ/mol)	Pre-exponential factor A, (min^{-1})
0.93	$ln(r_{char}) = 10.905 - 14795\frac{1}{T}$	123	54447
0.94	$ln(r_{char}) = 10.761 - 14600\frac{1}{T}$	121.3	47145
0.95	$ln(r_{char}) = 10.579 - 14362\frac{1}{T}$	119.4	39300
0.96	$ln(r_{char}) = 9.8673 - 13517\frac{1}{T}$	112.3	19289
0.97	$ln(r_{char}) = 9.3667 - 12861\frac{1}{T}$	106.9	11692
0.98	$ln(r_{char}) = 8.8081 - 12120\frac{1}{T}$	100.7	6688

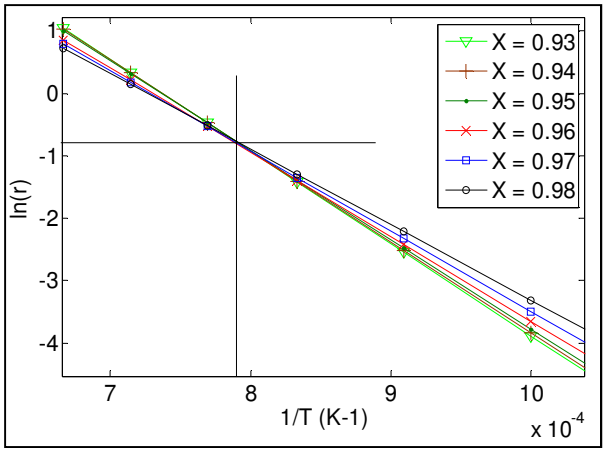

Figure IV-98. Arrhenius plot for conversions from 0.93 to 0.98 showing the isokinetic temperature and isokinetic reactivity

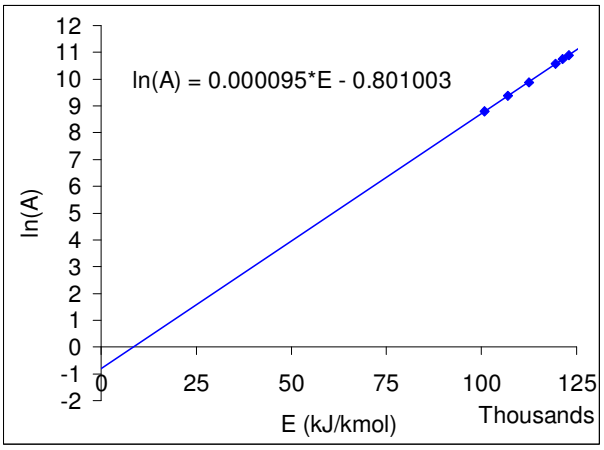

Figure IV-99. *Ln(A)* versus *E* for the conversion from 0.93 to 0.98

4.2.3. Gasification kinetics of woodchips char

The main constituent of char is carbon. Therefore the main reaction is the water gas reaction ($C+H_2O \Leftrightarrow CO + H_2$). Carbon-monoxide may undergo a water gas shift reaction ($CO + H_2O \Leftrightarrow CO_2 + H_2$). Based on these reactions carbon reactivity in char can be inferred from the molar flow rate of carbon-monoxide and carbon dioxide. For the purpose of measuring CO and CO_2 flow rates the mass spectrometer was used. CO_2 and CO flow rates were calculated by relating their partial pressures to the trace gas partial pressure. From the CO and CO_2 flow rate one can determine the carbon molar flow rate and total carbon yield. Consequently, this allowed for determining the history of carbon mass inside the reactor from the carbon flow rate-time relationship. Carbon conversion, *X*, is then determined using the total carbon yield and the carbon molar flow rate time relationship.

Figures IV-100, IV-101, IV-102 and IV-103 show the evolution of reaction rate with time at different gasifying agent partial pressures of 1.5, 1.2, 0.9 and 0.6 bars, respectively. Each

figure shows the results obtained from the two gasifying agents, steam and CO_2. Steam shows higher reactivity than that obtained with CO_2 as the gasifying agent. Results show that the time duration for gasification experiments with steam is about 22 minutes; however, the gasification duration with CO_2 is about 60 minutes. The duration of gasification with CO_2 being almost three times as that of steam gasification indicates that steam reactivity with char is almost three times faster than that of CO_2. Reaction rate in case of steam starts with a high value initially, followed by an increase in reaction rate to a peak value, followed by a steep decrease in reaction rate. On the other hand, reaction rate of char with CO_2 is characterized by a monotonically decreasing value over a longer period of time. Changing the gasifying agent partial pressure did not have a clear distinct effect on the reaction rate trend, values or gasification duration for both gasifying agents examined.

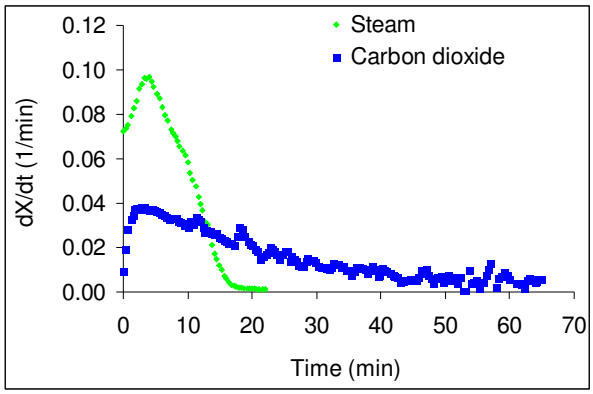

Figure IV-100. Evolution of reaction rate at gasifying agent partial pressure of 1.5 bars

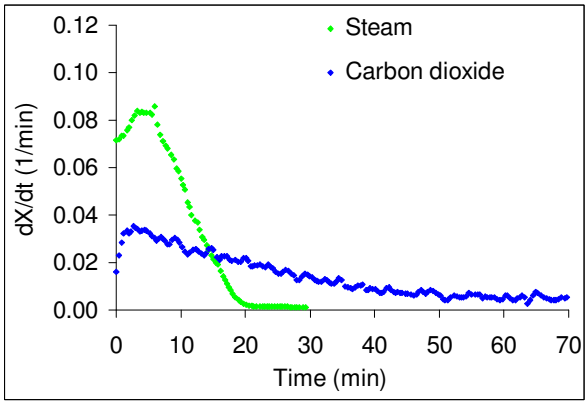

Figure IV-101. Evolution of reaction rate at gasifying agent partial pressure of 1.2 bars

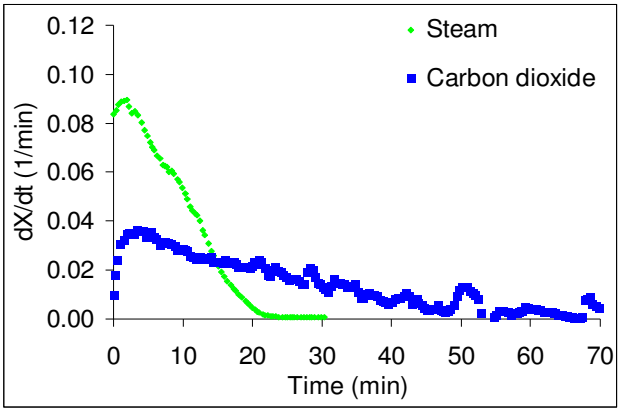

Figure IV-102. Evolution of reaction rate at gasifying agent partial pressure of 0.9 bars

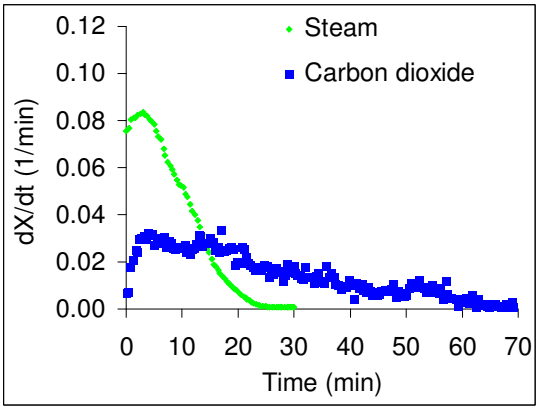

Figure IV-103. Evolution of reaction rate at gasifying agent partial pressure of 0.6 bars

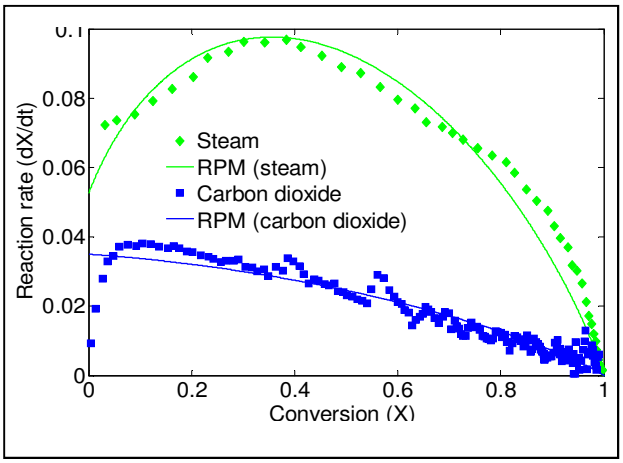

Figure IV-104. Reaction rate versus conversion and RPM fitting for gasifying agent partial pressure 1.5 bars

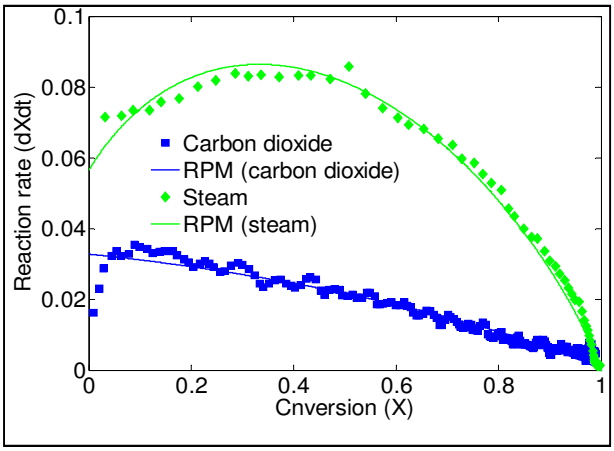

Figure IV-105. Reaction rate versus conversion and RPM fitting for gasifying agent partial pressure 1.2 bars

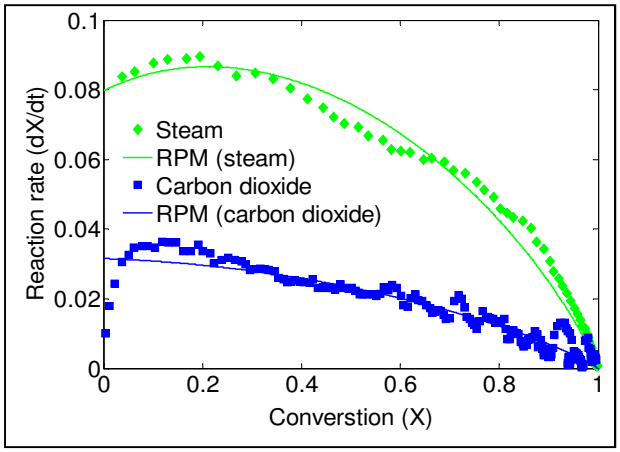

Figure IV-106. Reaction rate versus conversion and RPM fitting for gasifying agent partial pressure of 0.9 bars

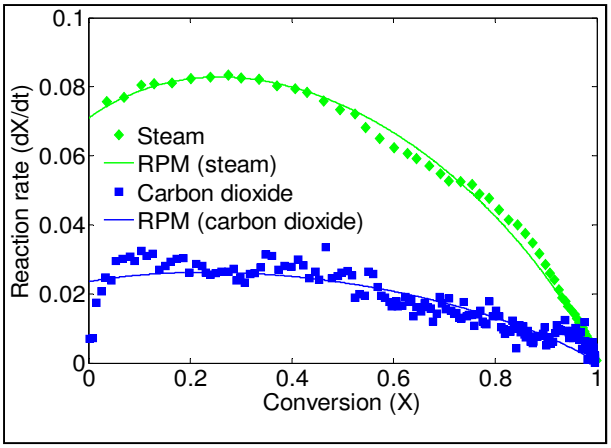

Figure IV-107. Reaction rate versus conversion and RPM fitting for gasifying agent partial pressure of 0.6 bars

Figures IV-104, IV-105, IV-106 and IV-107 show the change of reaction rate with conversion for gasifying agent partial pressures of 1.5, 1.2, 0.9 and 0.6. One can see that reaction rates of steam gasification experiments are higher than that of CO_2 gasification. Reaction rate of char with steam is showing a peak value at conversion value of approximately 0.3. However, for CO_2 it showed the peak value earlier at conversion value of approximately 0.1. Having a peak value of reaction rates indicates a geometrical change in sample pore structure which in turn affects the reaction rate as conversion progresses. The behavior of reaction rate versus conversion shown in figures IV-104 to IV-107 can be best fitted using the random pore model (RPM) [115]. In the random pore model (RPM), the reaction rate is given as a function of conversion via the following relationship.

$$\frac{dX}{dt} = K(1 - X)\sqrt{(1 - \Psi \ln(1 - X))}$$

where X, is the conversion, t is time, K is the rate constant and ψ is a structural parameter. Values of the rate constant, K, and structural parameter, ψ, for different partial pressure of gasifying agent are presented in table IV-3. The MATLAB curve fitting tool box was used to determine the rate constant, K, and structural parameter, ψ. Steam provided higher rate constant and higher structural parameter value, ψ, than CO_2 as the gasifying agent. Higher ψ values indicate higher progressive porosity of the sample and that more reactions are occurring at internal pores of the char. Also shown, in table IV-3 is the average rate, K, constant and average ψ for both steam and CO_2. Average values of rate constant, K, and structural parameter, ψ, were used to generate an average RPM fitting. The Average RPM was compared to reaction rate curves at the investigated partial pressures.

Table IV-3. Rate constants and structural parameters for both steam and CO_2 experiments

	Steam		**CO_2**	
Partial pressure	Rate constant, K_{H2O} (1/Sec)	Structural parameter, ψ_{H2O} (−)	Rate constant, K_{CO2} (1/Sec)	Structural parameter, ψ_{CO2} (−)
1.5	0.052	16.71	0.035	1.39
1.2	0.056	10.53	0.033	1.07
0.9	0.08	3.80	0.032	1.70
0.6	0.071	4.95	0.024	4.21
Average	***0.065***	***9.00***	***0.031***	***2.09***

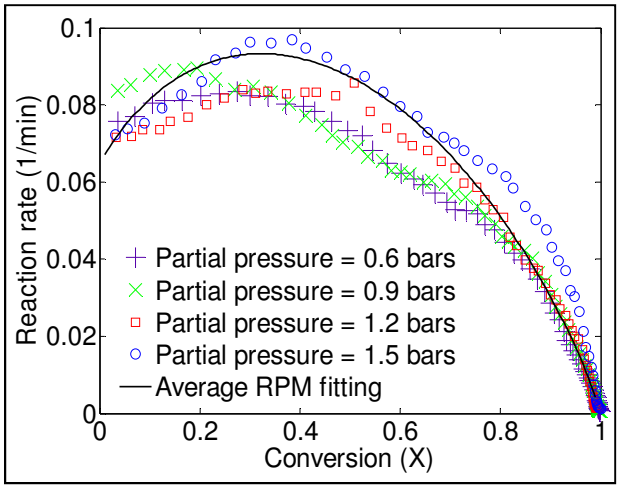

Figure IV-108. Reaction rates versus conversion and average RPM fitting for steam experiments

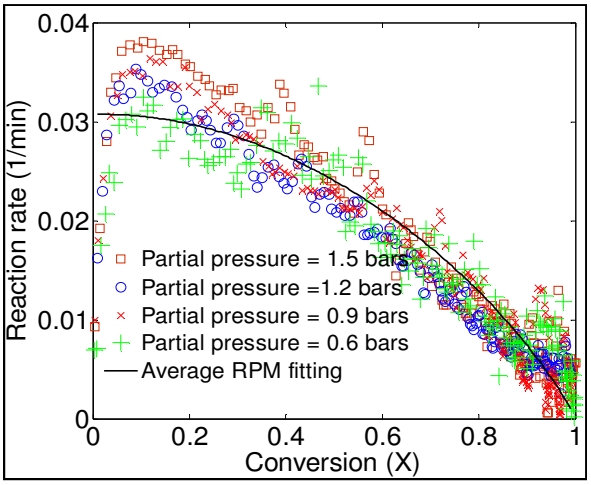

Figure IV-109. Reaction rates versus conversion and average RPM fitting for CO_2 experiments

Figure IV-108 show a comparison between the average RPM fit and reaction rates for steam-char experiments. Figure IV-109 show comparison between the average RPM fit and reaction rates for CO_2-char experiments. The results clearly show that the average RPM provides a good fit at the four investigated partial pressures. One can see that there is no clear effect of changing the gasifying agent partial pressure for both cases of steam and CO_2 gasification. The reaction rate curves at different gasifying agent partial pressures almost coincide with each other. Having negligible to no variation in reaction rate values as the partial pressure of gasifying agent varied from 1.5 to 0.6 bars, indicates a negligible to zero reaction order in the investigated range of partial pressure. In order to explain the reason for independency of reaction rate on gasifying agent partial pressure over the pressure range examined here, figure IV-110 is utilized [116]. In a chemically controlled surface reaction, the process undergoes three steps; first is a chemical adsorption to the solid surface, second is the surface reaction and third is the products desorption from the solid surface. If adsorption is the rate limiting step, then increase in gasifying agent

partial pressure would increase the reaction rate. However, if the surface reaction or desorption step is the rate limiting step then increase in the gasifying agent partial pressure would not have affected the reaction rate. This is because whatever is the gasifying agent concentration above the char surface, there is no free active sites available for gasifying agent molecules to be adsorbed.

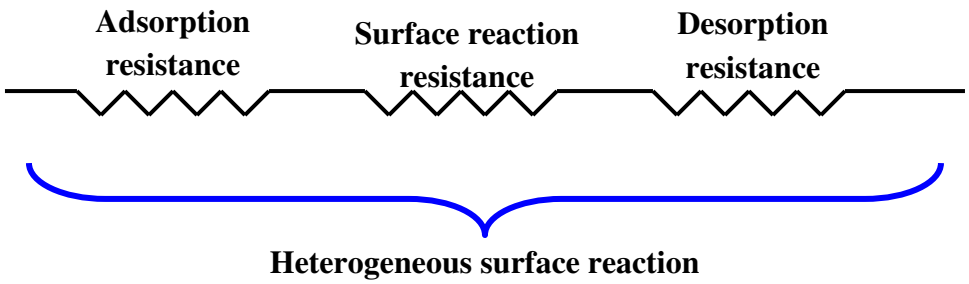

Figure IV-110. A schematic diagram of a chemically controlled surface reaction

4.2.4. Gasification kinetics of activated charcoal under diffusion resistance conditions

The effect of particle size, porosity and reactor temperature/reaction rate constant on the progress of a char particle conversion has been investigated numerically by solving the transport equation inside a reacting char particle. Numerical simulations have been conducted for three cases that include two extreme cases and one general case. The two extreme cases correspond to a very large Damkohler number ($3.2607*10^3$) and a very small Damkohler number (0.0042). The third case corresponds to an intermediate value of Damkohler number. For the very large Damkohler number case, concentration profiles of the gasifying agent showed a steep gradient across the particle and the reaction occurred mostly in outer layer of the particle. This behavior corresponds to a diffusion controlled process. For the very small Damkohler number case,

gasifying agent concentration was a straight line parallel to the x-axis, with a y-axis value of the surrounding concentration. The reaction occurred homogeneously across the particle and the degree of conversion was only a function in time. This behavior corresponds to a chemically controlled process. The total conversion of the char particle as a function of time has also been calculated for different particle sizes, initial porosity and reaction rate constant. Variation in conversion profiles as a function of time due to variation in initial porosity and reaction rate constant were limited to a certain extent.

Very high initial porosity values tend to shift the process towards a chemically controlled one; any further increase in porosity does not have a positive effect on the conversion-time relationship. Very high reaction rate constants tend to shift the process towards diffusion controlled process. Kinetic parameters have been determined experimentally using a chemically controlled process. The obtained parameters have been used in the model to determine the progress of char particle conversion at an increased reactor temperature of 1000^{o}C. The model has been compared to experimental results at the same temperature (1000^{o}C). The results showed very good agreement.

4.2.4.1. Model of char particle gasification

The char-gasifying agent reaction will be expressed using a single irreversible reaction, IV-R1.

$$Char + gasifying\ agent \longrightarrow products \qquad \text{(IV-R1)}$$

The gasifying agent concentration distribution inside the char particle is expressed using the transient transport equation, E1. $\frac{\partial C}{\partial t} = \frac{1}{r^2}\frac{\partial}{\partial r}\left[D_p r^2 \frac{\partial C}{\partial r}\right] - K(T)C^{n_{ga}} f(X) \qquad for\ \ 0 \le r \le r_p$

(IV-E1)

where, C is the concentration of gasifying agent, D_p is effective diffusivity of the gasifying agent inside the particle, $K(T)$ is the reaction rate constant, n_{ga} is the rate exponent with respect to gasifying agent and $f(X)$ is a function of conversion X.

The gasifying agent concentration distribution outside the particle is expressed using IV-E2

$$\frac{\partial C}{\partial t} = \frac{D_o}{r^2}\frac{\partial}{\partial r}\left[r^2 \frac{\partial C}{\partial r} \right] \quad for \;\; r > r_p \qquad \text{(IV-E2)}$$

where, D_o is the gasifying agent diffusivity in the gas phase

The char reaction rate, dX/dt, is expressed as a function in temperature, $K(T)$, gasifying agent concentration, C and char conversion, $f(X)$.

$$C_{carbon}\left(1-\varepsilon_o\right)\frac{\partial X}{\partial t} = K(T)C^{n_{ga}} f(X) \qquad \text{(IV-E3)}$$

where, C_{carbon} is the initial carbon concentration in the char particle and ε_o is the initial porosity of the particle.

4.2.4.2. Boundary and initial conditions

The boundary conditions for E1 are

$$\frac{\partial C}{\partial r} = 0 \quad at \;\; r = 0 \qquad \text{(IV-E4)}$$

$$D_p \left.\frac{\partial C}{\partial r}\right|_{r_p^-} = D_o \left.\frac{\partial C}{\partial r}\right|_{r_p^+} \quad at \;\; r = r_p \qquad \text{(IV-E5)}$$

The gradient of gasifying agent concentration at the particle center is zero, IV-E4, and the flux of gasifying agent diffusing into the particle just before the char-gasifying agent interface, r_p^-, is equal to the flux of gasifying agent diffusing just after the interface, r_p^+.

The boundary conditions for IV-E2 are:

$$C = C_S \quad at \quad r = r_p \qquad \text{(IV-E6)}$$

$$C = C_\infty \qquad at \quad r = \infty \qquad \text{(IV-E7)}$$

The initial condition is

$$X(r,t) = 0 \qquad at \; t = 0 \qquad \text{(IV-E8)}$$

4.2.4.3. Assumptions

The char reaction rate dependency on conversion is expressed by E9.

$$f(X) = (1 - X)^{n_{char}} \qquad \text{(IV-E9)}$$

The reaction exponent with respect to the gasifying agent is chosen as unity for simplicity; $n_{ga} = 1$. E3 will be reduced to IV-E10

$$C_{carbon}(1-\varepsilon_o)\frac{\partial X}{\partial t} = K(T)\,C\,(1-X)^{n_{char}} \qquad \text{(IV-E10)}$$

For short time intervals a quasi-steady state assumptions is used. Under the quasi-steady state assumption IV-E1 and IV-E2 are reduced to IV-E11 and IV-E12 respectively.

$$\frac{1}{r^2}\frac{\partial}{\partial r}\left[D_p r^2 \frac{\partial C}{\partial r}\right] - K(T)\,C\,(1-X)^{n_{char}} = 0 \qquad for \;\; 0 \le r \le r_p \qquad \text{(IV-E11)}$$

$$\frac{\partial}{\partial r}\left[r^2 \frac{\partial C}{\partial r}\right] = 0 \qquad for \;\; r > r_p \qquad \text{(IV-E12)}$$

Equations IV-E11 and IV-E12 state that for short time intervals the gasifying agent concentration profile does not change.

4.2.4.4. Solution

Integrating IV-E12 twice, a relation between gasifying agent concentration and radius r is obtained for $r > r_p$.

$$C = -\frac{r_p}{r}\left[C_\infty - C_S\right] + C_\infty \qquad for \;\; r > r_p \qquad \text{(IV-E13)}$$

And the gradient of gasifying agent just outside the particle concentration will be:

$$\left.\frac{\partial C}{\partial r}\right|_{r_p^+} = \frac{C_\infty - C_S}{r_p} \qquad \text{(IV-E14)}$$

Consequently, the flux of gasifying agent at $r = r_p^-$ will be:

$$D_p \left.\frac{\partial C}{\partial r}\right|_{r_p^-} = D_o \frac{C_\infty - C_S}{r_p} \qquad at \;\; r = r_p$$

$$or \qquad D_p r_p^2 \left.\frac{\partial C}{\partial r}\right|_{r_p^-} = r_p D_o \left(C_\infty - C_S\right) \qquad \text{(IV-E15)}$$

Diffusivity of the gasifying agent inside the particle, effective diffusivity, D_p, is expressed as a function of diffusivity of the gasifying agent in gaseous medium and the particle porosity.

$$D_p = \frac{D_o \varepsilon}{\lambda}, \qquad \lambda = 1/\varepsilon \qquad \Rightarrow \qquad D_p = D_o \varepsilon^2 \qquad \text{(IV-E16)}$$

where, D_o is the diffusivity of the gasifying agent in gaseous medium, $\varepsilon(X,t)$ is the porosity of the char particle at a given location and time, and λ is a tortuosity factor.

Porosity is expressed as a linear function of the conversion; $\varepsilon = a + bX$ with $\varepsilon = \varepsilon_o$ *at* $X = 0$ *and* $\varepsilon = 1$ *at* $X = 1$. Note that the effective diffusivity now is a function in conversion; consequently it became a function in r and t.

Diffusivity of the gasifying agent D_o was determined using the multicomponent diffusion coefficient expression developed by Fairbanks and Wilke, IV-E17 [117].

$$D_o = \frac{1 - y_{ga}}{\dfrac{y_B}{D_{ga-B}} + \dfrac{y_C}{D_{ga-C}} + ...} \qquad \text{(IV-E17)}$$

$D_{ga\text{-}B}$ and $D_{ga\text{-}C}$ are the respective binary diffusion coefficients of the gasifying agent in B and C. y_{ga}, y_B and y_C are the mole fractions of the components in the mixture.

For the purpose of determining the binary diffusion coefficients, the gasifying agent is assumed to be steam and gasification products are mainly carbon monoxide and hydrogen.

For a tertiary system, values of multi component diffusion coefficient of the gasifying agent are only affected by the ratio of *B* to *C* or *CO* to H_2. Consequently, for a certain *CO* to H_2 ratio, obtained D_o values will be valid for different gasifying agent concentrations/mole fractions. *CO* to H_2 ratio is assumed to be unity.

Now the second order boundary value problem, equations IV-E11, IV-E15 and IV-E4, can be solved numerically. The finite element method has been used. Detailed formulation of the finite element problem is given in **Appendix A**.

The dependency of the char conversion on time is determined by numerically integrating Eqn. E10 using the finite difference method.

$$X_{it+1}^{je} = X_{it}^{je} + \frac{K}{C_{carbon}(1-\varepsilon_o)} C_{it}^{je} \, f(X_{it}) \Delta t \qquad \text{(IV-E18)}$$

where, $je = 1$ to n_e+1 and $it = 1$ to n_{time}

Here, n_e represents the number of elements in the char particle and n_{time} is the number of time intervals.

In order to calculate the total conversion of the particle at time *t*, total number of moles inside the char particle is calculated at time *t*. The number of moles in each element *n* is calculated by the integral given in IV-E19.

$$N_e = \int_{r_e}^{r_{e+1}} 4\pi r^2 C_{carbon} (1-X)\, dr = 4\pi C_{carbon} \int_{r_e}^{r_{e+1}} r^2 (1-X)\, dr \qquad \text{(IV-E19)}$$

where, *X* is expressed as a linear function of *r* within each element; $X = a + br$ with $X = X_e$ at $r = r_e$ and $X = X_{e+1}$ at $r = r_{e+1}$

The total number of moles in the particle is calculated by summing all the number of moles in each element, eqn. IV-E20.

$$N_{total} = \sum_{e=1}^{e=n_e} N_e, \qquad \text{(IV-E20)}$$

Total conversion, X_{total}, of the char particle is then calculated using IV-E21.

$$X_{total} = 1 - \frac{N_{total}}{N_o}, \qquad \text{(IV-E21)}$$

where, $N_o = \frac{4}{3}\pi r_p^3 C_{carbon}$,

Calculation steps are as follows:

a) Concentration distribution of the gasifying agent, at time *t*, inside the particle is calculated using the finite element solution of the transport equation, IV-E1.

b) The initial concentration distribution is calculated based on the initial boundary condition, *X(r,0)= 0.*

c) The conversion at *time* = t_{+1} is calculated using the concentration profiles and conversion profiles obtained at time *t*

All the coding has been written using MATLAB software code.

4.2.4.5. Code validation

For the purpose of model and numerical solution validation, equation IV-E10 is rearranged and an observed reaction rate constant, $K_{observed}$ is defined; $K_{observed} = \frac{K(T)C}{C_{carbon}(1-\varepsilon_o)}$.

The rearranged conversion rate expression is:

$$\frac{\partial X}{\partial t} = K_{observed}(1-X)^{n_{char}} \qquad \text{(IV-E22)}$$

By integrating IV-E22, eqn. IV-E23 is obtained;

$$-\frac{(1-X)^{1-n_{char}}}{1-n_{char}} = K_{observed} * t + \text{constant} \qquad \text{(IV-E23)}$$

$K_{observed}$ and n_{char} were obtained by Fitting $-\frac{(1-X)^{1-n_{char}}}{1-n_{char}}$ versus t, see figure IV-111.

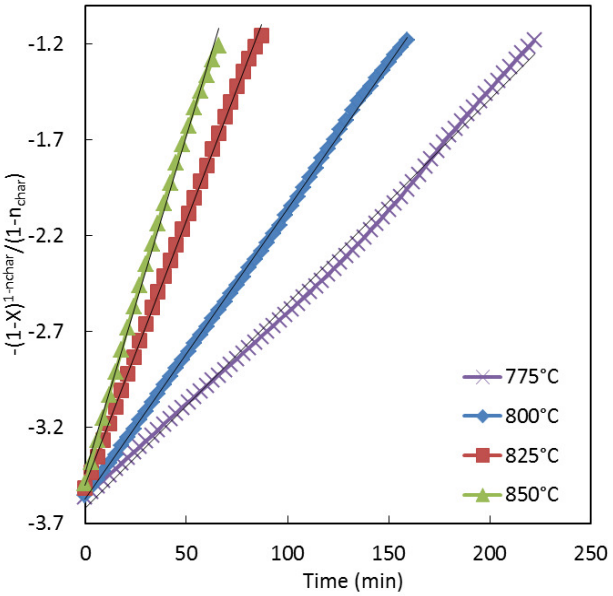

Figure IV-111. -(1-X) $^{1\text{-}nchar}$/(1-n_{char}) versus time

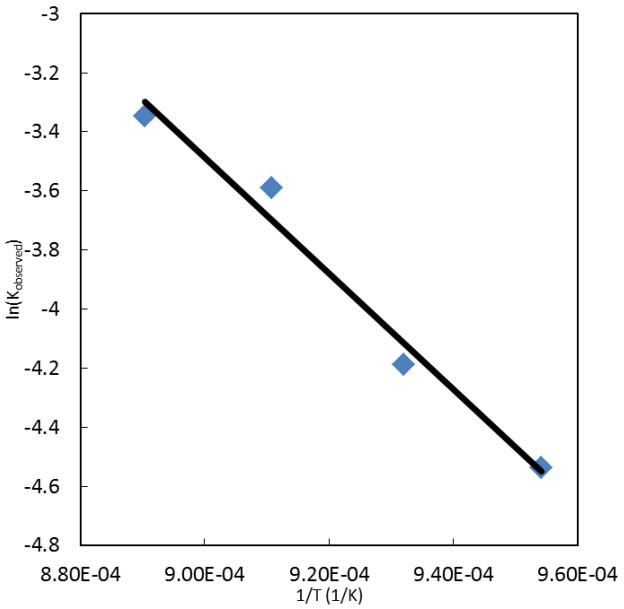

Figure IV-112. Ln($K_{observed}$) versus *1/T*

Table IV-4. Kinetic parameters of steam char reaction

A (1/min)	E_{act} (kJ/mole)	n_{char} (-)
1457160	163.3	0.722

The activation energy, E_{act}, and pre-exponential factor, A, were obtained by Fitting $\ln(K_{observed})$ versus $1/T$, see figure IV-112. Table IV-4 shows values of the kinetic parameters obtained.

Kinetic parameters obtained from the chemically controlled experiments were used in the simulations. In order to validate the numerical solution, the reactor temperature was increased to 1000°C and experimental results of char conversion versus time were compaerd to the numerical solution. Figure IV-113 shows the progress of total conversion with time for experimental and numerical results at 1000°C.

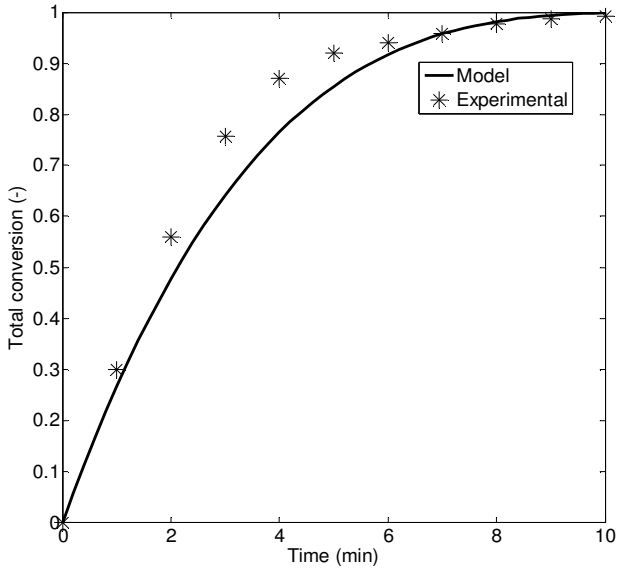

Figure IV-113. Progress of total conversion with time for experimental and numerical results at 1000°C

4.2.4.6. Results and discussion

Numerical simulations have been conducted for three cases; two extreme cases and one general case. The two extreme cases correspond to large Damkohler number and small Damkohler number while the third case corresponds to an intermediate value of Damkohler number.

Damkohler number, *Da*, is defined as [118]:

$$Da = \frac{KL^2 (C_S)^{n_{reaction}-1}}{D_{effective}} = \frac{K\left(2r_p\right)^2}{D_p} \quad \text{(IV-E24)}$$

where, K is the rate constant, L is the characteristic length, C_S is the concentration of the gasifying agent at the particle surface, $n_{reaction}$ is the reaction rate exponent with respect to the gasifying agent and $D_{effective}$ is the effective diffusivity inside the particle.

Damkohler number, *Da*, according to the above definition, represents the ratio between reaction rate and gasifying agent transport rate into the particle by diffusion or the ratio between chemical reaction time scale and diffusion time scale. It is worthy to note that, based on this definition, Damkohler number is similar to Thiele modulus which is also defined as the ratio between reaction rate and diffusion rate.

4.2.4.6.1. Effect of Damkohler number on Conversion and gasifying agent concentration profiles

Concentration and conversion profiles for extreme cases of initial values of *Da* have been investigated. Figure IV-114 shows the gasifying agent concentration profiles as function of *r* and *t* for a large initial value of *Da* number. Having a high *Da* number means that the reaction rate is much larger than the diffusion rate; the gasifying agent tends to react with the char particle as soon as it reaches the surface of the char particle. Consequently, the reaction mostly occurs at the outer layer of the car particle. Hence, the steep gradient in gasifying agent concentration occurs, especially during initial stages of the process. One can see that the gasifying agent concentration

dropped from a surface concentration to zero in less than 1mm distance from the outer surface of the particle.

A large *Da* number corresponds to a low porosity particle with a relatively large radius and high temperature with a high reaction rate constant.

After a certain time period into the process, the particle starts to shrink and its porosity increases. The smaller particle radius and higher porosity allows for less diffusion resistance and high effective diffusivity, and consequently a smaller Damkohler number. One can see in late stages of the particle reaction, the gasifying agent gradients get less steep, until they reach almost a horizontal line by the end of the process.

The initial value of *Da* number was $3.2607*10^{3}$ which corresponds to a particle radius of 1.3mm, initial porosity of 0.04, gas phase diffusivity of $5.91*10^{-4} m^2/s$ and a reactor temperature of 1200°C. It is important to note that the value of *Da* changes with time and the reported *Da* value here is the initial value of *Da* number.

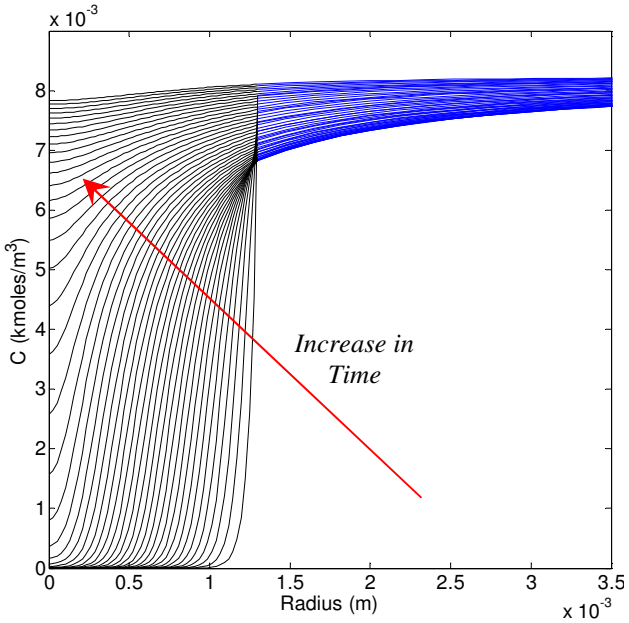

Figure IV-114. Concentration profiles for a large *Da* number case.

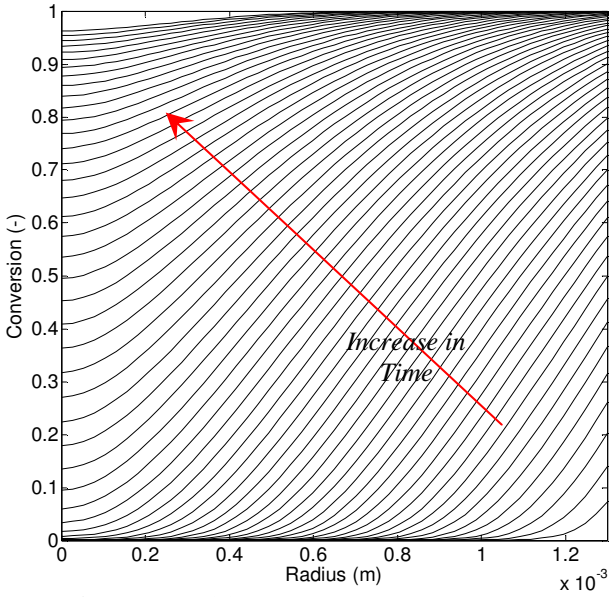

Figure IV-115. Conversion profiles for a large *Da* number case.

Figure IV-115 shows the local conversion as function of *r* and *t*. The conversion shows a steep variation with respect to the radius r, especially during the initial stages. This is attributed to the high value of reaction rate, large particle radius and low porosity; all of which results in high *Da* number. Notice that after a certain period of time the particle became small and porous enough to allow for more reaction in inner parts of the particle.

For the large *Da* number case, time step during simulations was one second. The gasification process has been simulated for two minutes duration. For conversion profiles shown in figure IV-114, profiles are plotted every two time interval, two seconds. For concentration profiles shown in figure IV-115, profiles are also plotted every two seconds. However, the last twelve plots, in figure IV-115, were deleted since concentration profiles tend to coincide on each other close to the asymptotic value of C_{∞}.

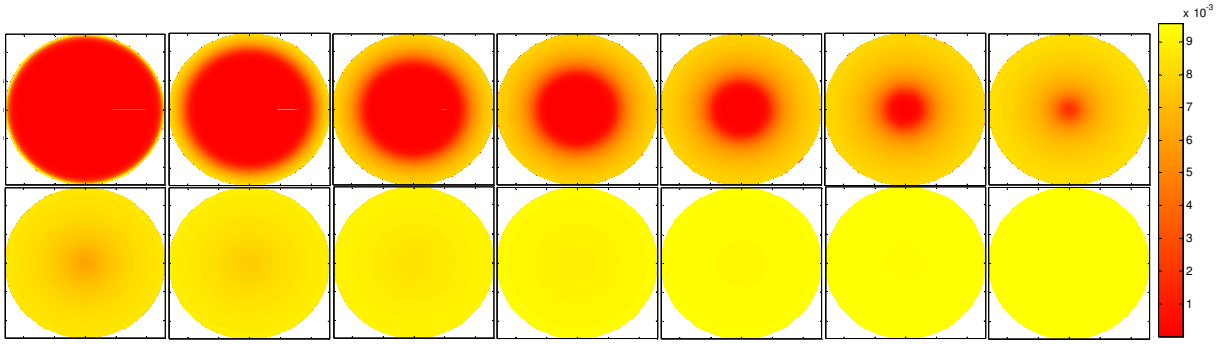

Figure IV-116. Progress of gasifying agent concentration inside the char particle for a large *Da* number case.

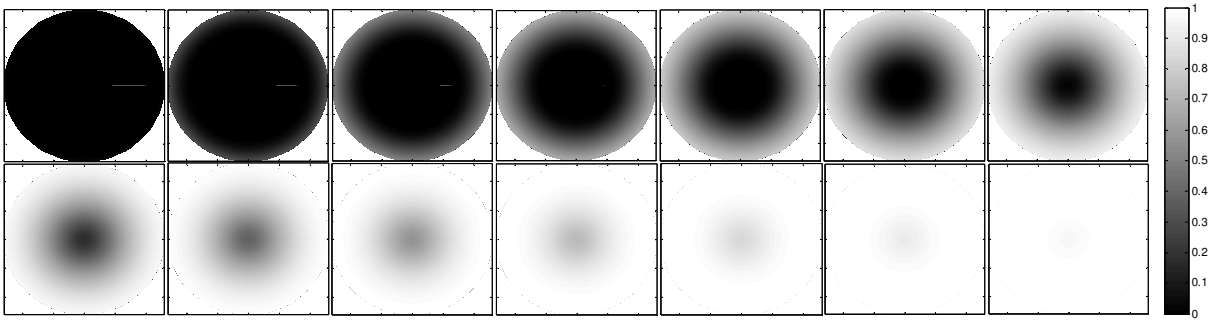

Figure IV-117. Progress of the char particle conversion with time for large *Da* number case.

Figure IV-116 and IV-117 show successive images of the gasifying agent concentration and char particle, respectively. Notice the distinct interface between the high gasifying agent concentration zone and the low concentration zone (see figure IV-116), as well as the high degree of conversion zone and the low conversion zone, see figure IV-117.

Figures IV-118 and IV-119 show the concentration profile and degree of conversion at successive time intervals for small *Da* case. *Da* number for this case is 0.0042, which is a very small value. This small value of *Da* number corresponds to chemical reaction controlling process; the reaction rate is much slower than the diffusion rate of gasifying agent. This allows enough time for the gasifying agent to diffuse inside the particle pores. One can see that the concentration profile is a constant horizontal line for all time intervals. The conversion profiles are straight horizontal lines parallel to the X-axis, which indicates that the whole particle reacts homogeneously.

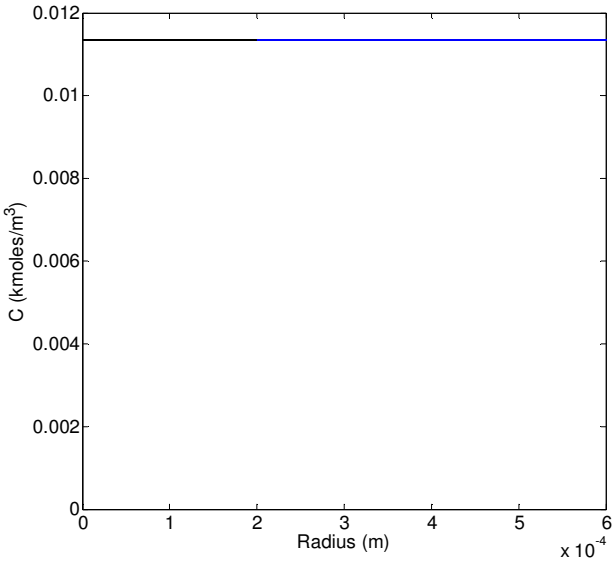

Figure IV-118. Concentration profiles for a small *Da* number case.

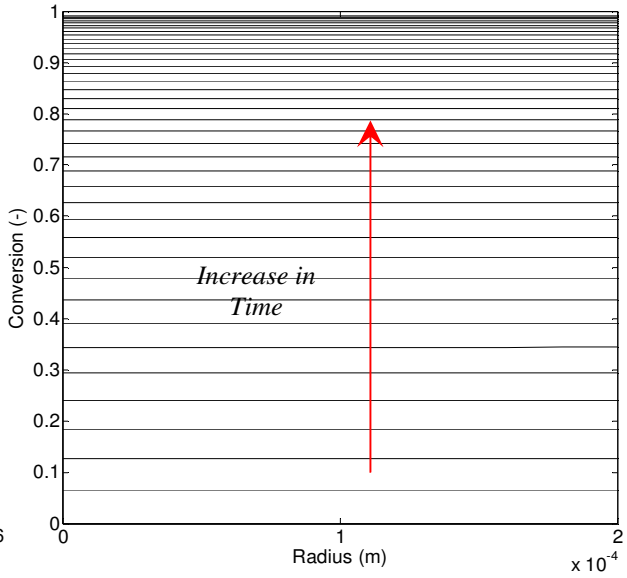

Figure IV-119. Degree of conversion for a small *Da* number case.

For the small *Da* number case, time step during simulations was one minute. The gasification process has been simulated for 162 minutes duration. Conversion profiles shown in figure IV-118 are plotted every four time intervals.

The constant concentration and the homogeneous conversion behavior are visualized in the images shown in figures IV-120 and IV-121; there is absolutely no gradient in the color of the conversion images. This case of chemically controlled process is used in determining the kinetic parameters of char-gasifying agent reactions.

The *Da* value of 0.0042 corresponds to a particle radius of 0.2mm, initial porosity of 0.4, gas phase diffusivity of $3.4353*10^{-4} m^2/s$ and a reactor temperature of 800^oC.

Figures IV-122 and IV-123 show the profiles of concentration and conversion for the general case. *Da* number has an intermediate value of 57.56. The gasifying agent concentration profiles show moderate slopes. Conversion profiles show a mild slope. The reaction occurs at the outer loops as well as inside the particle. The process is neither controlled by the chemical reaction nor the gasifying agent diffusion into the particle pores. Both affect the progress of the process.

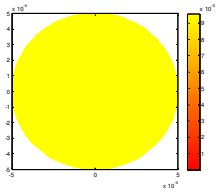

Figure IV-120. Gasifying agent concentration inside the char particle for a small *Da* number case.

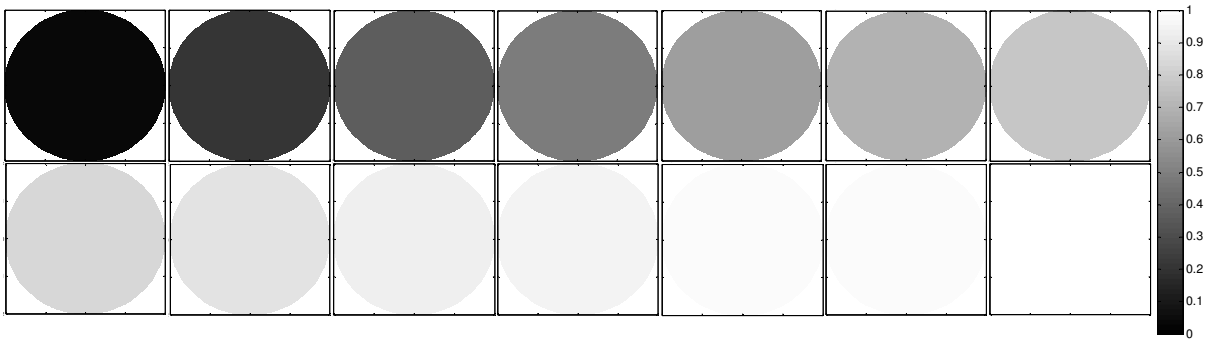

Figure IV-121. Progress of the char particle conversion with time for a small *Da* number case.

In this case, intermediate *Da* number, time step during simulations was four second. The gasification process has been simulated for 3.6 minutes duration. Conversion profiles shown in figure IV-122 are plotted every four seconds. Concentration profiles shown in figure IV-123 are also plotted every four seconds. The last twelve plots, in figure IV-123, were deleted since concentration profiles tend to coincide on each other close to the asymptotic value of C_∞.

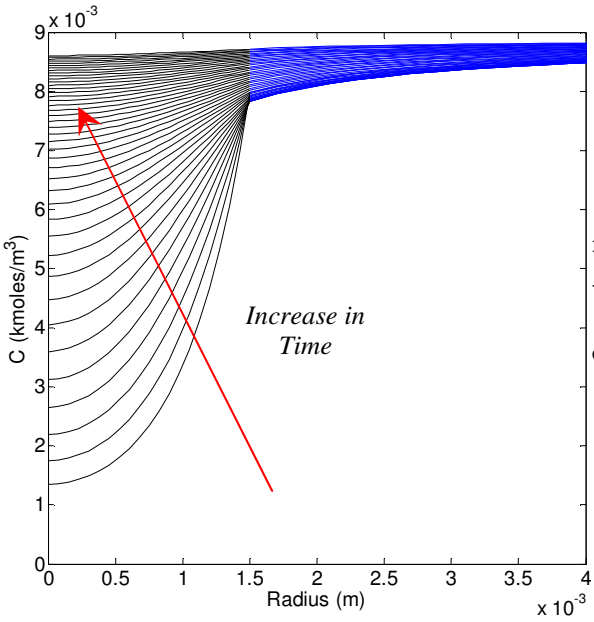

Figure IV-122. Concentration profiles for an intermediate *Da* number case.

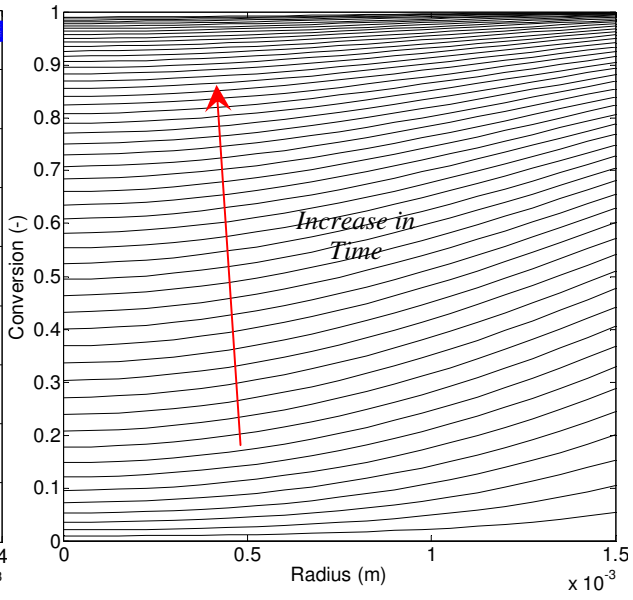

Figure IV-123. Conversion profiles for an intermediate *Da* number case.

Figures IV-124 and IV-125 show images of the gasifying agent concentration as well as the degree of conversion. One can see a smooth gradient of gasifying agent concentration and conversion at the initial stages of the process. After few minutes into the process the particle become smaller and porosity gets higher such that the effective diffusivity of the gasifying agent becomes high enough to have a chemically controlled process. This is confirmed by the near horizontal profiles of gasifying agent concentration shown in figure IV-122 as well as the even color shown in the concentration images at later stages of the process.

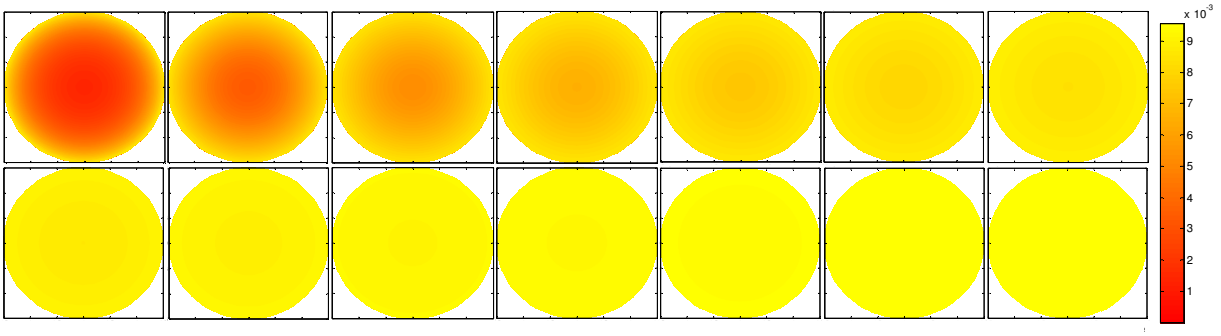

Figure IV-124. Progress of gasifying agent concentration inside the char particle for intermediate *Da* number case.

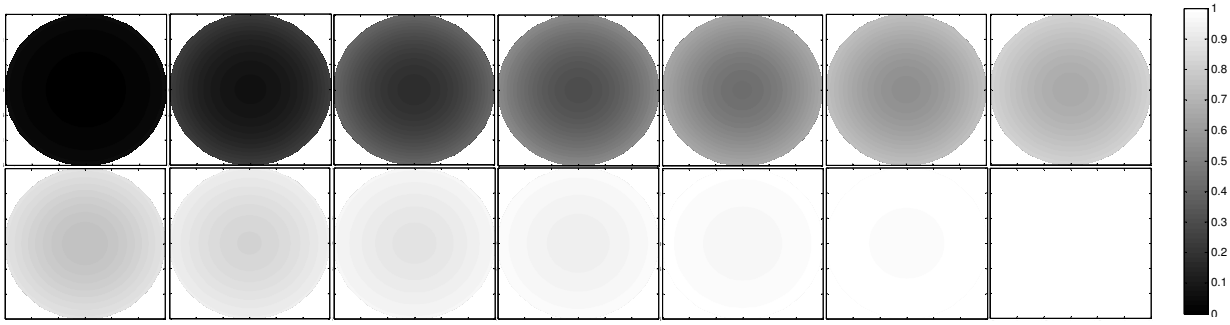

Figure IV-125. Progress of the char particle conversion with time for intermediate *Da* number case.

4.2.4.6.2. Effect of particle radius, r_p

The total conversion has been calculated using IV-E20 and IV-E21. Figure IV-126 represents the total conversion with time for different values of radii. Decrease in the particle radius decreases the resistance due to gasifying agent diffusion which consequently decreases the time duration for the conversion. One can see that the effect of decrease in the particle radius is sounder for big particles than that of small particles. This is attributed to the fact that reduction in diffusion resistance gets limited as the particle gets smaller.

4.2.4.6.3. Effect of initial porosity, ε_o

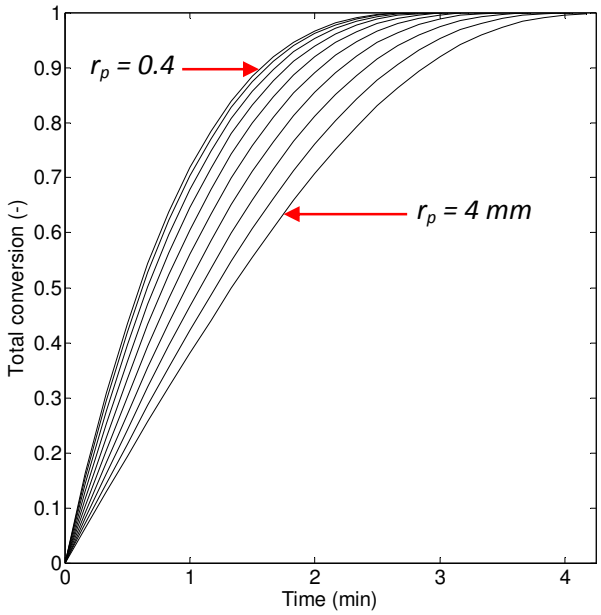

Figure IV-126. Total conversion versus time for different particle sizes, from r_p =0.4 to 4 mm in 0.4mms steps.

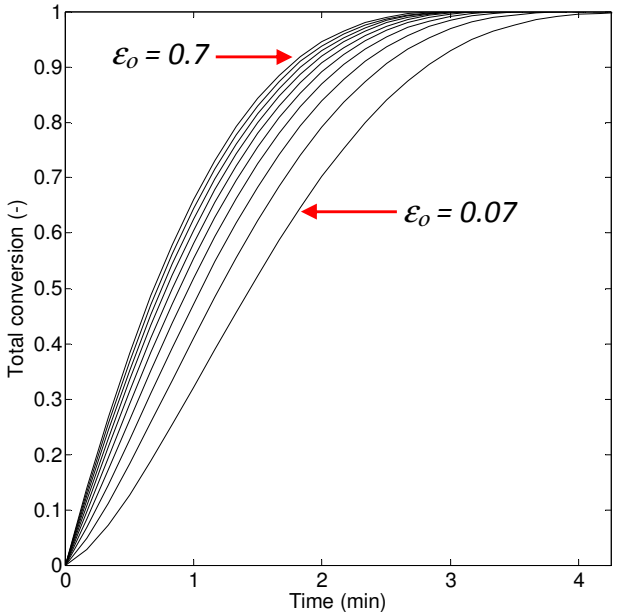

Figure IV-127. Total conversion versus time for different initial porosities, from ε_o = *0.07* to *0.7* in *0.07* steps.

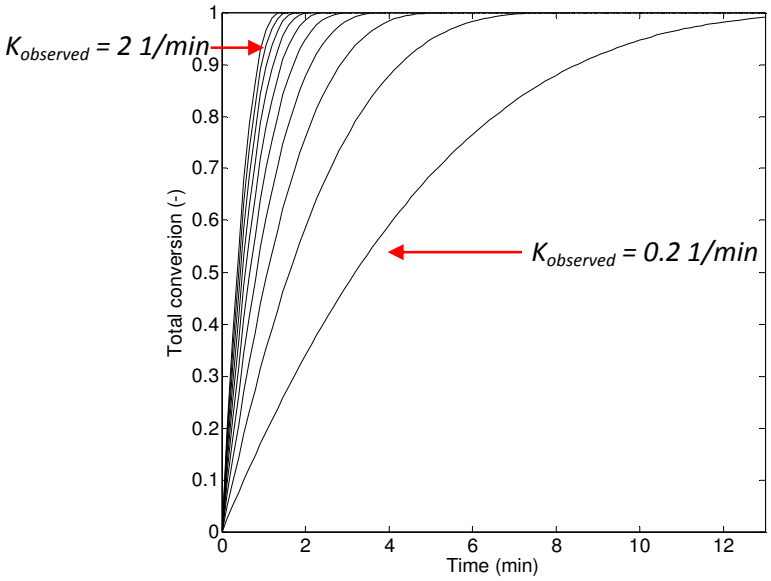

Figure IV-128. Total conversion versus time for different rate constants, from $K_{observed}$ =*0.2* to *2 1/min in 0.2 1/min* steps.

Figure IV-127 shows the effect of initial particle porosity on the progress of total conversion with time. The increase in initial porosity only affects the profile of total conversion-time relationship, i.e., the time duration required to reaches complete conversion, $t_{X=1}$, is almost the same for all initial porosity values. However, the time duration needed to reach *0.8* degree of conversion, for example, was affected by the increase in initial value of porosity. The reason for the weak dependency of $t_{X=1}$ on initial porosity is the progress of particle porosity towards a value of unity near $X=1$.

Increase in initial porosity is more effective in the low porosity range. One can see that for the higher initial porosity range the conversion-time profiles get closer to each other. This is attributed to the reduction in diffusion resistance with the increase in initial porosity, which results in shifting the problem towards a chemically controlled case, in which the reaction takes place homogeneously inside the particle.

Note that in equation IV-E10, the variation in initial porosity will vary the observed/effective rate constant value, $K_{observed} = \frac{K(T)C}{C_{carbon}(1-\varepsilon_o)}$. For consistent comparison between different values of initial porosity, *K(T)* was varied to keep constant value of the observed/effective rate constant, $K_{observed}$.

4.2.4.6.4. Effect of reaction rate constant, *K*

Figure IV-128 shows the effect of rate constant/reactor temperature on the progress of total conversion with time. The increase in rate constant decreased the time duration for complete conversion, especially at the low rate constant ranges. This effect decreases in the range of high rate constant values/reactor temperature. High values of reaction rate constants tend to shift the nature of the process towards being diffusion controlled.

4.3. Kinetics of syngas evolution during pyrolysis of solid wastes

4.3.4. Kinetics of Hydrogen evolution during polystyrene pyrolysis

Kinetics of hydrogen evolution from the PS pyrolysis is introduced. The Coats and Redfern method was used to determine the kinetic parameters, activation energy (E_{act}), pre-exponential factor (A) and reaction order (n). The model used is the nth order chemical reaction model. Kinetic parameters have been determined for three slow heating rates, namely 8, 10 and 12 ^{o}C/min. The averages values obtained from the three heating rates experiments were used to compare the model with the experimental data.

Considerable number of technical papers can be found that deal with the kinetics of thermal degradation of solid samples. However, not enough attention has been given to the kinetics of specific constituents resulting from thermal degradation of solid materials. In this study the kinetics of hydrogen evolution from PS is examined. In most cases the thermal

degradation rate is described as a function of reaction temperature and conversion of the sample. The hydrogen evolution will be treated in the same manor. The rate of hydrogen conversion will be a function of temperature and the hydrogen conversion. Hydrogen conversion is defined below in equation (IV-E25).

$$X = \frac{N_{H_2}}{N^*_{H_2}} \qquad \text{(IV-E25)}$$

where, X, N_{H_2} *and* $N^*_{H_2}$ are the conversion, number of hydrogen moles evolved at time (t) and total number of hydrogen moles evolved from the sample respectively. Reaction rate will be expressed as a function of the rate constant and hydrogen conversion, see equation (IV-E26).

$$\frac{dX}{dt} = k(T) * f(X) \qquad \text{(IV-E26)}$$

where, t , k, T, *and* $f(X)$ are the time, the rate constant, the temperature and a function that depends on the conversion, respectively. The rate constant is expressed using the Arrhenius equation given below in equation (IV-E27).

$$k(T) = A * \exp[-E_{act} / RT] \qquad \text{(IV-E27)}$$

where, A, E_{act} and R are the pre-exponential factor, activation energy and the universal gas constant respectively.

Coats and Redfern method is one of the most commonly used methods to determine the kinetics of thermal degradation of solids [119-124]. Coats and Redfern method will be used for the hydrogen evolution kinetics as well. Coats and Redfern method can be derived from the following equations:

$$\int_0^X \frac{1}{f(X)} dX = \int_0^t A * exp[-E_{act} / \bar{R}T\ ]\ dt \quad \text{(IV-E28)}$$

The sample was heated at a constant heating rate (q) and the temperature-time relation is given as:

$$T = T_o + q*t \quad \text{(IV-E29)}$$

$$\frac{dT}{q} = dt \quad \text{(IV-E30)}$$

$$\int_0^X \frac{1}{f(X)} dX = \frac{A}{q}\int_0^T \exp[-E_{act} / RT]\ dT \quad \text{(IV-E31)}$$

The right side of equation (IV-E31) does not have an exact solution. The approximation of Coats and Redfern is usually used.

$$\frac{A}{q}\int_0^T \exp[-E_{act} / RT]\ dT \approx \frac{ART^2}{qE_{act}}\left[1-\frac{2RT}{E_{act}}\right]\exp(-E_{act} / RT) \quad \text{(IV-E32)}$$

$$let\ g(X) = \int_0^X \frac{dX}{f(X)} \quad \text{(IV-E33)}$$

$$\ln\left(\frac{g(X)}{T^2}\right) = \ln\left(\frac{AR}{qE_{act}}\right) + \ln\left(1-\frac{2RT}{E_{act}}\right) - \frac{E_{act}}{R}\frac{1}{T} \quad \text{(IV-E34)}$$

For activation energies value corresponding to chemical reactions, 100 to 250 kJ/mol, the middle term from the right side of the equation can be neglected, since $RT/E_{act} << 1$. Based on this approximation one can find an estimate for activation energy (E_{act}) and pre-exponential factor (A) if $f(X)$ is known.

Finally, equation (IV-E34) can be simplified to equation (IV-E35)

$$F(X) = ln\left(\frac{g(X)}{T^2}\right) = ln\left(\frac{A\bar{R}}{qE_{act}}\right) - \frac{E_{act}}{R}\frac{1}{T} \quad \text{(IV-E35)}$$

Plotting $F(X)$ versus $(1/T)$ should give a linear relationship with the slope equal to $(-E_{act}/R)$ and an intercept of $ln(AR/qE_{act})$, provided the correct $f(X)$ is used.

The literature provides various expressions for $f(X)$ and consequently $g(X)$ based on the different mechanisms that could describe the process of solids thermal degradation. Table IV-5 presents examples of $f(X)$, $g(X)$ and the corresponding rate-determining mechanism.

Table IV-5 . Examples of $f(X)$, $g(X)$ and the corresponding rate-determining mechanism [120, 121].

Name of the function	$f(X)$	$g(X)$	**Rate-determining mechanism**
First order reaction	$(1-X)$	$-ln(1-X)$	Chemical reaction
Second order reaction	$(1-X)^2$	$(1-X)^{-1} - 1$	Chemical reaction
Third order reaction	$½(1-X)^3$	$(1-X)^{-2} - 1$	Chemical reaction
Mampel power law (n≠1)	$nX^{(n-1)/n}$	$X^{1/n}$	Nucleation
Avrami–Erofeev (n = 1.5, 2, 3, 4)	$n(1-X)[-ln(1-X)]^{(n-1)/n}$	$[-ln(1-X)]^{1/n}$	Random nucleation and its subsequent growth
Three-dimensional spherical symmetry, Jander equation	$1.5(1-X)^{2/3}[1-(1-X)^{1/3}]^{-1}$	$[1-(1-X)^{1/3}]^2$	Three-dimensional diffusion,
Three-dimensional spherical symmetry, Ginstling–Brounshtein	$1.5[(1-X)^{-1/3}-1]^{-1}$	$(1-2X/3)-(1-X)^{2/3}$	Three-dimensional diffusion,

Although the three dimensional diffusion models provided good fit for the experimental data, they have not been used. That's because in the derivation of the three dimensional diffusion models, the Jander model and Ginstling–Brounshtein model, a constant particle size was assumed [125]. These models would have been suitable for samples that yield char; however, it is considered not appropriate for use here since PS yields no char and the particle size is not constant.

On the other hand, Avrami–Erofeev model and Mampel power law did not provide a good fit, which indicate the process of hydrogen evolution from PS cannot be described using nucleation mechanisms.

Coats and Redfern method requires that the reaction order had to be fixed in advance to allow for the determination of activation energy (E_{act}) and pre-exponential factor (A) [126]. Both the second and third order reaction mechanism provided a good linear fit of $F(X)$ versus $(1/T)$. This means that the evolution of hydrogen from PS may be corresponding to a reaction order (n_{order}). Where (n) lies between 2 and 3. The process of determining (n) requires trial and error procedure. The procedure is given as follow:

- Assume (n)
- Fit $F(X)$ versus ($1/T$)
- Find the value of coefficient of determination (R_{cd}^2)
- Repeat above steps for different values of (n) between *2* and *3* in small increments
- The correct reaction order is the one corresponding to higher value of coefficient of determination (R^2)

For reaction order (n), $f(X)$ and $g(X)$ will take the following form of:

$$f(X)=\frac{(1-X)^n}{(n-1)} \quad and \quad g(X)=(1-X)^{1-n}-1 \qquad \text{(IV-E36)}$$

The experiments have been conducted at three heating rates of 8, 10 and 12^{o}C/min. The procedure of trial and error to find the maximum (R^2) value was repeated for the three heating rate. The corresponding kinetic parameters, (A), (E_{act}) and (n), were determined for each heating rate. Table IV-6 shows the kinetic parameters for the three heating rate as well as the average

value of (E_{act}), (A) and (n) at the three heating rate. The trial and error procedures were conducted using a Matlab code.

Figures IV-129a, IV-129b and IV-129c show a plot of $F(X)$ versus ($1/T$) and the linear fitting using the optimized values of (n) from the Matlab code. High values of coefficient of determination (R^2) indicate that the process can be adequately described by chemically controlled reaction model with a reaction order (n).

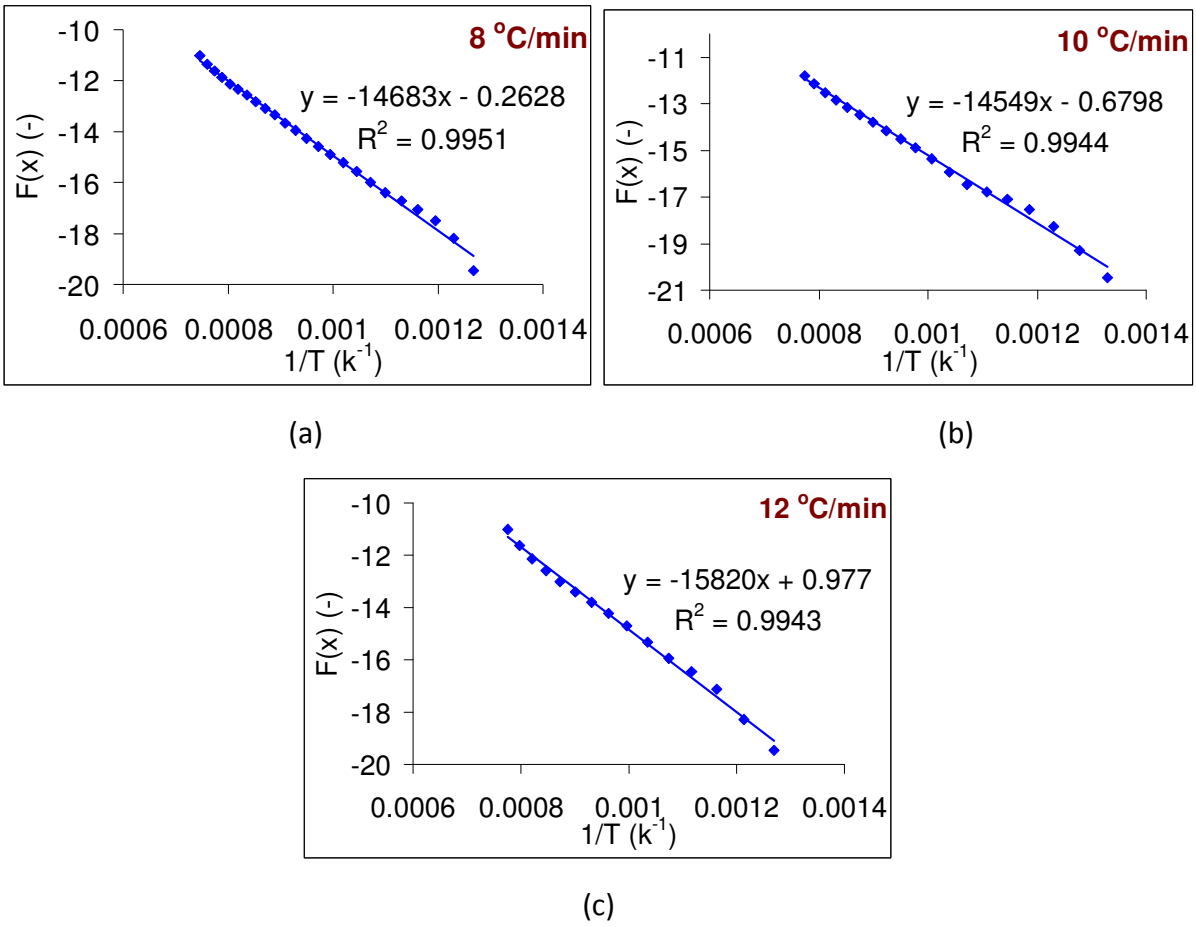

Figure IV-129. $F(X)$ versus ($1/T$) for heating rate (a) 8, (b) 10 and (c) 12°C/min.

After determining values of (A), (E_{act}) and (n) that best fits the experimental data for each heating rate, the average of these parameters has been used to compare the model results with the experimental results of conversion (X) versus temperature (T). Figures IV-130a, IV-130b and IV-

130c show a plot of conversion versus temperature for both the experimental data and the n^{th} order reaction model. Equation (IV-E35) was used to plot the conversion versus temperature for the model. One can see that the model follows the same trend as the experimental data with good proximity in conversion values.

Table IV-6 - Kinetic parameters for the three heating rate.

Heating rate(q) **(^{o}C/min)**	***Reaction order*** **(*n*)**	E_{act}/R **(K)**	$ln(AR/E_{act}q)$ **-**	E_{act} **(kJ/mol)**	***A*** **(min^{-1})**
8	2.411	14683	-0.26	122	90570.8
10	2.204	14549	-0.67	120.9	74448.48
12	2.2065	15192	0.0074	126.3	183658.1
Average	**2.273833**	**14808**	**-0.30753**	**123.1**	**116225.8**

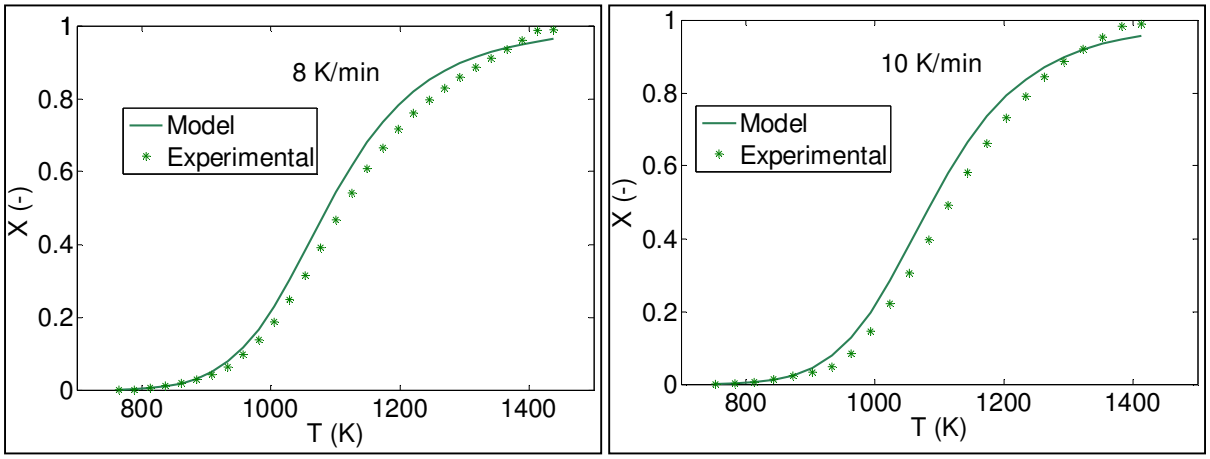

(a) (b)

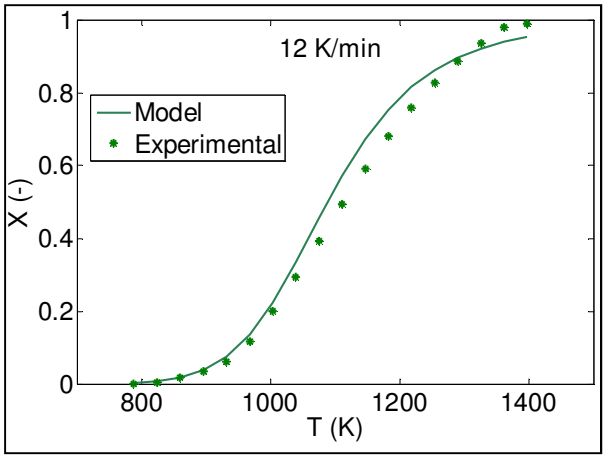

(c)

Figure IV-130. Conversion (X) versus temperature (T) for heating rates (a) 8, (b) 10 and (c) 12°C/min.

4.3.5. Kinetics of syngas evolution from paper pyrolysis

Evolution of main syngas constituents from the sample during pyrolysis such as H_2, CO, CO_2 and CH_4 have been modeled as a group of parallel first order reactions. The resulting conversion rate curve is a weighted sum of pseudo reactions conversion rates, $d\alpha_j/dt$, reaction rates, see equations IV-E37 and IV-E38. Each gas is assumed to be evolving from more than one pseudo precursors. Consequently, each gas is assumed to be evolving as a result of parallel independent reactions. These reactions are assumed to be first order reactions. The conversion from each reaction contributes the overall gas conversion by a fraction.

$$\frac{da_j}{dt} = \sum w_i \frac{da_i}{dt} \qquad \text{(IV-E37)}$$

$$and \ \frac{d\alpha_i}{dt} = K_i(1-\alpha_i) \qquad \text{(IV-E38)}$$

where, α_j is the overall conversion at time t for gas j, α_i is the conversion from pseudo reaction i, w_i is the weight of reaction i and K_i is the reaction rate constant for reaction i.

In order to evaluate the kinetics parameter for the first order model, paper sample was heated at a constant heating rate of 10°C/min from 200°C to 1000°C using the experimental facility. Integrating equation (IV-E38) provides one to obtain a relationship between conversion from reaction *i* and sample temperature, see equations (IV-E39) and (IV-E40),

$$\int \frac{d\alpha_i}{(1-\alpha_i)} = \int K\, dt \qquad \text{(IV-E39)}$$

$$or \quad \int \frac{d\alpha_i}{(1-\alpha_i)} = \int A\, e^{-\frac{E_{act)i}}{RT}}\, dt \qquad \text{(IV-E40)}$$

where, A, E_{act} R, and T are the pre-exponential factor, activation energy, universal gas constant and temperature respectively. For a constant heating rate, sample temperature is expressed as function of time.

$$T = T_O + q\,t \quad and \quad dT = q\,dt \qquad \text{(IV-E41)}$$

where, T_o is the initial sample temperature and q is the heating rate. Considering the relationship between time and reactor temperature from equation (IV-E41), equation (IV-E40) yields:

$$\int \frac{d\alpha_i}{(1-\alpha_i)} = \frac{A}{q}\int e^{-\frac{E_{act)i}}{\bar{R}T}}\, dT \qquad \text{(IV-E42)}$$

The expression on the right hand side of equation (IV-E42) has no exact solution. There are different methods to determine numerical integration of equation (IV-E42). The method is described in [122] and was developed by Coats and Redfern.

$$\ln\left[\frac{-\ln(1-\alpha_i)}{T^2}\right] = \ln\left[\frac{A\bar{R}}{q\,E_{act)i}}\left[1-\frac{2\bar{R}T}{E_{act)i}}\right]\right] - \frac{E_{act)i}}{\bar{R}T} \qquad \text{(IV-E43)}$$

Equation (IV-E43) is used to find a relationship between the conversion from reaction *i* and the sample temperature. Values of conversion from *i* and reaction rate are used in equation (IV-E38) to find a relation between temperature and the conversion rate. Note that these procedures are carried out for each reaction (*i*). For the preceding steps to be achieved, activation energy and pre-exponential factor have to be known. Different combinations of pre-exponential factor (*A*) and activation energy (E_{act}) can provide a good fit for experimental data. For this reason, the pre-exponential factor value (*A*) is often fixed. In a more detailed study about evolution of gases from coal pyrolysis by Porada [103], pre-exponential factors varied from *7.03E5 to 3.76E13 min*$^{-1}$. For simplicity, in this study the pre-exponential factor value was set to *1E10 min*$^{-1}$.The first order model parameters, $E_{act)i}$ and w_i were determined by trial and error. Values of activation energies ($E_{act)i}$) and pseudo reactions weights (w_i) where adjusted such that the overall conversion rate curve from the model matches the experimental conversion rate curve. Figure IV-131 shows the experimental value for conversion rate, the first order model fit and pseudo reactions *i* for H_2, CO, CO_2 and CH_4 evolution. Table IV-7 shows the first order model parameters for the main gases evolved.

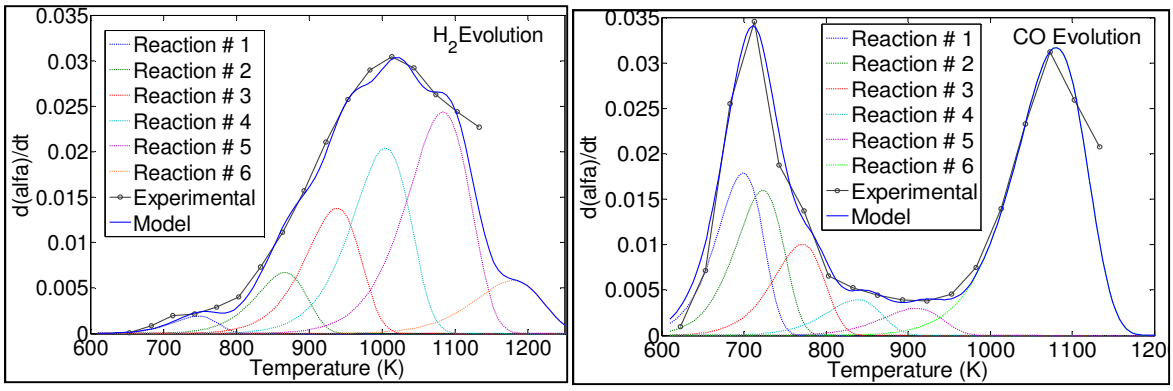

(a) **(b)**

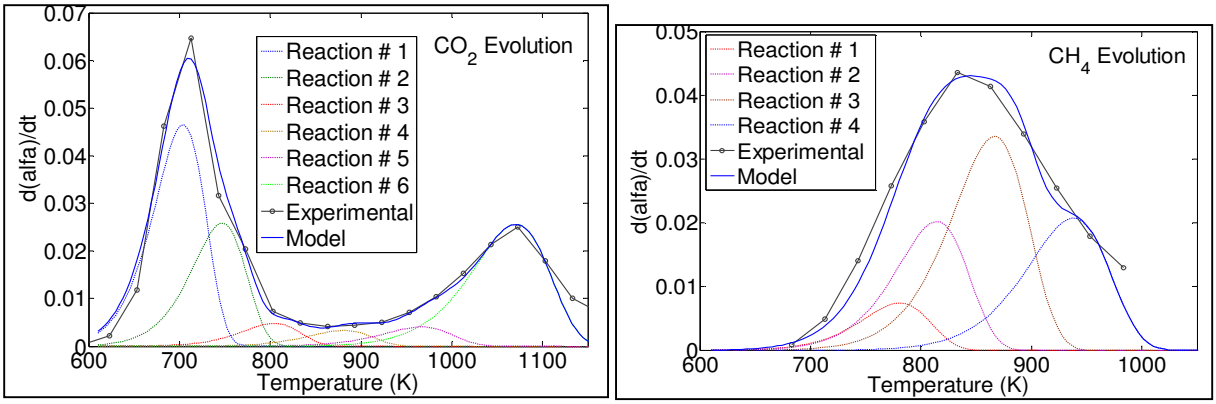

(c) **(d)**

Figure IV-131. Experimental conversion rates of main gases during pyrolysis and their first order model fit; (a) H_2, (b) CO, (c) CO_2 and (d) CH_4

Figures IV-131a, IV-131b, IV-131c and d show the change in conversion rate for H_2, CO, CO_2 and CH_4 with temperature. In each figure, the experimental change in conversion rate at various temperatures is represented by circles on the marked curve, while the solid continuous line represents the first order model. The solid continuous curve representing the model is the summation of dotted lines representing reactions IV-E37 to IV-E42 as the sample undergoes pyrolysis to evolve into the overall gas specie. Each dotted line represents the conversion rate from a single reaction. Thus, each dotted line represents a single reaction that contributes partially to the overall evolution curve of conversion rate.

Table IV-7. Kinetic parameters of the parallel first order reactions model*

	H_2	***CO***	***CO_2***	***CH_4***
E_{act1} (kJ/kmol)	*1.5E5*	*1.4E5*	*1.41E5*	*1.57E5*
E_{act2} (kJ/kmol)	*1.75E5*	*1.45E5*	*1.5E5*	*1.64E5*
E_{act3} (kJ/kmol)	*1.9E5*	*1.55E5*	*1.62E5*	*1.75E5*

E_{act4} **(kJ/kmol)**	*2.04E5*	*1.69E5*	*1.78E5*	*1.9E5*
E_{act5} **(kJ/kmol)**	*2.207E5*	*1.84E5*	*1.96E5*	----
E_{act6} **(kJ/kmol)**	*2.41E5*	*2.2E5*	*2.18E5*	----
w_1	*0.015*	*0.13*	*0.34*	*0.06*
w_2	*0.06*	*0.12*	*0.2*	*0.17*
w_3	*0.133*	*0.08*	*0.04*	*0.3*
w_4	*0.21*	*0.034*	*0.030*	*0.2*
w_5	*0.27*	*0.028*	*0.04*	----
w_6	*0.07*	*0.35*	*0.280*	----

***A is taken here as 1E10 min^{-1}**

E_{acti} in the above table is the activation energy of pseudo reaction *i,* and w_i is the weight of conversion rate from reaction *i* that contributes to the overall conversion rate.

Table IV-7 shows the numerical values of activation energies (E_{acti}) and reaction weights (w_i) for the group of first order reactions used to describe the overall curve. High values of activation energies represent reactions for which its peak value shifts towards higher temperatures. For example, the sixth pseudo reaction in hydrogen evolution has activation energy of 2.41E5 kJ/kmol. Conversion rate of the sixth pseudo reaction shows a peak at the highest temperature.

Chapter V: Experimental uncertainty analysis

5.1. Flow rates uncertainty [Systematic error]

Accuracy of syngas properties depends mainly on the accuracy of measuring syngas constituents. Individual flow rates of syngas constituents are calculated using equation 5.1

$$f_i = f_{N_2} \frac{MF_i}{MF_{N_2}} \qquad \text{(Eq. 5.1)}$$

The uncertainty in flow rates is calculated using equation 5.2

$$df_i = \frac{df_i}{df_{N_2}} \Delta f_{N_2} + \frac{df_i}{dMF_i} \Delta MF_i + \frac{df_i}{dMF_{N_2}} \Delta MF_{N_2} \qquad \text{(Eq. 5.2)}$$

The differentials in equation 5.2 are, $\frac{df_i}{dMF_i} = \frac{f_{N_2}}{MF_{N_2}}$, $\frac{df_i}{dMF_{N_2}} = -\frac{f_{N_2} MF_i}{(MF_{N_2})^2}$ and $\frac{df_i}{df_{N_2}} = \frac{MF_i}{MF_{N_2}}$.

The percentage of error in flow rate has been determined by dividing the variation in flow rate by the flow rate of the specific constituent i, (Eq. 5.3).

$$Percentage\ of\ error = \frac{df_i}{f_i} = \frac{\frac{df_i}{df_{N_2}} \Delta f_{N_2}}{f_i} + \frac{\frac{df_i}{dMF_i} \Delta MF_i}{f_i} + \frac{\frac{df_i}{dMF_{N_2}} \Delta MF_{N_2}}{f_i} \qquad \text{(Eq. 5.3)}$$

The share of each term in the percentage of uncertainty is calculated using equations 5.4a -5.4c.

$$\frac{\frac{df_i}{df_{N_2}} \Delta f_{N_2}}{f_i} = \frac{\frac{MF_i}{MF_{N_2}} \Delta f_{N_2}}{f_{N_2} \frac{MF_i}{MF_{N_2}}} = \frac{\Delta f_{N_2}}{f_{N_2}} \qquad \text{(Eq. 5.4a)}$$

$$\frac{\frac{df_i}{dMF_i} \Delta MF_i}{f_i} = \frac{\frac{f_{N_2}}{MF_{N_2}} \Delta MF_i}{f_{N_2} \frac{MF_i}{MF_{N_2}}} = \frac{\Delta MF_i}{MF_i} \qquad \text{(Eq. 5.4b)}$$

$$\frac{df_i}{dMF_{N_2}} \Delta MF_{N_2} \Big/ f_i = \frac{-\frac{f_{N_2} MF_i}{(MF_{N_2})^2} \Delta MF_{N_2}}{f_{N_2} \frac{MF_i}{MF_{N_2}}} = \frac{-\Delta MF_{N_2}}{MF_{N_2}} \qquad \text{(Eq. 5.4c)}$$

The percentage of uncertainty error is simplified to equation 5.5. The first term in the right hand side of equation 5.5 represents error in flow rate due to uncertainty in the nitrogen flow meter reading. The second and third term arose from the uncertainty in the GC reading.

$$Percentage\ of\ error = \frac{df_i}{f_i} = \frac{\Delta f_{N_2}}{f_{N_2}} + \frac{\Delta MF_i}{MF_i} + \frac{-\Delta MF_{N_2}}{MF_{N_2}} \qquad \text{(Eq. 5.5)}$$

$$\Delta f_{N_2} = 1.5\%\ of\ flow\ meter\ full\ scale, 0.075\ LPM$$

$$\Delta MF_i = 0.1\%\ [-]$$

$$\Delta MF_{N_2} = 0.1\%\ [-]$$

The first term in the percentage of error equation, Eq. 5.5, is constant and has a value of 3%. The second term is variable and ranges from 0.5% to 0.1% for nitrogen mole fraction ranging from 20% to 100%. The third term is variable as well. Variation of the third term is illustrated in figure V-1 below: the 5% percentage of error mark is corresponding to a mole fraction of 2%. Figure V-1 indicates that the percentage of error is magnified only near the very small values of mole fraction. The percentage of uncertainty error is negligible for mole fraction values higher than 5%. Very small values of mole fraction occur near the end of each experiment which is corresponding to very small values of syngas flow rate.

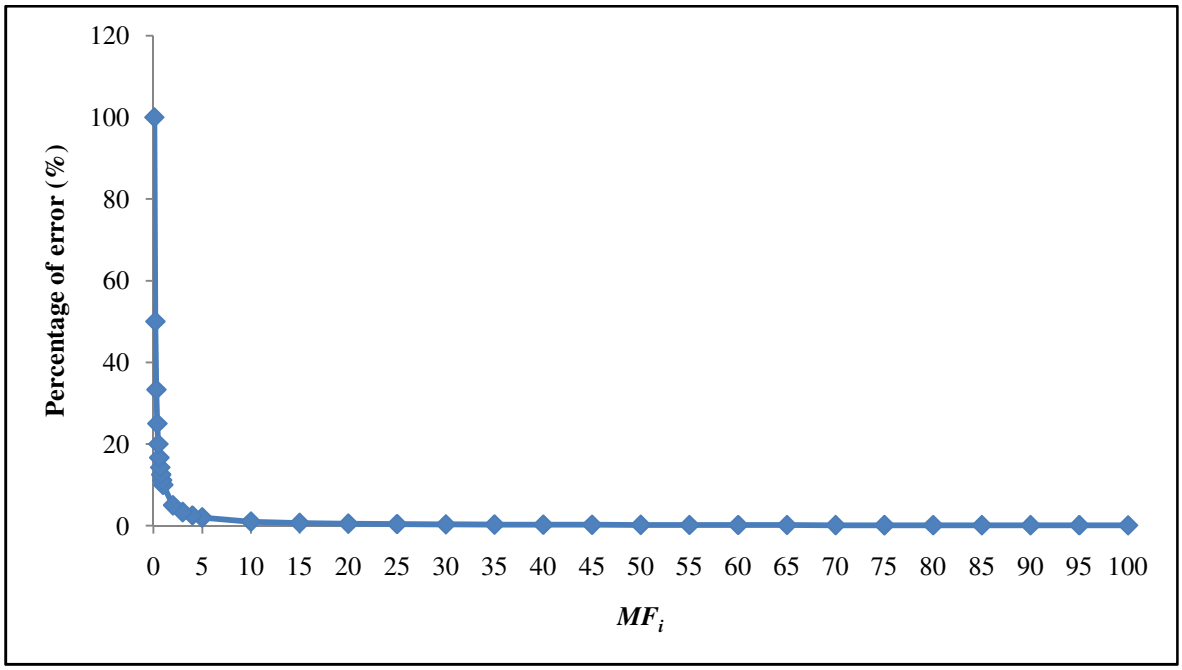

Figure V-1. Variation of percentage of uncertainty error due to uncertainty in MC reading as a function of syngas constituent mole fraction.

5.2. Data repeatability [Random error]

Formally random error should be calculated using equation 5.6

$$\sigma_y^2 = \sum_{i=1}^{n} \sum_{j=1}^{n} \left(\frac{\partial y}{\partial x_i}\right)\left(\frac{\partial y}{\partial x_j}\right)\sigma_{i,j} \quad \text{(Eq. 5.6)}$$

Where σ_y^2 is the variance of dependent variable y, n is the number of independent variables x and $\sigma_{i,j}$ is the covariance of x_i and x_j

However, since each run takes about 6 hours from start to finish and 8 hours for the reactor to cool down to start the next experiment, it is impossible to repeat the experiment enough time in order to find the means and standard deviations of measured properties. Consequently, assessment of random error will be achieved by checking for data repeatability.

In order to insure repeatability of the experimental results, some runs have been repeated and reported in the figures below. Sample results of paper gasification at 1000^{o}C are presented in

figure V-2 to show repeatability of the experiments. Evolution of syngas flow rate and hydrogen flow rate are plotted and shown in figure V-2. The repeated run (run# 2) showed the same trend as the first run (run#1) with a slight deviation in values. The plots reveal a good repeatability of the data.

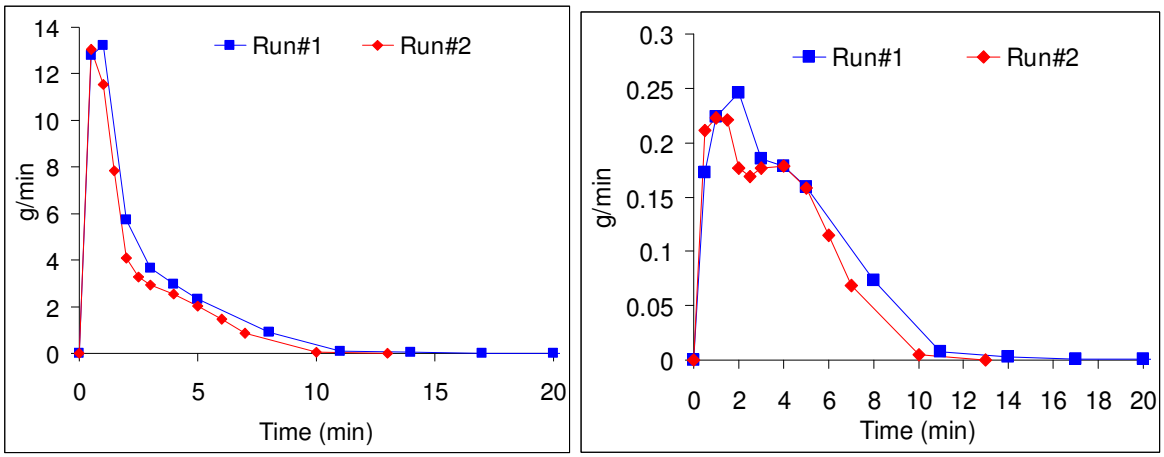

(a) (b)

Figure V-2. (a) Syngas flow rate and (b) H_2 flow rate at 1000°C for two runs

Repeatability of the data has been checked for the mixture experiments as well. The 80%PE-20%WC run was repeated two more times. Results of the three runs are shown in figure V-3 for syngas flow rate, hydrogen flow rate and output power. Excellent repeatability was obtained. The 80%PE-20%WC run was chosen because of the high synergistic effect noticed at this run. The deviation in total yield of syngas, hydrogen and energy among the three runs was 0.16%, 0.68% and 1.23% respectively.

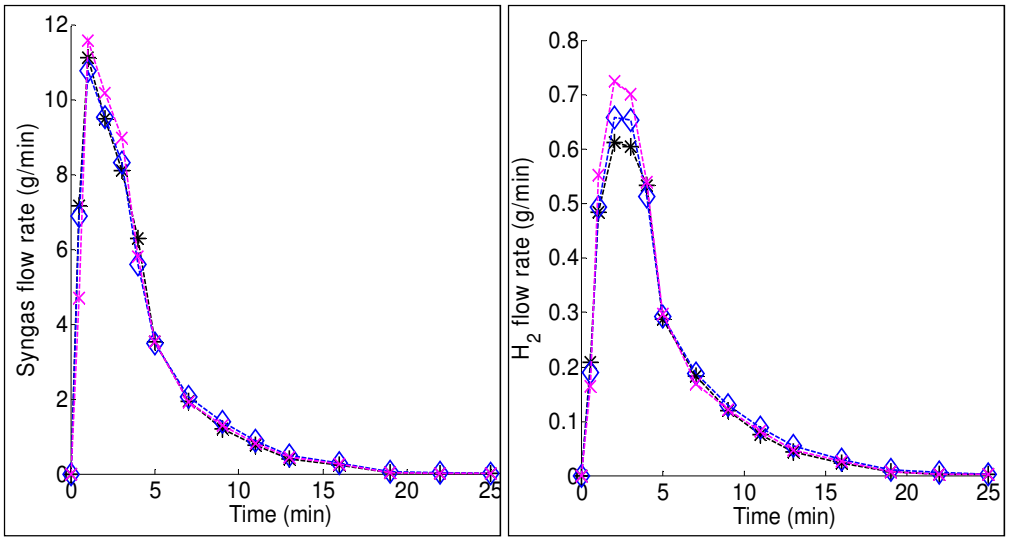

(a) (b)

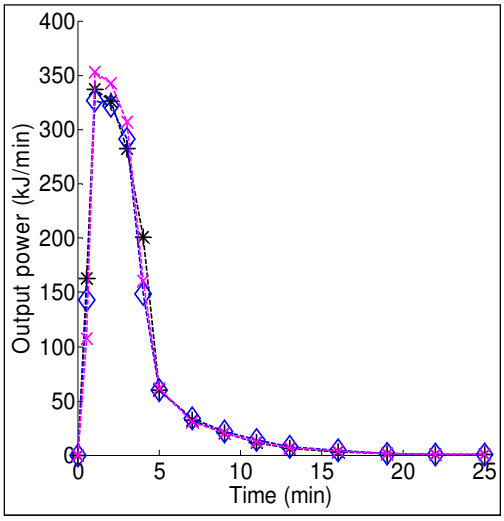

(c)

Figure V-**3.** Syngas flow rate, (b) hydrogen flow rate and (c) output power for three runs at 80% PE-20%WC mixture conditions

5.3. Variation in gasifying agent partial pressure

In the RPM experiments it is important to insure minimum variation in syngas partial pressure since reaction rate might be a function in gasifying agent partial pressure. Variation of gasifying agents' partial pressures has been calculated based on the gas analysis of the syngas.

Figure V-4 shows the variation of steam partial pressure with sample conversion for the investigated steam nominal partial pressure. It can be seen from the plots that there is only a negligible deviation of steam partial pressure from the nominal pressure.

Beside the fact that steam partial pressure is almost constant throughout the experiments, variation of steam partial pressure did not affect the reaction rate-conversion relationship. This conclusion is drawn from figure V-106, where the reaction rate is plotted versus conversion for steam partial pressures of 1.5, 1.2, 0.9 and 0.6 bars. It is confirmed from this plot that variation in steam partial pressure, in the tested range, does not affect the reaction rate. With this result in mind, the slight reduction in steam partial pressure with sample conversion would not affect reaction rate values.

Concerning the partial pressure variation of CO_2, figure V-4b, negligible variation in CO_2 partial pressure is observed for experiments at 0.6 and 0.9 bars. Moderate variation in CO_2 partial pressure is noticed initially at 1.5 and 1.2 bars. Figure V-107 shows the effect of CO_2 partial pressure on reaction rate-conversion relationship for CO_2 partial pressures of 1.5, 1.2, 0.9 and 0.6. Similar to what have been concluded in the case of steam gasification, the experiments confirm that variation of CO_2 partial pressure, in the tested range, did not affect the reaction rate-conversion relationship. Recalling that the CO_2 partial pressure varied from 1.5 bars down to 0.6 bars, it is confirmed that the initial decrease of CO_2 partial pressure for the 1.5 and 1.2 experiments would not have affected the reaction rate values. Based on the negligible variation of partial pressures and negligible reaction order with respect to steam and CO_2, in the tested range, a batch reactor analysis was followed.

The total pressure of the system was set constant to 2 bars. Argon was added to adjust the total pressure to 2 bars while maintaining a constant flow rate of gasifying agent. Negligible deviation

of gasifying agent partial pressure in most cases indicates negligible inhibitors concentrations, H_2 and CO. On the other hand, inhibition effect of H_2 and CO is considerable at higher pressures [31, 39].

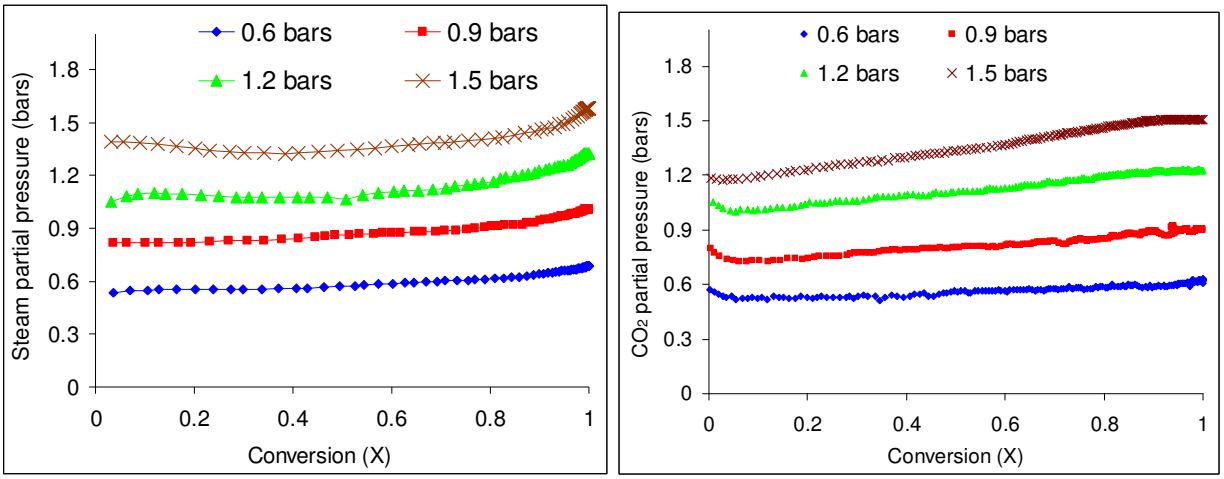

(a) **(b)**

Figure V-4. Variation of (a) steam and (b) CO_2 partial pressures with sample conversion

5.4. Experiments with different sample mass and different chips size

Implementing the RPM, requires that the reaction rate, *dX/dt (1/min)*, is independent on either the wood chips size or the amount of sample.

Dependency of reaction rate on sample mass and chips size was tested by repeating the "0.9 bars CO_2" experiment for a smaller sample mass (20 grams) and finer wood chips size. Figure V-5 shows the reaction rate, *dX/dt (1/min)*, as a function of sample conversion for the basic sample, finer chip size sample and a smaller mass sample. It can be seen from figure V-5 that the plots of reaction rate versus sample conversion coincide with each other. This indicates independency of reaction rate on wood chip size and sample mass.

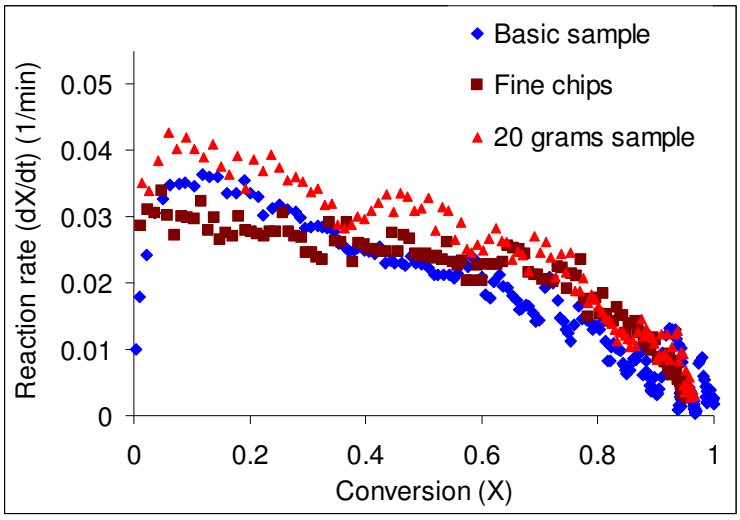

Figure V-**5.** Reaction rate versus sample conversion for finer chips sample and smaller mass sample

Chapter VI: Conclusions

6.1. Characteristics of syngas evolution from char based samples

In general the gasification process starts with a high flow rate of syngas that attribute to depolymerization and fragmentation of long chains of hydrocarbons; cellulose, lignin or hemicellulose. This high flow rate in the initial stage is followed by a steep decrease in syngas flow rate then an extended period of char gasification. Steam char gasification reaction is a strong function in reactor temperature; an increase in reactor temperature from 700 to 900^{o}C can result in a decrease in the duration of char gasification by 10 folds. The evolution of syngas in the first 2 to 6 minutes is mainly attributed to the sample pyrolysis; the chemical composition and flow rate form gasification coincides with that from pyrolysis during the first 2 to 6 minutes. The extent of overlap in chemical composition and flow rate overlap decreases by the increase in reactor temperature.

After the initial stage of high syngas flow rate, which is attributed mainly due to sample pyrolysis, there is a period of steam hydrocarbon reforming reactions and char gasification reactions which is then followed by an extended stage of char only gasification. In this middle stage one can have a flow rate of syngas from the pyrolysis experiment and a higher syngas flow rate from the gasification experiment. The presence of flow rate from pyrolysis experiments indicates the presence of volatile hydrocarbons which react partially with steam and contribute partially to the higher flow rate of syngas in this intermediate stage. The overlap between steam hydrocarbon reforming reactions and char gasification reactions increase with the increase in reactor temperature. This increase in overlap indicates stronger dependency of char gasification on temperature.

The difference in syngas flow rate/yield between gasification and pyrolysis at 600^{o}C is almost negligible. This indicates that Steam-hydrocarbons reactions and char gasification reactions are very slow at this temperature.

Dependency of syngas properties (flow rate and chemical composition) on steam flow rate is much weaker than the dependency of syngas properties on temperature. The increase in steam flow rate promotes steam hydrocarbon reforming reactions and water gas shift reaction and result in a higher hydrogen flow rate/yield. The increase in steam flow rate slightly increased the syngas yield and energy yield as well.

The total syngas yield and its main constituents did not have a clear trend during gasification. The syngas yield and its constituents are almost the similar for reactor temperatures of 700 to 1000^{o}C. However, results indicate the presence of a small peak at 900^{o}C for the syngas and hydrogen yields, during gasification. In the case of rice husk gasification a slight decrease in hydrogen yield was observed. The behavior of hydrogen yield as well as CO yield form gasification and pyrolysis can be explained in terms of hydrogen and carbon content in char, liquid hydrocarbons (HCs) and syngas. Under non-isothermal pyrolysis conditions, char yield is maximized at the conditions of low temperature and low heating rates. The liquid hydrocarbons yield is maximized at the conditions of intermediate reactor temperatures and high heating rates. The syngas yield is maximized for the conditions of high heating rate and high reactor temperatures. Hydrogen yield form gasification is attributed to the pyrolysis part as well the char gasification part. The increase in reactor temperature tends to increase the hydrogen yield in the form of syngas, but it also tends to increase the hydrogen content in the liquid hydrocarbons and tends to decrease the char formed. Having less char formed resulted in less yield of hydrogen in the syngas from the char gasification reaction: ($C+H_2O \rightarrow CO + H_2$). The existence of a slight

peak or decrease in the hydrogen yield for rice husk gasification is mainly attributed to competing effects of syngas increase due to increase in temperature and less char formed which in turn forms less hydrogen via the water gas reaction. Same discussion applies for the CO behavior; CO yield increases directly with the increase in reactor temperature and heating rate by pyrolysis. However, the carbon yield in form of char decreases as the reactor temperature increases. Although this competing effect, CO yield usually increases with temperature or at least results in a flat CO yield. The CO is known to be formed in competition with CO_2 in which CO is favored at high pyrolysis temperatures.

Despite this complicated behavior of hydrogen, CO and CO_2 behavior, energy yield and apparent thermal efficiency always increases with the increase in reactor temperature. Beside the dominate effect of CO increase, gaseous hydrocarbons usually increases with the increase in reactor temperature to result in consistent increase in energy yield and apparent thermal efficiency. Gaseous hydrocarbons are formed via fragmentation and tertiary reactions during pyrolysis. These reactions are promoted at high heating rates and high reactor temperatures.

The first step in biomass gasification is activation of cellulose, lignin and hemicellulose. After activation, the precursors undergo parallel reactions during initial stages of pyrolysis. The precursors may also undergo fragmentation reactions by carbon bonds scission, decarbonylation and decarboxylation, resulting in fragmented hydrocarbons; ketones, aldehydes and acetic acids. On the other hand the activated compounds may also undergo depolymerization to form cyclic and heterocyclic compounds. The fragmentation route is favored at high heating rates and high reactor temperatures. However, the depolymerization route is favored at high/medium heating rates and intermediate reactor temperatures. Cyclic compounds might undergo fragmentation through secondary reactions to yield gaseous hydrocarbons and fragmented hydrocarbons, which

in turn, might undergo tertiary reactions to yield gaseous hydrocarbons and carbon monoxide [35]. Char is formed by three routes; the first is charring and coke formation at low heating rates and low temperatures. The second route is aromatization and repolymerization from fragmented hydrocarbons. The third route is repolymerization of cyclic and heterocyclic compounds. Tar and carbon dioxide are formed by oligomerization of precursors such as levoglucosan to form oligomers. It has been reported in the literature that CO and CO_2 are formed from competing parallel routes [42]. CO production route is favored at high heating rates at high reactor temperatures. However CO_2 route is favored at intermediate heating rates and intermediate temperatures.

The behavior of syngas flow rate can be explained in lights of the presented reaction mechanism. The increase in reactor temperature results in an increase in the heating rate. Consequently routes of fragmentation, secondary fragmentation, tertiary reactions, steam-hydrocarbons reforming reactions and char gasification reactions are accelerated. As a result of the acceleration in these routes, syngas flow rate is increased. It is important to note that the precursors of char formation are the depolymerized cyclic and heterocyclic and fragmented hydrocarbons, which are consumed by tertiary reactions and steam reforming reactions. Consequently, the increase in reactor temperature results in less char formation and shorter time duration for char gasification.

6.2. Characteristics of syngas evolution from Polystyrene

In contrast to char based materials, polystyrene (PS) gasification yielded less syngas, hydrogen and energy than pyrolysis at 700^{o}C. However, the gasification of PS yielded more syngas, hydrogen and energy than pyrolysis at 900^{o}C temperature. Gasification of PS is affected by reactor temperature more than PS pyrolysis. Syngas, hydrogen and energy yield increased

exponentially with increase in temperature in case of gasification. However, syngas and energy yield increased linearly with temperature having rather a mild slope in the case of pyrolysis.

Steam gasification always increased the hydrogen yield for cellulosic material, and it was expected to see similar behavior for PS also. On the contrary a decrease in hydrogen flow rate and hydrogen yield with steam gasification at 700^{o}C and 800^{o}C was observed as compared to pyrolysis. Based on the observed syngas and hydrogen yield results one can conclude that the presence of a PS-steam reaction yields condensable hydrocarbons (liquid + wax). This reaction is competing with the gasification reactions. Consequently, in the simplest model, the gasification process can be represented by four competing parallel reactions as given below:

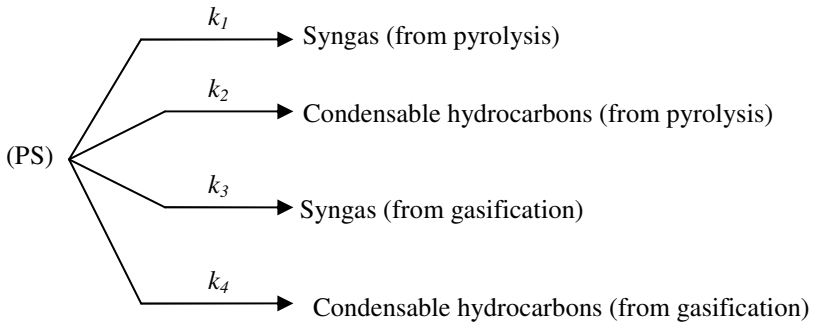

One can conclude the domination of reaction (k_4) at reactor temperature of 700^{o}C. However, at reactor temperature 900^{o}C, the third reaction (k_3), dominates.

For reactor temperature less than 800^{o}C, gasification yielded less energy and lower apparent thermal efficiency than pyrolysis. At reactor temperature of 900^{o}C, gasification yielded almost three times the amount of energy than that from pyrolysis. Energy yield and apparent thermal efficiency increased quasi-linearly with increase in temperature in case of the pyrolysis process. The increase in energy yield and apparent thermal efficiency with increase in temperature for gasification can be described by using an exponential function in temperature similar to that of

the Arrhenius equation. This indicates that the effect of temperature on energy yield is similar to that on the reaction rate.

6.3. Characteristics of syngas evolution from mixed samples

Gasification of polyethylene (PE) and woodchips (WC) mixtures have been investigated. Superior results in terms of syngas yield, hydrogen yield, total hydrocarbons yield, energy yield and apparent thermal efficiency have been shown from PE-WC blends as compared to expected weighed average yields from the individual components. Peak values of syngas yield, hydrogen yield energy yield, apparent thermal efficiency and carbon yield was obtained at PE percentage of approximately 60 to 80%. Results confirm synergistic interaction between PE and WC during high temperature steam gasification. A possible interaction mechanism is that PE acts as a hydrogen donor to radicals generated from WC pyrolysis, resulting in stabilizing those radicals and the production of higher yield of total hydrocarbons than that expected from the weighted average yield. Enhancement in HCs was ~ 4 grams at 80% PE. However the enhancement in syngas yield was ~ 18 grams at 80% PE. This means that there is ~ 14 grams increase in CO, H_2 and CO_2 which is not explained by the hydrogen donor mechanism. In order to explain the enhancement in CO, H_2 and CO_2 yield, the arrangement of WC with respect to PE should be considered. The PE was always located upstream from WC for all experiments for consistency. WC char might have played a role in adsorbing volatile matter evolved from PE, which in turn promoted steam-hydrocarbons reforming reaction to result in excess H_2, CO and CO_2 than that expected from the weighted average yield alone.

6.4. Kinetics of char gasification

Inorganic constituents in food char were found to have a catalytic effect. Char reactivity increased with the degree of conversion. In the conversion range from 0.1 to 0.9 the increase in

reactivity was accompanied by an increase in pre-exponential factor, suggesting an increase in gasifying agent adsorption rate to char surface.

Comparison between kinetics of woodchips char gasification using steam and CO_2 as gasifying agents has also been investigated. The average reaction rate for steam gasification was almost twice that of CO_2. Average rate constant at 900^oC was 0.065 min^{-1} for steam gasification and 0.031 min^{-1} for CO_2 gasification. Reaction rate peak for steam gasification was at a degree of conversion of approximately 0.3. However, for CO_2 gasification the reaction rate peak was found to be at conversion degree of approximately 0.1. Changing the partial pressure of the gasifying agent did not affect the reaction rate for both steam and CO_2 gasification, which indicates that the process is not controlled by the adsorption step. The process is controlled by either the surface reaction step or the desorption step.

The effect of particle size, porosity and reactor temperature/reaction rate constant on the progress of a char particle conversion has been investigated numerically using three different regimes of Damkohler numbers. For the very large Damkohler number case, concentration profiles of the gasifying agent showed a steep gradient across the particle and the reaction occurred mostly in the outer layer of the particle. This behavior corresponds to a diffusion controlled process. After a certain time period into the process, the particle starts to shrink and its porosity increases, allowing for high effective diffusivity. The gasifying agent gradients get less steep in late stages of the particle reaction until they reach almost a horizontal line by the end of the process. The conversion lines also get less steep and reached an asymptotic value of one for all radii.

For the case of very small *Da* number, gasifying agent concentration was found to be a straight line parallel to the x-axis, having a value of C_∞ for all values of r and was independent of time.

The reaction occurred homogenously across the particle and the degree of conversion was only a function in time. This behavior corresponds to a chemically controlled process.

Variation in conversion profiles as a function in time due to variation in initial porosity and reaction rate constant were limited to a certain extent. Very high initial porosity values tend to shift the process towards a chemically controlled one; any further increase in porosity was not found to have a positive effect on the conversion-time relationship. On the other hand, very high reaction rate constants tend to shift the process towards diffusion controlled process. Further increase in reactor temperature/rate constant resulted in a slight increase in conversion rate. The total conversion-time relationship for large values of K almost coincided with each other.

Chapter VII. Recommendations for future work

The gasification process is a very complicated process in which several disciplines have to be involved in order to have a complete understanding of the process. For example, the kinetics of pyrolysis reactions depends on the sample temperature, reactor pressure, concentration/partial pressure of other reactants and the environment of reaction whether being catalytic or not. Particle temperature depends on its physical properties, such as its conductivity and porosity as well as fluid dynamics inside the reactor which affects the convective heat transfer to the particle and consequently its temperature distribution. Partial pressure of reacting species is also a function of flow dynamics. It is important to point out that there is a mutual dependency between the chemistry of gasification and physical properties of reacting particles. For example, the reactor temperature, particle size, porosity and heating rate might favor certain reaction routes resulting in new physical properties of the particle such as the conductivity, composition and properties. On the other hand evolving gases, volatile matter changes the fluid dynamics of the flow which in turn affects the distribution/concentration of certain species inside the reactor. Due to this complex interaction between physical properties of the solid fuel and the chemistry of gasification it is important to design a small scale gasifier in which physical properties of the fuel and flow dynamics as well as evolution of chemical composition can be investigated.

7.1. Design procedures of small scale gasifier for experimental investigations

In order to design an experimental small scale facility, accurate numerical simulations of the process are essential. Chemical reactions kinetics can be simulated using CHEMKIN. Kinetic

parameters and models should be determined based on experimental results from a combined TGA-GC-MS setup. A reaction mechanism should be built based on results from a data base generated from different operation conditions. The reaction mechanism should model the pyrolysis process as well as the char gasification. Figure VII-1 shows the algorithm that can be used in the numerical simulations and gasifier design. Pyrolysis and gasification reactions mechanism should be build with the assistant of experimental results data base. A complete reactions mechanism will be build based on the pyrolysis and gasification mechanisms. Reactions will be simulated using the CHEMKIN software. Results will be compared to experimental results. Reaction mechanisms will be modified based on the comparison between numerical simulation results and experimental results. After reaching an accurate mechanism, it can be used in CFD simulations for the experimental small gasifier design. After reaching a final design, the gasifier should be utilized with enough ports and optical accesses for sampling and in situ diagnostics

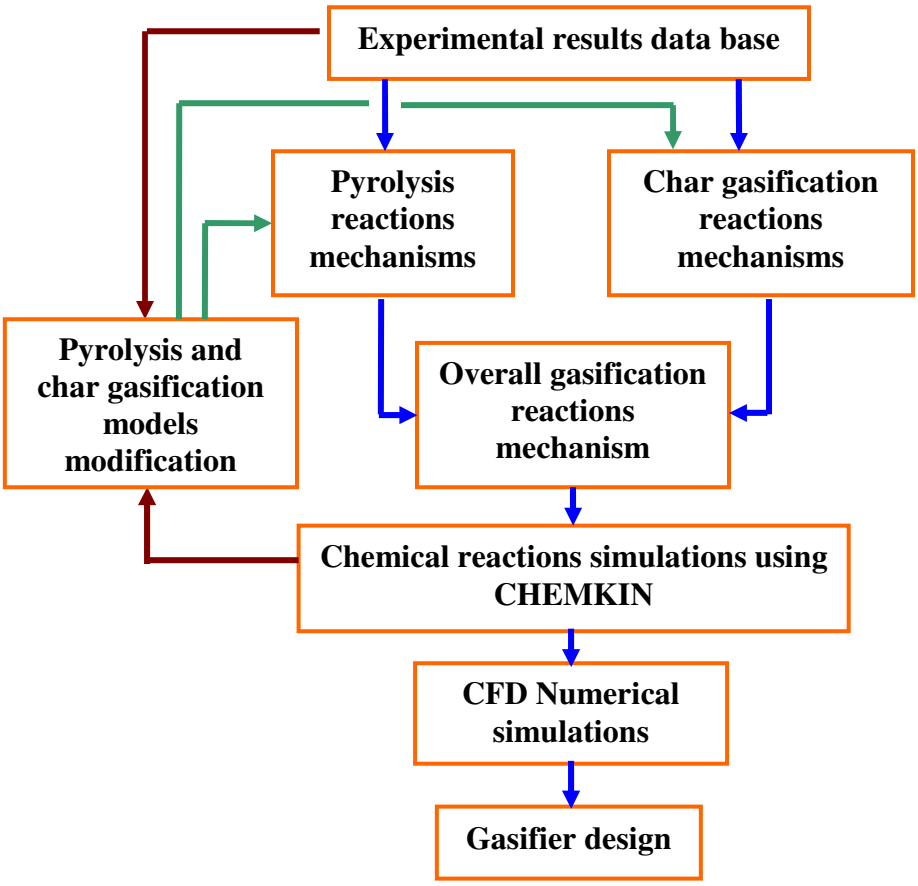

Figure VII-1. Algorithm of the gasification numerical simulations and gasifier design

7.2. Interaction between different samples

Gasification systems have the flexibility of introducing mixed feed stock to the same gasifier. Researchers tend to study the behavior of single samples only. Interaction between samples and their yields may change syngas characteristics and gasification duration as well. For example, ash content in some feed stock has proven to have a catalytic effect on the char gasification. Mixing a high ash content sample with a low ash content sample may reduce gasification duration of the mixture. Dual and triple interaction between different samples may be investigated. Because there are endless combinations of samples mixtures it is impossible to investigate all combinations. A good plan is to understand the dual interaction of all samples and construct a simple mechanism that accounts for dual sample interaction. For more than two or

three mixed samples, simulated mixtures that resemble the composition of real waste may be used.

7.3. Liquid fuels production by thermal/hydrothermal cracking of plastics

Preliminary experiments have been conducted in order to generate condensable hydrocarbons by pyrolysis or hydrothermal liquefaction of several samples; woodchips, paper, polypropylene and polystyrene. Reactor temperature ranged from 500 to 800^{o}C. Cellulose based samples, paper and woodchips, yielded tar as the condensable phase. Polyethylene yielded wax and gaseous fuels. However, with the polystyrene experiments we were successful in generating combustible liquid hydrocarbons in the temperature range of 500 to 700^{o}C. More investigation may be conducted in order to build a data base for the performance of different samples or mixture of samples over a wide range of operational conditions. Next step may be the understanding of reaction mechanism and identification of reaction pathways for process enhancement.

The obtained liquid hydrocarbons were highly combustible, which indicates that there is a good potential of liquid fuels production for power generation application. Following issues may be addressed:

- Investigating the potential of liquid fuel generation from other plastics and biomass samples
- Investigating the synergistic of a biomass-plastic and plastic-plastic samples
- Chemical composition analysis and determination of useful hydrocarbons percentage in the overall yield. Operational conditions should be altered to investigate their effect on desired hydrocarbons, C_8 to C_{15}

- Trying different liquefying agents; steam and hydrogen. Using hydrogen will increase the hydrogen to carbon ration in the hydrocarbons chain which will help in saturated hydrocarbons production, alkanes
- Investigating the effect of reactor pressure. Higher pressure is usually used in the Fischer Tropsch process for liquid fuels production from syngas. Consequently, it might be useful in direct liquids generation from plastics liquefaction
- Understanding the reaction mechanism of liquids generation for process enhancement and higher selectivity of desired C numbers

Appendix A: Formulation of the finite element problem

Multiplying E11 by the weight function, *w:*

$$\int_{r_1}^{r_2}\left[w\frac{\partial}{\partial r}\left[D_p r^2 \frac{\partial C}{\partial r}\right] - wr^2 K C f(X)\right] dr = 0 \qquad \text{A1}$$

Integrating by parts, the weak form will be:

$$w\left[D_p r^2 \frac{\partial C}{\partial r}\right]\Bigg|_{r_1}^{r_2} - \int_{r_1}^{r_2}\left[\frac{\partial w}{\partial r} D_p r^2 \frac{\partial C}{\partial r} + wr^2 K C f(X)\right] dr = 0 \qquad \text{A2}$$

Rearranging:

$$\int_{r_1}^{r_2}\left[\frac{\partial w}{\partial r} D_p r^2 \frac{\partial C}{\partial r} + wr^2 K C f(X)\right] dr = w\left[D_p r^2 \frac{\partial C}{\partial r}\right]\Bigg|_{r_1}^{r_2} \qquad \text{A3}$$

Defining the gasifying agent concentration across the element, C_{H2O}^{e} using the approximation function φ and choosing the weight function, *w*, same as the approximation function, one can write:

$$C^e = \sum_{j=1}^{2} C_j \varphi_j(r), \qquad w = \varphi_1 \;\&\; \varphi_2 \qquad \& \frac{\partial w}{\partial r} = \frac{\partial \varphi_1}{\partial r} \;\&\; \frac{\partial \varphi_2}{\partial r}$$

Substituting into A3 gives:

$$\int_{r_1}^{r_2}\left[\frac{\partial \varphi_1}{\partial r} D_p r^2 \sum_{j=1}^{2} C_j \frac{\partial \varphi_j}{\partial r} + \varphi_1 r^2 K \sum_{j=1}^{2} C_j \varphi_j f(X)\right] dr = \varphi_1(r_2) D_p r_2^2 \frac{\partial C}{\partial r}(r_2) - \varphi_1(r_1) D_p r_1^2 \frac{\partial C}{\partial r}(r_1) \qquad \text{A4}$$

$$\int_{r_1}^{r_2}\left[\frac{\partial \varphi_2}{\partial r} D_p r^2 \sum_{j=1}^{2} C_j \frac{\partial \varphi_j}{\partial r} + \varphi_2 r^2 K \sum_{j=1}^{2} C_j \varphi_j f(X)\right] dr = \varphi_2(r_2) D_p r_2^2 \frac{\partial C}{\partial r}(r_2) - \varphi_2(r_1) D_p r_1^2 \frac{\partial C}{\partial r}(r_1) \qquad \text{A5}$$

The approximation functions are chosen to be the linear hat functions with the following boundary conditions:

$$\varphi_2(r_2)=\varphi_1(r_1)=1 \quad \& \quad \varphi_2(r_1)=\varphi_1(r_2)=0$$

The approximation functions are defines as: $\varphi_1=\frac{r_2-r}{r_2-r_1}$ & $\varphi_2=\frac{r-r_1}{r_2-r_1}$ A6&7

and $\frac{\partial\varphi_1}{\partial r}=-\frac{1}{r_2-r_1}$ & $\frac{\partial\varphi_2}{\partial r}=\frac{1}{r_2-r_1}$

In matrix notations the linear algebraic equations for each element e can be written as:

$$\left[K^e_{stiff}\right]\left[C^e\right]=\left[J^e\right] \qquad \text{A8}$$

with:

$$k_{11}=\int_{r_1}^{r_2}\left[\left(\frac{\partial\varphi_1}{\partial r}\right)^2 D_p r^2+\varphi_1{}^2 r^2 Kf(X)\right]dr=\int_{r_1}^{r_2}\left[\left(-\frac{1}{r_2-r_1}\right)^2 D_p r^2+\left(\frac{r_2-r}{r_2-r_1}\right)^2 r^2 Kf(X)\right]dr$$

$$k_{12}=k_{21}=\int_{r_1}^{r_2}\left[\frac{\partial\varphi_1}{\partial r}D_p r^2\frac{\partial\varphi_2}{\partial r}+\varphi_1 r^2 K\varphi_2 f(X)\right]dr=\int_{r_1}^{r_2}\left[\left(-\frac{1}{r_2-r_1}\right)D_p r^2\left(\frac{1}{r_2-r_1}\right)+\left(\frac{r_2-r}{r_2-r_1}\right)r^2 K\left(\frac{r-r_1}{r_2-r_1}\right)f(X)\right]dr$$

$$k_{22}=\int_{r_1}^{r_2}\left[\frac{\partial\varphi_2}{\partial r}D_p r^2\frac{\partial\varphi_2}{\partial r}+\varphi_2 r^2 K\varphi_2 f(X)\right]dr=\int_{r_1}^{r_2}\left[\left(\frac{1}{r_2-r_1}\right)^2 D_p r^2+\left(\frac{r-r_1}{r_2-r_1}\right)^2 r^2 Kf(X)\right]dr$$

The average value of *X* within the element has been used to calculate *f(X)* and $D_p(\varepsilon(X))$ in the integration; $X=\frac{1}{2}\left(X_1^e+X_2^e\right)$

$$\left[C^e\right]=\begin{bmatrix}C_1^e\\C_2^e\end{bmatrix} \quad \& \quad \left[J^e\right]=D_p\begin{bmatrix}-r_1^2\frac{\partial C_{H_2O}}{\partial r}\left(r_1^e\right)\\ r_2^2\frac{\partial C_{H_2O}}{\partial r}\left(r_2^e\right)\end{bmatrix}$$

Assembling all the elements together, the global stiffness matrix and the force vector are obtained:

$$\left[K_{stiff}^{global}\right]\left[C^{global}\right]=\left[J^{global}\right] \qquad \text{A9}$$

where,

$$\left[K_{stiff}^{global}\right]=\begin{bmatrix} k_{11}^1 & k_{12}^1 & 0 & 0 & 0 & 0 \\ k_{21}^1 & k_{22}^1+k_{11}^2 & k_{12}^2 & 0 & 0 & 0 \\ 0 & k_{11}^2 & k_{22}^2+k_{11}^3 & . & 0 & 0 \\ 0 & 0 & . & . & 0 & 0 \\ 0 & 0 & 0 & . & k_{22}^{n-1}+k_{11}^n & k_{12}^n \\ 0 & 0 & 0 & 0 & k_{21}^n & k_{22}^n \end{bmatrix},$$

$$\left[C^{global}\right]=\begin{bmatrix} C_1 \\ C_2 \\ . \\ . \\ . \\ C_{n+1} \end{bmatrix} \qquad \& \left[J^{global}\right]=\begin{bmatrix} J_1^1 \\ J_2^1+J_1^2 \\ . \\ . \\ J_2^{n-1}+J_1^n \\ J_2^n \end{bmatrix}$$

Applying the boundary conditions on each arbitrary element, $J_2^{j-1}=-J_1^j$, boundary condition for the first element, $J_1^1=0$ and boundary condition of the last element,

$$J_2^n=D_p r_p^2\left.\frac{\partial C_{H_2O}}{\partial r}\right|_{r_p^-}=r_p D_o\left(C_\infty-C_S\right)$$

$$\left[J^{global}\right]=\begin{bmatrix} 0 \\ 0 \\ . \\ . \\ 0 \\ r_p D_o\left(C_\infty-C_S\right) \end{bmatrix} \quad moving\ r_p D_o C_{H_2O)surf.}\ to\ the\ left\ handside,\ \left[J^{global}\right]=\begin{bmatrix} 0 \\ 0 \\ . \\ . \\ 0 \\ r_p D_o C_\infty \end{bmatrix}$$

$$\& K_{n+1,n+1}^{global}=K_{n+1,n+1}^{global}+r_p D_o$$

Appendix B: List of Publications

- **Ahmed I**, Gupta AK. Evolution of syngas from cardboard gasification. Appl Energy 2009;86:1732-1740.
- **Ahmed I**, Gupta AK. Syngas yield during pyrolysis and steam gasification of paper. Appl Energy 2009;86:1813-1821.
- **Ahmed I**, Gupta AK. Characteristics of cardboard and paper gasification with CO_2. Appl Energy 2009;86:2626-2634.
- **Ahmed II**, Gupta AK. Hydrogen production from polystyrene pyrolysis and gasification: Characteristics and kinetics. Int J of Hydrogen Energy 2009;34:6253-6264.
- **Ahmed II**, Gupta AK. Pyrolysis and gasification of food waste: Syngas characteristics and char gasification kinetics. Appl Energy 2010;87:101-108.
- **Ahmed II**, Nipattummakul N and Gupta AK. Characteristics of Syngas from Co-gasification of Polyethylene and Woodchips. Appl Energy2011;88:165-174
- Nimit Nipattummakul, **Islam I. Ahmed**, Ashwani K. Gupta and Somrat Kerdsuwan. High Temperature Steam Gasification of Wastewater Sludge. Appl Energy 2010;87:3729-3734.
- Nimit Nipattummakul, **Islam I Ahmed**, Somrat Kerdsuwan, Ashwani K. Gupta. Hydrogen and syngas production from sewage sludge via steam gasification. Int J of Hydrogen Energy 2010; 35:11738-11745.
- **Ahmed II**, Gupta AK. Kinetics of woodchips char gasification with steam and carbon dioxide. Applied Energy 2011;88 (5):1613-1619.

- Nimit Nipattummakul, **Islam I. Ahmed**, Ashwani K. Gupta and Somrat Kerdsuwan. Hydrogen and Syngas Yield from Residual Branches of Oil Palm Tree using Steam Gasification. International Journal of Hydrogen Energy 2011;36(6): 3835-3843
- **Ahmed I**, Gupta AK. Characteristic of hydrogen and syngas evolution from gasification and pyrolysis of rubber. International Journal of Hydrogen Energy 2011;36(7):4340-4347.
- **Ahmed II,** Gupta AK. Particle Size, Porosity and Temperature Effects on Char Conversion. Appl Energy (2011), doi:10.1016/j.apenergy.2011.06.001.
- **Ahmed II,** Gupta AK. Sugarcane Bagasse Gasification: Global Reaction Mechanism of Syngas Evolution. Submitted to the Journal of Applied energy, accepted.
- **Ahmed II**, Jangsawang W, Gupta AK. Energy Recovery from Pyrolysis and Gasification of Mangrove. Submitted to the Journal of Applied energy, accepted.

References

[1] Summary of the Resource Conservation and Recovery Act, EPA: http://www.epa.gov/lawsregs/laws/rcra.html

[2] Klein, A., Gasification: An Alternative Process for Energy Recovery and Disposal of Municipal Solid Wastes, M. Sc. Thesis, Department of Earth and Environmental Engineering, Columbia University, May 2002.

[3] http://www.landfill-gas.com

[4] Gupta AK, Lilley DG. Incineration of plastics and other wastes for efficient power generation: a review. 41st Aerospace Sciences Meeting and Exhibit, Reno, Nevada, January 6-9, 2003.

[5] He M, Hu Z, Xiao B, Li J, Guo X, Luo S, Yang F, Feng Y, Yang G, Liu S. Hydrogen-rich gas from catalytic steam gasification of municipal solid waste (MSW): Influence of catalyst and temperature on yield and product composition. Int J Hydrogen Energy 2009;34:195-203.

[6] Tongamp W, Zhang Q, Saito F. Hydrogen generation from polyethylene by milling and heating with Ca(OH)2 and Ni(OH)2. Int J Hydrogen energy 2008;33:4097-4103.

[7] He M, Xiao B, Hu Z, Liu S, Guo X, Luo S. Syngas production from catalytic gasification of waste polyethylene: Influence of temperature on gas yield and composition. Int J of Hydrogen Energy 2009;34:1342-1348.

[8] Gupta AK, Lilley DG. Energy recovery opportunities from wastes. Journal of Propulsion and Power 1999;15(2):175-180.

[9] Kaminsky W, Schmidt H, Simon CM. Recycling of mixed plastics in a fluidized bed. Macromol. Symp 2000;152:191-199.

[10] Higman, C. and van der Burgt, M., Gasification, Elsevier Science, 2003.

[11] Ahmed I, Gupta AK. Evolution of syngas from cardboard gasification. Appl Energy 2009;86:1732-1740.

[12] Ahmed I, Gupta AK. Characteristics of cardboard and paper gasification with CO_2. Appl Energy 2009;86:2626-2634.

[13] Ahmed I, Gupta AK. Syngas yield during pyrolysis and steam gasification of paper. Appl Energy 2009;86:1813-1821.

[14] Ahmed II, Gupta AK. Hydrogen production from polystyrene pyrolysis and gasification: Characteristics and kinetics. Int J of Hydrogen Energy 2009;34:6253-6264.

[15] Junqing Caia, Yiping Wang, Limin Zhou, Qunwu Huang, Thermogravimetric analysis and kinetics of coal/plastic blends during co-pyrolysis in nitrogen atmosphere fuel processing technology 2008;89:21–27.

[16] Sharypov VI, Beregovtsova NG, Kuznetsov BN, Cebolla VL, Collura S, Finqueneisel G, Zimny T, Weber JV. Influence of reaction parameters on brown coal–polyolefinic plastic co-pyrolysis behavior. J. Anal. Appl. Pyrolysis 2007;78:257-264.

[17] Yamashita T, Fujii Y, Morozumi Y, Aoki H, Miura T. Modeling of gasification and Fragmentation Behavior of Char Particles Having Complicated Structures. Combustion and Flame 2006; 146:85–94.

[18] Ahmed II and Gupta AK, Kinetics of Woodchips Char Gasification with Steam and Carbon Dioxide, International Conference on Applied Energy (ICAE 2010), 21-23 April 2010, Singapore.

[19] Kajitani S, Matsuda SHH. Gasification Rate Analysis of Coal Char with a Pressurized Tube Furnace. Fuel 2002;81:539-546.

[20] Roberts DG, Harris DJ. Char Gasification with O_2, CO_2, and H_2O: Effects of Pressure on Intrinsic Reaction Kinetics Energy & Fuels 2000, 14, 483-489.

[21] Sun Q, Li W, Chen H, Li B. The CO2-Gasification and Kinetics of Shenmu Maceral Chars with and without Catalyst. Fuel 2004;83:1787–93.

[22] Zou JH, Zhou ZJ, Wang FC, Zhang W, Dai ZH, Liu HF, et al. Modeling Reaction Kinetics of Petroleum Coke Gasification with CO2. Chem Eng Process 2007;46:630–636.

[23] Bhatia SK, Perlmutter DD. A Random Pore Model for Fluid-Solid Reactions: I. Isothermal kinetics control. AIChE Journal 1980;26(3):379-385.

[24] Klose W, Wolki M. On the Intrinsic Reaction Rate of Biomass Char Gasification with Carbon Dioxide and Steam Fuel 2005;84:885–892.

[25] Tancredi N, Cordero T, Mirasol JR, Rodriguez JJ. CO_2 Gasification of Eucalyptus Wood Chars. Fuel 1996;75(13):1505–1508.

[26] Montesinos FM, Cordero T, Mirasol JR, Rodriguez JJ. CO_2 and Steam Gasification of a Grapefruit Skin Char. Fuel 2002;81:423–429.

[27] Ahmed II, Gupta AK. Pyrolysis and gasification of food waste: Syngas Characteristics and Char Gasification Kinetics. Applied Energy 2010;87:101–108.

[28] Everson RC, Neomagus HW, Kasaini H, Njapha D. Reaction Kinetics of Pulverized Coal Chars Derived from Inertinite-Rich Coal Discards: Gasification with Carbon Dioxide and Steam. Fuel 2006;85:1076–1082.

[29] Wall TF, Liu G, Wu H, Roberts DG, Benfell KE, Gupta S, Lucas JA, Harris DJ. The Effects of Pressure on Coal Reactions During Pulverized Coal Combustion and Gasification. Prog. Energy Combust Sci. 2002;28:405-433.

[30] Cetin E, Moghtaderi B, Gupta R, Wall TF. Biomass Gasification Kinetics: Influence of Pressure and Char Structure. Combust Sci. Technol. 2005;177:765–791.

[31] Mann MD, Knutson RZ, Erjavec J, Jacobsen JP. Modeling Reaction Kinetics of Steam Gasification for a Transport Gasifier. Fuel 2004;83:1643–1650.

[32] Molina A, Mondrago F. Reactivity of coal gasification with steam and CO_2. Fuel 1998;77(15):1831-1839.

[33] Marcio L. de Souza-Santos. Solid Fuels Combustion and Gasification; Modeling Simulations and Equipment Operation. ISBN: 0-8247-0971-3, Marcel Dekker, Inc. 2004.

[34] Reddy JN. An Introduction to the Finite Element Method. Second Edition. ISBN: 0-07-051355-4. McGraw-Hill, Inc. 1993.

[35] Shin EJ, Nimlos MR. Evans RJ. Kinetic analysis of the gas-phase pyrolysis of carbohydrates. Fuel 2001;80: 1697-1709.

[36] Balat M. Mechanisms of Thermochemical Biomass Conversion Processes. Part 1: Reactions of Pyrolysis. Energy Sources Part A 2008;30:620–635.

[37] Shafizadeh F. The Chemistry of Pyrolysis and Combustion. The chemistry of solid wood, Chapter 13, pp 489–529, ISBN 9780841207967, 2005, 1984 Copyright © 1984 American Chemical Society.

[38] Yan-fen L, Shu-rong W, Xiao-Qian M. Study of Reaction Mechanisms in Cellulose Pyrolysis. Am. Chem. Soc., Div. Fuel Chem. 2004;49(1):407-411.

[39] Vatirhegyi G, Antal MJ, Jakab E, Szabo P. Kinetic Modeling of Biomass Pyrolysis. Journal of Analytical and Applied Pyrolysis 1997;42:73-87.

[40] Luo Z, Wang S, Liao Y and Cen K. Mechanism study of cellulose rapid pyrolysis. Ind. Eng. Chem. Res. 2004;43:5605-5610.

[41] Diebold JP. A unified, global model for the pyrolysis of cellulose. Biomass Bioenergy 1994;7:75-85.

[42] Banyasz JL, Li S, Lyons-Hart JL, Shafer KH. Gas Evolution and the Mechanism of Cellulose Pyrolysis. Fuel 2001;80:1757–1763.

[43] Lin Y, Cho J, Tompsett GA, Westmoreland PR, Huber GW. Kinetic and Mechanism of Cellulose Pyrolysis. J. of Phys. Chem. C 2009;113:20097-20107.

[44] Petrocelli FP and Klein MT. Model Reaction Pathways in Kraft Lignin Pyrolysis. Macromolecules 1984, 17, 161-169

[45] Gil, J., Aznar, M. P., Caballero, M. A., Frances, E. and Corella, J., Biomass Gasification in Fluidized Bed at Pilot Scale with Steam-Oxygen Mixtures. Product Distribution for Very Different Operating Conditions, Energy & Fuels, Vol. 11, No. 6, 1997, pp. 1109 -1118.

[46] Narvaez , I., Orıo, A., Aznar, M. P. and Corella, J., Biomass Gasification with Air in an Atmospheric Bubbling Fluidized Bed Effect of Six Operational Variables on the Quality of the Produced Raw Gas, *Ind. Eng. Chem.* Res. Vol. 35, 1996, pp. 2110-2120.

[47] Sugiyama, S., Suzuki, N., Kato, Y., Omino, K. Y. A., Ishii, T., Yoshikawa, K. and Kiga, T., Gasification Performance of Coals Using High Temperature Air, Energy, Vol. 30, 2005, pp. 399–413.

[48] Garcıa, L., Salvador, M. L., Arauzo, J. and Bilbao, R., Catalytic Steam Gasification of Pine Sawdust; Effect of Catalyst Weight/Biomass Flow Rate and Steam/Biomass Ratios on Gas Production and Composition, Energy & Fuels, Vol. 13, 1999, pp. 851-859.

[49] Franco, C., Pinto, F., Gulyurtlu, I. and Cabrita, I., The Study Of Reactions Influencing the Biomass Steam Gasification Process, Fuel, Vol. 82, 2003, pp. 835–842.

[50] Lee, J. G., Kim, J. H., Jin, H., Park, T. J. and Kim, S. D., Characteristics of Entrained Flow Coal Gasification in Drop Tube Reactor, Fuel, Vol. 75, No. 9, 1996, pp. 1035-1042.

[51] Kim, Y. J., Lee, J. M. and Kim, S. D., Coal Gasification Characteristics in an Internally Circulating Fluidized Bed With Draught Tube, Fuel, Vol. 76, No. 11, 1997, pp. 1067-1073.

[52] Pinto F., Franco, C., Andre, R.N., Miranda, Gulyurtlu, M. I. and Cabrita, I., Cogasification Study of Biomass Mixed with Plastic Wastes, Fuel, Vol. 81, 2002, pp. 291-297.

[53] Chaudhari, S. T., Dalai, A. K. and Bakhshi, N. N., Production of Hydrogen and/or Syngas (H_2 + CO) via Steam Gasification of Biomass-Derived Chars, Energy & Fuels Vol. 17, 2003, pp. 1062-1067.

[54] Olivares, A., Aznar, M. P., Caballero, M. A., Gil, J., Frances, E. and Corella, J., Biomass Gasification: Produced Gas Upgrading by In-Bed Use of Dolomite, Ind. Eng. Chem. Res.**,** Vol. 36, 1997, pp. 5220-5226.

[55] Pinto, F., Franco, C., Andre, R. N., Tavares, C., Dias, M., Gulyurtlu, I., and Cabrita, I., Effect of Experimental Conditions on Co-Gasification of Coal, Biomass and Plastics Wastes With Air/Steam Mixtures in a Fluidized Bed System, Fuel, Vol. 82, 2003, pp. 1967–1976.

[56] Ocampoa, A., Arenasb, E., Chejnea, F., Espinela, J., Londonoa, C., Aguirrea, J. and Pereza, J. D., An Experimental Study on Gasification of Colombian Coal in Fluidized Bed, Fuel, Vol. 82, 2003, pp. 161–164.

[57] Demirbas, A., Gaseous Products from Biomass by Pyrolysis and Gasification: Effects of Catalyst on Hydrogen Yield, J. Energy Conversion and Management, Vol. 43, 2002, pp. 897–909.

[58] Corella, J., Aznar, M. P., Gil, J. and Caballero, M. A., Biomass Gasification in Fluidized Bed: Where To Locate the Dolomite To Improve Gasification?, Ind. Eng. Chem. Res.**,** Vol. 36, 1997, pp. 5220-5226.

[59] Milosavljevic, I., Oja, V. and Suuberg, E. M., Thermal Effects in Cellulose Pyrolysis: Relationship to Char Formation Processes, Ind. Eng. Chem. Res., Vol. 35, 1996, pp. 653-662.

[60] Matsumura, Y., Evaluation of Supercritical Water Gasification and Biomethanation for Wet Biomass Utilization in Japan, Energy Conversion and Management, Vol. 43, 2002, pp. 1301–1310.

[61] Encinar JM, González JF. Pyrolysis of synthetic polymers and plastic wastes: kinetic study. Fuel Processing Technology 2008;89:678-686.

[62] Westerhout RWJ, Waanders J, Kuipers JAM, Van Swaaij WPM. Kinetics of the low-temperature pyrolysis of polyethene, polypropene, and polystyrene modeling, experimental determination, and comparison with literature models and data. Ind Eng Chem Res 1997;36:1955-1964.

[63] Lin KS, Wang HP, Liu SH, Chang NB, Huang YJ, Wang HC. Pyrolysis kinetics of refuse-derived fuel. Fuel Processing Technology 1999;60:103-110.

[64] Cozzani V, Nicolella C, Petarca L, Rovatti M, Tognotti L. A fundamental study on conventional pyrolysis of a refuse-derived fuel. Ind Eng Chem Res 1995;34:2006-2020.

[65] Dong C, Yang Y, Jin B, Horio M. The pyrolysis of sawdust and polyethylene in TG and U-shape tube reactor. Waste Management 2007;27:1557-1561.

[66] Bockhorn H, Hornung A, Hornung U. Stepwise pyrolysis for raw material recovery from plastic waste. Journal of Analytical and Applied Pyrolysis 1998;46:1-13.

[67] Ponzio A, Kalisz S, Blasiak W. Effect of operating conditions on tar and gas composition in high temperature air/steam gasification (HTAG) of plastic containing waste. Fuel Processing Technology 2006;87:223-233.

[68] Kaminsky W, Schlesselmann B, Simon C. Olefins from polyolefins and mixed plastics by pyrolysis. Journal of Analytical and Applied Pyrolysis 1995;32:19-27.

[69] Simon CM, Kaminsky W, Schlesselmann B. Pyrolysis of polyolefins with steam to yield olefins. Journal of Analytical and Applied Pyrolysis 1996;38:75-87.

[70] Gonzalez JF, Encinar JM, Canito JL, Rodrıguez JJ. Pyrolysis of automobile tyre waste. Influence of operating variables and kinetics study. J Anal Appl Pyrol 2001;58e59:667e83.

[71] Leung DYC, Wang CL. Kinetic study of scrap tyre pyrolysis and combustion. J Anal Appl Pyrol 1998;45(2):153e69.

[72] Williams PT, Besler S. Pyrolysis-thermogravimetric analysis of tyres and tyre components. Fuel 1995;74(9):1277e83.

[73] Castaldi MJ, Kwon E, Weiss B. Beneficial use of waste tires: an integrated gasification and combustion process design via thermogravimetric analysis (TGA) of styreneebutadiene rubber (SBR) and polyisoprene (IR). Environ Eng Sci 2007;24 (8):1160-78.

[74] San Miguel G, Geoffrey D, Fowler GD, Sollars CJ. Pyrolysis of tire rubber: porosity and adsorption characteristics of the pyrolytic chars. Ind Eng Chem Res 1998;37:2430-5.

[75] Helleur R, Popovic N, Ikura M, Stanciulescu M, Liu D. Characterization and potential applications of pyrolytic char from ablative pyrolysis of used tires. J Anal Appl Pyrol 2001; 58-59:813-24.

[76] San Miguel G, Fowler GD, Sollars CJ. A study of the characteristics of activated carbons produced by steam and carbon dioxide activation of waste tyre rubber. Carbon 2003; 41(5):1009-16.

[77] Gonzalez JF, Encinar JM, Garcia CM, Sabio E, Ramiro A, Canito JL, et al. Preparation of activated carbons from used tyres by gasification with steam and carbon dioxide. Appl Surf Sci 2006;252(17):5999-6004.

[78] Vizuete EM, Garcia AM, Gisbert AN, Gonzalez CF, Serrano VG. Preparation of mesoporous and macroporous materials from rubber of tyre wastes. Micropor Mesopor Mater 2004;67(1):35-41.

[79] Aznar MP, Caballero MA, Sancho JA, Frances E. Plastic waste elimination by co-gasification with coal and biomass in fluidized bed with air in pilot plant. Fuel Processing Technology 2006;87:409-420.

[80] Vélez JF, Chejne F, Valdés CF, Emery EJ, Londoño CA. Co-gasification of Colombian coal and biomass in fluidized bed: An experimental study. Fuel 2009;88:424-430.

[81] Sharypov VI, Marin N, Beregovtsova NG, Baryshnikov SV, Kuznetsov BN, Cebolla VL, Weber JV. Co-pyrolysis of wood biomass and synthetic polymer mixtures. Part I: influence of experimental conditions on the evolution of solids, liquids and gases. Journal of Analytical and Applied Pyrolysis 2002;64:15-28.

[82] Kumabe K, Hanaoka T, Fujimoto S, Minowa T, Sakanishi K. Co-gasification of woody biomass and coal with air and steam. Fuel 2007;86:684-689.

[83] Lapuerta M, Hernández JJ, Pazo A, López J. Gasification and co-gasification of biomass wastes: Effect of the biomass origin and the gasifier operating conditions. Fuel processing technology 2008;89:828-837.

[84] Sakurovs R. Interactions between coking coals and plastics during co-pyrolysis. Fuel 2003;82:1911-1916.

[85] Sjostrom K, Bjornbom E, Chen G, Brage C, Rosen C, Yu Q. Synergetic effects in co-gasification of coal and biomass. In: APAS Clean Coal Technology Programme, vol. 3. 1992–1994. p. C3.

[86] De Jong W, Andries J, Hein KRG. Coal-biomass gasification in a pressurized fluidized bed gasifier. In: ASME International GT and Aerospace Congress, Stockholm, SE, June 2–5, 1998. p. 1–7.

[87] Rudiger H, Greul U, Spliethoff H, Hein KRG. In: APAS clean coal technology program, 1992–1994, Volume 3, C4.

[88] Kuznetsov BN, Sharypov VI, Kuznetsova SA, Taraban'ko VE, Ivanchenko NM. The study of different methods of bio-liquids production from wood biomass and from biomass/polyolefine mixtures. Int J Hydrogen Energy 2009;34:7051-7056.

[89] Kuznetsov BN, Catalytic methods in coal processing to syn-gas, carboneous and liquid fuels contributing to sustainable development. International Journal of Hydrogen Energy 2009;34: 7057-7063.

[90] Ochoa J, Cassanello MC, Bonelli PR, Cukierman AL. CO2 gasification of Argentinean coal chars: A kinetic characterization. Fuel Process Technol 2001;74:161–76.

[91] Sangtong-Ngam K, Narasingha MH. Kinetic study of Thai-lignite char gasification using the random pore model. Thammasat Int J Sci Technol 2008;13(3):16–26.

[92] Bhat, A., Bheemarasetti, J.V. and Rao, T. R., Kinetics of Rice Husk Char Gasification, Energy Conversion and Management, Vol. 42, 2001, pp. 2061-2069.

[93] Marsh H, Taylor DA., Lander JR. Kinetic study of gasification by oxygen and carbon dioxide of pure and doped graphitizable carbons of increasing heat treatment temperatures. Carbon 1981;19(5):375-381.

[94] Agrawal, RK. On the compensation effect. Journal of Thermal Analysis 1986;31; 73-86.

[95] Dhupe AP, Gokarn AN, Doraiswamy LK. Investigations into the compensation effect at catalytic gasification of active charcoal by carbon dioxide. Fuel 1991;70(7):839-844.

[96] Feistel PP, Van Heek KH, Juntgen H, Pulsifer AH. The compensation effect in the steam gasification of coal, Carbon, 1976;14(6):363-364.

[97] Gokarn AN, Muhlen HJ. Catalysis of char gasification by mixed lignosulfonates: quantification of role of each component. Fuel 1996;75(1):96-98.

[98] Li S, Cheng Y. Catalytic gasification of gas-coal char in CO_2. Fuel 1995;74(3):456-458.

[99] Iwaki, H., Ye, S., Katagiri, H. and Kitagawa, K., Wastepaper Gasification with CO_2 or Steam using Catalysts of Molten Carbonates, Applied Catalysis A, General 270, 2004, pp. 237–243.

[100] Tomishige, K., Asadullah, M. and Kunimori, K., Syngas Production by Biomass Gasification Using $Rh/CeO_2/SiO_2$ Catalysts and Fluidized Bed Reactor, Catalysis Today, Vol. 89, 2004, pp. 389–403.

[101] Asadullah, M., Tomishige, K. and Fujimoto, K., A Novel Catalytic Process for Cellulose Gasification to Synthesis Gas, Catalysis Communications, Vol. 2, 2001, pp. 63-68.

[102] Watanabe, M., Inomata, H. and Arai, K., Catalytic Hydrogen Generation from Biomass (Glucose and Cellulose) with ZrO_2 in Supercritical Water, Biomass and Bioenergy, Vol. 22, 2002, pp. 405–410.

[103] Porada S. The reactions of formation of selected gas products during coal pyrolysis. Fuel 2004;83:1191-1196

[104] Becidan M, Varhegyi G, Hustad JE, and O Skreiberg O. Thermal Decomposition of Biomass Wastes. A Kinetic Study. Ind. Eng. Chem. Res. 2007; 46:2428-2437

[105] Braun RL and Burnham AK. Analysis of Chemical Reaction Kinetics Using a Distribution of Activation Energies and Simpler Models. Energy & Fuels 1987;1: 153-161

[106] Albina, D. O., Millrath, K. and Themelis, N. J., Effects of Feed Composition on Boiler Corrosion in Waste-to-Energy Plants, 12th North American Waste to Energy Conference, Savannah, Georgia USA, May 2004.

[107] Biomass Energy Foundation: http://www.woodgas.com/proximat.htm)

[108] Gaur S, Reed TB. An atlas of thermal data for biomass and other fuels. NREL/TP-433-7962; June 1995.

[109] Gray T, Tire Derived Fuel: Environmental Characteristics and Performance. The Southeast Regional Scrap Tire Management Conference Nashville, Tennessee, November 6, 1997.

[110] Salvador S., Quintar M., David C.. Combustion of a substitution fuel made of cardboard and polyethylene: influence of the mix characteristics experimental approach. Fuel 83 (2004) 451–462.

[111] http://www.patentstorm.us/patents/5672794/description.html

[112] Ahmed I, Noosai N, Gupta AK. Evolutionary Behavior of Gas Yield from Cardboard Pyrolysis. 46th AIAA Aerospace Sciences Meeting and Exhibit 7-10 January 2008, Reno, Nevada.

[113] Li S, Lyons-Hart J, Banyasz J, Shafer K. Real Time Evolved Gas Analysis by FTIR Method: An Experimental Study for Cellulose Pyrolysis. Fuel 2001;80: 1809-1817.

[114] Antal JM, Varhegyi G. Cellulose Pyrolysis Kinetics: The Current State of Knowledge. J. Ind. Eng. Chem. Res. 1995;34: 703-717.

[115] Bhatia SK, Perlmutter DD. A random pore model for fluid–solid reactions: I. Isothermal kinetics control. AIChE J 1980;26(3):379–85.

[116] Fogler HS. Elements of chemical reaction engineering, 4th ed., Pearson Education, Upper Saddle River, NJ 07458; 2006, p. 669–71.

[117] Fairbanks DF, Wilke CR. Diffusion Coefficients in Multicomponent Gas Mixtures. Industrial and Engineering Chemistry 1950;42(3):471-475.

[118] Belfiore LA. Transport Phenomena for Chemical Reactor Design. ISBN 0-471-20275-4, John Wiley 2003.

[119] Vyazovkin S. Kinetic concepts of thermally stimulated reactions in solids: A view from a historical perspective. Int Reviews in Physical Chemistry 2000;19(1):45-60.

[120] Capart R, Khezami L, Burnham AK. Assessment of various kinetic models for the pyrolysis of a microgranular cellulose. Thermochimica Acta 2004;417:79-89.

[121] Turmanova SC, Genieva SD, Dimitrova AS, Vlaev LT. Non-isothermal degradation kinetics of filled with rise husk ash polypropene composites. Express Polymer Letters 2008;2(2):133-146.

[122] Vlaev LT, Markovska IG, Lyubchev LA. Non-isothermal kinetics of pyrolysis of rice husk. Thermochimica Acta 2003;406:1-7.

[123] Sharma A, Rajeswara T. Kinetics of pyrolysis of rice husk. Bioresource Technology 1999;67(1): 53-59.

[124] Liu NA, Weicheng F, Dobashi R, Huang L. Kinetic modeling of thermal decomposition of natural cellulosic materials in air atmosphere. Journal of Analytical and Applied Pyrolysis 2002;63:303-325.

[125] Carter RE. Kinetic model for solid-state reactions. The Journal of Chemical Physics 1961;34(6):2010-2015.

[126] Tsamba AJ, Yang W, Blasiak W. Pyrolysis characteristics and global kinetics of coconut and cashew nut shells. Fuel Processing Technology 2006; 87:523-530.